

The Baldwin-effect in Wolf-Rayet stars

The Baldwin-effect in Wolf-Rayet stars

Het Baldwin-effect
in Wolf-Rayet sterren
met een samenvatting in het Nederlands

Proefschrift

ter verkrijging van de graad van doctor aan de Universiteit Utrecht
op gezag van de Rector Magnificus, Prof. Dr. H. O. Voorma,
ingevolge het besluit van het College voor Promoties
in het openbaar te verdedigen
op maandag 6 november 2000 des middags te 2.30 uur

door

Jeroen Ivar van Gent

geboren op 17 januari 1969 te Amsterdam

Promotor: Prof. Dr. H. J. G. L. M. Lamers
Sterrenkundig Instituut, Universiteit Utrecht

Cover: Extract from an image of the giant galactic nebula NGC 3603, showing stars in the outer regions of a massive star cluster. The cluster contains many early type O-stars and Wolf-Rayet stars.
Credit: Wolfgang Brandner (JPL/IPAC), Eva K. Grebel (Univ. Washington), You-Hua Chu (Univ. Illinois Urbana-Champaign), and NASA

Cover design: Hester J. van Gent
Robert Buizer

Printed by: Ponsen & Looijen, Wageningen, The Netherlands

© Copyright 2000 J. I. van Gent

All rights reserved. No part of this publication may be reproduced, stored in a retrieval system or transmitted, in any form or by any means, electronic, mechanical, photocopying, recording, or otherwise, without the prior written permission of the author.

ISBN 90-393-2534-0

Aan mijn ouders

Contents

Voorwoord	xi
1 Introduction	1
1.1 WR star classification	2
1.2 Physical properties of Wolf-Rayet stars	5
1.3 Wolf-Rayet stars as a phase of massive star evolution	8
1.4 The distances of early type stars	9
1.5 The Baldwin-effect	10
1.6 Outline of this thesis	11
2 Observations and interstellar extinction	13
2.1 Introduction	13
2.2 Spectroscopic data	13
2.2.1 Ultraviolet data	16
2.2.2 Optical data	16
2.2.3 Near infrared data	16
2.3 Interstellar extinction	16
2.4 Colour excesses in the study of the Baldwin-effect	18
2.4.1 Colour excesses derived from the ratio of intrinsic line fluxes	18
2.4.2 Colour excesses from the correction of the interstellar 2175 Å absorption bump	20
2.5 Discussion	21
3 On the Baldwin Effect of He II emission lines in WR (WN) stars	23
3.1 Introduction	23
3.2 A simple explanation of the Baldwin-effect	24
3.2.1 Optically thin wind	24
3.2.2 Optically thick continuum and optically thin line	25
3.2.3 Optically thick wind for continuum and line	27
3.3 Model atmospheres	30
3.3.1 Chemical composition	30
3.3.2 Atmosphere structure	31
3.3.3 Convergence	32
3.3.4 Synthetic spectra	32
3.4 The synthetic Baldwin effect	33
3.4.1 Grid parameters	33
3.4.2 Spectra	33

3.4.3	Ionization.	33
3.4.4	Equivalent widths and luminosities.	36
3.4.5	Effective temperature, T_{eff} , versus stellar temperature, T_*	42
3.4.6	Parametrizations	44
3.5	Discussion	46
4	Model atmospheres in the study of Wolf-Rayet type stars	49
4.1	Introduction	49
4.2	Model atmospheres	49
4.2.1	Geometry	49
4.2.2	Density and velocity of spherically symmetric winds	50
4.2.3	Radiative transfer in a spherically symmetric geometry	52
4.2.4	Temperature structure.	53
4.3	Assumptions in the ISA-WIND model atmospheres	55
4.3.1	The ISA-WIND model atmosphere code	55
4.3.2	The influence of hydrogen and nitrogen on the model atmospheres	55
4.3.3	The temperature structure	61
4.3.4	Clumping and electron scattering	63
4.3.5	Line blanketing and photon loss	64
4.3.6	Discussion	65
4.4	ISA versus CMF	66
4.4.1	The POTSDAM model atmosphere code	66
4.4.2	Grid comparison	66
4.4.3	Model comparison	68
4.5	Discussion and conclusions	71
5	The validation of predicted Baldwin-relations from He-N models for WN stars	79
5.1	Introduction	79
5.2	Observations	80
5.3	Model atmospheres	80
5.3.1	Atmosphere structure	81
5.3.2	Chemical composition	82
5.3.3	Convergence	82
5.3.4	Synthetic spectra	83
5.4	The synthetic Baldwin-effect for He-N models	83
5.4.1	Grid parameters	83
5.4.2	Line profiles and ionization	84
5.4.3	Theoretical Baldwin-relations for WN stars	87
5.5	Model assumptions	87
5.5.1	Nitrogen abundance	87
5.5.2	Clumping	95
5.5.3	Thomson scattering in lines	97
5.6	Testing the Baldwin-relations: stars with a well known distance	99
5.7	A new strategy for determination of WN star distances	102
5.8	Discussion	111

6	Distances of WN stars from the Baldwin-effect	113
6.1	Introduction	113
6.2	Observations	114
6.3	Mass-loss rate determinations	114
6.3.1	Mass-loss rates from detailed modelling	114
6.3.2	Mass-loss rates from optical and radio observations	115
6.3.3	Average mass-loss rates as function of spectral subtype	116
6.4	Strategy	119
6.5	Distance to Galactic WN stars	119
6.5.1	Mass-loss rates from observations	119
6.5.2	Mass-loss rate as function of spectral subtype	121
6.6	Discussion	122
	Summary and prospects	127
	Summary of the thesis	127
	Prospects	129
	Het Baldwin-effect in Wolf-Rayet sterren	131
	Sterren, wat zijn ze en waarom is kennis over hun afstand belangrijk?	132
	Afstandsbepalingen van sterren	132
	Sterrenwinden, spectra en Wolf-Rayet sterren	133
	De afstand van Wolf-Rayet sterren: het Baldwin-effect	135
	Overzicht van dit proefschrift	135
	Curriculum Vitae	137
	List of Figures	139
	List of Tables	143
	References	145

Voorwoord

Het boekje dat voor u ligt beschrijft de resultaten van een aantal jaren sterrenkundig onderzoek. Op de kaft is weliswaar mijn naam vermeld, maar vele andere personen hebben, ieder op eigen wijze, bijgedragen aan het welslagen van dit proefschrift.

Allereerst noem ik Henny Lamers, mijn promotor. Henny, wat moet onderzoek makkelijk zijn met jouw diepe inzicht en brede kennis van zaken. Heel erg bedankt voor alle steun. Ook Trudi bedankt (“U woont werkelijk heel erg leuk”).

Then there is the guy from the “Appelflappendienst”, Pat Morris. Thanks you for both astrophysical and moral support throughout the project; thanks also to you and Kim for the hospitality in and around Pasadena.

Alex de Koter, je maakte de toegang tot de wereld van modelatmosferen eindeloos veel makkelijker. Er zijn veel dingen die ik graag nog eens met je zou willen onderzoeken.

Lars Koesterke, with inexhaustible patience you answered my endless stream of questions and provided me with whatever I needed. I really wish we can write something together on this model business. And of course I still admire your beautiful hair.

Tante grazie to Luciana Bianchi, for enabling my visits to Baltimore and guiding me on my first steps in the field of Wolf-Rayet star observations.

My stays in that big and dangerous city knew many pleasant times, thanks to Thomas Gäng. Believe me, I even cherish those long nights when we were wrestling with line profiles, while eating pizza. Thanks to you and Amanda for introducing me to “America outside the office”.

Harry Blom bedankt voor de gastvrijheid in Mexico en voor het regelen van mijn praatje aldaar.

Dichter bij huis: veel dank aan mijn kamergenoten op SRON en het Sterrenkundig Instituut, Lucky, Pat en Willem-Jan. W.-J., je hebt me vaak verbaasd met je doorzettingsvermogen en je grote menselijke inzicht. Ik vond het een leuke tijd. Heel veel succes nog in het laatste jaar.

Sake en Ed bedankt voor het mogen gebruiken van jullie computer-wijsheid. Dank aan Marion en Gé voor werkelijk van alles en nog wat.

Jorick, meestal zijn we het wel eens, alleen: Amsterdam is een mooie stad, leer dat nu toch. Maar het is goed om lotgenoten in de buurt te hebben tijdens het afronden van een proefschrift. Hetgeen me brengt bij Marco; een bolhoed schijnt ons goed te staan. Bij ons volgende optreden wisselen we van hoed, ok? Robert, je bent inmiddels opnieuw collega. Ik mag en zal van je opbouwende kritiek blijven genieten. Maureen, dankzij jou eet ik snickers nu met mes en vork. Eric, het was leuk. Ferdi, Jacco, Joeri, Mariëlle, Thijs, Wouter en alle anderen op het instituut en op SRON, bedankt voor alle vrolijke, serieuze, gezellige en chaotische momenten.

Het Leids Kerkhoven-Bosscha Fonds en de Nederlandse Organisatie voor Wetenschappelijk Onderzoek dank ik voor de financiële steun voor mijn reizen naar het buitenland.

Zonder steun van mensen buiten het vakgebied is het voltooien van een proefschrift haast onmogelijk. Heel veel dank aan al mijn vrienden, voor het meegenieten van hoge toppen en de

steun bij het klimmen uit diepe dalen. Mijn zus Hester, heel erg bedankt voor het ontwerpen van de mooie omslag en Robert Buizer voor de hulp daarbij.

Tot slot dank ik mijn ouders, voor alle steun en vertrouwen, bij de keuze voor een vak waarover ik zo weinig vertelde.

Jeroen van Gent
Utrecht, September 2000

1

Introduction

It all started in 1867, when C.J.E. Wolf and G. Rayet discovered broad emission lines ($\sim 10^3 \text{ km s}^{-1}$) in the spectra of three stars in the constellation of Cygnus (Wolf & Rayet 1867, see Fig. 1.1). Almost a century and a half later, these *Wolf-Rayet* stars are known to form an important phase in the evolution of stars with an initial mass of $M \gtrsim 25 M_{\odot}$. Wolf-Rayet stars are among the most luminous stars known and have a high impact on their environment, due to their strong radiation field and violent mass-loss. Along with their short lifetimes (a few times 10^5 yr) and their role in the nucleosynthesis of heavy chemical elements, they are important contributors to the chemical enrichment of the interstellar medium.

The spectrum of Wolf-Rayet stars is characterised by broad emission lines that indicate mass-loss in the shape of a strong stellar wind. The density of this wind is such, that it hides the underlying star from vision. There are also less massive stars that show the Wolf-Rayet phenomena in their spectrum. These are population II stars, relatively old and located in the centres of planetary nebulae. Although the name *Wolf-Rayet* is also being used for this class of stars, the subject of this thesis is the class of the much younger population I stars, which are thought to be the descendents of O-stars. It is this population I class of stars to which will be referred if we use the name Wolf-Rayet.

Because of their peculiar spectral characteristics and high luminosities, Wolf-Rayet stars are detected at large distances. To date, 227 Wolf-Rayet (WR) stars have been detected in the Milky Way galaxy. Because of the widespread and capriciously distributed interstellar matter in the Galaxy, many more are likely to await their discovery. Many WR stars have also been detected in other Local Group galaxies. Their detectability at large distances would make WR stars suitable candidates to function as galactic and intergalactic candles.

Unfortunately, their intrinsic luminosities are hard to determine, as the absolute visual magnitudes of WR stars do not correlate well with temperature or intrinsic colours (e.g. Conti & Vacca 1990; van der Hucht 2000). WR star distances are therefore often poorly known, particularly if the star is not a member of a stellar cluster or OB association with a known distance.

However, it was found by Morris et al. (1993a) that the strength of helium emission lines in the spectra of nitrogen rich WR stars shows a relation with the luminosity of the underlying continuum. This means that information on the luminosities of WR stars, and therefore on their distance, can be obtained purely from their spectral characteristics!

This discovery followed the observation of a similar relation in the spectra of galaxies with Active Galactic Nuclei (AGN, Baldwin 1977; Baldwin et al. 1978). It is the *Baldwin-effect in Wolf-Rayet stars* that is the subject of this thesis.

The spectral criteria by which WR stars are classified will be briefly reviewed in Sect. 1.1. The main physical properties of these stars is described in Sect. 1.2. The position of the Wolf-Rayet phase in massive star evolution is the subject of Sect. 1.3. Subsequently, the importance of knowing the distances of early type stars is discussed (Sect. 1.4). The Baldwin-effect in WR

ASTRONOMIE. — *Spectroscopie stellaire*. Note de MM. WOLF et RAYET, présentée par M. Le Verrier.

« Parmi les nombreuses étoiles dont la lumière a été étudiée à l'aide du prisme, on n'en connaît qu'une seule, γ de Cassiopée, dont le spectre offre constamment des lignes brillantes. Nous avons l'honneur de signaler à l'Académie l'existence de semblables lignes dans trois étoiles de la constellation du Cygne. Ce sont les étoiles suivantes du Catalogue de Bonn (1850) :

Argelander. Zone + 35	8,5	$\lambda = 20.4.49,3$	$\Omega = + 35.45,1$
Zone + 35	8,0	$\lambda = 20.6.27,3$	$\Omega = + 35.46,1$
Zone + 36	8,0	$\lambda = 20.9.6,7$	$\Omega = + 36.13,3$

» Elles ont été observées par Bessel, à Königsberg ; et alors, comme aujourd'hui, leurs grandeurs étaient celles qu'indique Argelander. Ces étoiles ne doivent donc pas, jusqu'à nouvel ordre, être considérées comme variables. Elles ne présentent non plus aucune trace de nébulosité. Mais elles se distinguent immédiatement de leurs voisines par leur teinte jaune : la première est franchement jaune, la deuxième jaune orangé, la troisième jaune verdâtre.

» Leur spectre se compose d'un fond éclairé dont les couleurs sont à peine visibles, et qui paraît manquer de rouge et de violet, sans doute à cause de la faiblesse de la lumière. Ce fond semble interrompu par des lignes noires, mais il est impossible de l'affirmer, et à plus forte raison d'assigner la position de ces lignes. Tous trois présentent une série de lignes brillantes.

» Le plus beau spectre est celui de la deuxième étoile. Il possède quatre lignes lumineuses, dont nous avons pu déterminer les positions par rapport

Figure 1.1: The first page of the article by Wolf & Rayet (1867), in which they discuss the discovery of three stars that show bright lines in their spectrum. Source: *Comptes Rendus de l'Académie des Sciences Paris, 1867; Vol. 65*.

stars is described in Sect. 1.5. Finally, in Sect. 1.6, an overview is given of the content of this thesis.

Recent reviews on Wolf-Rayet stars have been given by Abbott & Conti (1987), van der Hucht (1992). A new overview of the properties and distribution of Galactic WR stars will soon appear in the VIIth *catalogue of Galactic WR stars* (van der Hucht 2000).

1.1 WR star classification

Nowadays, population I Wolf-Rayet stars are subdivided in three major classes, WN, WC, and WO, according to whether their optical spectrum distinguishes itself by spectral features of nitrogen, carbon, or oxygen, respectively. The WN stars were subdivided in WN-A and WN-B

stars by Hiltner & Schild (1966); these two subclasses respectively refer to stars with either narrow, weak lines and a strong continuum spectrum and stars with a weak continuum, but relatively strong and broad lines¹.

Many attempts have been made to find suitable schemes for classifying the stars within each of the three major WR star classes mentioned above. One of the most widely used schemes for WR stars is that of Smith (1968). In this scheme, WR stars are classified on basis of the strength and ratios of spectral lines in their optical spectrum, similar to the MKK classification scheme of “normal” stars (Morgan et al. 1943). Table 1.1 lists the classification scheme of Smith (1968), including extensions and modifications of later years. The WN stars are classified WN2-11, mainly based on the ratios of different ion species of nitrogen. Analogously to the MKK system, WNE2-6 stars are called “early” types (WNE), and the WN7-11 stars are considered “late” type (WNL) stars (Conti et al. 1989; Conti & Massey 1989; Conti et al. 1990). Similarly, one discriminates between WCE stars (WC4-7) and WCL stars (WC8-9) (Smith et al. 1990). Examples of WN star spectra are shown in Fig. 1.2.

For normal stars, the classification is based on the *absorption* line spectrum, which is formed close to the stellar *photosphere* where also the continuum radiation originates. The appearance of the absorption spectrum therefore gives a good representation of some basic physical properties of the star, such as luminosity and effective temperature.

On the other hand, the optical spectrum of WR stars is dominated by *emission lines*, which are formed in an optically thick *stellar wind*. Ratios of emission line strength therefore are a good representation of neither effective temperature nor luminosity. Even a radius is hard to define for WR stars, because the inner regions of the stellar wind are optically thick for continuum radiation. Any definition of the radius of the star therefore intrinsically depends on the wavelength at which the star is observed.

The WR classification scheme of Smith (1968) thus mainly reflects ionization and excitation conditions in the stellar wind. The system is “one-dimensional”, as it only describes an ionization sequence among WR stars. New studies gradually adopt the three-dimensional classification scheme for WN stars of Smith et al. (1996), which uses spectral line characteristics to describe ionization, line width classes (discriminating between broad lined and narrow lined spectra) and hydrogen content. Conti (1999) however advised against the classifications based on line width, as the dividing line between these classes is rather arbitrary and does not clearly reflect a division of physical properties in WR stars.

Similar classification criteria as those of Smith et al. (1996) were already adopted by Hamann et al. (1995), amending the system of Smith (1968) to discriminate between strong lined and weak lined WNE stars (assigning the labels WNE-s and WNE-w, respectively and bringing back to live the system of Hiltner & Schild 1966) and to account for the presence of hydrogen in the spectrum. According to Smith et al. (1996), the WNE-s and WNE-w classification *does* reflect differences in physical WR star properties (e.g. mass-loss rate). Although the division line may not be a sharp one, the “s” and “w” labels at least indicatively discriminate between WNE stars with dense winds (WNE-s) and less dense winds (WNE-w). Therefore, the classification criteria for WN stars from Hamann et al. are adopted throughout this thesis.

¹This hints already at the Baldwin-effect, of which the physical explanation is presented in Ch. 3.

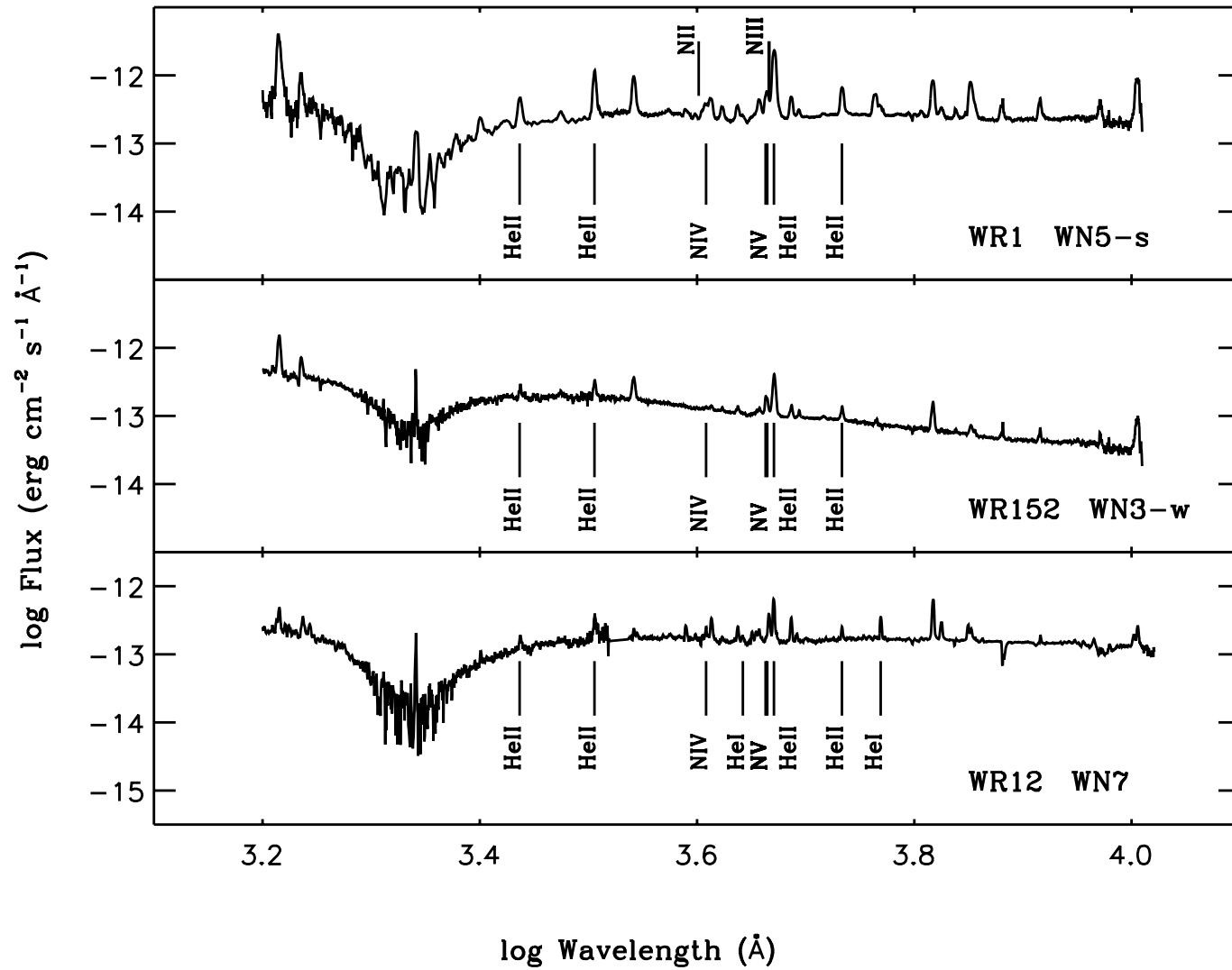


Figure 1.2: Spectrum of a WNE-s (top), WNE-w (middle), and WNL star. Some spectral features that are characteristic for their class are indicated, as well as some omnipresent helium lines.

Table 1.1: WR classification scheme by Smith (1968).

WN subtypes	Nitrogen emission lines	Other emission criteria
WN2	N V weak or absent	He II strong
WN2.5	N IV present; N IV absent	
WN3	$N IV \ll N V$; N III weak or absent	
WN4	$N IV \approx N V$; N III weak or absent	
WN4.5	$N IV > N V$; N III weak or absent	
WN5	$N III \approx N IV \approx N V$	
WN6	$N III \approx N IV$; N V present but weak	
WN7	$N III > N IV$; $N III < He II \lambda 4686$	He I weak P Cygni
WN8	$N III \gg N IV$; $N III \approx He II \lambda 4686$	He I strong P Cygni
WN9 ^a	$N III > N II$; N IV absent	He I strong P Cygni
WN10	$N III \approx N II$	Balmer lines; He I P Cygni
WN11	$N II \approx He II$; N III weak or absent	Balmer lines; He I P Cygni
WC subtypes	Carbon emission lines	Other emission criteria
WC4	C IV strong; C II weak or absent	O V moderate
WC5	$C III \ll C IV$	$C III < O V$
WC6	$C III \ll C IV$	$C III > O V$
WC7	$C III < C IV$	$C III \gg O V$
WC8	$C III > C IV$	C II absent; O V weak or absent
WC9	$C III > C IV$	C II present; O V weak or absent
WO subtypes^b	Oxygen emission lines	Other emission criteria
WO1	O VI strong; O IV absent	$C IV \leq O V$; C III absent
WO2	O VI strong; O IV absent	$C IV > O V$; C III absent
WO3	$O VI > O IV$	$C IV \gg O V$; C III absent
WO4	$O VI \approx O IV$	$C IV \gg O V$; C III absent
WO5	$O IV > O VI$	$C IV \gg O V$; C III absent

^aWalborn (1977) suggested the possible necessity of subtypes WN9 and higher; The current definitions of subtypes WN9 to WN11 were set by Crowther et al. (1995a)

^bThe WO class was introduced by Barlow & Hummer (1982). An extension to their classification scheme was presented by Kingsburgh et al. (1995).

1.2 Physical properties of Wolf-Rayet stars

A Wolf-Rayet star can be considered as the core remaining of a normal O supergiant star, after the outer layers of the star have been expelled during an era of violent mass-loss in the shape of a stellar wind. Sometimes the core may be the result of Roche-lobe overflow when the star is in a binary system.

Some of the basic physical parameters of WR stars, discussed below, are shown in Table 1.2, in comparison with the same parameters of O-stars and the Sun (remember that the solar wind is not driven by its radiation field). As mentioned before, the spectra of WR stars are characterised by strong, broad emission lines, sometimes containing a blue-shifted absorption component, caused by P Cygni scattering of radiation. These emission lines and P Cygni profiles in WR

Table 1.2: Basic physical parameters of Wolf-Rayet stars, compared to those of O-stars and the Sun.

	R_* (R_\odot)	T_{eff} (K)	\dot{M} ($M_\odot \text{ yr}^{-1}$)	$\log(L)$ (L_\odot)	M (M_\odot)	v_∞ (km s^{-1})
WR stars	1 – 60	$25 - 100 \times 10^3$	$0.2 - 10 \times 10^{-5}$	4.5 – 6.5	5 – 50	900 – 4500
O stars	10 – 35	$30 - 55 \times 10^3$	$0.5 - 20 \times 10^{-6}$	5.0 – 6.5	20 – 130	900 – 3500
Sun	1	5800	10^{-14}	0	1	400 – 800

spectra are the signatures of a strong stellar wind. Indeed, a photospheric absorption spectrum, like encountered in O star spectra, is absent in the spectra of WR stars, since the high wind density blocks the underlying stellar core from view. The physical properties of WR stars can thus only be inferred from line characteristics and the shape of a continuum *formed in the stellar wind*.

The dense forest of emission lines often prevents a straightforward determination of the continuum level; in WC star spectra, the continuum can even disappear due to large overlap of strong emission features.

The line profiles however nicely reflect the velocity structure in the wind outflow and the terminal wind velocity (v_∞) is therefore readily measured from the stellar spectrum. Values of v_∞ in WR star winds range from ≈ 900 to $4500(!)$ km s^{-1} . The highest velocities occur for the most compact stars, as indicated by the theory of radiation driven winds, which states that the terminal velocity is proportional to a star's escape velocity (e.g. Lamers & Cassinelli 1999).

Parameters other than the wind velocity, such as temperature, radius, mass-loss rate and luminosity are not easily inferred from the spectrum. Moreover, the classical definitions of radius and effective temperature are useless in the case of WR stars, because they depend on the observed wavelength.

One of the most widely used methods to derive the basic physical parameters of WR stars is through model atmosphere calculations. By prescribing the wind structure, velocity and temperature distribution, chemical composition, and atomic states in the wind, an artificial WR atmosphere is created. Radiative transfer theory then provides a synthetic spectrum, which can be compared to the spectral observations.

The inner boundary of the synthetic atmosphere functions as *stellar radius* or *core radius*, R_* , mostly corresponding to a Rosseland optical depth of $\tau_{\text{Ross}} \approx 20$. Correspondingly, a *stellar temperature*, T_* , is defined by means of the familiar Stefan-Boltzmann law, $L = 4\pi R_*^2 \sigma T_*^4$ (e.g. Hillier 1987, 1990, Schmutz et al. 1989; Hamann et al. 1994).

One of the boundary conditions for the derivation of stellar parameters is that the distance of the star is known; the distance is required to infer the stellar radius from the shape and strength of the observed continuum spectrum; the continuum shape and the line strength subsequently provide information on the temperature and mass-loss rate. Distances of WR stars can be quite uncertain however, as we will see in Sect. 1.4.

For almost all known WR stars in the Galaxy and the Large and Small Magellanic Clouds (LMC and SMC, respectively), model atmospheres have provided stellar parameters (e.g. Crowther & L. J. Smith 1997; Crowther 2000; Gräfener et al. 1998; Hamann & Koesterke 1998, 2000). The use of model atmosphere calculations in the study of WR stars is the subject of Ch. 4.

The most obvious aspects in which Wolf-Rayet stars distinguish themselves from their predecessors, the O-stars, is their high rate at which they expel their outer layers into the interstellar medium. The mass-loss rate (\dot{M}) of WR stars is commonly about $10^{-5} - 10^{-4} M_{\odot} \text{ yr}^{-1}$, some 10 times higher than for O-stars. Much attention has been paid to understanding and deriving the mass-loss rates of early type stars, as they play an important role in the late stages of evolution of massive stars and in the enrichment and dynamics of the interstellar medium.

It is generally accepted that the mass-loss rates of both O-stars and Wolf-Rayet stars is at least for the major part driven by the pressure of their strong radiation field. In this mechanism, photon scattering processes in both continuum and spectral lines result in a, nett radially outward directed, transfer of momentum from the stellar radiation field to the outer layers of the stellar atmosphere. Due to Doppler-shifting, a spectral line can absorb a large frequency range of continuum photons, which results in an efficient acceleration of the outflowing matter into a full blown stellar wind, with a high terminal velocity.

The theory of line driven winds in O-stars has been developed by Castor et al. (1975, CAK). The CAK theory has led to the basic understanding of the origin of the winds of early type stars. Improvements have been made through the detailed calculations of momentum transfer of thousands of spectral lines, e.g. by Abbott (1982) and Pauldrach et al. (1986).

The momentum of the stellar wind and that of the star's radiation field are related as

$$\dot{M}v_{\infty} = \eta \frac{L_{*}}{c}, \quad (1.1)$$

in which L_{*} is the luminosity of the star and c is the speed of light. The variable η is the wind efficiency factor, describing the fraction of radiative momentum transferred to the wind outflow.

One would expect that the maximum mass-loss rate that can be driven by the star's radiation field is found if the full radiative momentum is transferred to the wind, i.e. $\eta = 1$. However, observations indicate that early type stars, and particularly Wolf-Rayet stars, often show much stronger outflows than can be explained by the momentum from the radiation they emit. In other words, values of η much larger than 1 are observed (Lamers & Leitherer 1993; Puls et al. 1996). This *momentum problem* appears to be largest for stars with the highest wind densities.

A probable solution for the momentum problem lies in the mechanism of multiple scattering, in which photons are scattered more than one time at spectral lines before they escape from the stellar wind. Recently, Vink et al. (2000) carefully took multiple scattering processes into account in Monte Carlo calculations of radiative transfer through the winds of O and B type stars. For the O stars, good agreement was found between the predicted and observed mass-loss rates.

For the Wolf-Rayet stars, the momentum problem is larger ($\eta \approx 1 - 50$) and is unlikely to be solved by multiple scattering alone. In recent years however, evidence has risen that WR star mass-loss rates have been overestimated. The reason is that stellar winds have always been considered to be spherically symmetric and have a wind density structure that drops monotonically with radial distance to the star. Over recent years, however, both theory and observations have indicated irregular wind structures for WR stars (e.g. Hillier 1984; Moffat et al. 1988; Nugis et al. 1998). These "clumping" phenomena in WR star winds affect the derived mass-loss rates. The emission features in WR star spectra are in majority formed by recombination processes, which scale with ρ^2 . Therefore, in a clumped wind, a lower mass-loss rate is required to get the same strength of emission lines as in a "smooth" wind. The derivation of clumping corrected mass-loss rates have lowered the wind efficiency factor η to values of $\eta \approx 1 - 20$ (e.g. Nugis & Lamers 2000). The remaining discrepancy can probably largely be resolved by taking into

account multiple scattering processes, although much is still to be known about the exact processes that actually initiate the mass-loss of early type stars (e.g. Schmutz 1997; Vink et al. 1999).

1.3 Wolf-Rayet stars as a phase of massive star evolution

Nowadays, virtually everyone in the astrophysical community agrees that Wolf-Rayet stars are to be considered as the representation of an advanced phase in the evolution of massive stars ($M \gtrsim 25 M_{\odot}$). Although opinions to the contrary exist (Bhatia & Underhill 1986, 1988, 1990), it is generally accepted that WR stars are the successors of O stars that have expelled their outer envelope by means of a strong stellar wind and possibly eruption like events. In this scenario, the rich spectrum of nitrogen, carbon and oxygen lines is the result of the way massive, early type stars burn their nuclear fuel: the CNO fusion cycle for conversion of hydrogen to helium; triple-alpha processes to create carbon out of helium. The products of these nuclear fusion cycles are shown at the stellar surface, after the outer layers of the star are blown away. The transitional phase, from O star to Wolf-Rayet star is not well understood, however, and the subject of ongoing research.

The first observational support for the mechanism where O stars turn into Wolf-Rayet stars through mass-loss in a stellar wind came from Conti (1976). This *Conti scenario* has remained alive ever since, though with varying details.

An example of the success of the Conti scenario is the luminosity of WR stars. With respect to stars on the main-sequence in the Hertzsprung-Russel diagram, WR stars are overluminous for their mass. Their luminosities do however agree with those predicted for bare cores (e.g. Smith & Maeder 1989).

Stellar evolution calculations over the years have provided many variations on the details of the Conti scenario. Below we give the evolution scheme from Maeder (1996), who comprised the scheme from suggestions by Chiosi & Maeder (1986); Crowther et al. (1995d), and Langer & Maeder (1995).

$M \geq 60 M_{\text{sun}}$

O \Rightarrow Of \Rightarrow WNL + a \Rightarrow WN7 \Rightarrow (WNE) \Rightarrow WCL \Rightarrow WCE \Rightarrow SN

$M \approx 40 - 60 M_{\text{sun}}$

O \Rightarrow Of \Rightarrow LBV \Rightarrow WN8 \Rightarrow WNE \Rightarrow WCE \Rightarrow SN

$M \approx 25 - 40 M_{\text{sun}}$

O \Rightarrow (BSG) \Rightarrow RSG \Rightarrow (BSG) \Rightarrow WNE \Rightarrow (WCE) \Rightarrow SN

In the above scheme, WNL + a refers to a WNL phase in which the star still shows absorption lines, additional to the typical WR emission features; BSG stands for “blue supergiant”, and RSG for “red supergiant”. LBV denotes the phase of “luminous blue variable”, in which the star shows brightness variations on time scales of a few weeks to many years; meanwhile the star’s total luminosity is high ($\log(L_*/L_{\odot}) \gtrsim 5.5$) and the star loses mass in a stellar wind at rates that are similar to those of WR stars, but with a much lower terminal velocity of a few hundred kilometres per second. SN abbreviates “supernova”, the catastrophic phenomenon

through which the most massive stars end their lives. Of stars are O stars that show the He II $\lambda 4686$ feature and the N III $\lambda 4634-41$ complex in emission. In spectral appearance they are situated between O stars and WNL + a and WN7 stars, suggesting the evolutionary connection from O, via Of, to WNL. This connection is also found from mass-loss properties of these types of stars (Lamers & Leitherer 1993). WN8 stars seem to be placed in the evolutionary scheme of intermediate mass stars. Based on, among other criteria, their lower luminosity than WNL + a and WN7 stars and the occurrence of circumstellar nebulae around WN8 stars, a resemblance of WN8 stars with LBVs is suggested (Crowther et al. 1995d).

Many factors exist that can change the details of the presented evolution scheme. For example, different metallicities, Z , change the mass-loss behaviour of stars; the lifetime of certain phases or some stages of the above scheme may even be skipped (e.g. Langer & Maeder 1995). Also, there are indications that LBVs do not follow directly the O star phase, but experience an intermediate red supergiant phase. Many LBVs are namely observed to have a circumstellar nebula, that seems to be the expelled outer layers of red supergiants, based on their abundance and dust properties (e.g. Smith et al. 1997; Voors et al. 2000). This despite the fact that no RSGs are observed with sufficient luminosity to explain their LBV descendants. Based on abundances in the nebulae and the photospheres of LBVs and the velocities of the nebulae, Lamers et al. (2000) argue against a RSG descent of LBVs. Rather, an LBV may have experienced a brief red phase during which they had an optically thick wind. The star then *resembles* a RSG.

1.4 The distances of early type stars

The importance of early type stars in the derivation of Galactic and extra-galactic distance scales is through their large luminosities. O stars and Wolf-Rayet stars have been detected in many Local Group galaxies and distant WR stars are particularly easily recognised because of their peculiar spectral features. For stars of spectral type B and later, the determination of the distance is relatively easy. Intrinsic colours correlate well with absolute magnitude and photometric observations. Combined with the determination of interstellar extinction, stellar distances are readily obtained (e.g. Eggen 1981).

For O, B, and A supergiants, another distance estimator is provided through the “wind momentum - luminosity relation” (WLR, Kudritzki et al. 1995). This relation states that the so called *modified wind momentum*, $\Pi \equiv \dot{M} v_{\infty} R_{*}^{0.5}$ is proportional to $L^{1/\alpha}$, where α is a parameter depending on the ionization in the wind and the strength of spectral lines. Such a relation has indeed been found from O star observations (e.g. Puls et al. 1996). Good agreement between theoretically predicted and observed wind momenta, found by Vink et al. (2000), supports the power of the WLR as a distance estimator.

The WLR does not apply for WR stars, nor are WR star colours well correlated with their absolute visual magnitudes. But then, from the above, we derive that the distances of Wolf-Rayet stars can be found if these stars are a member of a stellar cluster or OB association. WR star cluster/association membership has been looked into by Lundström & Stenholm (1984), and 50 WR candidates for membership were found.

By far not every WR star, however, is associated with an open star cluster or OB star association. Furthermore, the determination of cluster/association membership is not an easy task, as cluster boundaries may be not well determined, and because the cluster distance may be uncertain itself. An interesting example in this respect is the star γ Velorum (also known as WR 11), which is important for the study of absolute visual magnitudes and colours of WR stars, because

it is the nearest WR star known. This WC8 type star with an O star companion has been long considered as member of the Vela OB2 association, at a distance of ≈ 450 pc. Measurements from the HIPPARCOS satellite however (van der Hucht et al. 1997) revised the distance of this binary system to 258_{-31}^{+41} pc (1σ limits). Two years later, de Zeeuw et al. (1999) argued the star to be a member again, based on its directional position and proper motion. Membership was also confirmed by Pozzo et al. (2000), arguing γ Velorum to be associated with a new discovered group of pre-main sequence stars.

Similar distance uncertainties occur for WR 6, a WN5 star, associated with the open cluster Collinder 121 (Col 121). This cluster has a distance of ≈ 910 pc (Lundström & Stenholm 1984). The strength of interstellar lines however, indicate that WR 6 is at a distance of at least 1800 pc (Howarth & Schmutz 1995). Again, de Zeeuw et al. (1999) concluded the star to be a member of Col 121; this conclusion was based on the HIPPARCOS parallax and proper motion of the star, although HIPPARCOS parallaxes alone are unreliable for distances larger than ≈ 500 pc.

1.5 The Baldwin-effect

So, for WR stars not in a cluster or association, or for those WR stars with uncertain membership, distance information is not easily obtained. Yet, gathering information about the distances of WR stars is important, as the way they are distributed through the Galaxy provides information on the chemical enrichment of the interstellar medium, and information on (local) stellar evolution and the initial mass-function. Furthermore, as we have seen, the basic stellar parameters of WR stars are not easily derived if the distance is unknown. Therefore, well known distances of WR stars first of all provide insight in the Wolf-Rayet phenomenon itself.

With respect to this latter statement, one ideally would have a method to estimate WR star distances that depends on spectral characteristics alone, and does not depend on predicted or derived physical properties of these stars. Such a method may be available through *the Baldwin-effect in Wolf-Rayet stars*, an observed relationship between the equivalent width, W , of emission lines in WR star spectra and the monochromatic luminosity of the stellar continuum at the central wavelength of the line, $L_c^{\lambda_0}$ (Morris et al. 1993a). These authors found that for the WN stars in the LMC, W decreases with larger $L_c^{\lambda_0}$. They found this effect for emission lines of N V, C IV, and He II. The trends found for He II lines are shown in Fig. 1.3. Comparison to a set of model atmosphere calculations (with constant mass-loss rate and constant terminal wind velocity) suggested that the Baldwin-effect is caused by a difference in wind density among stars. The physical details were not studied, however. The spread in the relations was assumed to be of a gaussian nature and due to measurement uncertainties in the line equivalent width values and the determination of the continuum level in their spectral observations. By using least-square fits to the observed *Baldwin-relations*, Morris (1995) estimated the distance of Galactic WN stars, with promising results. For stars of which the distance is known from their membership of an open cluster or OB association, Morris (1995) confirmed the distance modulus, mostly within a few tenths of a magnitude.

A complete understanding of the Baldwin-effect in Wolf-Rayet stars may improve its application as a distance estimator. Once the physics of the Baldwin-effect are understood, model atmosphere calculations may provide relations between line equivalent width and continuum luminosity. Theoretically predicted Baldwin-relations may then even function as a method to provide distances of extra-galactic WR stars, as they can be calibrated for environments of

different metallicities.

1.6 Outline of this thesis

In the chapters to follow, the Baldwin-effect in WN stars is further investigated. For this project we have obtained a large set of spectral observations, by courtesy of Pat Morris, which is for the larger part equal to that used by Morris (1995). We will not investigate the Baldwin-effect for WC stars, as the continuum level in these spectra is often hard to determine due to extensive line blending. Our spectral observations and the colour excesses, used to correct the spectra for the effects of interstellar extinction, are discussed in Ch. 2.

The physics of the Baldwin-effect in WN stars is the subject of Ch. 3. In this chapter we use model atmosphere calculations to investigate the mechanisms that cause the Baldwin-effect and to find out over which range of the basic physical parameters of WN stars (such as radius, temperature, mass-loss rate) a Baldwin-effect can be expected. Also, a first idea is given on how theoretically predicted relations between equivalent width and continuum luminosity can be used to estimate stellar distances.

The results from model atmosphere calculations are always a simplification of the real physical circumstances. Assumptions in the calculations need to be made, either because not all physical process acting in a star are fully understood, or because including all physics is beyond the capability of today's computer power. Nevertheless, it is important to understand the effect of the made assumptions, particularly if predictions are made that are based on simplified model calculations. Ch. 4 therefore discusses the use of model atmosphere calculations in the study of WN stars, with the Baldwin-effect in mind. The possibilities and limitations of today's model atmosphere computer codes is discussed. Also, the results from two different model atmosphere coded are compared.

In Ch. 5, the stage is set to actually apply theoretically predicted Baldwin-relations to estimate the distances of WN stars. New theoretical Baldwin-relations are presented. The calibration of these relations is discussed by investigating the main assumptions, and by predicting continuum luminosities of WN stars in the LMC.

Further testing of theoretically predicted Baldwin-relations is done in Ch. 6. Moreover, estimates are made of the distances of Galactic WN stars. Focusing on WN stars in open star clusters and OB associations, we will get further insight in the accuracy of theoretically predicted Baldwin-relations as distance estimators.

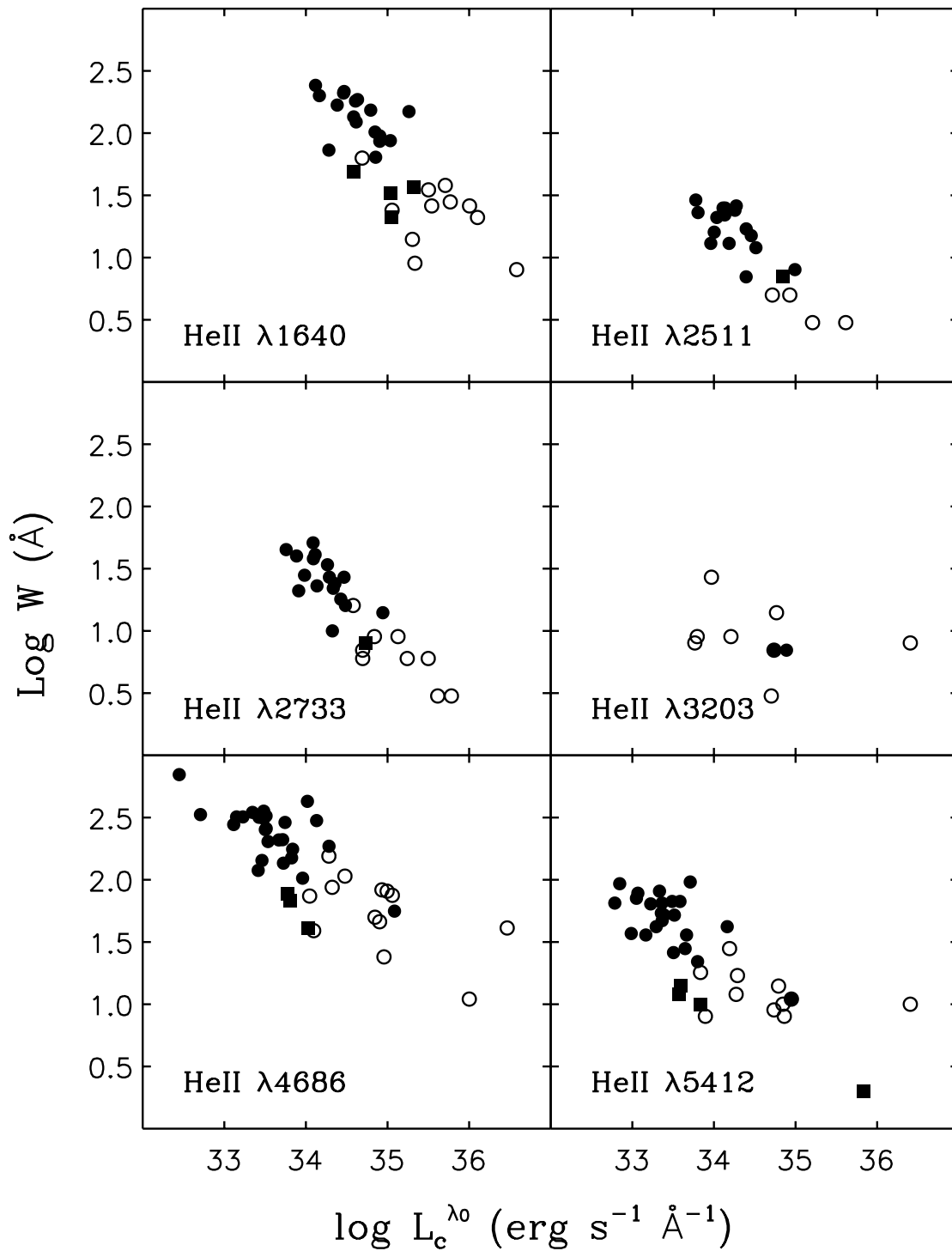


Figure 1.3: The Observed *Baldwin-effect* for He II transitions in the spectra of WN stars in the LMC. Open circles represent WNL stars; filled circles are WNE stars. Stars with absorption lines in their spectra are indicated by filled squares.

Observations and interstellar extinction

2.1 Introduction

The observational data set used for this thesis project is for the major part the same as that of Morris (1995). It consists of ultraviolet (UV) spectra from the *International Ultraviolet Explorer* (IUE) satellite and ground based spectra in optical and near infrared (NIR) wavelength regions.

The spectral data set covers most of the WN stars in the Milky Way galaxy and the Large Magellanic Cloud (LMC). The LMC spectra are used in Ch. 5 to validate the use of the theoretical relation between helium line equivalent widths and monochromatic continuum luminosity (the Baldwin-effect, see Ch. 3). In Ch. 6 the theoretical Baldwin-effect will be applied to the spectra of Galactic WN stars, to measure their distances. In both cases knowledge about the affection of the spectra by interstellar extinction is required. In this chapter, we will therefore also treat the methods by which the spectral data have been “de-reddened”.

An overview of the spectral data used in this thesis is given in Sect. 2.2; general de-reddening methods, to correct the spectrum for interstellar extinction, are discussed in Sect. 2.3; two of these methods, used for de de-reddening of our data set, are the subject of Sect. 2.4.

2.2 Spectroscopic data

The spectral data used in this thesis cover most of the known WN stars in the Galaxy and the LMC. Galactic objects are listed in Table 2.1; LMC objects are listed in Table 2.2.

Table 2.1: Galactic WN stars. Bullets indicate that the indicated wavelength range is present in our dataset.

WR ^a	Spectral subtype ^b		UV	Optical	NIR	$E(B - V)^c$	σ
	Smith 1968	SSM 1996					
1	WN5-s	WN4b	•	•	•	0.73	0.05
2	WN2-w	WN2b	•	•		0.52	0.01
3	WN3a-w+c	WN3b+04	•	•		0.34	0.02
6	WN5-s+c?	WN4b	•	•	•	0.03	0.01
7	WN4-s	WN4b	•	•	•	0.53	0.02
10	WN4.5-w	WN5h(+OB)	•	•	•	0.57	0.02
12	WN7	WN8b	•	•	•	0.84	0.04
16	WN8	WN8h	•	•	•	0.47	0.02

Continued on next page

Table 2.1, *continued.*

WR	Spectral subtype		UV	Optical	NIR	$E(B - V)$	σ
	Smith 1968	SSM 1996					
18	WN5-s	WN4b	•	•	•	0.77	0.04
21		WN5+O4-6	•	•	•	0.60	0.03
22	WN7a+c	WN7ha	•	•	•	0.29	0.02
24	WN7a	WN6ha	•	•	•	0.19	0.01
25	WN7a	WN6ha		•	•	0.40	0.03
31		WN4+O8 V	•	•	•	0.61	0.06
40	WN8	WN8h	•	•	•	0.41	0.01
44	WN4-w	WN4o	•	•	•	0.53	0.02
46	WN3pec-w	WN3b pec	•	•	•	0.33	0.03
47		WN6+O5 V	•	•	•	1.11	0.03
55	WN7	WN7o	•	•	•	0.70	0.04
61	WN4.5-w	WN5	•	•		0.55	0.05
71		WN6+OB?	•	•	•	0.33	0.04
75	WN6-s	WN6b	•	•		0.97	0.06
78	WN7	WN7h	•	•	•	0.54	0.04
85		WN6h+OB?	•	•	•	0.84	0.03
108	WN9	WN9ha	•	•	•	1.12	0.02
110	WN6-s	WN5-6b	•	•	•	1.15	0.01
123	WN8	WN8o	•	•	•	0.72	0.04
127		WN3+O9.5 V	•	•		0.46	0.03
128	WN4-w+c	WN4(h)	•	•	•	0.28	0.02
133		WN5+O9 I	•	•		0.30	0.03
134	WN6-s+c	WN6b	•	•	•	0.51	0.03
136	WN6-s+c	WN6b(h)	•	•	•	0.52	0.01
138	WN6a-w+c	WN5o+B?	•	•		0.64	0.04
139		WN5+O6 III-V	•	•		0.88	0.04
141	WN6-w+c	WN5o+OB	•	•		1.12	0.05
148	WN7+c	WN8h	•	•		0.87	0.07
151		WN4+O5 V	•	•	•	1.13	0.02
152	WN3-w	WN3(h)	•	•		0.48	0.03
153		WN6/WCE+O6I	•	•		0.64	0.02
155	WN7+c	WN6o+O9 II/Ib	•	•	•	0.54	0.03
156	WN8	WN8h	•	•	•	1.09	0.04
157	WN4.5-w	WN5o(+B1 II)	•	•	•	0.65	0.05
158	WN7	WN7h	•	•	•	1.17	0.05

^aWR numbers are from van der Hucht et al. (1981)

^bSpectral subtype classification from Smith (1968) (column 2) and Smith et al. (1996) (SSM, column 3). The Smith 1968 classification is only shown for those stars that have been analysed by Hamann & Koesterke 1998a; these authors extended the classification with the “s” and “w” labels to discriminate between strong and weak lined early type stars, respectively.

^cColour excesses are taken from Morris et al. (1993b) and Conti & Morris (1990). For stars in common in these studies average values have been adopted.

Table 2.2: WN stars in the LMC. Bullets indicate that the indicated wavelength range is present in our dataset.

Br ^a	Spectral subtype ^b		UV	Optical	NIR	$E(B - V)^c$	σ
	Smith 1968	SSM 1996					
1	WN3-s	WN3b	•	•	•	0.00	0.03
3		WN4b	•	•		0.14	0.05
6	WN2.5-s	WN4b	•	•	•	0.00	0.04
12	WN4-s	WN4b	•	•	•	0.04	0.05
13	WN8	WN8h	•	•	•	0.03	0.02
14		WN4	•	•	•	0.11	0.04
15		WN4(h)	•	•		0.11	0.03
16	WN2.5-s	WN4b+OB?	•	•	•	0.00	0.03
18		WN9h	•	•	•	0.05	0.01
23		WN4b	•	•		0.05	0.04
24	WN7	WN6h	•	•	•	0.05	0.02
25		WN3b	•	•	•	0.17	0.03
26	WN7	WN6(h)+abs?	•	•	•	0.09	0.04
27	WN3-w	WN3o	•	•		0.01	0.03
29	WN3/CE-s	WN4b/CE	•	•	•	0.04	0.04
35		WN4b	•	•		0.10	0.05
36		WN8h	•	•	•	0.08	0.03
37	WN3-w+abs	WN4+OB	•	•		0.00	0.01
38		WN4o	•	•		0.01	0.03
40	WN4-s	WN4b	•	•		0.03	0.04
46		WN4b	•	•		0.08	0.03
47	WN8	WN6h	•	•	•	0.05 ^d	
48		WN4o?+B	•	•	•	0.01	0.02
52	WN4-w+abs	WN4h+abs	•	•		0.00	0.01
56	WN6-w	WN50?+OB	•	•	•	0.36 ^d	
57	WN7	WN7h+OB	•	•	•	0.85	0.15
64	WN9	WN9h	•	•	•	0.34	0.09
65			•	•	•	0.39	0.06
85	WN3-4p-s	WN4b	•	•	•	0.25 ^d	
87	WN6		•	•	•	0.20	0.05
89	WN6	WN6h	•	•	•	0.08	0.05
90	WN6	WN6(h)	•	•	•	0.22	0.04
92	WN6	WN5(h)	•	•	•	0.26	0.04

^aBr numbers are from Breysacher (1981).^bSpectral subtype classification from Smith (1968) (column 2) and Smith et al. (1996) (SSM, column 3). The Smith 1968 classification is only shown for those stars analysed by Hamann & Koesterke 2000; these authors extended the original classification with the “s” and “w” labels to discriminate between strong and weak lined early type stars, respectively.^cColour excesses are taken from Morris et al. (1993b).^d $E(B - V)$ value adopted from Morris (1995).

2.2.1 Ultraviolet data

The ultraviolet spectral data used for this study are observations by the IUE satellite. All UV spectra were taken with the SWP and LWP and/or LWR cameras in low dispersion mode (≈ 6 Å resolution). The SWP camera has an effective wavelength range of 1150-2000 Å. For the LWP and LWR cameras this is 1850-3300 Å. Temperature drift in the camera head amplifier was corrected for, using values for the mean amplifier temperature recorded during observation (Thompson 1983; Thompson & Turnrose 1983). Corrections for sensitivity degradations were made, using routines from the Regional Data Analysis Facility at the University of Colorado (CURDAF).

2.2.2 Optical data

The optical Wolf-Rayet data were taken at Kitt Peak National Observatory (KPNO) and Cerro Tololo Inter-American Observatory (CTIO) over the period 1981 - 1986. For part of the data set, the observations and reduction techniques are described in Massey (1984) and Torres-Dodgen & Massey (1988); the remaining spectra are described in Morris (1995) and Brownsberger (1995). They used absolute spectrophotometry to derive so called line-free *ubvy* continuum colours of Galactic stars, and intrinsic colours and absolute magnitudes of LMC stars.

2.2.3 Near infrared data

The near infrared (NIR) spectra were for the larger part obtained at the European Southern Observatory (ESO) over the period 1980-1883, and CTIO in December 1989. Of these data, spectra of southern LMC and Galactic WR stars can be found in Vreux et al. (1983) and Vreux et al. (1989). Northern and other southern Galactic stars are published in Conti et al. (1990). All ESO spectra cover the wavelength range from 5800 to 10350 Å at a resolution of about 8 Å.

The CTIO observations are spectrophotometric data of LMC and Galactic WR stars performed at the 1.5m telescope. A detailed description of the observational method and data analyses can be found in Morris et al. (1993b)

2.3 Interstellar extinction

One of the reasons the stellar parameters of Galactic Wolf-Rayet stars are poorly known is the often high degree of reddening in their spectrum due to extinction of stellar light by interstellar matter. The interstellar extinction prevents the direct determination of a stars intrinsic colour and continuum energy distribution. Reviews on the theory and the observational influence of interstellar extinction are given by Savage & Mathis (1979) and Mathis (1990).

Several methods have been developed over the years to determine the extinction of stars and correct for it to get intrinsic colours:

1. A star of the same spectral subclass is found close enough to the sun for the extinction to be negligible. Its colour can then be determined directly. Although this method has been applied to many stellar subclasses, it does not work for the more massive stars such as O stars and also Wolf-Rayet stars; they are relatively rare and the nearest of them are already a few hundred parsecs from the sun.

2. A star of the same subclass is found in the Large Magellanic Cloud(LMC), where the foreground Galactic extinction and intrinsic LMC extinction are low and known. This means that the observed flux levels can be corrected for interstellar extinction with suitable reddening laws. This method assumes that stars of the same subtype also have the same colours; Though this assumption is justified for many stellar subtypes it is not for Wolf-Rayet stars (see below).
3. If the star or one of the same subclass is a member of a stellar cluster or association the reddening can be determined from the extinction values of other member objects. Lundström & Stenholm (1984) used stars in Galactic clusters to determine the extinction in front of member WR stars.
4. For WN stars, the ratio of fluxes of several emission lines appears to be independent of spectral subtype (Conti & Massey 1989; Conti & Morris 1990). Observed flux ratios of these lines are therefore a measure of the interstellar extinction. Conti & Morris (1990) used this property to determine colour excesses for Galactic Wolf-Rayet stars, based on intrinsic line flux ratios of WR stars in the LMC (Sect. 2.4.1).
5. The strength of the 2175 Å absorption feature is used as a measure for the interstellar extinction. The method involves the use of an extinction law that models the absorption bump and succeeding de-reddening of the observed spectrum to find a value for the colour excess $E(B-V)$ (e.g. Fitzpatrick & Massa 1988; Fitzpatrick & Massa 1990). This method was used for an extensive study on Wolf-Rayet star colours by Vacca & Torres-Dodgen (1990) using IUE spectra only, and later by Morris et al. (1993b) using IUE and ground-based optical and near-infrared spectra of a larger set of Galactic and LMC WR stars (Sect. 2.4.2).
6. Schmutz & Vacca (1991) showed the existence in WN star spectra of a tight correlation between the intrinsic colours $(b-v)_0$ and the strength of the He II $n = 4$ continuum jump. The observed strength of continuum jumps therefore is a measure of the interstellar extinction.
7. The energy distribution and colour of the star of interest are determined from model atmospheres. For Wolf-Rayet stars this method was for example used in a series of papers on stellar parameters by Crowther and coworkers (Crowther & Smith 1997 and references therein).

Several of the above methods rely on the assumption that stars of the same spectral subclass have the same intrinsic colours. Although this may be true for many subclasses of “normal” stars (e.g. O stars), it is not automatically the case for Wolf-Rayet stars. Indeed, some scatter between measured intrinsic colour and subtype was found for WR type stars by Smith (1968), though already at the time part of it was suspected to be caused by the presence of emission lines within the band passes of the photometric system.

This line contribution was confirmed by Massey (1984), who derived “line free” colour indices in the optical continuum from 10 Å resolution spectrophotometry. The line contribution for WN stars in the Smith system of indices appeared to be small, but is significant for WC stars, as is expected from the fact that in WC spectra lines may overlap to the extent that no (pseudo)-continuum is visible (see Ch. 1).

With the newly derived line free indices and new spectrophotometric observations intrinsic colours were derived for LMC Wolf-Rayet stars by Torres-Dodgen & Massey (1988) and for

both LMC and Galactic Wolf-Rayet stars Vacca & Torres-Dodgen (1990). From this it became clear that there is indeed significant scatter between intrinsic colour and subclass for these stars.

2.4 Colour excesses in the study of the Baldwin-effect

The initial observational basis for the Baldwin-effect (Morris et al. 1993a) hinges very little on corrections for interstellar extinction of continuum fluxes, since reddening is low towards LMC stars (with exception of the 30 Doradus region). However, the application of the Baldwin-effect for measuring distances of Galactic stars will clearly depend on reddening corrections, which can often be significant. We will therefore briefly review the two methods that were used to derive colour excesses for the Galactic WN stars that we will rely upon.

Where de-reddened continuum fluxes are needed in our analyses of the Baldwin-effect as a distance estimator of Galactic WN stars (Chs. 5 and 6), we have adopted the reddening corrections derived by Conti & Morris (1990) and Morris et al. (1993b), who applied methods 4 and 5, respectively, of the description in Sect. 2.3. The two, independent, methods show good mutual agreement in their results. For the many Galactic stars that were analysed in common by the two methods, we will adopt the mean value of the colour excesses. For stars in the LMC, we will use values from Morris et al. (1993b). Below follows a brief description of each of the two mentioned methods to derive colour excesses.

2.4.1 Colour excesses derived from the ratio of intrinsic line fluxes

This method for the derivation of the interstellar extinction towards Wolf-Rayet stars was devised by Conti & Morris (1990). The method relies on the wavelength dependence of the extinction and involves the determination of colour excess $E(B - V)$ for Galactic WR stars from the ratio of observed spectral line fluxes and known $E(B - V)$ values for WR stars in the LMC.

The classification of WN stars in spectral subtype is based on the strength of numerous emission lines in their spectra. However, it was shown by by Conti & Massey (1989) and Conti & Morris (1990) that in WN star spectra many emission features are generally weak or strong together and that the ratios of the intrinsic line fluxes and the ratios of line equivalent widths do not vary with WR spectral subtype. This is particularly true if lines of the same ion species are compared. The reason is that for any two lines that are formed roughly in the same wind region, variations of wind density and temperature among stars affect the line strengths in the same way. Only at the weak line end of this relationship there is a small difference, since lines formed further out in the wind become optically thin due to lower temperature and density.

Furthermore, the ratio of equivalent widths is not influenced by distance or interstellar extinction, as both line and continuum flux are changed in the same way. However, extinction does influence the ratio of line *fluxes*. This makes that the difference between intrinsic and observed line flux ratios is a measure for the interstellar extinction, as already suggested by Conti & Massey (1989). Conti & Morris (1990) used this property to derive $B - V$ colour excesses from He II lines. Their method is shown below.

First of all we note that the difference between the intrinsic magnitude $m_0(\lambda)$ and the observed magnitude $m_{\text{obs}}(\lambda)$ determines the total extinction at a certain wavelength λ :

$$A(\lambda) \equiv m_{\text{obs}}(\lambda) - m_0(\lambda)$$

$$\begin{aligned}
&= 2.5\{\log F_0(\lambda) - F_{\text{obs}}(\lambda)\} \\
&\equiv 2.5\Delta\log F,
\end{aligned} \tag{2.1}$$

where F_0 and F_{obs} are the intrinsic and observed line fluxes, respectively. The $\lambda - V$ colour excess, according to the *UBV* photometric system, is defined as

$$E(\lambda - V) = A(\lambda) - A_V \tag{2.2}$$

This way, the $B - V$ colour excess can be related to the extinction as

$$A(\lambda) = E(B - V)(R_V + k(\lambda)) \tag{2.3}$$

where R_V is the ratio $A_V/E(B - V)$ and $k(\lambda)$ is the reddening law, defined as

$$k(\lambda) \equiv E(\lambda - V)/E(B - V) \tag{2.4}$$

Let us have a look at two lines in the spectrum with wavelength λ_1 and λ_2 , respectively. Then we can define a reddening slope S as the ratio of the extinction at the line wavelengths:

$$S \equiv \frac{A(\lambda_1)}{A(\lambda_2)} \tag{2.5}$$

This way we can express the colour excess $E(B - V)$ in terms of line flux differences:

$$\begin{aligned}
E(B - V) &= 2.5 \frac{\Delta\log\{F(\lambda_1)\}}{R_V + k(\lambda_1)} \\
&= 2.5 \frac{S}{1 - S} \frac{\log\{F_{\text{obs}}(\lambda_1)\} - \log\{F_{\text{obs}}(\lambda_2)\} - b}{R_V + k(\lambda_1)}
\end{aligned} \tag{2.6}$$

and similarly

$$\begin{aligned}
E(B - V) &= 2.5 \frac{\Delta\log\{F(\lambda_2)\}}{R_V + k(\lambda_2)} \\
&= 2.5 \frac{1}{S - 1} \frac{\log\{F_{\text{obs}}(\lambda_2)\} - \log\{F_{\text{obs}}(\lambda_1)\} + b}{R_V + k(\lambda_2)}
\end{aligned} \tag{2.7}$$

In this, b is the y-axis intercept of the line with slope S at the point $(x, y) = (\log F_{\lambda_2}, \log F_{\lambda_1})$.

The above result means that we can find the $E(B - V)$ extinction value from accurately measuring line flux ratios in the stellar spectrum.

For the method to work, the two lines under consideration need to be sufficiently separated in wavelength, since otherwise the reddening slope S will be too close to unity, leading to unrealistic results for $E(B - V)$. Furthermore, the *intrinsic* line flux ratios need to be determined accurately enough. That is the reason LMC spectra were used for this, as the reddening of those is relatively low; Morris et al. (1993b) used average $E(B - V)$ values from Vacca & Torres-Dodgen (1990) and Schmutz & Vacca (1991) for the LMC stars to derive intrinsic line flux ratios from their spectra.

Finally, we want to remark that using the intrinsic fluxes of LMC stars to find those of Galactic stars means that the lines of which flux ratios are determined should be of the same atomic species, in order to avoid the influence of abundance differences.

The power of this method for the dereddening of Galactic spectra is the fact that no theoretical assumptions are involved. The uncertainty in the derived colour excesses therefore completely consists of observational aspects, which are mainly the used reddening law and the quality of the observed spectral data.

2.4.2 Colour excesses from the correction of the interstellar 2175 Å absorption bump

This method is based on the derivation of values for the colour excess $E(B - V)$ from the strength of the 2175 Å absorption feature that is present in the UV spectrum of WR stars. This broad absorption is probably due to interstellar graphite grains that scatter stellar light out of the line of sight (e.g. Spitzer 1978). The strength of the absorption is a measure for the interstellar extinction. Therefore colour excess values can be derived by correcting the spectra for the absorption bump, applying a suitable reddening law.

In the method described here, the “nulling” of the 2175 Å bump is achieved by assuming that the intrinsic stellar continuum spectrum can be represented by a power law:

$$F_0(\lambda) \propto \lambda^{-\alpha} \quad (2.8)$$

This idea was proposed for by Vacca & Torres-Dodgen (1990), who applied the method for the first large scale study on WR star colours.

The further procedure to derive a value for the $E(B - V)$ colour excess is as follows: first a number of continuum points are found in the spectrum by eye. For each continuum point λ_i (with $i = 1, \dots, N$; $35 \leq N \leq 55$) the intrinsic flux $F_0(\lambda_i)$ relates to the observed flux $F_{\text{obs}}(\lambda_i)$ by

$$F_0(\lambda_i) = F_{\text{obs}}(\lambda_i) + 0.4E(B - V)(k(\lambda_i) + R_V). \quad (2.9)$$

Since for the intrinsic flux a power law was assumed, one also has $\log F_0(\lambda_i) = C - \alpha \log \lambda_i$. Combining this with Eq. 2.9 one can express the accuracy of fitting a power-law to the spectrum as

$$\chi^2 = \sum_i^N \left[\frac{1}{\sigma_i} \log F_{\text{obs}}(\lambda_i) + 0.4E(B - V)\{k(\lambda_i) + R_V\} - \{C - \alpha \log \lambda_i\} \right]^2 \quad (2.10)$$

in which σ is the error in the logarithmic flux. In this expression the reddening law k_{λ_i} and the value of R_V are specified, whereas $E(B - V)$, α , and C are free parameters whose values are derived from the best fit.

For the Galactic stars in our data set, the reddening law of Seaton (1979) was used. For the LMC stars, the total extinction is composed of a contribution of the Galactic foreground and of the intrinsic LMC extinction. For the Galactic extinction, a constant foreground colour excess of $E(B - V) = 0.03$ was assumed and the observations were corrected for this with the reddening law of Seaton (1979). For the remaining extinction, due to the interstellar medium of the LMC, the above described method was applied, using the average LMC extinction law of Vacca (1992).

The assumption of a power law continuum appears to be justified when looking at spectra of WR stars with low reddening level, such as stars in the LMC. Figure 2.1 shows the uncorrected spectra of both an LMC and a Galactic WN star of the same spectral type. It is readily seen that the deviation from a power law spectrum is small, considering the uncertainty in the continuum level. Bound-free continuum edges are too weak to be observed and therefore to spoil the power law behaviour.

Vacca & Torres-Dodgen (1990) tested the validity of the method with model spectra for the IUE wavelength range of 1200-3200 Å. They reddened the spectra with a certain value of $E(B - V)$ and added random noise to it. Then they applied the dereddening method and compared the resulting colour excess with the input value. They found differences between

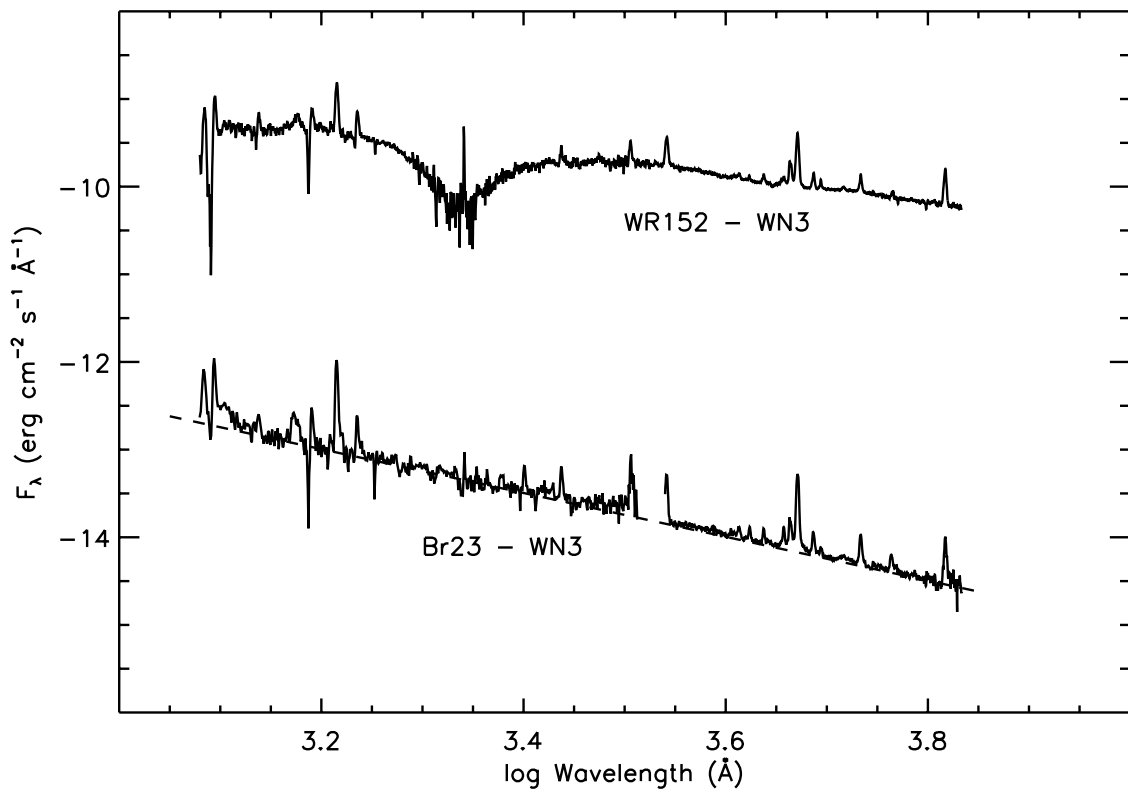


Figure 2.1: Observed Spectra of a Galactic (top) and an LMC WN3 star. Because of the low reddening of the LMC star ($E(B-V)=0.05$), the power-law shape of its spectrum is clearly visible. Dashes indicate a continuum power law, fitted “by eye”. Interstellar extinction severely affects the Galactic spectrum ($E(B-V)=0.38$). For clarity, the Galactic spectrum is offset by 3 dex.

input and output values for the colour excess up to 0.04 magnitudes, which lies for most of their stars within the 2σ error of the method itself. Similar quality tests of the method were performed by Morris et al. (1993b). These authors showed that the power law behaviour of the continuum exists from the ultraviolet until near infrared wavelengths. Through this broader wavelength coverage than in the study of Vacca & Torres-Dodgen (1990), a more accurate determination of the continuum spectral indices (α in Eq. 2.8) and therefore the colour excesses could be achieved.

2.5 Discussion

An extensive set of spectral data is available for the study of the Baldwin-effect in Wolf-Rayet stars. Two independent dereddening methods, described in Sects. 2.4.2 and 2.4.1, have provided accurate colour excesses, suitable for the validation and application of the Baldwin-effect in the chapters to follow. These colour excesses are listed in Tables 2.1 and 2.2, respectively.

On the Baldwin Effect of He II emission lines in WR (WN) stars

J. I. van Gent, H. J. G. L. M. Lamers, A. de Koter, P. W. Morris
Submitted to Astronomy & Astrophysics

Abstract

We investigate the relation between the equivalent width of He II emission lines and the monochromatic continuum luminosity at the line wavelength in the spectra of Wolf-Rayet stars. Model stellar atmospheres and spectra are used to show that the equivalent width inversely correlates with the monochromatic continuum luminosity. We find the effect in Wolf-Rayet star models over a large range of stellar parameters. The effect is shown to be connected to density differences among Wolf-Rayet star winds. The conclusion is drawn that the Baldwin-effect may provide a new method for the determination of Wolf-Rayet star distances.

3.1 Introduction

Spectral observations of Wolf-Rayet (WR) stars of the WN sequence in the optical, near infrared (NIR), and ultraviolet (UV), have shown an inverse proportionality between continuum luminosity and the line equivalent width of emission lines (Morris et al. 1993a). This phenomenon was found among WN stars in the Large Magellanic Cloud, where distance and reddening properties are relatively well-determined. The relation between line and continuum luminosity is called the Baldwin-effect after a similar correlation found in quasar spectra (Baldwin 1977). Morris et al. (1993a) suggested the effect in WN stars to be the result of differences in wind density and effective radius among stars. If the Baldwin-effect appears to be a general phenomenon in Wolf-Rayet spectra, it can be of great importance as it may indicate a way to derive absolute luminosities and distances from the spectra.

The determination of Galactic Wolf-Rayet star distances is known to be problematic, since a clear temperature - luminosity relation does not exist among stars with strong stellar winds (Conti & Underhill 1988; van der Hucht 2000).

The most reliable WR distances are most often based on membership in OB associations and clusters and average reddening properties. Membership may be tenuous, though, and cluster or

association distance can be uncertain. Less than one third of the known Galactic WR stars outside the Galactic Centre, however, appear in clusters or associations (van der Hucht et al. 1988). Alternatively, distances can be estimated from a *general* trend of spectral subtype with absolute magnitude (based on members of clusters or associations or the Magellanic Clouds), but the spread in any one subtype bin is large, $\Delta M_v \simeq 2$ mag. or more (e.g. Hamann & Koesterke 1998a) and suffers from low number statistics. Any independent method to derive distances should therefore be investigated. The Baldwin-effect may provide such a method. In the Baldwin-effect the continuum luminosity is affected by distance and reddening, but not the line equivalent widths. Moreover, the Baldwin-effect of several emission lines can be used to determine the stellar distance from the equivalent width - luminosity relation.

In this paper we will investigate the underlying physics that causes the Baldwin-effect in Wolf-Rayet stars. By means of model atmosphere calculations we will show the range of basic stellar parameters for which the Baldwin-effect applies, and gain some insight into the intrinsic scatter in the equivalent width - luminosity relations. This knowledge is needed to assess the viability of the Baldwin-effect as a distance estimation tool, and provides a new perspective on line and continuum coupling in terms of the fundamental stellar parameters. We will not try to give a ready-to-use formalism for the distance determination of WN stars, but restrict ourselves to explaining the physics behind the Baldwin-effect. The absolute calibration of the Baldwin-effect will be the subject of a future study, where we will introduce a scheme to apply the Baldwin-effect as a spectroscopic method to estimate WN star distances in the Milky Way.

A simple explanation of the Baldwin-effect from a theoretical viewpoint is given in Sect. 3.2; Sect. 3.3 describes the assumptions and the computer code used for the model atmospheres. The results of the calculations are presented in Sect. 3.4, which is followed by a general discussion and prospects for observational applications.

3.2 A simple explanation of the Baldwin-effect

In this section we will use simple expressions in order to get an empirical understanding about the basic processes that determine the relation between the luminosity of the continuum and the equivalent width of spectral lines. We will discriminate between optically thick and thin winds. Also, we will assume that the atmosphere is in local thermodynamic equilibrium (LTE) and is isothermal at a temperature $T = T_*$. The reason why we first adopt LTE and a constant temperature is because we want to investigate the Baldwin-effect in an analytical way. We will drop both assumptions in Sect. 3.4, where we present results of detailed non-LTE calculations.

3.2.1 Optically thin wind

We will first look at the case where the stellar wind is optically thin for both line and continuum radiation. In that case, the continuum radiation originates from the photosphere, roughly at the stellar radius R_* . We will call R_* the *core* radius, describing the size of the star underlying the wind. If we consider an emission line transition with rest wavelength λ_0 , the monochromatic continuum luminosity at λ_0 can be expressed as

$$L_c^{\lambda_0} \simeq 4\pi R_*^2 \pi B_{\lambda_0}(T(R_*)). \quad (3.1)$$

The energy emitted in the line and escaping from the atmosphere is given by the integral over the wind volume of the emissivity, corrected for the photons that are emitted towards the

stellar core. The line luminosity thus is

$$L_l = 4\pi A_{ul} h\nu_0 \int_{R_*}^{\infty} n_u(r) r^2 [1 - W_D(r)] dr \quad (3.2)$$

where n_u is the population density of the upper level of the line transition, ν_0 is the rest frequency of the transition, and A_{ul} is the corresponding Einstein coefficient for spontaneous emission. W_D is the geometrical dilution factor, which represent the angular size of the stellar core as seen from radial distance r :

$$W_D = \frac{1}{2} \left\{ 1 - \sqrt{1 - \left(\frac{R_*}{r}\right)^2} \right\} \quad (3.3)$$

In the following, we will ignore the factor $[1 - W_D(r)]$, for simplicity reasons. This will influence the luminosity by a factor of two, at most, and is not important for the qualitative description.

For recombination lines in an isothermal LTE atmosphere, the ratio n_u/ρ^2 has a constant value over the wind volume. With help of the equation of mass continuity,

$$\dot{M} = 4\pi r^2 \rho(r) v(r), \quad (3.4)$$

with mass-loss rate \dot{M} and velocity field $v(r)$, we can express the line luminosity as

$$\begin{aligned} L_l &= 4\pi A_{ul} h\nu_0 \frac{n_u^*}{(\rho_*)^2} \int_{R_*}^{\infty} \rho(r)^2 r^2 dr \\ &= A_{ul} h\nu_0 \frac{n_u^*}{(4\pi\rho_*)^2} \left(\frac{\dot{M}}{v_\infty}\right)^2 \frac{1}{R_*} EM_1 \end{aligned} \quad (3.5)$$

with ρ_* and n_u^* are the density and the upper level population at the core, respectively; v_∞ the terminal wind velocity and we defined the dimensionless radius and velocity parameters: $x \equiv r/R_*$ and $w \equiv v/v_\infty$. EM_1 is the normalised emission measure for an optically thin wind, given by

$$EM_1 = 4\pi \int_1^{\infty} \frac{dx}{x^2 w^2} \quad (3.6)$$

For a certain type of velocity law, the integral in Eq. (3.6) solves to a constant value, so we see that we can expect the line luminosity to scale as $L_l \propto \dot{M}^2 v_\infty^{-2} R_*^{-1}$.

The line equivalent width W is the ratio L_l/L_c , so

$$W \propto \dot{M}^2 v_\infty^{-2} R_*^{-3}. \quad (3.7)$$

3.2.2 Optically thick continuum and optically thin line

For dense winds, as they occur in Wolf-Rayet stars, the continuum radiation field may originate at a radius $r_c \equiv R_* x_c$ that is substantially larger than R_* . The exact value of this effective radius depends on the density and the observed wavelength. For now, we assume that the wind volume above r_c is still optically thin for line radiation, because of the high velocity gradient in the wind. The optically thick continuum and thin line limit is only expected to be valid for weak lines, i.e. *not* the diagnostic lines used to study the Baldwin-effect. However, a discussion

of this limit is important as it helps in understanding the more realistic case of optically thick continuum and partly optically thick line limit, presented in Sect. 3.2.3.

The approximate expression for the continuum luminosity is given by:

$$L_c^{\lambda_0} \simeq 4\pi R_*^2 x_c^2 \pi B_{\lambda_0}(T(x_c)) \quad (3.8)$$

For the line luminosity we get

$$L_l = A_{ul} h\nu_0 \frac{n_u^*}{(4\pi\rho_*)^2} \left(\frac{\dot{M}}{v_\infty}\right)^2 \frac{1}{R_*} EM_{x_c} \quad (3.9)$$

in which the normalised emission measure is now determined by the wind volume above the dimensionless radius x_c , where the continuum is formed:

$$EM_{x_c} = 4\pi \int_{x_c}^{\infty} \frac{dx}{x^2 w^2} \quad (3.10)$$

The line equivalent width now scales as

$$W \propto \dot{M}^2 v_\infty^{-2} R_*^{-3} x_c^{-2} EM_{x_c} \quad (3.11)$$

The emission measure decreases as x_c increases. An increase of x_c occurs when the wind density is enhanced, either due to an increase of the mass-loss rate, a decrease of the stellar radius, or a decrease of the terminal velocity.

An estimate for the value of x_c can be found if it is assumed that the continuum opacity is mainly free-free absorption. This assumption is reasonable for optical and infrared wavelengths (see e.g. Morris 1995, chapter 4). In fact, electron scattering may be the dominating factor in the continuum opacity, but as it neither creates nor destroys photons, it will not have a strong effect on the star's energy distribution (Lamers & Waters 1984). Therefore we will ignore electron scattering in our determination of x_c , in this simple description of the Baldwin-effect. The opacities for free-free and bound-free processes can be expressed together as (Brussaard & van de Hulst 1962)

$$\begin{aligned} \kappa_\lambda &= 1.370 \cdot 10^{-23} Z^2 \{g_{\text{ff}}(\lambda, T) + g_{\text{bf}}(\lambda, T)\} \\ &\times \gamma n_i^2 \lambda^3 T^{-\frac{1}{2}} \left(1 - e^{-\frac{hc}{\lambda kT}}\right) \text{ cm}^{-1} \end{aligned} \quad (3.12)$$

with Z the mean atomic charge, n_i the ion density, γ the ratio of electron and ion density, and $g_{\text{ff}}(\lambda, T)$ and $g_{\text{bf}}(\lambda, T)$ the free-free and bound-free gaunt factors, respectively. For a spherically symmetric, extended atmosphere, the effective radius is the radius where the optical depth is about $\frac{1}{3}$, so from $\tau_\lambda(x_c) = 1/3$ we get

$$CR_*^{-3} \left(\frac{\dot{M}}{v_\infty}\right)^2 \int_{x_c}^{\infty} T^{-\frac{1}{2}} \left(1 - e^{-\frac{hc}{\lambda kT}}\right) \frac{dx}{x^4 w^2} = \frac{\lambda^{-3}}{3}, \quad (3.13)$$

with C is a constant that depends on Z , γ , and the free-free and bound-free gaunt factors:

$$C = 8.676 \cdot 10^{-26} \frac{Z^2}{\mu^2 m_{\text{H}}^2} \gamma (g_{\text{ff}} + g_{\text{bf}}) R_*^{-3} \quad (3.14)$$

In this, μ is the mean ionic mass. In the derivation of Eq. (3.13), we assumed that the gaunt factors have a constant value over the wind volume, and also that Z , μ , and γ are constants. Again, for simplicity, we will assume the atmosphere to be isothermal, with a temperature of $T = T_*$. Then Eq. (3.13) reduces to

$$\int_{x_c}^{\infty} \frac{dx}{x^4 w^2} = \frac{1}{\Gamma_\tau} \frac{\lambda^{-3}}{3}, \quad (3.15)$$

where we defined

$$\Gamma_\tau = CR_*^{-3} \left(\frac{\dot{M}}{v_\infty} \right)^2 T_*^{-\frac{1}{2}} \left(1 - e^{-\frac{hc}{\lambda k T_*}} \right). \quad (3.16)$$

Following Morris (1995), we will call the scaling factor Γ_τ the optical depth parameter.

We numerically calculated x_c from Eq. (3.13) with a β -type velocity law:

$$v(r) = v_\infty \left(1 - \frac{R_*}{r} \right)^\beta. \quad (3.17)$$

For our qualitative description here, the value of β is not important, and $\beta = 1$ was adopted in Eqs. (3.8), (3.9), and (3.11) to determine line and continuum luminosities and equivalent widths.

Figure 3.1 shows the dependence of the normalised effective radius x_c on the optical depth parameter Γ_τ , for different values of β . For the figure we used a wavelength of $\lambda = 1640 \text{ \AA}$ (the central wavelength of the He II 3-2 transition), typical gaunt factor values of $g_{ff} = g_{bf} = 1$ (Waters & Lamers 1984), and $\gamma = 1$. We see that for thin winds (small Γ_τ), the atmosphere becomes transparent, so x_c approaches unity. For dense winds, the continuum is formed at radii that are much larger than the stellar core. In those regions, the velocity does not differ much from the terminal velocity ($w \simeq 1$). From Eq. (3.15) we then understand that for dense winds $\log x_c$ increases proportional to $\log \Gamma_\tau$, with a slope of $\frac{1}{3}$.

In Fig. 3.2, the relationship is shown between line and continuum luminosity (panel a) and between equivalent width and continuum luminosity (panel b), for different values of the stellar temperature T_* . Since we are interested in recombination lines, we will express the equivalent width of emission lines as positive values and ignore absorption dominated profiles, throughout this paper.

The thick and thin wind regimes in the figure distinguish themselves by the sudden change in slope of the relations. For thin winds, where $x_c = 1$, the relation has a constant slope of $\alpha = -1/2$ in the $L_l - L_c$ plane and $\alpha = -\frac{3}{2}$ in the $W - L_c$ plane. *So for thin isothermal winds a Baldwin-effect exists.* For thick winds a Baldwin relation is still present, although the slope is rather flat. This is because of the influence of the effective radius on the wind volume that emits line radiation. However, an enhanced wind density due to an increase in mass loss rate at constant R_* never increases x_c enough to lower the equivalent width. The slopes of the relations in Fig. 3.2 are not constant for the thick wind regime, due to the behaviour of x_c as function of the optical depth parameter, Γ_τ .

3.2.3 Optically thick wind for continuum and line

In the more realistic case of a wind that is (partially) optically thick for both continuum and line radiation, the radiation observed around the central line wavelength originates further from

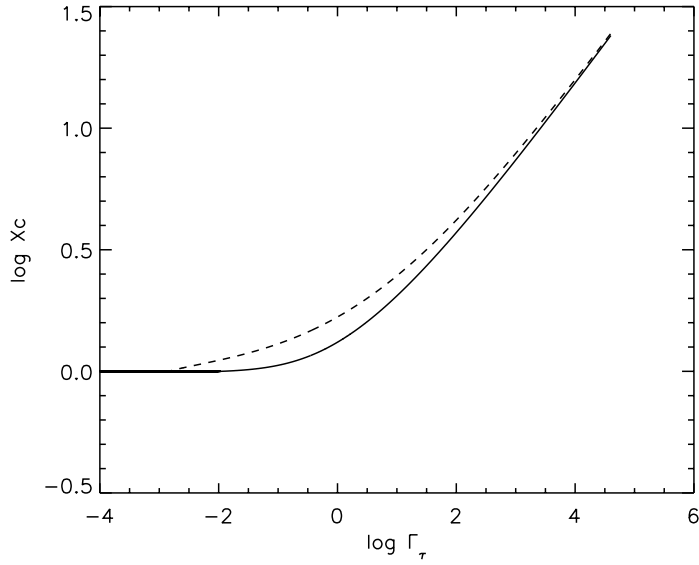


Figure 3.1: Dimensionless effective radius, $x_c = r_c/R_*$, vs. optical depth parameter, Γ_τ , for different β -type velocity laws. Full line: $\beta = 1$, dotted line: $\beta = 2$. Γ_τ is defined by Eq. (3.16). For the figure, a wavelength value of $\lambda = 1640 \text{ \AA}$ is used.

the star than the continuum effective radius r_c . Although the radius where the line radiation originates can depend strongly on the line of sight, we can at least find an estimate for the optical thickness of the atmosphere from the tangential Sobolev optical depth (e.g. Leitherer 1988; 199, p 203). In the Sobolev theory, it is assumed that a spectral line can emit photons of a certain observed frequency only over a very small region around the *Sobolev point*. This is due to Doppler shifting caused by the atmospheric outflow. Within this small volume the physical circumstances are not expected to change significantly, which simplifies the equations of radiative transfer. For a line of sight at impact parameter p , the tangential Sobolev optical depth is

$$\tau_{v,p}^S = \frac{\pi e^2}{m_e c} f_{lu} \lambda_0 n_l \left(1 - \frac{n_u g_l}{n_l g_u} \right) \frac{r}{v} \quad (3.18)$$

with all quantities evaluated at the Sobolev point. The variables n_l and n_u are the number densities of the lower and upper level of the transition, respectively, g_l and g_u are the corresponding statistical weights, and f_{lu} is the transition's oscillator strength.

Let us now assume that the continuum radiation originates again from the dimensionless radius x_c , so the continuum luminosity is given by Eq. (3.8). If the atmosphere above x_c is optically thick for line radiation until a radius $x_1 > x_c$, the line emission is given by

$$L_l = L_1 + L_2 \quad (3.19)$$

where L_1 is the line luminosity of the sphere of radius x_1 :

$$L_1 = 4\pi R_*^2 x_1^2 \pi S(x_1) \quad (3.20)$$

with $S(x_1)$ the line source function at x_1 . L_2 is the luminosity emitted in the optically thin layer above x_1 :

$$L_2 = A_{ul} h\nu_0 \frac{n_u^*}{4\pi\rho_*^2} \left(\frac{\dot{M}}{v_\infty} \right)^2 \frac{1}{R_*} EM_{x_1} \quad (3.21)$$

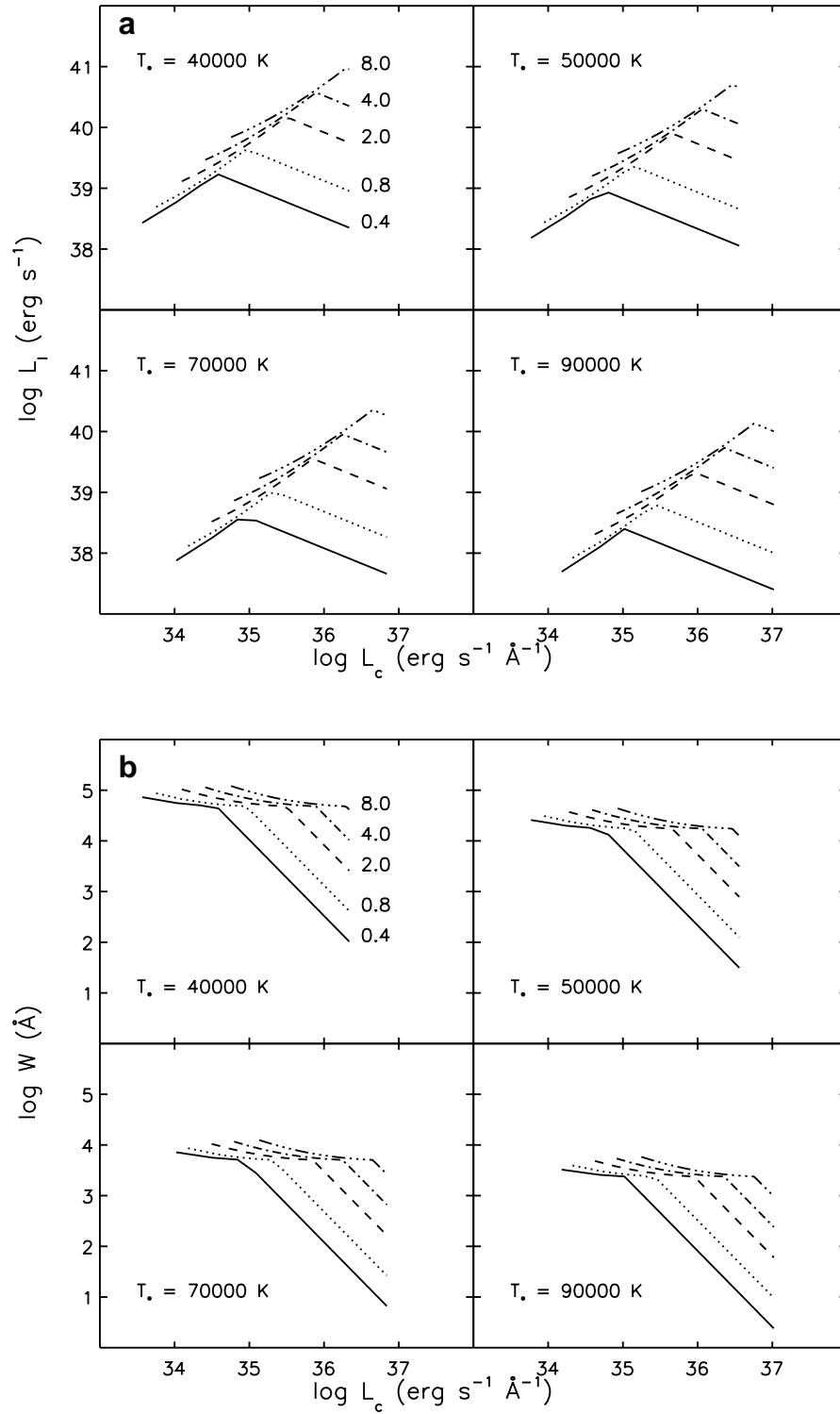


Figure 3.2: Line luminosity L_l (panel a) and equivalent width W (panel b) vs. continuum luminosity for the He II λ 1640 transition for isothermal atmospheres. Labels indicate values of \dot{M}/v_∞ , with the mass-loss rate in $10^{-5}M_\odot \text{ yr}^{-1}$ and the terminal velocity in 10^3 km s^{-1} .

If the total line luminosity is dominated by L_1 , and we still assume an isothermal LTE atmosphere, then the equivalent width scales as $W \propto (x_1/x_c)^2$, whereas if L_2 dominates, the equivalent width varies as

$$W \propto \dot{M}^2 v_\infty^{-2} R_*^{-3} x_c^{-2} EM_{x_1} \quad (3.22)$$

in which the expression for the emission measure is similar to Eq. (3.10), but with x_1 as the lower boundary for x . Since $x_1 > x_c$, we have $EM_{x_1} < EM_{x_c}$, and therefore lower equivalent width values compared to the case of optically thin lines.

From the above description for different type of stellar atmospheres, we conclude that the Baldwin-effect naturally follows from differences in wind density among stars, and will be generally present in both optically thin and optically thick atmospheres, albeit with different slopes. The main stellar parameters, core radius, mass-loss rate, terminal wind velocity, and stellar temperature, all play a role in the exact relation between line equivalent width and monochromatic continuum luminosity. The Baldwin relation of Wolf-Rayet stars is mainly caused by differences in core radius between stars. The relation is broadened by differences in temperature and the ratio of the mass-loss rate and terminal velocity. For a real sample of Wolf-Rayet stars, these three parameters are not fully independent, as the star's radiation field depends on radius and effective temperature and it is the radiation field that drives the mass loss rate. A given sample of Wolf-Rayet stars therefore will cover only part of the diagram shown in Fig. 3.2. However, our goal here is merely to show the influence of each of the basic stellar parameters on the relation between line equivalent width and continuum luminosity. A more realistic description follows from the detailed model atmosphere calculations, given below.

3.3 Model atmospheres

We calculated model stellar atmospheres to study the physical details behind the Baldwin-effect and to be able to predict the relation between line equivalent width and continuum luminosity. For the synthetic atmospheres we used the non-LTE code ISA-WIND (de Koter et al. 1993, 1997), that produces model atmospheres in a spherically symmetric geometry. Both the photospheric and the stellar wind structure are calculated (unified atmosphere), as opposed to the core-halo approach, in which the photospheric radiation field is defined as input at the base of the extended envelope of the model star.

The equations that describe the transfer of the continuum radiation through the atmosphere are solved under the constraint of statistical equilibrium, through the method of approximate lambda iteration. Here, we do not give a detailed description of this method, but instead refer to de Koter et al. (1993, 1997). For the line radiation transfer an improved Sobolev approximation (ISA) is used, which takes into account the diffuse radiation field in the outflowing atmosphere, as well as continuum processes within the line resonance volume (Puls & Hummer 1988).

3.3.1 Chemical composition

We calculated model atmospheres that consist purely of helium. WN stars are generally hydrogen depleted and, compared to helium, their nitrogen abundance is rather low, so the helium lines are not influenced much by the presence of other chemical elements (e.g. Hamann & Koesterke 1998a). This provides the purest way of studying the relation between continuum

luminosity and line equivalent width for helium. The complexity of the He atom in the models is the same as used by de Koter et al. (1997).

Besides thermal motions, for the calculation of the synthetic spectra no additional turbulent velocity fields that could broaden the line profiles were taken into account in the calculation of the synthetic spectra. This way, the line equivalent width is completely due to the bulk wind velocity field and thermal motions. We will discuss the implications of the simplifications made here in Sect. 3.5.

3.3.2 Atmosphere structure

The photospheric density structure in each model is determined by an inner radius, R_* , which determines the size of the core underlying the atmosphere, the effective gravity acceleration, g_{eff} , and the density at the core, ρ_* . The latter is chosen such, that the total Rosseland optical depth, κ_R , has a value between 20 and 25. Following Hamann (1985a), and follow up papers, we set the scale height in the photosphere by assuming $\log(g_{\text{eff}}) = 3.5$. With the above parameters setting the boundary conditions, the density structure then follows from the solution of the momentum equation for a stationary wind. This equation is given by

$$v \frac{dv}{dr} + \frac{1}{\rho} \frac{dp}{dr} + \frac{GM(1-\Gamma)}{r^2} = 0 \quad (3.23)$$

with velocity field v , gas pressure p , and stellar mass M . Radiative acceleration by electron scattering is included in the equation by the parameter Γ , which denotes the ratio between radiative and gravitational acceleration:

$$\Gamma = \frac{g_{\text{rad}}}{g_{\text{N}}} = \frac{\sigma_e L}{4\pi c GM} = 7.66 \times 10^{-5} \sigma_e \left(\frac{M}{M_\odot} \right)^{-1} \left(\frac{L}{L_\odot} \right) \quad (3.24)$$

where L is the stellar luminosity and σ_e is the Thompson scattering coefficient. In the subsonic region the velocity structure follows from the density structure by using the equation of mass continuity (Eq. (3.4)).

In the wind region a β -type velocity law is used

$$v(r) = v_\infty \left(1 - \frac{r_0}{r} \right)^\beta. \quad (3.25)$$

and the corresponding density structure follows from mass continuity. The photosphere and wind regions are smoothly connected by requiring continuity of both the velocity field and its gradient. These conditions are met by iteratively solving for the radius where the two regions are connected, r_{con} and the parameter r_0 in Eq. 3.25. It turns out that r_{con} lies close to the sonic radius.

The luminosity is specified by the *stellar temperature*, T_* , as

$$L = 4\pi R_*^2 \sigma T_*^4, \quad (3.26)$$

where T_* corresponds to the effective temperature that describes the flux at the core radius, R_* , of the model. T_* is not the real effective temperature T_{eff} , as R_* is not the effective stellar radius. A unique radius is hard to define, as it is intrinsically wavelength dependent. We will define the effective radius, R_{eff} , as the radial distance where the thermalization optical depth equals $1/\sqrt{3}$

Table 3.1: He II transitions for which the Baldwin-effect was studied.

Central wavelength (\AA)	Levels $n-m$
1640	3-2
3203	5-3
4686	4-3
5411	7-4
10124	5-4

at $\lambda = 5500 \text{ \AA}$ (Schmutz et al. 1990). This radius thus follows from the model output, as does T_{eff} , through the luminosity and the radius.

The temperature structure follows from the assumption of radiative equilibrium in a grey atmosphere in LTE. We allow the temperature to drop with radius down to a minimum temperature T_{min} , after that it remains constant. For T_{min} we use the value of $T_*/2$, suggested for O-stars by Drew (1989). We keep in mind that there are indications that for Wolf-Rayet stars lower values for T_{min} are more realistic (e.g. Hamann et al. 1994).

3.3.3 Convergence

Most models were found to converge well. As a criterium for convergence we required that for two succeeding iteration steps the populations of all atomic levels at all radii not to differ by more than 0.1 %.

For some models this criterium was not met; those models kept “flipping” between two solutions that generally differed less than 1 percent. In those cases it was also found that the two solutions result in almost identical synthetic spectra, with less than one percent difference in flux levels at all wavelengths. Therefore we included those cases in our model sample.

3.3.4 Synthetic spectra

We calculated synthetic spectra by solving the radiative transfer equations through the model atmospheres. We selected five He II transitions as being suitable for studying the Baldwin-effect. These lines are listed in Table 3.1.

The reason for selecting these lines is that they belong to the strongest He II lines in observed Wolf-Rayet star spectra, and that they are relatively free of blends by other lines. For example, in many observed Wolf-Rayet spectra the He II Balmer lines from even numbered upper levels suffer from blends from the hydrogen Lyman series. This may hamper the applicability of the Baldwin-effect in those WN stars that have still significant hydrogen left (i.e. mostly the WNL-type stars).

In both the calculations of the atmosphere and the spectrum, the effects of electron scattering in lines are not included. Although electron scattering wings can contribute significantly to the equivalent width of a line, we ignore the effect as we are currently only interested in the qualitative explanation of the Baldwin-effect, which is unlikely to be altered by electron scattering processes.

Other simplifications in our modelling that should be mentioned are the assumptions of (i) spherical symmetry, (ii) a homogeneous density distribution, i.e. we ignore the effects of clumping. We will discuss these assumption in more detail in Sect. 3.5.

Table 3.2: Input parameters of the ISA-Wind model atmospheres

R_* (R_\odot)	1,2,3,5,10,15,20,25, 27,28,29,30
T_* (kK)	10,20,30,40,50,60, 70,80,90
v_∞ (km s^{-1})	1250, 2000, 2500
\dot{M}/v_∞ ($10^{-5}M_\odot\text{yr}^{-1}$)/(10^3 km s^{-1})	0.4, 0.8, 2, 4, 8
$\log g$	3.5
β	1

3.4 The synthetic Baldwin effect

3.4.1 Grid parameters

We calculated a large grid of atmosphere models. The stellar temperature, T_* , ranges from 10 to 90 kK, and the core radius R_* from 1 to $30 R_\odot$. This way both parameters cover the range that is thought to occur in real WN stars (Hamann & Koesterke 1998a). The parameters of our model grid are presented in Table 3.2.

3.4.2 Spectra

Most lines in our model spectra show pure emission profiles, resulting from recombination processes followed by cascading events. For the cooler models, the lines may contain a P Cygni component, due to scattering processes. The equivalent width of each line was measured over the full profile. As long as the scattering region of the atmosphere around the star is large compared to the stellar core size, only few photons will be scattered back to the stellar core and lost from the radiation field. The absorption component will thus be of about equal size as the scattering emission component. The net equivalent width, measured over the full line profile, therefore is a good representation of the equivalent width of the emission profile formed by recombination processes.

As can be seen from Table 3.2, we used three different values of the terminal velocity v_∞ in our model atmospheres, such that for each value of v_∞ the same set of values of \dot{M}/v_∞ was obtained. A well known phenomenon in synthetic spectra of Wolf-Rayet stars is that models with the same so called transformed radius show approximately the same normalized spectrum. This was found by Schmutz et al. (1989). The transformed radius is given by

$$R_t = R_* \times \left(\frac{v_\infty}{2500 \text{ km s}^{-1}} / \frac{\dot{M}}{10^{-4} M_\odot \text{ yr}^{-1}} \right)^{\frac{2}{3}} \quad (3.27)$$

One therefore expects a similar Baldwin-effect for star samples that have the same value of the ratio \dot{M}/v_∞ .

3.4.3 Ionization.

A major role in the presence of the Baldwin-effect and its characteristics is played by the ionization structure in the atmosphere. In our simple explanation of the Baldwin-effect (Sect. 3.2),

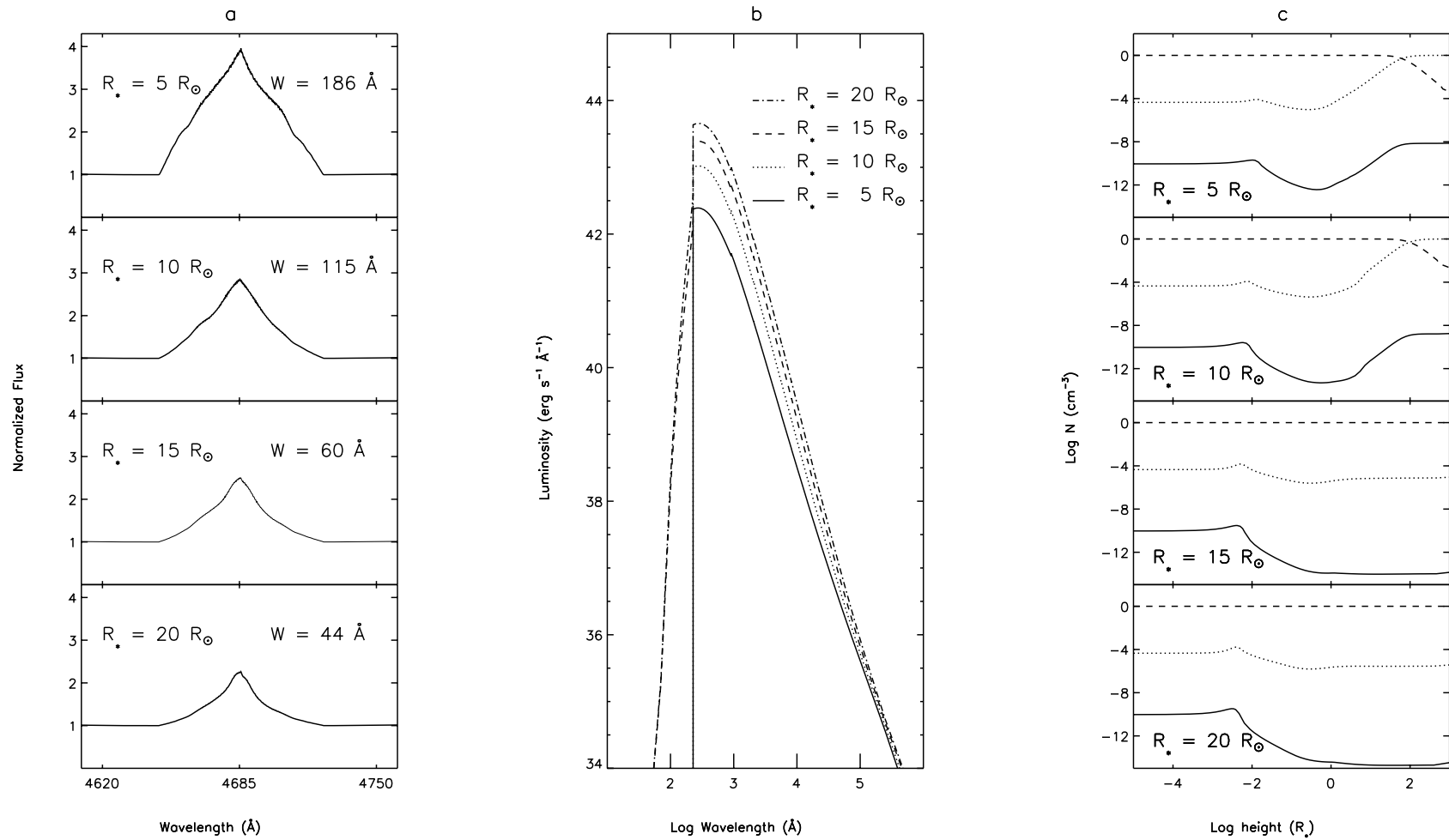


Figure 3.3: Four models that show the Baldwin-effect. Panel a: Continuum normalized line spectra of He II $\lambda 4686$ for different core radii. W indicates the line equivalent width in \AA . Panel b: The corresponding spectral energy distributions. Panel c: Ionization structure of the same models, as function of height above the core. Full line: He I; dotted line: He II; dashed line: He III. In all three panels, R_* indicates the core radius. For all models: $T_* = 60 \text{ kK}$, $\dot{M} = 5 \times 10^{-5} M_\odot \text{ yr}^{-1}$, and $v_\infty = 2500 \text{ km s}^{-1}$. For increasing core radius, the continuum luminosity increases, whereas the line equivalent width decreases: the Baldwin-effect.

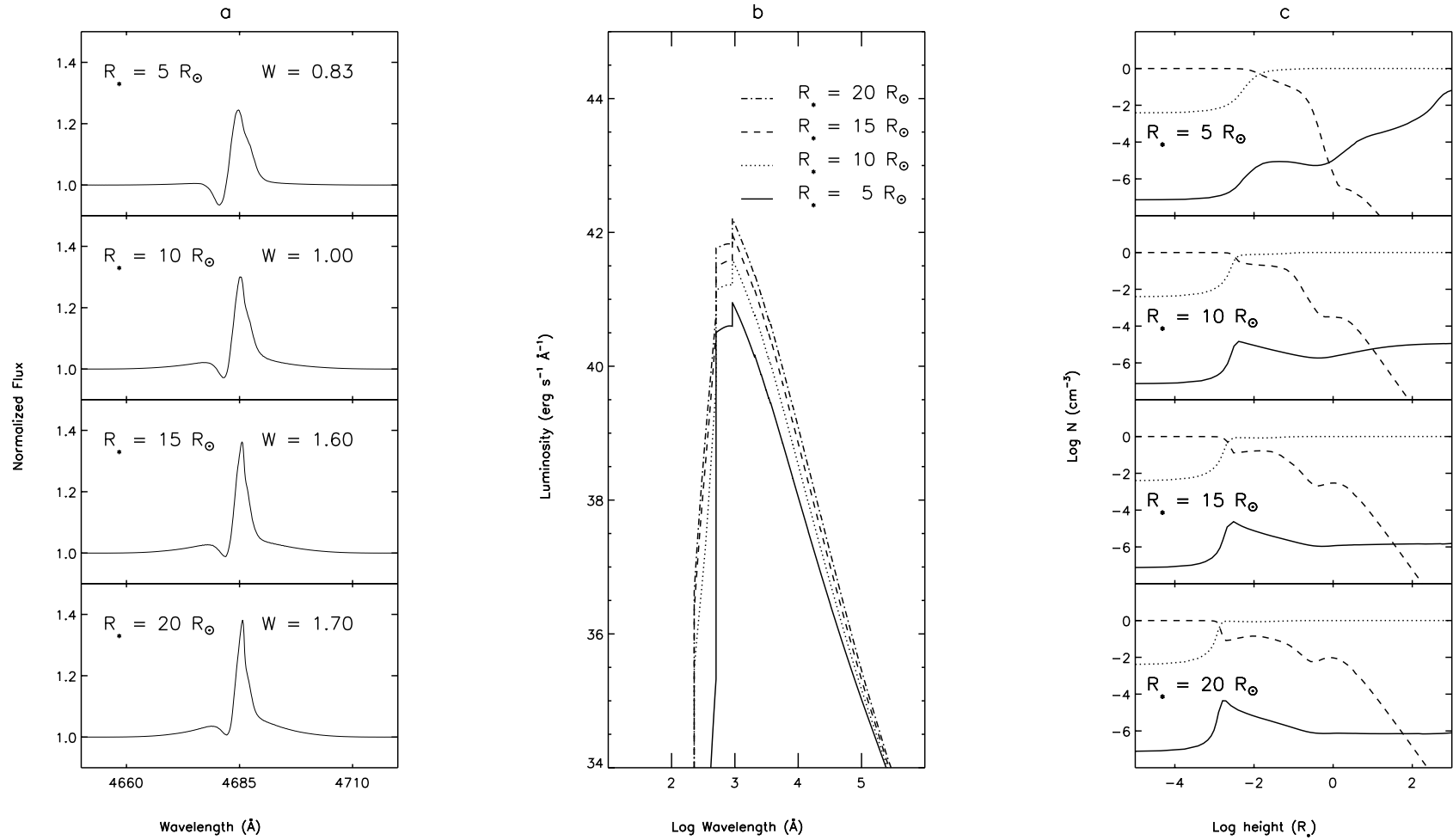


Figure 3.4: Four models that do not show the Baldwin-effect. For all models: $T_* = 30 \text{ kK}$ and $\dot{M} = 1 \times 10^{-5} M_\odot \text{ yr}^{-1}$, and $v_\infty = 2500 \text{ km s}^{-1}$. For explanation of the labels: see text with Fig. 3.3.

we assumed an isothermal atmosphere in LTE, so the stratification of the ionization was only determined by the density. In a real Wolf-Rayet star atmosphere the temperature structure drops with radial distance, so a more complex ionization stratification is to be expected. Based on the dependence of the $W - L_c$ relations on the basic stellar parameters, a sample of stars should have a similar degree of ionization over the line forming region in their atmospheres, in order to show a Baldwin-effect. Since the degree of ionization depends on mass density, temperature, and the radiation field, an arbitrary sample of Wolf-Rayet stars will expose a range of ionization structures. To illustrate the influence of the ionization structure, Figs. 3.3 and 3.4 show some line profiles along with the spectral energy distribution (SED) and helium ionization structure of the corresponding model atmospheres. Fig. 3.3 shows models with stellar temperature $T_* = 60$ kK. From top to bottom the core radius increases from $5 R_\odot$ to $20 R_\odot$.

From the line profiles and the values of equivalent width and monochromatic continuum luminosity we see that this small sample of models shows a Baldwin-effect. Indeed, as already seen in Sect. 3.2, the equivalent width is inversely proportional to the monochromatic continuum luminosity, whereas the integrated line luminosity scales directly proportional to it. From the ionization stratifications we see that helium is fully ionized over a large volume of the wind. We can therefore understand the occurrence of a Baldwin-effect from the explanation in Sect. 3.2. Recombination of He III to He II only takes place in the outer regions of the wind, where it no longer influences the line profiles.

At a stellar temperature of $T_* = 30$ kK (Fig. 3.4) the relation between line equivalent width and continuum luminosity is opposite from a Baldwin-effect. At this low temperature He III is not the dominant ionization stage in the line forming wind regime. Emission due to recombination therefore is much less than at $T_* = 60$ kK. Furthermore, towards larger core radii, the ionization balance shifts in favour of He III, as a result of reducing wind density. Therefore at larger core radii there is more line emission, leading to an increase in equivalent width with core radius, as opposed to a decrease at higher values of T_* .

3.4.4 Equivalent widths and luminosities.

In Sect. 3.2 we used simple expressions to determine the relation between line luminosity and equivalent width on one hand and the monochromatic continuum luminosity on the other hand (Fig. 3.2). Figs. 3.5 to 3.9 show similar relations for line equivalent width versus continuum luminosity, but this time from the model atmosphere calculations and for the five helium lines He II $\lambda 1640$, He II $\lambda 3203$, He II $\lambda 4686$, He II $\lambda 5411$, and He II $\lambda 10124$. Each panel shows models for a certain stellar temperature, T_* , but for different values of the mass-loss rate, \dot{M} , and core radius, R_* . For clarity, we only show the models with $v_\infty = 2500 \text{ km s}^{-1}$. For other values of v_∞ the relations are almost the same, because the spectrum is invariant for $R_* (\dot{M}/v_\infty)^{2/3}$.

From the figures we see that there is a Baldwin-effect present in our model stars, be it not over the whole parameter range. For the regions in parameter space where a Baldwin-effect occurs the results agree very well with our simple estimates in Sect. 3.2, in a qualitative way. The model atmospheres confirm that the Baldwin-effect is mainly caused by differences in wind density among the stars. However, there are two important differences between the result of these simple predictions and those from the detailed model atmospheres. Both are caused by the fact that the model atmospheres are not isothermal, but have a more realistic temperature stratification that drops with radial distance. First of all, the Baldwin-effect breaks down for models with low stellar temperature and high wind density. The reason for this is the ionization

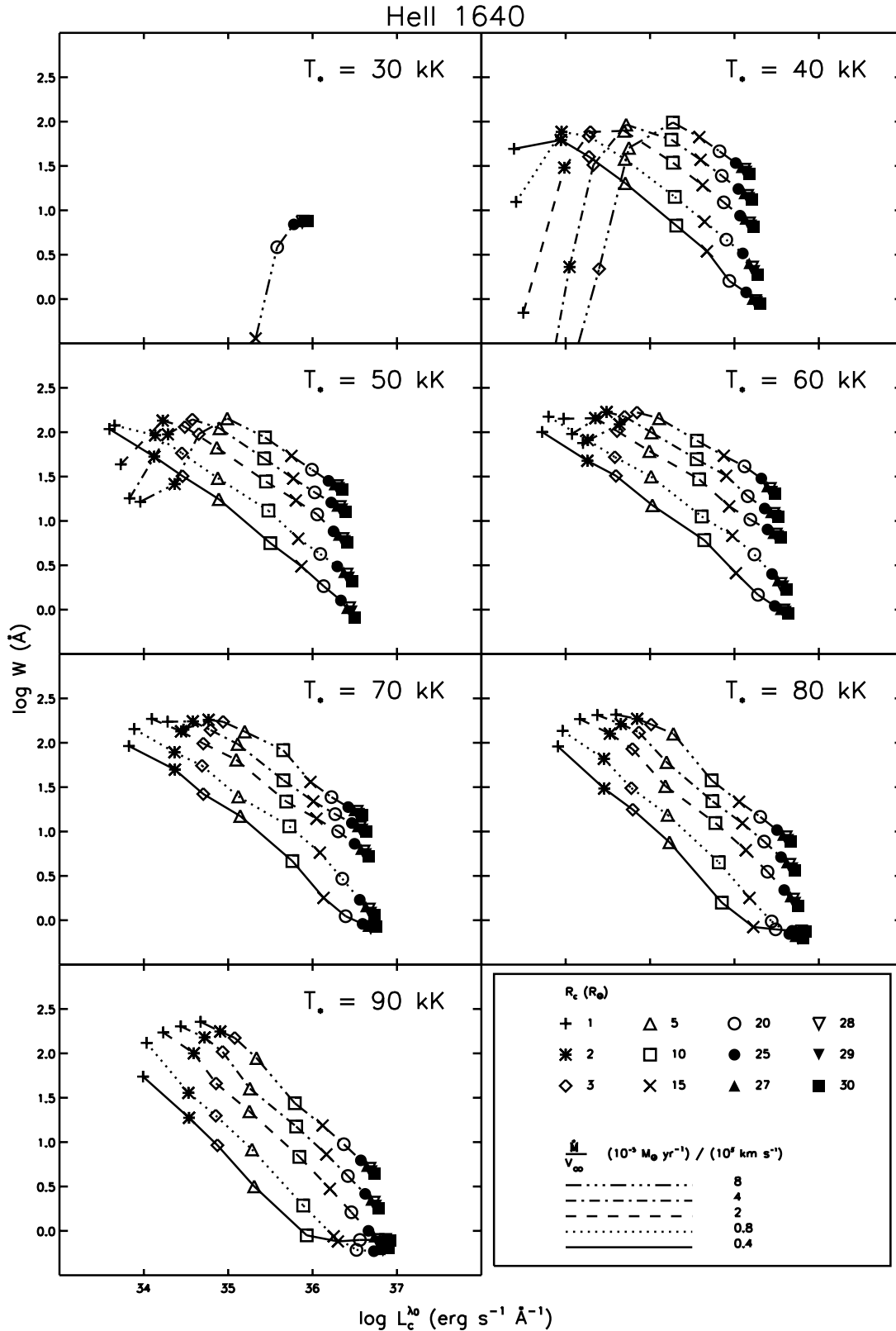


Figure 3.5: Line equivalent width vs. monochromatic continuum luminosity for the He II $\lambda 1640$ line. Each panel shows $\log(W)$ as function of $\log(L_c)$ for models with the same value of T_* , and for different values of the mass-loss rate, \dot{M} , and the core radius, R_* . $v_\infty = 2500 \text{ km s}^{-1}$. Models with the same value of \dot{M} are connected by lines; the values of R_* are indicated by symbols. Line style and symbols are explained in the bottom right panel.

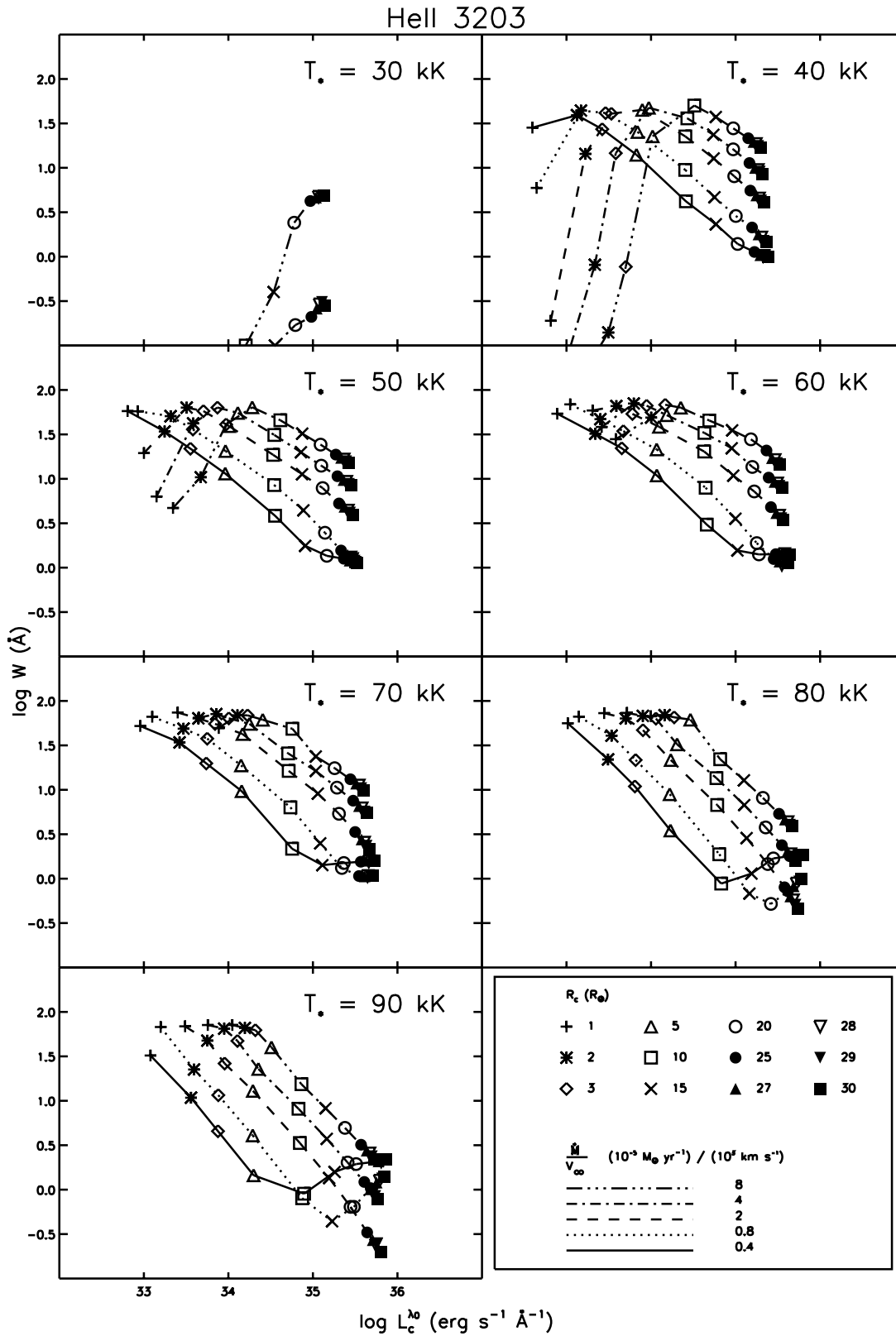


Figure 3.6: Line equivalent width vs. monochromatic continuum luminosity for the He II $\lambda 3203$ line. For explanation, see the text below Fig. 3.5.

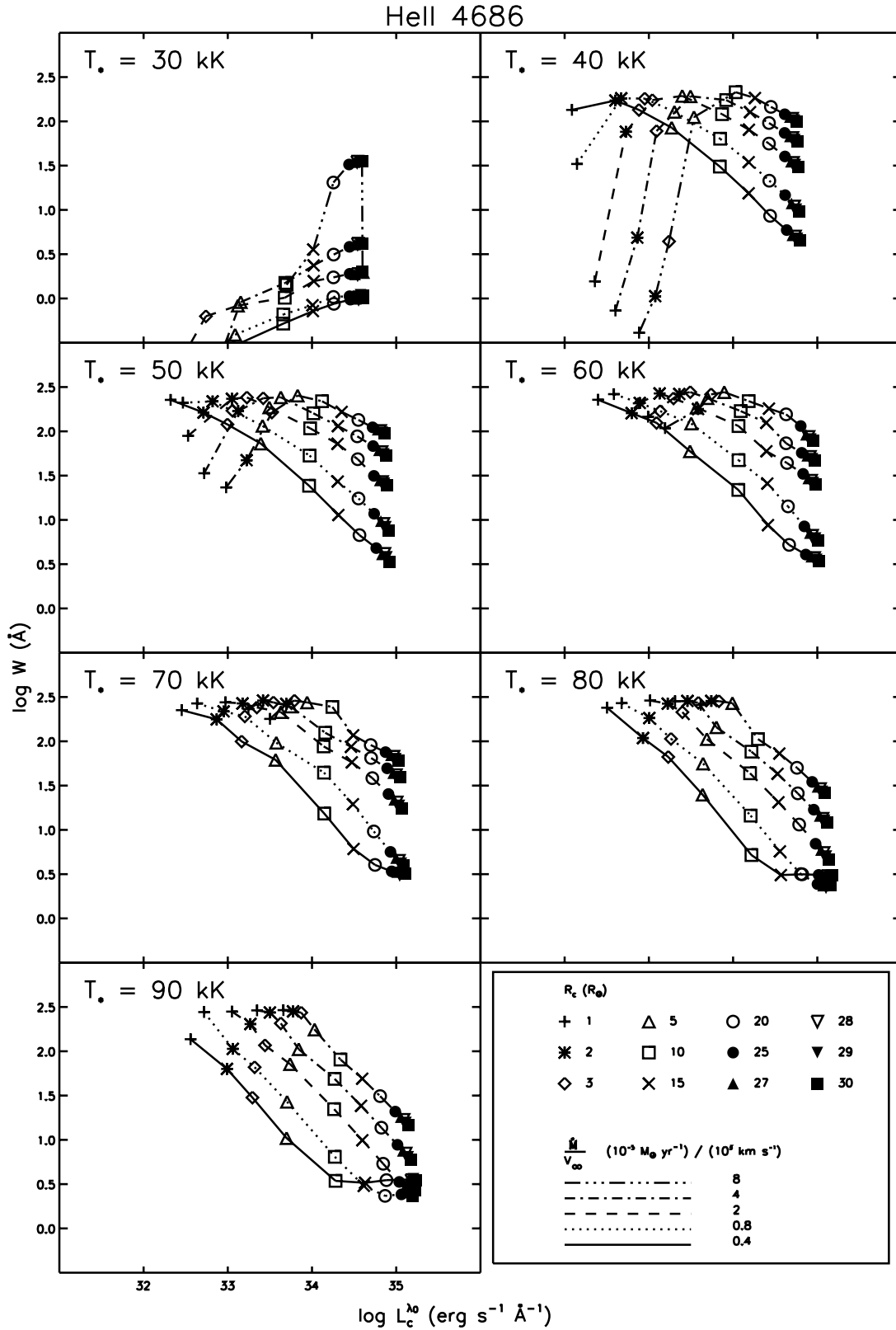


Figure 3.7: Line equivalent width vs. monochromatic continuum luminosity for the He II $\lambda 4686$ line. For explanation, see the text below Fig. 3.5.

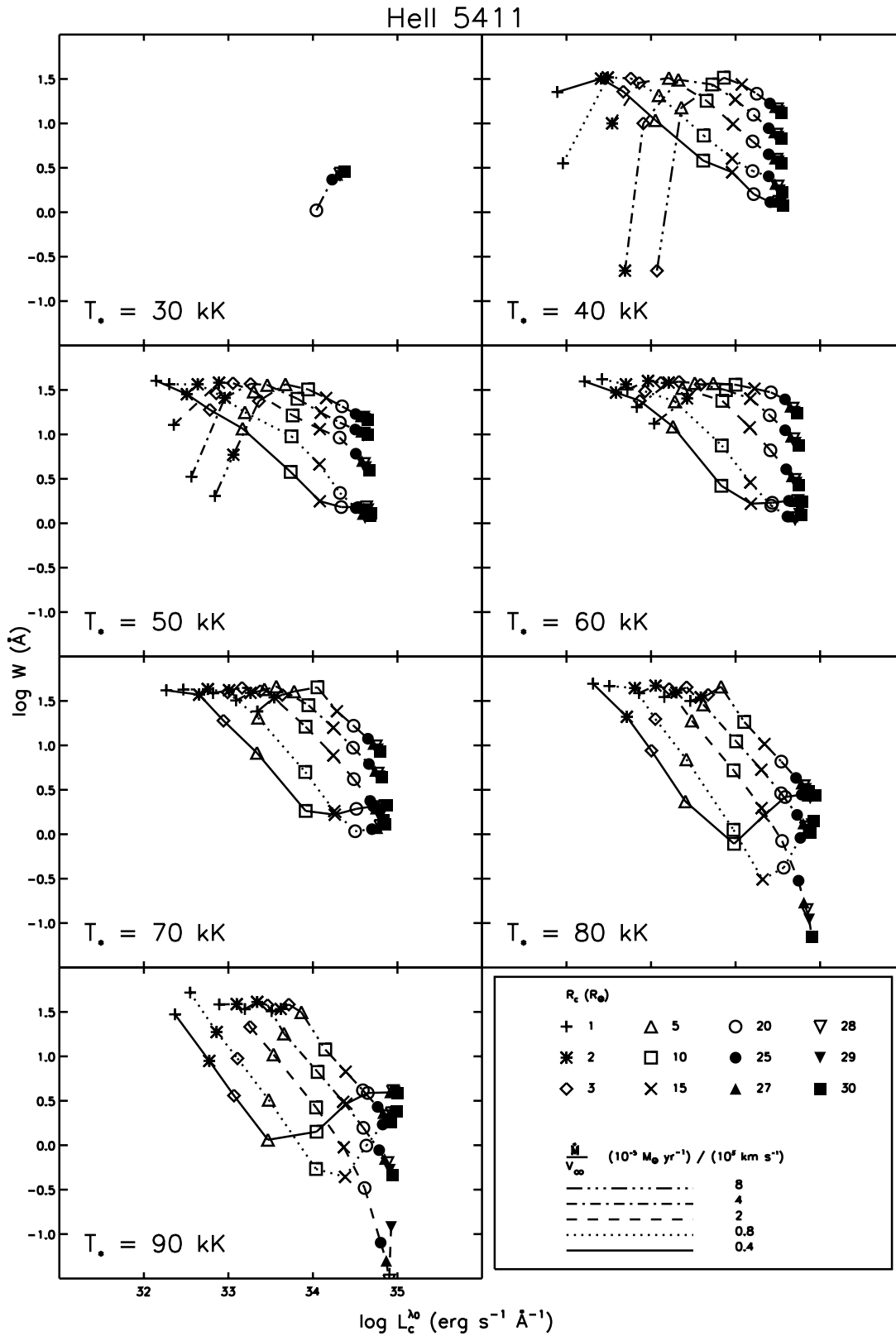


Figure 3.8: Line equivalent width vs. monochromatic continuum luminosity for the He II $\lambda 5411$ line. For explanation, see the text below Fig. 3.5.

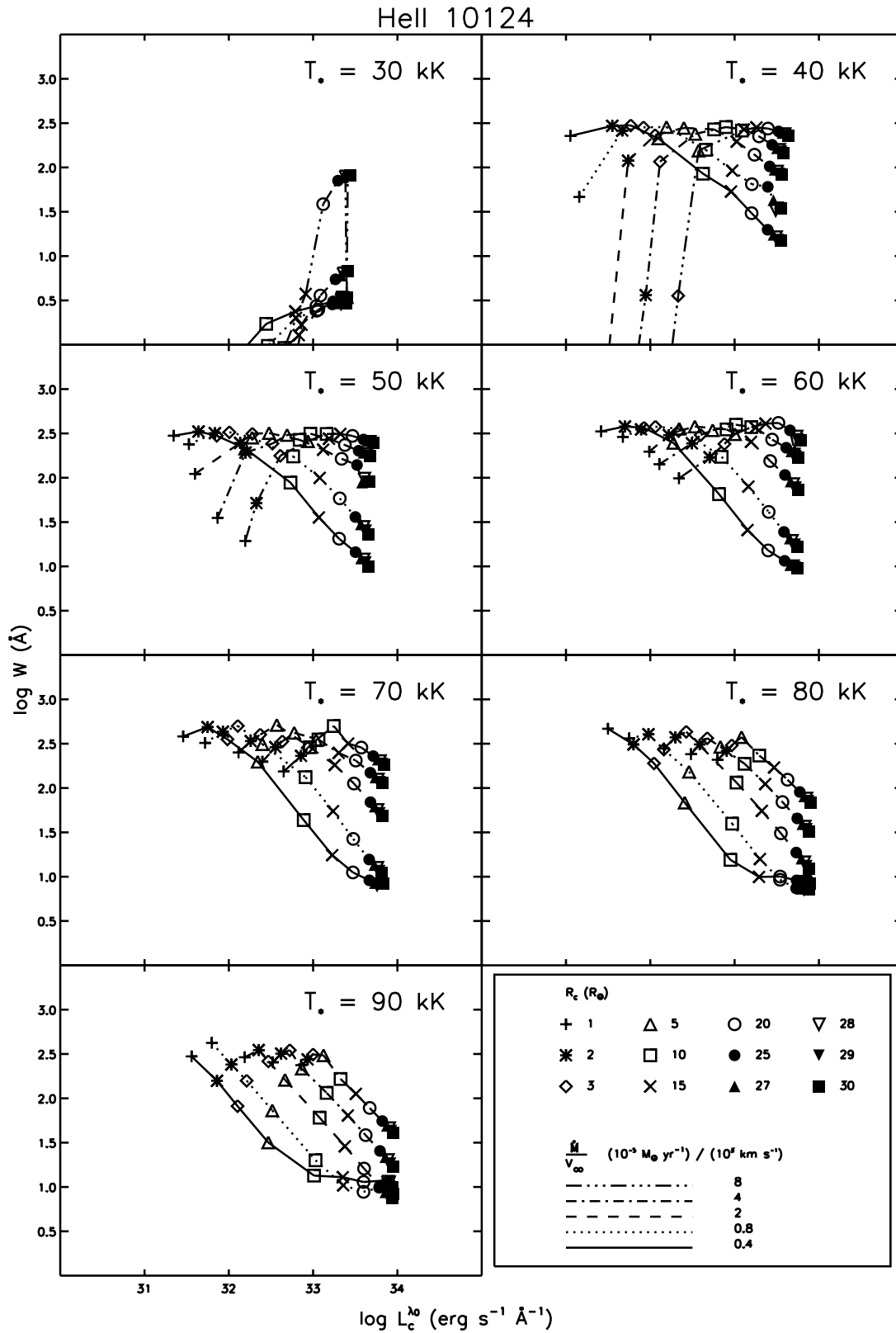


Figure 3.9: Line equivalent width vs. monochromatic continuum luminosity for the He II $\lambda 10124$ line. For explanation, see the text below Fig. 3.5.

structure, which plays a major role in the presence of the Baldwin-effect. As mentioned above, at relatively low temperatures and high densities the dominant ionization stage shifts from He III to He II, reducing the emission of the He II lines.

The second important difference with the simple results of Sect. 3.2 is that there is no Baldwin-effect for the models with the least dense winds in our grid. Again this is caused by the fact that the model atmospheres are non isothermal. At the lowest mass-loss rates, in going from small to large core radius, the stellar wind can become optically thin for continuum radiation (cf. Fig. 3.1). The steep increase in temperature close to the photosphere then causes an enhanced line emission as compared to the optically thick winds. This disrupts the Baldwin-relation.

Besides these differences, the detailed calculations shown in Fig. 3.5 also confirm some important results from the simple picture drawn in Sect. 3.2. In the parameter range where the Baldwin-effect applies, differences in wind density among models due to different core radii cause the Baldwin-effect; a density enhancement (either due to increasing mass-loss rate or decreasing core radius) increases the line equivalent width even though this causes the effective radius to increase. Fig. 3.5 shows that differences in mass-loss rate at constant core radius show approximately the same continuum luminosity (roughly given by Eq. (3.8)). This is because the increase of x_c with mass loss rate is compensated by the lower temperature at x_c . At large wavelength and for dense winds x_c is large enough to lie in the isothermal regions of the wind, leading to a higher continuum luminosity.

In Sect. 3.2 we saw that if the continuum is formed in the wind, the Baldwin relations are steeper at higher densities, due to the influence of the continuum effective radius on the emission measure (see Fig. 3.2 and the text in Sect. 3.2.2). This behaviour is opposite from what is seen in the detailed model calculations, where the relations appear to flatten when going to higher density (i.e. smaller core radius), as seen in Figs. 3.5 to 3.9. The reason for this lies in the line optical depth. As mentioned in paragraph 3.2.3, for optically thick lines, the effective radius for the line, x_l , can be (much) larger than the continuum effective radius, x_c , reducing the line emission measure.

Indeed, for high wind densities the lines can be optically thick. For the He II $\lambda 1640$ line, this is shown in Fig. 3.10, which depicts the tangential Sobolev optical depth (Eq. (3.18)) of the model atmospheres at a radius of $r = 1.5R_c$. The increasing line optical depths, visible in denser winds, explains the flattening of the Baldwin relations. We conclude from the detailed model calculations that the Baldwin-effect in He II recombination lines is a general phenomenon in Wolf-Rayet stars, where the continuum radiation field is formed in the wind. For thin winds (small mass flux) the Baldwin relations breaks down, due to the steep temperature rise at the base of the wind. Also for very thick and cool winds, there is no Baldwin-effect, as recombination from He III to He II weakens the line emission.

Effective temperature, T_{eff} , versus stellar temperature, T_* .

In the above description of the Baldwin-effect for Wolf-Rayet stars, we presented the results for different values of the stellar temperature, T_* (defined in Eq. (3.26)). As mentioned before, this temperature does not equal the effective temperature, T_{eff} (see Sect. 3.3.2). Furthermore, the stellar temperature is a quantity that cannot be derived from observations, whereas the effective temperature can. In applying the Baldwin relations one would therefore rather present them for certain values of T_{eff} than for T_* .

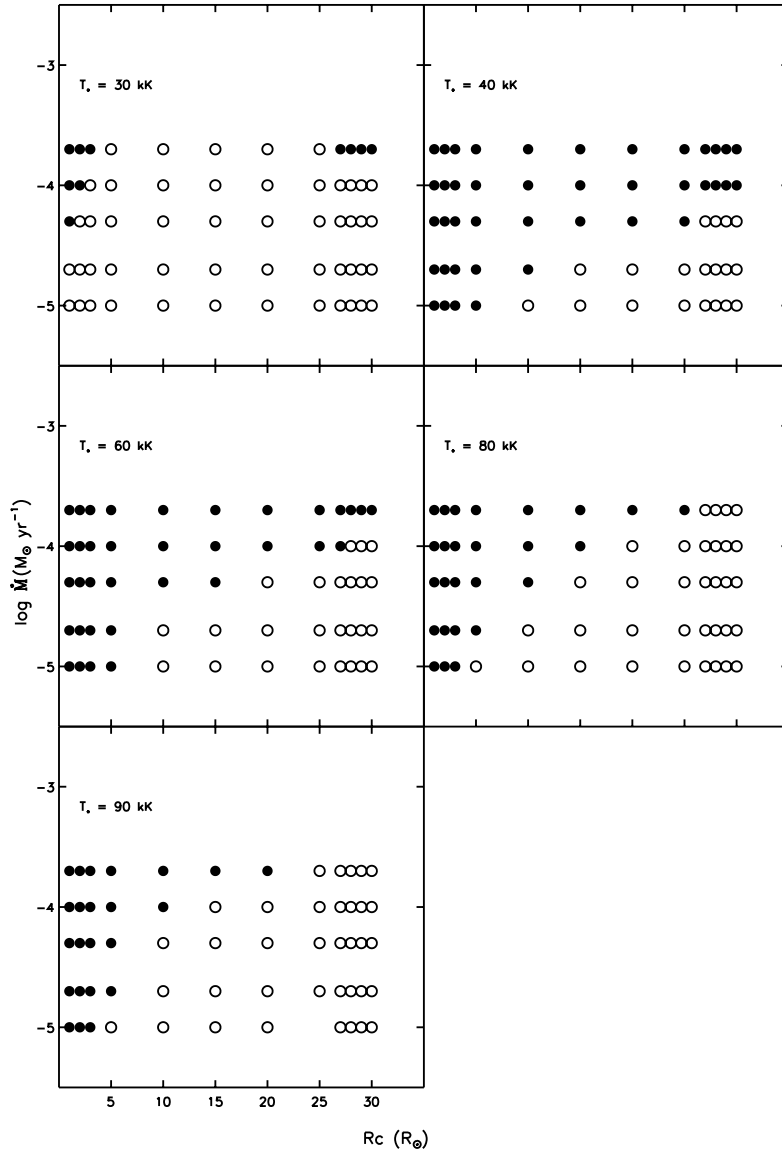


Figure 3.10: Tangential Sobolev optical depth, τ_{tan} , for the He II $\lambda 1640$ line, as function of core radius (x-axis) and mass-loss rate (y-axis) for different stellar temperatures. Open circles represent models with $\tau_{\text{tan}} < 1$, full circles represent models with $\tau_{\text{tan}} > 1$.

To get a feeling of how a representation for different values of T_{eff} (instead of T_*) alters the Baldwin relations, Fig. 3.11 shows again the relation between line equivalent width and monochromatic continuum luminosity, for the He II $\lambda 1640$ line, this time as function of T_{eff} instead of T_* .

Note, however, that the value of T_{eff} is not an input parameter, but result from the model output. Because the value of T_{eff} essentially depends on wind density, a sample of Wolf-Rayet star models with the same value of T_* will cover a range in T_{eff} . Each panel in Fig. 3.11 groups together those models for which the value of T_{eff} is within 5000 kK from the value indicated.

Clearly, the largest differences between Fig. 3.11 (as function of T_{eff}) and Fig. 3.5 (as function of T_*) are at the lowest and highest values of T_{eff} . Since $T_{\text{eff}} < T_*$, and the highest value

of T_* is 90 kK, there are only a few models with $T_{\text{eff}} = 90$ kK, whereas there are many models with T_{eff} around 30 kK. For the latter no Baldwin-effect is visible, because, although for those models T_{eff} lies around 30 kK, they have different stellar temperatures, T_* , and therefore show different degrees of ionization in the line forming region. Despite all this, the relation between equivalent width and continuum luminosity does not alter much when this relation is presented for a certain effective temperature instead of stellar temperature.

3.4.6 Parametrizations

To describe the Baldwin relations of our model grid, we present a set of expressions that give the continuum luminosity at the line wavelength, as a function of equivalent width and mass-loss rate, for a certain stellar temperature, T_* . Note that these equations do *not* provide the absolute calibration of the Baldwin-effect, as our models do not yet contain all relevant effects such as clumping and electron scattering in line wings. As explained in Sect. 3.1, we prefer a somewhat simplified approach as the main aim of this paper is to investigate the basic physics of the Baldwin-effect.

For each value of T_* , and each spectral line, we selected by eye the region in Figs. 3.5 to 3.9 for which $\log W$ varies more or less linearly with $\log L_c^{\lambda_0}$. For these regions we applied a two dimensional linear regression technique to express $\log L_c^{\lambda_0}$ as function of $\log W$ and $\log(\dot{M}/v_\infty)$. The result is a set of equations of the form

$$L_c^{\lambda_0} = a(T_*) \log W + b(T_*) \frac{\dot{M}}{v_\infty} + c(T_*), \quad (3.28)$$

with W in \AA , \dot{M} in $M_\odot \text{ yr}^{-1}$, and v_∞ in km s^{-1} . The limits of the range where Eq. (3.28) applies, as well as the temperature dependent fit coefficients $a(T_*)$ and $b(T_*)$ are given in Table 3.3.

The best results are obtained when applying the expressions for as many spectral lines as possible, taking into account the quality of the line features in the considered spectrum. For some stellar temperatures no data can be given, since for some equivalent width values more than one solution is possible for the continuum luminosity. In other words: for those stellar temperatures, the area in the $\log W$ - $\log L_c^{\lambda_0}$ plane where the Baldwin relations behave linearly, is too small to provide useful parametrisations.

Table 3.3: Fit coefficients and parameter range limits for the Baldwin relations as described by Eq. (3.28).

T_*	30000	35000	40000	50000	60000	70000	80000	90000
He II λ 1640								
a	-	-1.27	-1.17	-1.36	-1.39	-1.31	-1.18	-1.07
σ_a	-	0.07	0.03	0.02	0.03	0.04	0.02	0.03
b	-	1.23	1.20	1.26	1.25	1.10	1.16	1.14
σ_b	-	0.07	0.04	0.03	0.03	0.04	0.02	0.03
c	-	46.60	46.24	47.02	47.13	45.83	45.87	45.39
Min. $\log L_c^{\lambda_0}$	35.	35.2	35.	34.8	34.9	35.0	35.1	34.8
Max. $\log L_c^{\lambda_0}$	34.	36.5	36.3	36.5	36.7	36.5	37.0	36.0

Continued on next page

Table 3.3, *continued.*

T_*	30000	35000	40000	50000	60000	70000	80000	90000
Min. log W	0.0	0.5	-0.5	-0.5	-0.1	-0.1	-0.1	0.0
Max. log W	0.0	0.5	-0.5	-0.5	-0.1	-0.1	-0.1	0.0
He II λ 3203								
a	-	-1.37	-1.21	-1.34	-1.39	-1.31	-1.11	-1.02
σ_a	-	0.09	0.05	0.05	0.05	0.03	0.02	0.02
b	-	1.21	1.17	1.25	1.29	1.19	1.09	1.17
σ_b	-	0.08	0.05	0.04	0.04	0.02	0.02	0.01
c	-	45.48	45.01	45.76	46.22	45.30	44.06	44.36
Min. log $L_c^{\lambda_0}$	35.	34.3	34.2	34.5	34.1	32.9	32.9	32.9
Max. log $L_c^{\lambda_0}$	34.	35.5	35.2	35.5	35.7	35.9	36.0	35.8
Min. log W	-0.5	0.4	-0.1	0.2	0.2	0.3	0.4	0.4
Max. log W	2.5	1.7	1.7	1.7	1.7	1.6	1.7	1.4
He II λ 4686								
a	-	-0.82	-1.12	-1.22	-1.17	-1.10	-1.11	-1.05
σ_a	-	0.07	0.06	0.06	0.06	0.05	0.02	0.01
b	-	0.87	1.07	1.19	1.12	1.07	1.16	1.20
σ_b	-	0.07	0.07	0.06	0.06	0.05	0.02	0.01
c	-	42.48	44.49	45.62	45.04	44.51	44.86	44.89
Min. log $L_c^{\lambda_0}$	35.	34.	34.	34.0	34.0	34.0	32.3	32.3
Max. log $L_c^{\lambda_0}$	34.	34.8	35.0	35.0	34.9	36.7	35.2	35.3
Min. log W	2.0	0.4	0.5	0.5	0.5	0.5	0.6	0.6
Max. log W	-0.5	2.3	2.4	2.3	2.3	2.4	2.2	2.4
He II λ 5411								
a	-	-0.74	-1.15	-1.39	-	-	-0.97	-0.95
σ_a	-	0.04	0.06	0.07	-	-	0.02	0.03
b	-	1.32	1.01	1.23	-	-	1.08	1.15
σ_b	-	0.05	0.05	0.06	-	-	0.01	0.01
c	-	44.95	42.88	44.91	-	-	42.95	43.32
Min. log $L_c^{\lambda_0}$	35.	33.4	33.9	33.6	34.4	34.0	32.1	32.1
Max. log $L_c^{\lambda_0}$	34.	34.3	34.8	34.8	34.0	34.0	35.0	35.0
Min. log W	2.0	-0.2	0.1	0.2	0.3	0.3	0.5	0.7
Max. log W	-1.5	1.0	1.5	1.5	1.5	1.5	1.4	1.4
He II λ 10124								
a	-	-0.96	-1.13	-	-0.97	-0.86	-0.96	-1.00
σ_a	-	0.03	0.05	-	0.03	0.02	0.02	0.02
b	-	1.39	1.17	-	1.39	1.27	1.16	1.21
σ_b	-	0.05	0.05	-	0.04	0.02	0.01	0.01
c	-	46.00	44.67	-	46.19	45.02	43.85	44.10

Continued on next page

Table 3.3, *continued.*

T_*	30000	35000	40000	50000	60000	70000	80000	90000
Min. $\log L_c^{\lambda_0}$	35.	32.6	32.6	32.6	32.6	32.7	32.2	32.0
Max. $\log L_c^{\lambda_0}$	34.	33.6	33.8	32.0	33.9	33.9	34.0	34.0
Min. $\log W$	3.5	0.7	1.0	1.0	1.0	1.0	1.1	1.3
Max. $\log W$	0.0	2.0	2.0	2.0	2.1	2.1	2.3	2.2

3.5 Discussion

Extensive studies exist on the behaviour of the equivalent width of spectral lines and continuum luminosity in Wolf-Rayet spectra with basic stellar parameters (e.g. Hamann & Koesterke 1998a; Nugis et al. 1998). Morris et al. (1993a) were the first to show a relation between the two quantities for Wolf-Rayet stars. The purpose of our study is mainly to indicate the existence of the Baldwin-effect for almost the whole range of Wolf-Rayet stellar parameters and to explain the physics that cause the effect. The model calculations have shown that the effect is mainly caused by differences in radius among the stars. Differences in stellar temperature and mass-loss rate cause a broadening of the relation. Variations of the normalized effective radius x_c cannot cause the Baldwin-effect (as was proposed by Morris et al. 1993a) but do determine the slope of the Baldwin-relations. The ionization structure determines the parameter region where the Baldwin-effect applies.

The fact that sufficiently dense atmospheres are required in order to show a Baldwin-effect, explains why the effect has been observed in Wolf-Rayet stars and not in normal O-stars. Indeed, for O-stars the continuum spectrum is not formed in the wind, except for wavelengths in the infrared and longer. We calculated also a few O-star models, i.e. with parameters similar to our Wolf-Rayet star model grid, but with lower mass-loss rates: $-7 < \log(\dot{M}) < -5.5$. We found no clear correlation between line equivalent width and monochromatic continuum luminosity.

The influence of stellar temperature, and mass-loss rate, has implications for the applicability of the Baldwin-effect in the determination of stellar distances. The broadening of the $W - L_c$ relation is mainly caused by differences in the mass-loss rate. This indicates that a star's absolute luminosity (and through that it's distance) is difficult to obtain from a single relation between equivalent width and continuum luminosity due to this intrinsic spread. Indeed, without some knowledge of a star's mass-loss rate (which already depends on it's luminosity!), we cannot guarantee to derive a distance from a single equivalent width versus L_c relation with error bars systematically any smaller than currently found in the literature. However, it may be possible to define *separate* equivalent width versus L_c relations for the three groups of late-type, strong-lined early-type, and weak-lined early-type WN stars. These groups tend to cluster in parameter space (see, e.g., Hamann & Koesterke 1998a), and will thus occupy limited regions of our grids of Baldwin relations for the HeII lines.

Before making use of the Baldwin relations, however, we must fully account for deficiencies in our model calculations that will contribute to uncertainties in the equivalent width measurements. The line equivalent width in the stellar spectra may be influenced by additional Doppler broadening arising from unaccounted for turbulent motion in, e.g., shocks. Also, the neglect of nitrogen has a slight influence on the He line profiles (Hamann & Koesterke 1998a). Over recent

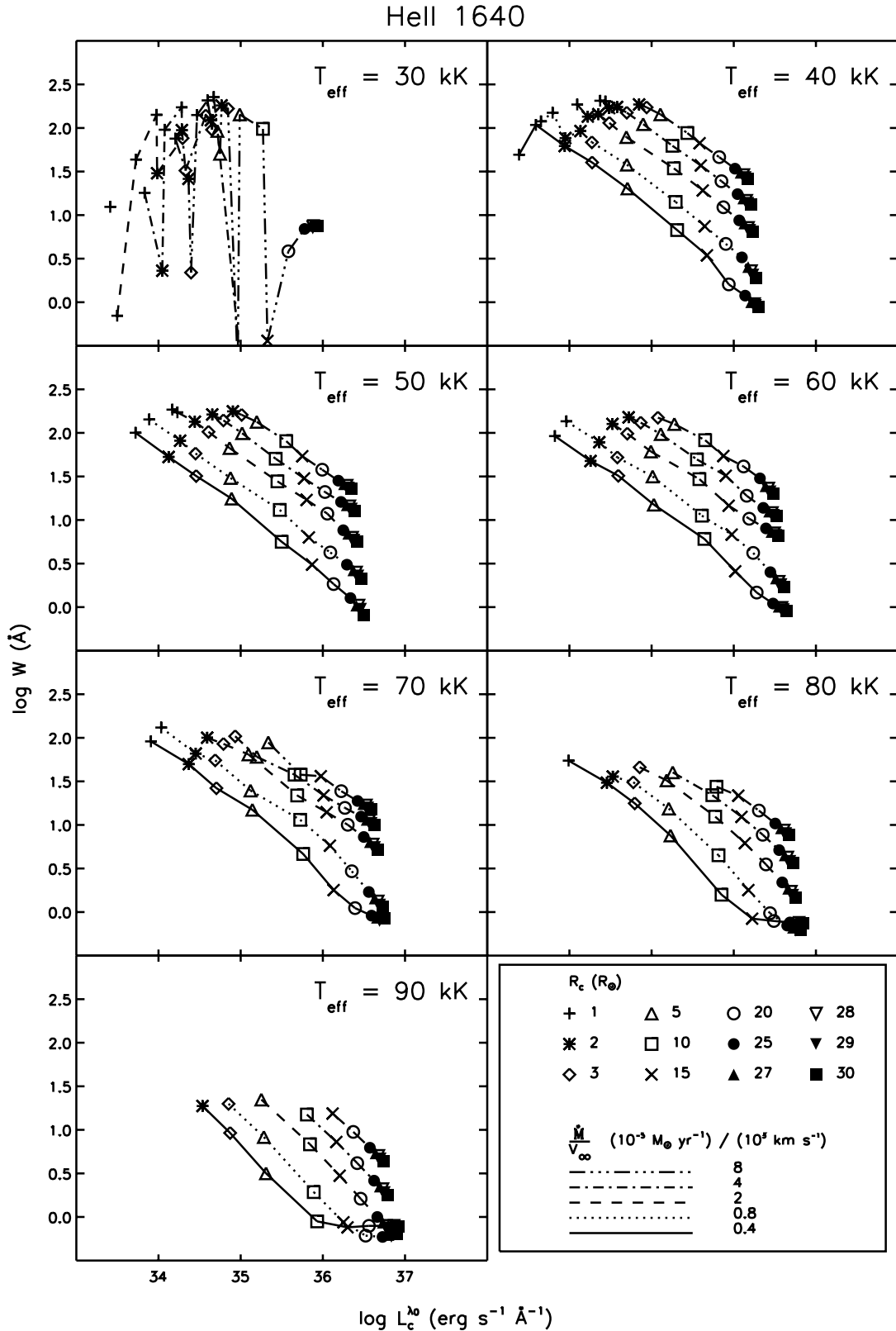


Figure 3.11: The Baldwin relations of the the He II $\lambda 1640$ line, but now as a function of T_{eff} rather than T_* (compare with Fig. 3.5). Each panel shows $\log(W)$ as function of $\log(L_c)$ for models with the same value of T_{eff} , and for different values of the mass-loss rate, \dot{M} , and the core radius, R_* . Models with the same value of \dot{M} are connected by lines; the values of R_* are indicated by symbols. Line style and symbols are explained in the bottom right panel.

years, furthermore, it has become more obvious that the spherically symmetric, homogeneous approach in model atmosphere calculations does not suffice to describe spectral observations; wind clumping phenomena may influence both the line profile shape (in the electron scattering wings) and the overall SED, as shown by Hillier (1984). Observational evidence for clumping can be found in e.g. Lépine & Moffat (1999). The impact of clumping in terms of the stellar parameters is chiefly in the estimated values of \dot{M} , and may therefore alter the manner in which the Baldwin relations are applied on a source by source basis.

In a forthcoming paper we will treat some of these effects, such as the inclusion of nitrogen and influence of clumping. The final calibration of the Baldwin-relations will be done by means of observations of stars with well known distances. This will set the stage for application of the Baldwin-effect to Galactic WR star observations.

Acknowledgements

AdK acknowledges support from NWO Pionier grant 600-78-333 to L. B. F. M. Waters and from NWO Spinoza grant 08-0 to E. P. J. van den Heuvel.

Model atmospheres in the study of Wolf-Rayet type stars

4.1 Introduction

The observed inverse correlation between the equivalent width of emission lines in Wolf-Rayet (WR) star spectra and the continuum luminosity at the line wavelength has been shown to be predicted by model calculations of WR atmospheres and spectra (chapter 3). This correlation is called the Baldwin-effect after a similar observationally found property of the spectra of Active Galactic Nuclei (AGN) by Baldwin (1977).

When properly calibrated, the *Baldwin-relations* in WR spectra can be used to derive the distance of WR stars from their spectrum. The calibration of the Baldwin-relations of spectral lines in Wolf-Rayet (WR) stars depends on a comparison between observed line strengths and those predicted by detailed models of WR atmospheres. The purpose of this chapter is to discuss critically the model atmospheres of WR stars and the accuracy of the line profile calculations. We compare the results of two methods for the calculation of spectra of WR stars: a) the ISA-WIND computer code of de Koter et al. (1993), which is based on the Improved Sobolev Approximation (ISA), and b) the POTSDAM code¹ of Hamann 1985b; Hamann & Wessolowski 1990, based on the co-moving frame (CMF) method. We will not only discuss the two methods, but particularly look at the differences in the calculation of the atmospheric structure, such as temperature, density, and the chemical composition.

In Sect. 4.2 we give a brief general overview of the basic methods used in the construction of model atmospheres of stars with winds. In Sect. 4.3 we describe the assumptions of one of these codes, the ISA-WIND code, and we discuss their accuracy. Sect. 4.4 compares the spectral features predicted by the ISA-WIND code with those predicted by the POTSDAM code.

4.2 Model atmospheres

4.2.1 Geometry

Early attempts to model the spectrum of stars use a hydrostatic, plane parallel representation of the outer layers of the star, where the observed radiation originates (the photosphere). It is assumed that the observed spectrum originates from a layer of gas that is relatively thin when compared to the radius of the star, so the curvature of the layer can be neglected. This, of

¹ This code has been traditionally known as the KIEL code. Since the developers of this code moved to Potsdam, references to the code increasingly use the name POTSDAM code. Therefore, we will refer to the code as POTSDAM code throughout this chapter.

course, strongly simplifies the radiative transport problem and the method has proved to be very successful for the modelling of the atmospheres and spectra of main sequence stars (e.g. the sun) and giants without strong stellar winds.

Indeed, for stars with high mass loss rates, a different approach is required for modelling the atmospheric structure and the emitted stellar spectrum. For these stars, the radial distance over which the expanding atmosphere contributes to the observed radiation is generally too large for the plane parallel approximation to hold. This is certainly true for (strong) spectral lines, but for very dense winds also the continuum radiation field can be formed in extended, curved atmospheric layers. In the latter case the star is described as having an “extended” atmosphere. The simplest approach used for the modelling of stars with extended atmospheres is to adopt a spherical symmetric geometry, assuming a monotonically accelerating, homogeneous outflow. Wolf-Rayet stars are among the stars with the densest winds. A plane parallel approach in the modelling of these stars is useless, as many features in the spectra of these stars originate in the rapidly out-flowing part of the atmosphere. Departures from spherical symmetry and homogeneity, e.g. clumping, have been the study subject of recent years. We will discuss the effects of clumping on the stellar spectrum in Sect. 4.3.4.

4.2.2 Density and velocity of spherically symmetric winds

In a spherically symmetric, homogeneous outflow, the determination of the density and velocity stratifications throughout the stellar atmosphere would require the solution of two hydrodynamical equations. The first one describes mass conservation:

$$\dot{M} = 4\pi r^2 \rho(r)v(r), \quad (4.1)$$

with r the radial distance from the centre of the star, and with mass loss rate \dot{M} , density ρ and velocity v . The second equation is the equation of motion:

$$v \frac{dv}{dr} + \frac{1}{\rho} \frac{dp}{dr} + g_N - g_{\text{rad}} = 0, \quad (4.2)$$

where p is the gas pressure, g_N is the Newtonian gravity acceleration, and g_{rad} is the acceleration due to radiation pressure.

The radiative acceleration term contains both continuum processes (bound-free, free-free, and Thomson electron scattering) and line acceleration. This requires, that the Eqs. 4.1 and 4.2 be solved simultaneously with the equations that describe the state of the gas and the radiative transport through the atmosphere. For today’s standards, the computational demands on performing this task accurately are too high. Furthermore, the physical mechanisms that drive the mass loss of hot stars are not fully understood. For this reasons, some assumptions have to be made about the hydrodynamic structure in stellar atmospheres. For example, the equation of motion can easily be solved if line radiation terms in g_{rad} are ignored. For that purpose, it is often assumed that the dominating opacity term is due to Thomson scattering. For hot stars with winds, this is valid in the atmosphere layers far below the sonic point, where the velocity gradient of the outflow is small. The equation of motion without line accelerations reduces to:

$$v \frac{dv}{dr} + \frac{1}{\rho} \frac{dp}{dr} + \frac{GM(1 - \Gamma_e)}{r^2} = 0, \quad (4.3)$$

where we used Newton's gravity law and introduced Γ_e , which is the ratio between the electron scattering acceleration and the gravitational acceleration. Γ_e is given by

$$\Gamma_e = \frac{g_{\text{rad}}}{g_{\text{N}}} = \frac{\sigma_e L}{4\pi c G M} = 7.66 \times 10^{-5} \sigma_e \left(\frac{M}{M_\odot} \right)^{-1} \left(\frac{L}{L_\odot} \right), \quad (4.4)$$

where L is the stellar luminosity; σ_e is the Thompson scattering coefficient; M and L are the stellar mass and luminosity, respectively, and G is the gravitational constant. Eq. (4.3) can be solved for a given temperature structure, that couples the density and pressure through the ideal gas law:

$$p = \frac{\rho(r) k T(r)}{\mu m_{\text{H}}}, \quad (4.5)$$

where k is Boltzmann's constant and μ is the mean atomic weight in units of the proton mass, m_{H} . Solving Eq. (4.3) results in a density and velocity structure, valid in the subsonic part of the stellar wind.

Further out in the atmosphere, though already below the sonic point, acceleration of the wind by spectral lines becomes important. It is mainly the line driving that determines the mass loss rate of the star. For OB-stars, recent studies have shown that line driving of iron or iron-like elements, at the base of the wind, determines the star's mass-loss rate, whereas acceleration by lines of lighter elements (carbon, nitrogen, oxygen) determines the velocity in the supersonic wind region (Vink et al. 1999; Puls et al. 2000).

The calculation of the line acceleration is rather complex, because it involves the simultaneous solution of the ionization and excitation structure of many ions, as well as the equation of motion (Eq. 4.2) and the radiative transfer equations. Therefore, instead of solving the equation of motion, including line driving, in the largest part of the wind region some parametrisation of the velocity structure is used. The corresponding density structure then follows from mass conservation (Eq. 4.1). This parametrisation mostly describes a monotonically increasing velocity with radial distance from the star. An often used parametrisation for the supersonic wind region is the so called β -law (Lamers & Rogerson 1978):

$$v(r) = v_0 + (v_\infty - v_0) \left(1 - \frac{R_*}{r} \right)^\beta, \quad (4.6)$$

where R_* is the inner radius of the model, v_∞ is the terminal velocity of the wind and v_0 is the velocity at the base of the wind: $v_0 = v(r = R_*)$. In stellar atmosphere codes the β law is often rewritten in a slightly different form:

$$v(r) = v_\infty \left(1 - \frac{r_0}{r} \right)^\beta, \quad (4.7)$$

In this form, the β -law, that describes the velocity in the supersonic wind region, can be smoothly connected at a radius r_{con} to the velocity structure in the subsonic region (which followed from solving Eq. 4.3) by requiring continuity of both $v(r)$ and its derivative dv/dr . By an iterative technique both r_0 and r_{con} are then determined. Although parametrisations are always approximations of the situation as it occurs in nature, they have the advantage that they can be used to study the influence of the velocity on the atmosphere structure and spectrum of the star.

The β -law is used in several well known stellar atmosphere codes, e.g. ISA-WIND (de Koter et al. 1993, 1997) and the model traditionally called the KIEL model, but that is now known as the POTSDAM model (Hamann 1985b; Hamann & Wessolowski 1990 and papers thereafter).

The model CMFGEN (Hillier 1987; Hillier 1990a) uses a somewhat different expression for $v(r)$, using two *beta* parameters:

$$v(r) = \frac{v_0 + (v_\infty - v_0 - v_{\text{ext}})(1 - R_*/r)^{\beta_1} + v_{\text{ext}}(1 - R_*/r)^{\beta_2}}{1 + (v_0/v_*)e^{(r-R_*)/h_{\text{eff}}}}, \quad (4.8)$$

where v_* is $v(r = R_*)$ and h_{eff} is the effective scale height in the subsonic part of the atmosphere. In the numerator of Eq. (4.8) we recognise the β -law (Eq. 4.6), although in this form, a distinction is made between $v(r = R_*)$ and the free parameter v_0 . Besides that, an extra velocity parameter v_{ext} is used to control the velocity behaviour in the outer wind regions. In this way a shallower velocity law than the classical β -law can be obtained, which seems to be a more realistic approach to the actual velocity structure in WR star winds, as derived from observational evidence. The denominator of Eq. (4.8) is such that close to the core, the velocity structure of isothermal atmosphere in near hydrostatic equilibrium is recovered.

4.2.3 Radiative transfer in a spherically symmetric geometry

We will present some basic radiative transfer theory in this section, valid for a spherically symmetric radial outflow. We will use the expressions given in this section to study the electron temperature distribution in the atmosphere (Sect. 4.2.4). For a time-independent, spherically symmetric expanding atmosphere, the equation of radiative transfer in the observer's frame is given by:

$$\mu \frac{\partial I_\nu}{\partial r} + \frac{1}{r}(1 - \mu^2) \frac{\partial I_\nu}{\partial \mu} = \eta_\nu - \chi_\nu I_\nu, \quad (4.9)$$

In this expression I_ν is the intensity with dimension [$\text{erg cm}^{-2} \text{s}^{-1} \text{Hz}^{-1} \text{sterad}^{-1}$]; μ is the cosine of the angle between the radial direction, r , and the direction in which I_ν is emitted; η_ν is the emissivity ([$\text{erg cm}^{-3} \text{s}^{-1} \text{Hz}^{-1} \text{sterad}^{-1}$]); and χ_ν is the opacity ([cm^{-1}]).

Widely used in the theory of radiative transfer are the so called *moments of intensity*, where the n th moment of intensity is given by

$$\frac{1}{2} \int_{-1}^1 I_\nu \mu^n d\mu. \quad (4.10)$$

The zero order moment ($n=0$) physically represents the mean intensity J_ν , which is the averaged, integrated intensity over all solid angles; the first moment is called the Eddington flux, denoted by H_ν ; and the second moment is denoted by K_ν . Knowing this we can write the zero order moment of the transfer equation (Eq. 4.9) as:

$$\frac{1}{r^2} (r^2 H_\nu) = \eta_\nu - \chi_\nu J_\nu. \quad (4.11)$$

Similarly, the first order moment of the transfer equation is given by:

$$\frac{\partial(f_\nu J_\nu)}{\partial r} + \frac{1}{r}(3f_\nu - 1)J_\nu = -\chi_\nu H_\nu, \quad (4.12)$$

were we used the variable Eddington factor

$$f_v \equiv \frac{K_v}{J_v}. \quad (4.13)$$

This Eddington factor is a measure for the isotropy of the radiation field. Far from the stellar surface, the radiation field is pointed in the outward direction and $f_v = 1$; deep in the star, the radiation field is isotropic and $f_v = 1/3$.

4.2.4 Temperature structure.

The prediction of the variation of the electron temperature with radial distance in hot star atmosphere models has known some significant developments in recent years. Nowadays, basically two approaches are used, both based on the assumption of hydrostatic equilibrium. Since we will treat the implications of both methods on model spectra in Sect. 4.4, we will give a brief description here.

Radiative equilibrium The assumption of radiative equilibrium (RE) states that at every radius in the stellar atmosphere the total energy of the radiation field absorbed by the gas is equal to the total emitted radiative energy. In mathematical form, this can be expressed as:

$$\frac{dL}{dr} = \int_0^\infty 4\pi r^2 \chi_\nu \{J_\nu - S_\nu\} d\nu = 0, \quad (4.14)$$

in which L is the bolometric luminosity. Indeed, the main energy transport in the winds of early type stars, is thought to be through the radiation field (and not, e.g., through advection, convection, conduction, waves, or shocks). This implies that energy released or consumed in the expanding atmosphere can be neglected. This is justified because the kinetic energy loss in WR star winds is 10^{-1} of the radiative energy loss, and the thermal energy loss is only 10^{-4} of the radiative loss of energy (Lamers & Cassinelli 1999, p 197). It is the condition of radiative equilibrium that can be used to determine the temperature structure in the wind. By considering all important radiative processes in the wind, the temperature of the gas that produces a constant luminosity is calculated. An important cooling term in hot star winds, for example, is through spectral lines. Hillier (1988) showed a strong effect of cooling by collisional excitations followed by line emission of nitrogen and carbon on the temperature distribution.

The condition of radiative equilibrium is at the basis of two methods to calculate the electron temperature distribution in hot star winds, which are described below.

I. Grey temperature structure of an LTE atmosphere For a number of years, most spherical symmetric atmosphere codes used this method for describing the electron temperature stratification. The calculation of this kind of temperature structure is relatively straightforward. In the case of a grey atmosphere, the opacity is assumed to be frequency-independent. This is definitely not true in a real stellar atmosphere. The temperature structure can still be calculated with the grey approximation, however, if a suitable frequency-averaged mean opacity can be found. There are several possible approaches in finding the mean opacity (Mihalas 1978, p. 37 ff) . Here we will follow de Koter et al. (1993) and define a mean opacity $\bar{\chi}$ such that the first moment of the transport equation (Eq. 4.12), when integrated over all frequencies, has the

same shape in the grey case as in the non grey case. This ensures that the total flux is conserved. We thus define:

$$\frac{1}{\bar{\chi}_g} \equiv \frac{\int_0^\infty \chi_v^{-1} \left\{ \frac{\partial}{\partial r}(f_v J_v) + \frac{1}{r}(3f_v - 1)J_v \right\} dv}{\int_0^\infty \left\{ \frac{\partial}{\partial r}(f_v J_v) + \frac{1}{r}(3f_v - 1)J_v \right\} dv} \quad (4.15)$$

The next step involves the Rosseland mean opacity, which is defined as:

$$\frac{1}{\chi_R} \equiv \frac{\pi}{4\sigma T^3} \int_0^\infty \chi_v \frac{\partial B_v}{\partial T} dv, \quad (4.16)$$

where B_v is the Planck curve. Deep in the photosphere, the so called first Eddington approximation holds, which states that $f_v \approx 1/3$ and $J_v \approx B_v$. Assuming the validity of this throughout the whole atmosphere, we may use $\bar{\chi}_g \approx \chi_R$. If we then integrate over frequency, the first order moment of the transfer equation becomes:

$$\frac{\partial}{\partial r}(fJ) + \frac{1}{r}(3f - 1)J = -\chi_R H. \quad (4.17)$$

Integrated quantities over frequency are denoted here by omission of the frequency index.

Under the assumption of radiative equilibrium (Eq. 4.14), we have for our grey atmosphere: $S = J$. As a final assumption for calculating the temperature structure, we suppose the atmosphere to be in local thermodynamic equilibrium (LTE), from which we find

$$J = S = B = \frac{\sigma T^4}{\pi}. \quad (4.18)$$

We can now express the temperature distribution, by combining the expression for the total luminosity, $L = 4\pi r^2 \sigma T^4(r)$ with Eqs. 4.14, 4.17, and 4.18 and find:

$$\frac{dT}{dr} = -\frac{1}{16\pi} \frac{\chi_R}{f T^3} \frac{L}{4\pi r^2} - \frac{T}{4f} \left\{ \frac{df}{dr} + \frac{1}{r}(3f - 1) \right\} \quad (4.19)$$

Instead of performing the formal solutions of the radiative transfer equations to find the Eddington factors $f(r)$, suitable approximations can be made. For an explanation we refer to Lucy (1971) and Wessolowski et al. (1988).

The expression for the temperature structure given in Eq. (4.19) is used in the ISA-WIND model atmosphere code.

II. Temperature structure in a non-grey, non-LTE atmosphere. The full determination of the electron temperature structure in a non-LTE atmosphere, with all opacities being frequency dependent (non-grey) is understandably more complex than the derivation of the grey LTE temperature structure (Eq. 4.19). Strictly, to find a physically realistic temperature structure in the non-grey, non-LTE way requires that, at every radius in the atmosphere, all major continuum and line processes are taken into account. From the condition of radiative equilibrium one can then derive the temperature required to preserve a constant bolometric luminosity. This process is computationally demanding, which is why the calculation of the temperature structure in this way has only been possible in recent years. This method to calculate the temperature structure has been used in the POTSDAM code for the calculation of Wolf-Rayet star winds.

4.3 Assumptions in the ISA-WIND model atmospheres

In chapter 3 we used model atmosphere calculations of the ISA-WIND code to explain the physics behind the Baldwin-effect in WN stars. At that stage, we merely wanted to understand the Baldwin-effect and didn't try to give a full calibrated set of Baldwin-relations applicable for the determination of WN star distances. However, since the physical mechanism of the Baldwin-effect has become clear in chapter 3, it will be worthwhile to calibrate the Baldwin-relations, both in equivalent width and continuum luminosity. To do so, it has to be realized that some assumptions were made in the ISA-WIND model calculations which may influence both of these physical quantities. In this section we will discuss the most important of these assumptions and study their effect on the line and continuum spectrum.

4.3.1 The ISA-WIND model atmosphere code

We will briefly mention the main characteristics of the ISA-WIND code. A more extensive explanation of the different aspects of the code can be found in de Koter et al. (1993, 1997) and in chapter 3, Sect. 3.3. Furthermore, we discussed the fundamental characteristics of model atmosphere codes in general in Sect. 4.2.

The ISA-WIND code treats the model atmosphere in a spherically symmetric geometry. The main input parameters of the model atmospheres are the inner radius, R_* , which determines the size of the stellar core underlying the atmosphere, the effective gravity acceleration, g_{eff} , and the density at the core, ρ_* . The latter is chosen such, that the total Rosseland optical depth, κ_R , has a value between 20 and 25. Following Hamann (1985a), and papers thereafter, we set the scale height in the photosphere by assuming $\log(g_{\text{eff}}) = 3.5$.

The velocity structure in the subsonic wind region follows from solving the equation of motion, were it is assumed that acceleration of the wind by radiation is only through Thomson scattering processes (Eq. 4.3). In the supersonic region of the wind, a β -law is used (Eq. 4.7).

The luminosity is specified by the *stellar temperature*, T_* , as

$$L = 4\pi R_*^2 \sigma T_*^4, \quad (4.20)$$

where T_* corresponds to the effective temperature at the core radius, R_* , of the model. Note that T_* is not the real effective temperature T_{eff} , as R_* is not the stellar radius. The real stellar radius of Wolf-Rayet stars is intrinsically wavelength dependent.

The temperature structure is that of an atmosphere in LTE, under the assumption of a frequency independent (“grey”) opacity (Eq. 4.19). We artificially limit the drop of the temperature with radius to a value $T_{\text{min}} = 13$ kK. The choice of this value is explained in Sect. 4.3.3.

4.3.2 The influence of hydrogen and nitrogen on the model atmospheres

In chapter 3, where we described the theory behind the Baldwin effect of helium lines for WN stars, we used pure helium model atmospheres from the ISA-WIND code, neglecting the influence of hydrogen and metals on the strength and shape of both the helium lines and the spectral energy distribution. The argument for this assumption is, that the abundances of hydrogen and metals are small in WN star atmospheres. In this section we will discuss the validity of this assumption by studying the influence of hydrogen and nitrogen on the model atmospheres and the Baldwin-relations.

Most WNL stars and some WNE stars with weak emission lines (WNE-w stars) show clear signs of the presence of hydrogen in their spectra. Derived H/He ratios range from 0.20 to 3.0 in the LMC (Crowther & Smith 1997); Galactic WN stars show hydrogen contents up to $\approx 50\%$ of the mass (e.g. Hamann et al. 1995), corresponding to a number ratio of $H/He = 4.0$ for a star of H-He composition. The presence of hydrogen in the model atmospheres may therefore influence the ionization balance and affect the helium spectrum and through that the Baldwin-relations of the helium lines.

Several authors have stated that the inclusion of other chemical elements than hydrogen and helium (mainly carbon and nitrogen) in the model calculations has little effect on the predicted helium spectrum, at least for the WNL and strong lined WNE stars. (e.g. Hillier 1988; Crowther et al. 1995b; Hamann et al. 1994; Hamann & Koesterke 1998a). Indeed, when looking at a large grid of models, that covers the space of the basic WN star parameters, the presence of nitrogen in the stellar atmosphere on average seems to have little effect on the helium spectrum (Hamann & Koesterke 1998a)².

However, if additional chemical elements have some effect on the temperature and the helium ionization stratification in the model atmospheres, the effect on the helium spectrum may be more severe for the relatively cool WNL stars, where the helium ionization balance can be between He II and He III, and where both He I and He II lines are therefore very sensitive to small differences in ionization.

To get a better feeling of the effect of including H and N on the predicted helium spectrum, we compare model atmospheres and spectra from the ISA-WIND code for different chemical compositions.

As an example, Fig. 4.1 shows the profiles of He lines for a model of a WNL type star, for H/He ratios (by number) of 0.0, 0.8, and 1.5. These models do not contain nitrogen.

The reduction of the helium line equivalent width with increasing hydrogen content simply reflects the relative lower helium populations, as can be seen from the ionization structure, shown in Fig. 4.2. Despite the reduction of the He II line equivalent width we consider the pure helium approximation for the model atmospheres very satisfactory. Even for the highest ratio of $H/He = 1.5$ (a hydrogen content of $\approx 30\%$ by mass) the influence on the line equivalent width is not dramatic (some 10-15 % lower equivalent width). Considering this, we find it justified to ignore the presence of hydrogen in the prediction of the Baldwin-relations for WN type stars.

The consequence of the inclusion of nitrogen in the models is more severe. Hillier (1988) found that collisional excitation of nitrogen and carbon has a strong cooling effect on the wind. Hence, particularly for those models with a relatively low stellar temperature, T_* , and high wind densities, the effect of including nitrogen and or carbon in the calculations may have a significant effect on the equivalent width of the He II lines. This is because under those conditions helium is no longer fully ionized and the degree of ionization is very sensitive to the temperature structure.

To illustrate this, Fig. 4.3 shows a comparison between spectral lines from a hydrogen-

²Hamann & Koesterke (1998a) have compared their new He-N models with former pure helium models. We want to note that the two model sets do not only differ in chemical composition. The pure He atmospheres use a temperature distribution of a grey atmosphere in LTE, whereas in the He-N models the electron temperature is calculated in non-LTE, from the assumption of radiative equilibrium. Including nitrogen in the models and using a non-LTE temperature structure may have opposite effects on the helium ionization balance, resulting in little difference of the helium line equivalent widths between the two model sets. We will discuss the separate effects on the helium ionization of the nitrogen content in model atmospheres and the used temperature structure in Sect. 4.4.

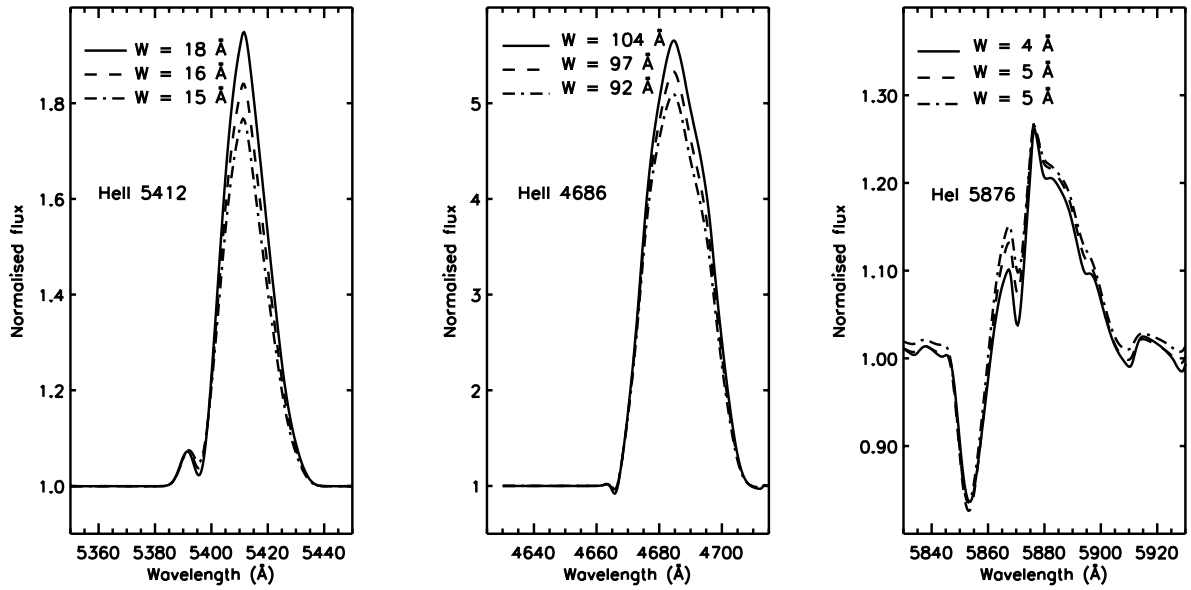


Figure 4.1: Helium spectral lines for a WNL type H-He model for three different H/He abundance ratios. The ratios are (by number): 0.0 (full line), 0.8 (dashed line), and 1.5 (dashed-dotted line). The basic stellar parameters are: $T_* = 33.5\text{kK}$, $R_* = 19R_\odot$, $\dot{M} = 9 \times 10^{-5} M_\odot \text{yr}^{-1}$, and $v_\infty = 1500\text{km s}^{-1}$. W denotes the equivalent width in Å.

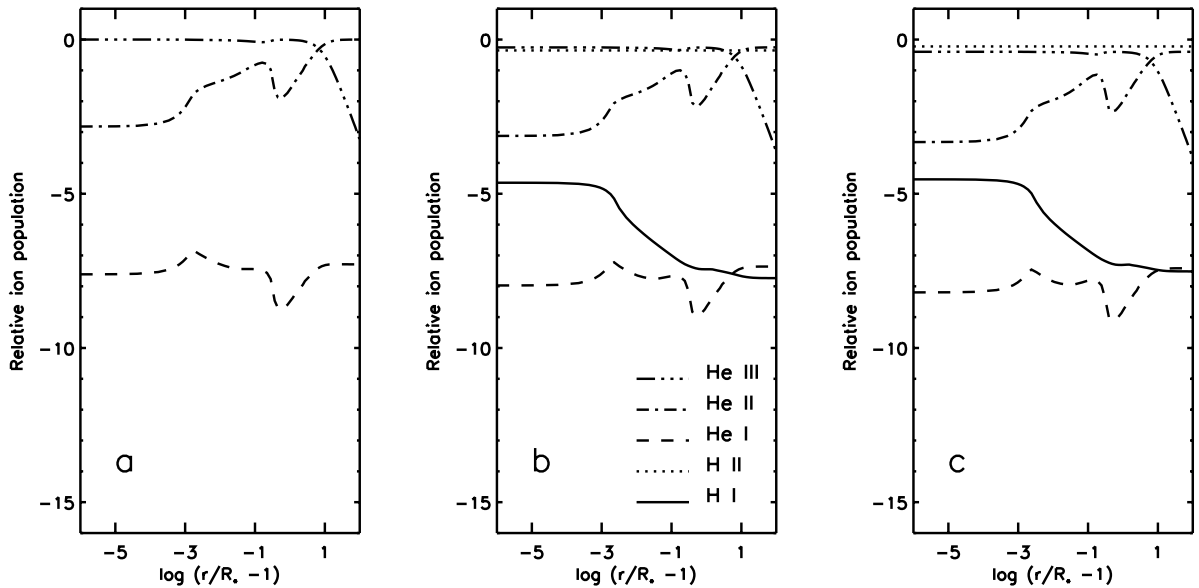


Figure 4.2: Hydrogen and helium ionization structure of the models for which helium lines are shown in Fig. 4.1. The H/He ratios shown are 0.0 (panel a), 0.8 (panel b), and 1.5 (panel c). The stellar parameters are the same as in Fig. 4.1.

helium model and the same lines from a model that also includes nitrogen. The corresponding ionization stratification of hydrogen and helium are shown in Fig. 4.4. The stellar temperature is $T_* = 33\text{kK}$. We have used a nitrogen content of 1.5% by mass, following Hamann et al. (1994), as a typical value for a galactic WN star. This corresponds to a number ratio of $\text{N/He} =$

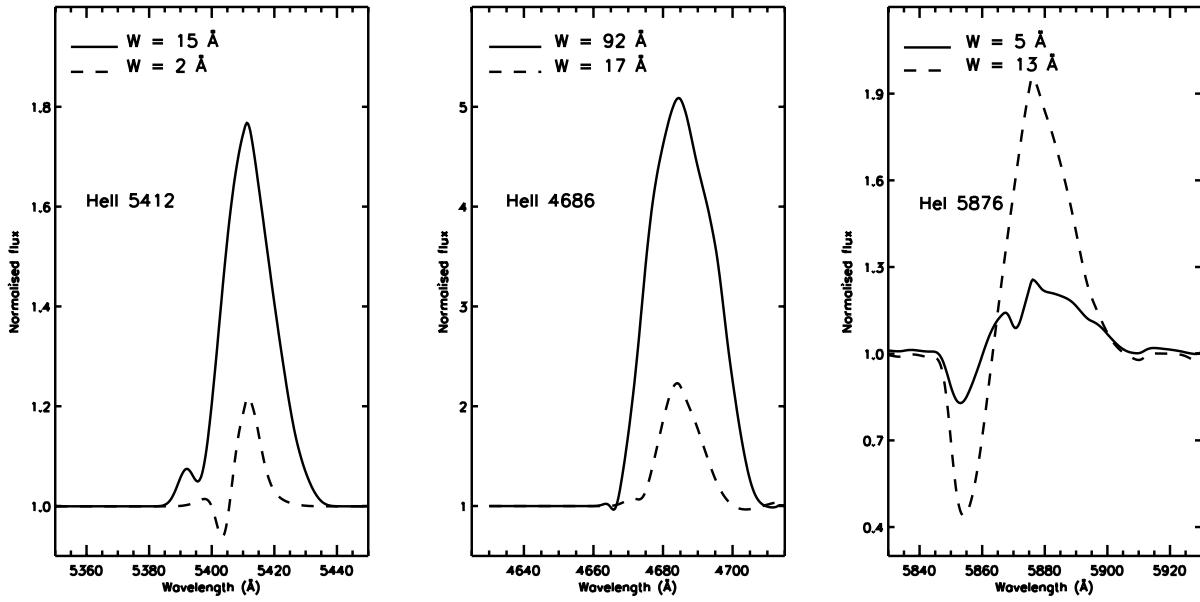


Figure 4.3: Model spectra of helium lines for the H-He model (full lines) and a model with the same stellar parameters but consisting of H-He-N (dashes). $T_* = 33$ kK, $R_* = 19.0 R_\odot$, $\dot{M} = -4.05 M_\odot \text{yr}^{-1}$, and $v_\infty = 1500 \text{km s}^{-1}$.

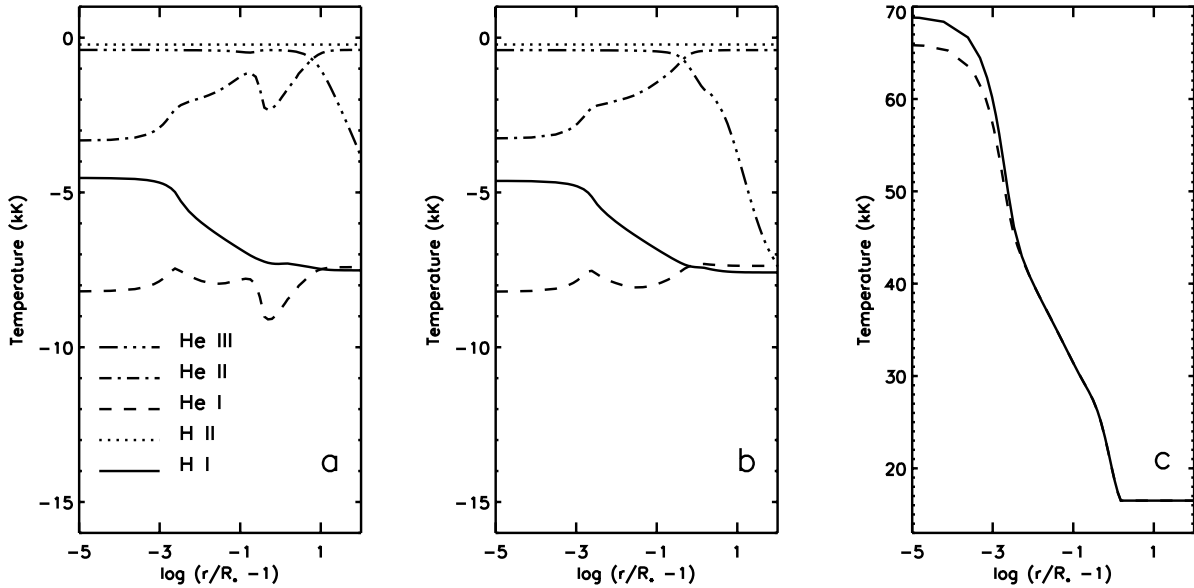


Figure 4.4: Ionization structure for the $T_* = 33$ kK H-He model (panel a) and H-He-N model (panel b). Panel c shows the temperature stratification for the H-He (full line) and H-He-N (dashes) models. The stellar parameters are the same as in Fig. 4.3.

0.006. The adopted hydrogen content is $\text{H}/\text{He} = 1.5$, by number. Apart from the chemical composition, the input parameters of both models are the same.

The helium ionization structure of the H-He model, depicted in Fig. 4.4 a, shows that helium is doubly ionized in the major part of the wind. However, when we look at the model that includes nitrogen (Fig. 4.4 b), the population of doubly ionized helium (He III) has reduced in

favour of He II. As a result, in the model containing nitrogen, the He II lines appear strongly reduced in strength, compared to the H-He model, while at the same time the equivalent width of the He I line at 5876 Å has increased (Fig. 4.3).

To understand why the presence of nitrogen has such a dramatic effect on the equivalent width of the He lines, we have to compare in detail the He ionization structures of the H-He and the H-He-N model (Fig. 4.4 a and 4.4 b, respectively). In the H-He model, we see that the drop of the electron temperature with radius (Fig. 4.4 c, full line) causes a gradual increase of the He II population, at the expense of He III. This takes place in the height range above the core of $\log h \equiv \log(r/R_* - 1) \approx -3.5$ to -0.8 . But, because the wind density drops in the accelerating outflow, re-ionization is enabled at larger height, causing a dip in the He II population. In the most outer parts of the wind, the density of the radiation field has become too low to keep He fully double ionized and He II becomes the dominant helium ionization stage.

In the H-He-N model, the helium ionization is somewhat different. The main difference with the H-He model is that the dip in the He II ionization around $\log h = -0.5$ is not observed. The reason behind this are non-LTE effects, due to the presence of nitrogen. We can understand the influence of nitrogen on the helium ionization if we look at the spectral energy distributions (SEDs) of both the H-He and the H-He-N model (Fig. 4.5). In both models, the flux in the He II Balmer continuum (below 912 Å) is much stronger than in the He II Lyman continuum, which remains optically thick up until the outer radius of the models. The He ionization balance is therefore mainly determined by the $n = 2$ level of He II. However, for the H-He-N model, the He II Balmer continuum interferes with the continua of the N III $2p^2$ level (continuum edge at 261 Å) and the N III $2p^4$ (edge at 307 Å). The result is that, in the H-He-N model, the radiation field below 307 Å remains optically thick until the outer boundary, leading to a stronger coupling between the radiation field and the gas than in the H-He model³. This means that in the H-He-N model, the helium ionization is much more determined by the electron temperature structure than in the H-He model. For the H-He-N model, the dropping temperature with radius therefore causes the He II population to keep rising throughout the whole line forming wind region. This is the reason why the He II lines in the H-He-N model are weaker than in the H-He model, whereas the He I line is stronger⁴. The difference in line equivalent width between the H-He and the H-He-N model are completely caused by differences in flux of the *lines*; the continuum flux at the central wavelength of the lines is not affected by nitrogen, as can be seen from Fig. 4.5.

For models with a larger value of the stellar temperature, T_* , we expect less influence of

³At this stage we want to note that caution has to be taken with frequency ranges for which a model atmosphere is still optically thick at the outer boundary. As there is no inward flux at the outer boundary, the boundary condition for the radiation field is physically unrealistic if the atmosphere is still optically thick at that location. Since in the above comparison of models with and without nitrogen we are dealing with such optically thick continua, we cannot trust the absolute flux levels in the “thick” frequency range. The influence of the nitrogen continuum edges on the helium ionization, described above, can however be trusted. This is based on findings by Werner Schmutz, who found that differences in e.g. level and ion populations that occur deeper in the atmosphere than the last 5 layers in his radius grid, can be trusted (de Koter, private communication). On similar grounds we trust the finding in the above comparison of the He and the He-N model. This kind of comforting results are crucial in the modelling of Wolf-Rayet star atmospheres, since the radius where, e.g., the He II Lyman continuum becomes optically thin can be several hundred to several thousand core radii from the stellar center.

⁴Note that the difference in electron temperature between the two models at deeper layers of the atmosphere ($\log h < -2$) cannot be the reason for the differences in line equivalent width: At the wavelength of the lines the radiation field is already thermalized as far out as $\log h \approx -1.22$. The temperature differences at deeper layers therefore cannot cause the large differences in ionization further out in the wind.

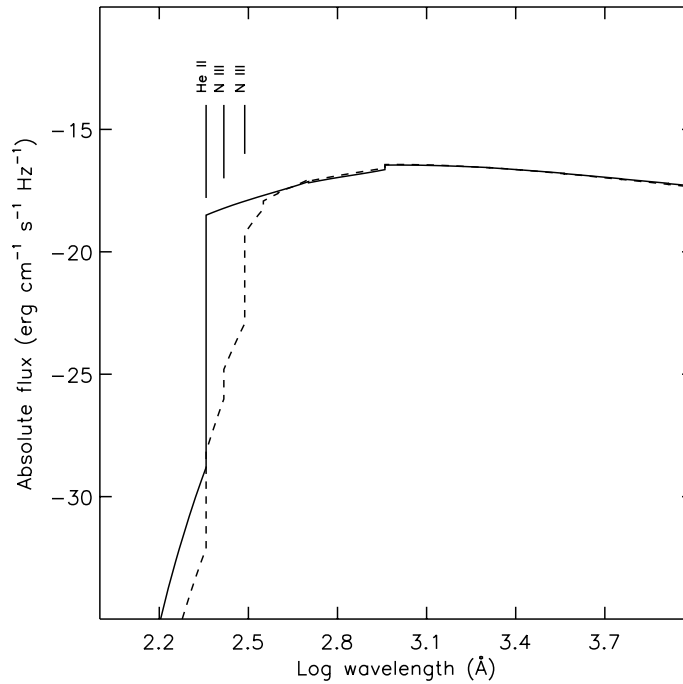


Figure 4.5: Spectral energy distributions of the H-He model (full line) and the H-He-N model (dashes) at $T_* = 33$ kK. The labels in the figure indicate the He II Lyman continuum edge at 227 \AA and the N III edges at 261 \AA and 307 \AA , respectively. The stellar parameters are the same as in Fig. 4.3.

the nitrogen content on the He II equivalent width and the continuum luminosity. This is partly because for values of T_* higher than ≈ 50 kK (depending also on the density), the temperature is high enough throughout the whole atmosphere to keep helium almost completely ionized to He III. Furthermore, at higher temperatures the N III population reduces in favour of higher nitrogen ions, reducing the optical depth in the N III $2P^2$ and $2P^4$ continua. From this, we expect the addition of nitrogen in the model to have more influence on the helium spectrum of late type Wolf-Rayet stars than on early types.

We have tested this by again comparing a H-He model with a H-He-N model, this time at a stellar temperature of $T_* = 50$ kK. For these models, helium line profiles are shown in Fig. 4.6. The corresponding ionization structures are shown in Fig. 4.7. The agreement between the H-He model and the H-He-N model is much better than at a temperature of $T_* = 33$ kK. Both the $2P^2$ and the $2P^4$ continuum of N III get optically thin around $\log h = -1.4$.

From the above study on the influence of hydrogen and nitrogen on model atmospheres and model helium spectra, we find that the equivalent width values of helium lines are not strongly affected by hydrogen. Considering the range of hydrogen abundances derived for WNL stars, an average reduction of $\approx 10\%$ of the He II line equivalent width can be expected due to the presence of hydrogen. From the smaller hydrogen content or even absence of hydrogen in WNE stars, we conclude that the helium lines for WNE type models are not or very little affected by the inclusion of hydrogen.

The inclusion of nitrogen in the model calculations does have a very significant effect on the equivalent width values of He lines in WNL models. A reduction of the He II line equivalent

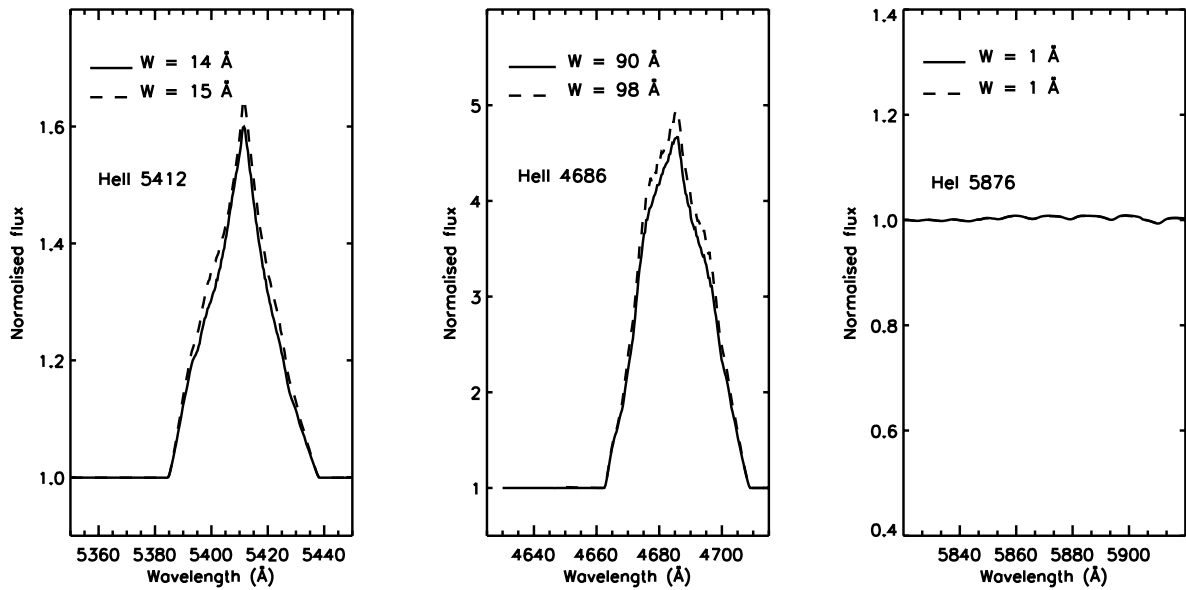


Figure 4.6: Model spectra of helium lines for a H-He model (full lines) and a model with the same stellar parameters but consisting of H-He-N (dashes). $T_* = 50$ kK; other parameters are the same as for Fig. 4.3.

width of a factor 6-7 was observed for a WNL type model with a nitrogen content of only 1.5 % by mass, whereas an equivalent width increase by more than a factor 2 was observed for He I. The differences between models with and without nitrogen disappear at higher values of T_* .

The overall conclusion can be drawn that the inclusion of metals in WR model atmospheres have a significant influence on the helium spectrum of WNL type models. For the calibration of the Baldwin-relations of helium lines, it is therefore not sufficient to use pure helium model atmospheres.

4.3.3 The temperature structure

As mentioned in Sect. 4.3.1, the temperature stratification in the ISA-WIND model atmospheres is that of a quasi grey atmosphere in LTE (Eq. 4.19), with a properly defined mean opacity, independent of frequency. More advanced model atmosphere codes nowadays are capable of calculating the electron temperature structure in the atmosphere in non-LTE from the assumption of radiative equilibrium, and with a correct, frequency dependent opacity.

This more advanced way of the treatment of the electron temperature in the model atmosphere was also in the studies which conclude that the inclusion of nitrogen in the model calculation has little effect on the helium spectrum (e.g. Hamann & Koesterke 1998a). Since we noted that, particularly for the WNL stars, the helium spectrum can be clearly altered by the presence of nitrogen, the question rises whether this may be (partly) due to our assumption of a temperature stratification of a “grey” atmosphere in LTE.

Hillier (1988) discussed the differences of a calculated, non-LTE temperature structure between a H-He model and a model cooled by collisional excitation of nitrogen and compared the result to a “grey” temperature law (his figure 1). The overall temperature structure for the non-LTE H-He model is higher than a grey structure. In fact, in the non-LTE H-He case, after an

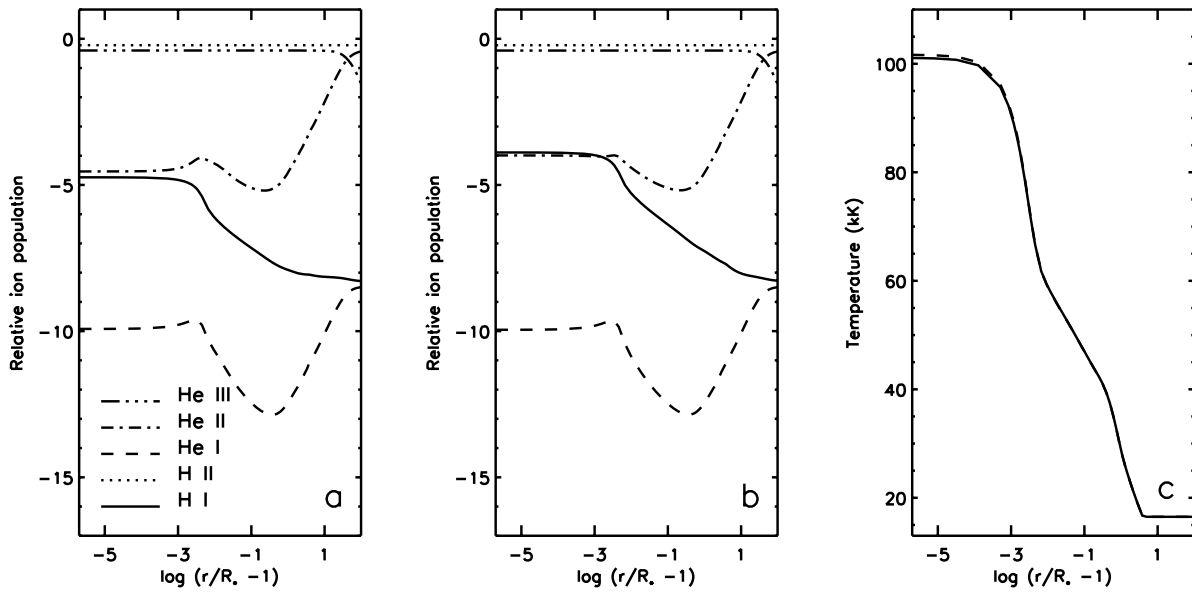


Figure 4.7: Ionization structure for the $T_* = 50$ kK H-He model (panel a) and H-He-N model (panel b). Panel c shows the temperature stratification for the H-He (full line) and H-He-N (dashes) models. The stellar parameters are the same as in Fig. 4.6.

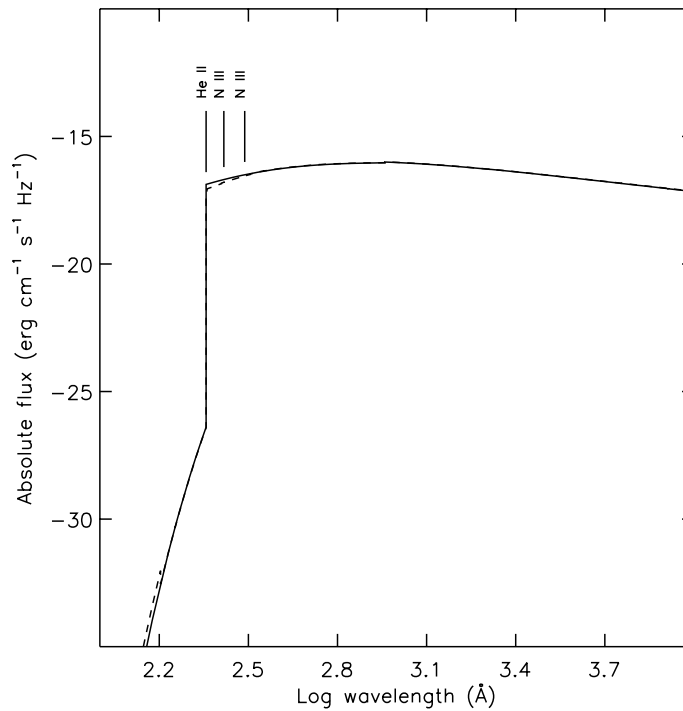


Figure 4.8: Spectral energy distributions of the H-He model (full line) and the H-He-N model (dashes) at $T_* = 50$ kK. The locations are indicated of the same continuum edges as in Fig. 4.5. The stellar parameters are the same as in Fig. 4.6.

initial outward decrease, the temperature rises again. This is due to non-LTE-processes, causing heating of the outer layers of the atmosphere by the radiation of low level continua (Mihalas 1978). So, for H-He models, the non-LTE temperature structure may deviate strongly from that of the grey LTE atmosphere.

Interestingly, Hillier found that collisional cooling processes of nitrogen lead to a temperature structure that decreases monotonically outward, which agrees much closer with the grey case than the non-LTE temperature structure of the H-He model. Inclusion of more chemical elements in the model atmosphere calculations may therefore lead to an even better agreement with the grey distribution (de Koter, private communication). In conclusion, the grey temperature structure seems a reasonable assumption. The Non-LTE effects of nitrogen on the helium spectrum, as shown in Sect. 4.3.2, therefore are not expected to disappear when a full non-LTE calculation of the temperature stratification would be included in our model atmospheres.

Although the assumption of a grey-type temperature structure seems to be justified, its mathematical description (4.19) shows that the temperature will keep dropping with radius, whereas non-LTE temperature distributions approach a constant temperature in the outer wind regions. Physically, a temperature that keeps dropping is not realistic in an expanding, outflowing atmosphere. In our model calculations with ISA-WIND we therefore limit the temperature drop to a value T_{\min} and assume a constant temperature at larger radii. The choice of T_{\min} can have some influence on the line spectrum.

Model atmosphere calculations of Wolf-Rayet stars with a non-LTE, non-grey temperature structure, indicate that the temperature drops to a value around between ≈ 9 and ≈ 15 kK, irrespective of the stellar temperature, T_* (Koesterke, private communication). Studies of single WN stars by Hillier (1988) and Hamann et al. (1994) both show a temperature stratification that drops to 13 kK in the outer regions of the stellar wind. We therefore adopted a value of $T_{\min} = 13$ kK for our grey temperature structure in our model calculations.

4.3.4 Clumping and electron scattering

Emission lines in hot stars often show broad wings, extending to several times the wind terminal velocity from both sides of the line centre. The lines are caused by scattering of light by fast moving free electrons in the wind (Thomson scattering). Since scattering processes neither create nor destroy photons, the effect of electron scattering on continuum radiation is small (Lamers & Waters 1984). For spectral lines, however, the effects of electron scattering can be large; many spectral lines in WR star spectra are optically thick. Redistribution in frequency of line photons by electron scattering can de-saturate the lines. This way electron scattering processes can significantly increase the line equivalent width. The effect of electron scattering on line equivalent width is different for different line transitions, as it depends very much on how deep in the wind the line is formed. The effect of scattering on the equivalent width can be severe. For helium emission line in Wolf-Rayet stars, Hillier (1991) found an increase in equivalent width up to 85% for He II lines; more modest increments (up to 20%) were found for the He I lines.

Modern model atmosphere codes include Thomson scattering processes in the calculations (e.g. Hamann et al. 1994; Hillier 1991). It is not included in the ISA-WIND code and therefore the equivalent widths of spectra predicted by ISA-WIND may be slightly in error. Since the contribution of scattering wings to the total line equivalent width can be large, it is important for our study of the Baldwin-relations. Therefore it would be valuable to have at least an esti-

mate for the contribution of the scattering wings to the equivalent width in different locations of the R_t, T_*, \dot{M} parameter space. We postpone this problem to chapter 5, where we will use model spectra from the POTSDAM code to provide such an estimate.

Theoretical and observational evidence indicates that the winds of real O-stars and WR stars are *clumped*, which means that they contain inhomogeneities in their winds (Hillier 1984; Moffat et al. 1988; Nugis et al. 1998). Most model atmosphere codes that take clumping into account define some density enhancement D , which denotes the density contrast of the clumped material with respect to a homogeneous (i.e. non clumped) model with equal mass-loss rate (Schmutz 1997). Correspondingly a volume filling factor f of the clumps is defined as $f = 1/D$, if the wind medium between the clumps is considered void. Emission lines in WR stars are mainly formed by processes that scale with ρ^2 . Therefore, for a model with a certain clumping factor D , the same line equivalent width can be obtained as in the un-clumped model, by scaling down the mass-loss rate with a factor \sqrt{D} . This way clumping can be included in the expression for the transformed radius (Eq. 3.27), which then becomes:

$$R_t = R_* \times \left(\frac{v_\infty}{2500 \text{ km s}^{-1}} / \frac{\dot{M} \sqrt{D}}{10^{-4} M_\odot \text{ yr}^{-1}} \right)^{\frac{2}{3}} \quad (4.21)$$

Note that a constant value of R_t only guarantees equivalent width invariance of the part of the lineprofile that is formed by ρ^2 processes. The Thomson scattering wings are formed by processes that scale linear to the density, and increasing the clumping factor will not alter the strength of the wings, since the density enhancement is compensated by the smaller volume filling factor f . However, if at the same time mass loss is reduced to keep R_t constant, the Thomson scattering opacity is reduced, resulting in weaker scattering wings. Comparison of observations and model calculations show that smooth, un-clumped models overestimate the strength of the electron scattering wings. Since the inclusion of clumping in the models can reduce the strength of the wings, the too strong scattering wings in models with smooth wings are considered evidence for the presence of clumped winds around WR stars (Hillier 1984).

Hamann & Koesterke (1998b) used model spectra to derive clumping factors from observed galactic WR spectra. They found best fits of the models to the observations for a density enhancement of $D \approx 4$ for WN stars. Analysis of the optical and radio spectra of Galactic WR stars by Nugis et al. (1998) revealed values for WN stars of D between 0.7 and 8.7, with an average of $D = 2.4$.

Good estimates for the clumping factor are important for our study of the Baldwin-relations. If the clumping factor can be derived from the observed spectrum, or if a suitable average of D can be found, then clumping can be accounted for in the Baldwin-relations by scaling them with help of Eq. (4.21).

4.3.5 Line blanketing and photon loss

The last assumption in our ISA-WIND calculations that we want to discuss is the omission of line blanketing processes. The presence of millions of line transitions, mainly present in the photospheric region of the atmosphere and in the frequency domain mainly in the ultraviolet, can have dramatic influence on the ionization structure in the wind and on the star's spectral energy distribution. The ISA-WIND code does not yet include line blanketing processes; we therefore want to have an estimate of blanketing on the Baldwin-relations.

A thorough study of the influence of line blanketing processes on Wolf-Rayet star spectra has been done by Hillier & Miller (1998). One of their conclusions is that the inclusion of blanketing has far less influence on WN star spectra than it has on the spectra of WC stars.

For the WN star model they studied, they found noticeable weakening of the N III $\lambda 4640$ and the N IV $\lambda 4058$ features. However, for the optical and UV He I and He II lines, only small differences were found (mostly a few percent in line equivalent width). The reason for this is that the He I and He II transitions are mainly formed by recombination processes. In the wind volume region where the He II lines are formed, helium is almost fully double ionized. The He II transitions are therefore expected to be even less sensitive to ionization changes by blanketing than the He I lines.

We also want to mention the *photon loss* mechanism (Schmutz 1997). Photon loss is the assigned name for blending of one or more spectral lines with a strong line that is crucial in the settling of the ionization structure in the stellar wind (Schmutz 1997). A significant fraction of the photons of the optically thick radiation field of this strong line can escape through transitions of the blending lines. This can change the ionization balance in the wind. Photon loss mechanisms have been studied for Wolf-Rayet stars with the ISA-WIND code (Crowther et al. 1999). These authors found that photon loss processes, like line blanketing, seem to affect the ionization of WC star winds more severely than the wind ionization of WN stars. The reason is for the larger part the occurrence of strong photon loss of He II Lyman α radiation through transitions of blending oxygen lines (De Marco, private communication).

From the above we conclude that for the study of the Baldwin-effect of helium lines in WN spectra, line blending and blanketing processes are only of small influence. In chapter 5, where Baldwin-relations for WN stars will be presented, based on He-N models, we will therefore ignore blanketing processes in the models. Some caution is to be taken for models of WNL stars. As we saw in Sect. 4.3.2 for WNL models the degree of ionization of N can be of influence of the He ionization stratification. Since we saw above that the N ionization is affected by line blanketing, ignoring of line blanketing processes in the calibration of the Baldwin-relations may be less accurate for WNL stars.

4.3.6 Discussion

From the above study of assumptions in the ISA-WIND model atmosphere code, we conclude that pure helium models provide a good description for the helium spectrum of early WN type (WNE) stars. This is because we found that the influence of hydrogen content on the helium lines is low and most WN stars do not even contain significant amounts of hydrogen. The influence of nitrogen on the helium ionization was found to be small for WNE type models; only for the coolest WNE the inclusion of nitrogen is important.

For the modelling of late type WN stars (WNL), the conclusion is drawn that a good description of the nitrogen content is required. The accurate knowledge of the nitrogen content is necessary because of the strong affection of the helium continuum radiation field by N III continua. The resulting influence on the strength of the helium line spectrum illustrates the importance of an accurate determination of the nitrogen abundance for the calibration of the Baldwin-relations.

4.4 ISA versus CMF

Before the Baldwin-relations can be applied for the determination of stellar distances, we want to test the accuracy of the prediction of the Baldwin-relations with the ISA-WIND code. In the previous section we discussed the physical assumptions made in the ISA-WIND code. In this section, we will compare model calculations from the ISA-WIND code with those from the co-moving frame code from (Hamann 1985a; Hamann & Koesterke 1998a). We shall refer to the latter code as the POTSDAM code (see footnote on page 49). Before we shall compare the predictions of the ISA-WIND code and the co-moving frame code for different Wolf-Rayet star models, we give a brief outline of the method by which the POTSDAM code operates.

4.4.1 The POTSDAM model atmosphere code

The POTSDAM model atmosphere code calculates the radiative transfer from the co-moving frame of reference (CMF). The clear advantage of calculating the radiative transfer within the CMF is the fact that the mean line intensity is determined by a region that extends over only a few Doppler widths. However, to compute a synthetic spectrum, the radiative transfer has to be converted to the observers's frame. In general, CMF calculations are computationally more demanding but treat the line transfer correctly, whereas calculations with the Sobolev approximation (used in ISA-WIND) are significantly faster, due to simplifications in the radiative transfer equations.

Apart from the method to solve the radiative transfer, the ISA-WIND and POTSDAM codes have other differences:

- The POTSDAM code determines the density structure at the base of the wind from the assumption of hydrostatic equilibrium. In the ISA-WIND code, the equation of motion (Eq. 4.3) is solved.
- The electron temperature distribution in the POTSDAM code is calculated in non-LTE, with frequency dependent opacities (non-grey), from the assumption of radiative equilibrium. The ISA-WIND code uses the temperature structure of a grey atmosphere in LTE (see Sect. 4.2.4).
- In the POTSDAM code frequency redistribution of line radiation by electron scattering can be taken into account. In ISA-WIND this is not yet possible. In order to make a better comparison between the results from the two codes, we used POTSDAM models in which electron scattering was not included.
- Blanketing processes are currently being included in the POTSDAM code (Hamann & Koesterke 2000). Our grid of POTSDAM models does not yet include line blanketing. However, first results confirm previous findings that WN star spectra are less affected by blanketing processes than the spectra of WC stars (see Sect. 4.3.5).

4.4.2 Grid comparison

We obtained a grid of He-N models of the POTSDAM code for a luminosity of $\log(L/L_{\odot}) = 5.3$ and a terminal wind velocity of $v_{\infty} = 1600 \text{ km s}^{-1}$ (Koesterke, private communication). In Fig. 4.9 we compare equivalent width contours of the POTSDAM grid with a those of a grid of

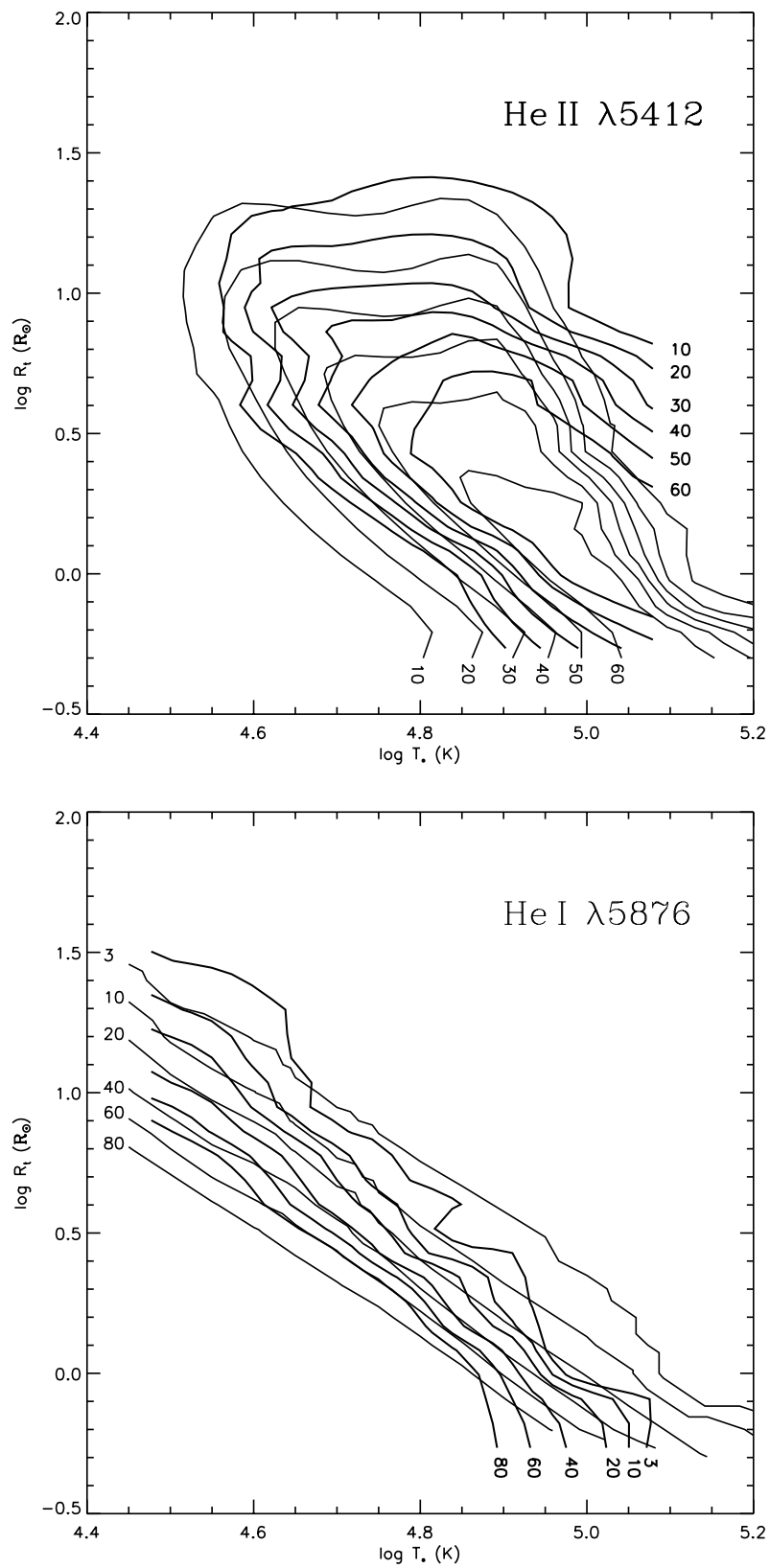


Figure 4.9: Equivalent width contours for the He II $\lambda 5412$ line (left panel) and the He I $\lambda 5876$ line (right panel). Countours are labeled with their equivalent width value in \AA . Thin lines represent the POTSDAM code models; the ISA-WIND models are shown as thick lines.

Table 4.1: Number of explicitly treated levels and line transitions for the ISA-WIND and the POTSDAM codes.

Ion	POTSDAM		ISA-WIND		ISA-WIND Crowther et al. (1999)	
	levels	lines	levels	lines	levels	lines
He I	17	55	17	136	17	136
He II	16	120	20	190	20	190
He III	1	0	1	0	1	0
N II	1	0	5	10	3	3
N III	33	118	14	91	40	780
N IV	38	153	12	66	44	561
N V	17	80	14	91	26	325
N VI	1	0	1	0	1	0

ISA-WIND models, for the diagnostic helium lines He II $\lambda 5412$ and He I $\lambda 5876$. These ISA-WIND models will be used in chapter 5 to present new, calibrated Baldwin-relations. The ISA-WIND models all have a terminal wind velocity of $v_\infty = 2000 \text{ km s}^{-1}$; the luminosity of the models lies between $\log(L/L_\odot) = 5.0$ and 5.5 .

Overall, the differences in equivalent width between the POTSDAM and the ISA-WIND models are not large. Differences mostly are between 10 and 20%, which is to be expected from the different methods used for the radiative transfer in the two codes and differences in atomic data. However, differences in the predicted equivalent width values of the two codes seem larger in the regime of low T_* values and high values of R_t , which covers the WNL type models. More specific, in this parameter domain, the equivalent width values of the He II line are lower in the ISA-WIND models, whereas for the He I line they are higher. The presence of differences in equivalent width for the WNL models is not surprising, as for WNL models the helium ionization structure is very sensitive to relatively small differences in temperature. The differences between the two code for the WNL models seem to be systematic. Since understanding the differences between the results of the two codes are important for the calibration of the Baldwin-relations, we will try to get more insight in the differences by comparing some specific POTSDAM and ISA-WIND models in the next section.

4.4.3 Model comparison

In this section we will present a comparison between model calculations from the POTSDAM and the ISA-WIND code. We are mainly interested in comparing those aspects that have a large influence on the outgoing line spectrum, as we keep the validation of the Baldwin-effect in mind. We will compare models for different temperatures and wind densities, so we can expect different ionization structures. We used POTSDAM models from the grid described in Sect. 4.4.2. We calculated specific ISA-WIND models to be able to compare both equivalent width values of the two codes as well as line profiles and atmosphere structures. In the calculated ISA-WIND models, we used the condition of hydrostatic equilibrium to calculate the density structure in the subsonic region of the atmosphere. This facilitates the direct comparison of the results of both codes, even though for the dense winds of WR stars models, the exact density structure of the subsonic wind region has little influence on the calculated spectrum.

Table 4.2: Basic parameters of the four WR star models for which the ISA-WIND code and the POTSDAM code are compared.

	A	B	C	D
T_* (kK)	89.1	50.1	44.7	31.6
R_t	2.51	12.59	3.98	10.0
R_* (R_\odot)	1.90	5.92	7.50	11.88
$\log \dot{M}$ ($M_\odot \text{ yr}^{-1}$)	-4.40	-4.69	-3.78	-4.08
v_∞ (km s^{-1})	1600	1600	1600	1600

Table 4.1 shows the number of atomic levels and line transitions explicitly treated in the two codes. Also listed are the atom data used in a study on WR star nebulae (Crowther et al. 1999), which in our discussion below will be of importance for WNL type models.

We will compare the ISA-WIND and POTSDAM codes for four different type of WR stars models. The main parameters of these models are give in Table 4.2. For each of the four models we will compare the results of the He II $\lambda 5412$ and the He I $\lambda 5876$ transitions, which are widely used as diagnostic lines in the study of WR spectra (e.g. Hamann & Koesterke (1998a)).

MODEL A First we look at a model with relatively high temperature. The stellar temperature of $T_* = 89.1$ kK is such, that the dominant ionization state is He III for most of the wind volume; this can be seen in Fig. 4.10. The agreement of the helium line profiles of the two codes is reasonable. Also the helium ionization stucture does compare well. The differences in the helium ionization are probably due to a combination of several effects, such as differences between the used model atoms, atom data (cross sections etc.), and the used method for the radiatibe transfer (Improved Sobolev Approximation versus co-moving frame). The differences in the line profiles is also partly caused by differences in the temperature structure. Although the He ionization structures of the two codes match well, the slightly lower temperature in the ISA-WIND code in part of the wind is sufficient to increase the recombination rate from He III to higher levels of He II. The result is a stronger He II $\lambda 5412$ feature in the ISA-WIND code. Indeed, the wavelength were the enhancement of the He II line in ISA-WIND is largest, corresponds to the velocity region were the largest discrepancy in the electron temperature is observed.

Although for our validation purposes of the Baldwin-effect we are mainly interested in the helium transitions, we also compare the nitrogen ionization balance in Fig. 4.10 for the ISA-WIND and the POTSDAM model. Clearly, differences in the N ionization are visible between the two models; although this may be partly due to the difference in the temperature structure, the discrepancies between the two codes for the nitrogen ionization are larger than for the helium ionization. However, due to the high stellar temperature of $T_* = 89.1$ kK, the nitrogen ionization balance does not affect the ionization balance of He, and no nitrogen continuum edges are visible in the spectral energy distribution of the two models (Sect. 4.3.2).

MODEL B Model B represents a slightly cooler star, with larger radius. The compared model characteristics are shown in Fig. 4.11. The dominant helium ionization stage is still He III, throughout the major part of the wind. The agreement of the spectral line profiles, is excellent, although because of the high He ionization, the He I line is barely visible. Of all models we

studied, model B shows the best agreement in the helium line profiles between the two codes.

The agreement between the two codes in the diagnostic helium lines gives good confidence in the comparability in result from ISA-WIND and the POTSDAM code.

Like for model A, the helium ionization structures agree well, whereas the nitrogen ionization shows larger differences. Again, however, there is no apparent influence of the nitrogen ionization on the helium spectrum.

MODEL C Model C represents a relatively cool star ($T_* = 44.7$ kK), with a high mass flux. The comparison for this model between the ISA-WIND and the POTSDAM code is shown in Fig. 4.12. The agreement for all helium lines, between the two codes, is reasonably good (see Fig. 4.12). If we look at the $3d^3$ level population (the upper level of the He I $\lambda 5876$ transition), we see that in the wind acceleration zone there is a disagreement of about one decade between the results of the two codes. This is reflected in the ionization balance. Compared to the POTSDAM code, He I and He II are overpopulated in ISA-WIND at the expense of the He III population. This explains He II $\lambda 5412$ to be slightly weaker in ISA-WIND whereas He I $\lambda 5876$ is stronger.

The differences between the two codes in the helium level populations can partly be explained by the difference in temperature structure at $h \approx 1 R_*$ and higher. A noticeable discrepancy in the helium ionization, however, is already present at lower heights above the stellar core, starting at $h \approx 0.01 R_*$. Indeed we find that not the temperature causes the main difference in helium ionization, but the effect of nitrogen in the atmosphere. From the spectral energy distribution, we notice the influence of N III continuum edges on the He II Balmer continuum; the influence of this on the helium ionization structure was discussed in Sect. 4.3.2.

Here we find that the N III $2p^2$ continuum edge at 261 \AA is much more prominent in ISA-WIND than in the POTSDAM code. It is likely, therefore, that the difference in the He II Balmer continuum between the codes is probably due to the different treatment of the nitrogen model atom (see Table 4.1).

MODEL D This model represents a relatively cool, low density wind. Fig. 4.13 shows the comparison between the ISA-WIND and the POTSDAM code for this model. The He line profiles don't agree well between the two codes. The equivalent width of the He I $\lambda 5876$ is $\approx 75\%$ higher in the ISA-WIND model than in the POTSDAM model, whereas the He II $\lambda 5412$ equivalent width is about 5 times lower.

From the He ionization balance and the temperature structure, it can be seen that the differences in line strength are caused by differences in temperature. In the major part of the wind, the temperature is lower in the ISA-WIND model than in the POTSDAM model, reducing the He III population in favour of He II and He I in the ISA-WIND model. Accordingly the He II line is weaker and the He I line stronger. The lower ISA-WIND temperature increases the N III population in the ISA-WIND model, affecting the He continua. This enhances the disagreement between the line profiles of the two codes.

Above, we compared the results from the ISA-WIND code and the POTSDAM code for four different WR star models. Agreement between the result of both codes was found to be good for models with a high value of T_* ; for cooler stars ($T_* \lesssim 45 - 50$ kK) larger differences between the results of the two codes were found. Differences in the predicted He line profiles from the two codes were found to be caused by a different treatment of the electron temperature structure and

possibly because of differences in the ionization balance of nitrogen, which affects the helium ionization.

We do not have a good explanation for the sometimes large differences in the nitrogen ionization. Partly, the differences seem to be caused by differences in the temperature structure, since, when moving outward to larger radii, the deviations of the N ionization start at approximately the same height as the discrepancies of the temperature structure (Figs. 4.10 to 4.13). However, the large difference in N ionization between the ISA-WIND and the POTSDAM code in the outer wind region is not explained by this. One explanation of these differences may be the lower number of N levels taken into account in the ISA-WIND than is used in the POTSDAM code (see Table 4.1). To test this we again show the comparison of the ISA-WIND and POTSDAM code results for model C (Fig. 4.14). This time, however, we used a more extensive model atom (De Marco, private communications), which was used in a study of WR 124 and its nebula M 67 (Crowther et al. 1999). Surprisingly, the agreement between ISA-WIND and the POTSDAM code is worse than for our result with the simpler model atom (Fig. 4.12). The stronger disagreement is caused by a stronger reduction of the He II Balmer continuum by N III continua. We can not explain the larger difference between the results from the two codes when a more sophisticated model atom is used in ISA-WIND.

4.5 Discussion and conclusions

Model atmosphere calculations over the years have proved to be a powerful tool in deriving stellar parameters for almost all Wolf-Rayet stars in the Galaxy and the Magellanic clouds. They have largely improved the knowledge about the structure and evolution of these stars. Nevertheless, different approaches have been followed in developing the spectral atmosphere codes, each with its own advantages and disadvantages. Comparisons between the results of different model atmosphere codes are scarce.

In Sect. 4.3, we studied the major assumptions of the ISA-WIND model atmosphere code, which treats the radiation transfer in the Sobolev approximation. It was found that pure helium models, as used to calculate the Baldwin-relations in Chapter 3, do not give an accurate prediction of the line equivalent width. To derive calibrated Baldwin-relations, nitrogen needs to be included. For accurate prediction of the Baldwin-relations with ISA-WIND models, the processes of wind clumping and Thomson scattering redistribution of line radiation have to be included in the model calculations. However, clumping can be accounted for by scaling of the Baldwin-relations, if a suitable average clumping factor can be found.

In Sect. 4.4, the results from the ISA-WIND code were compared to results from the POTSDAM co-moving frame code. The main conclusion drawn from the comparison is that particularly for WNL type models (low values of T_*), large differences can occur in the calculated line spectra, with a factor 5 difference in line equivalent width in extreme cases. These differences were found to be due to differences in the nitrogen ionization balance and to the different way in which the electron temperature structure is treated.

We were not able to explain the discrepancies in the nitrogen ionization of the two codes. It was found that the nitrogen ionization balance is highly sensitive to the used model atom, although increasing the number of atomic levels does not automatically lead to a more trustworthy ionization structure.

Interesting in this respect is the work of De Marco et al. (1999). They compared the ISA-WIND and POTSDAM codes for the WC8 star WR 135 and found good agreement for the helium

profiles. Nitrogen does not play a role in their study, which is why the helium spectra agree in their model comparison. However, in their model comparison they found disagreement between the two codes for the carbon ionization. A definitive explanation was not given, although it was suggested that the discrepancies are due to differences in the used model atoms. As a second possible cause for the different results of the two codes, the authors mentioned the different treatment of the radiative transfer: the Improved Sobolev Approximation in ISA-WIND and the co-moving frame method in the POTSDAM code. We think it possible that in our model comparisons the difference in the method used for the radiative transfer causes the differences in ionization; we found the discrepancies in the nitrogen ionization between the two codes to be largest in the outer regions of the wind, where the velocity gradient is low and the Sobolev approximation is less accurate.

Overall, we conclude that the cause of the different results between the ISA-WIND and the POTSDAM code is twofold:

- I.** Discrepancies between spectra from the two codes can largely be explained from the different treatment of the electron temperature distribution. Since the calculation of the NLTE temperature structure from the condition of radiative equilibrium is not straightforward and depends strongly on the chemical elements included and line transitions in the model, it is not *a priori* clear that this kind of temperature structure is to be preferred above the temperature structure of a grey atmosphere in LTE.
- II.** The inclusion of nitrogen in the modelling of WN type stars has influence on the helium ionization structure. Differences between the nitrogen model atoms used in the two codes probably have a different effect on the helium spectrum, causing discrepancies in the helium line profiles. It is not clear which code treats the nitrogen in the most correct way.

Based on the above two statements, we conclude that our ISA-WIND model calculations have a sufficiently physical temperatures structure and a sufficiently accurate treatment of the nitrogen atom structure. However, the differences in equivalent width between our model calculations and those from the POTSDAM code remain a source of uncertainty in the calibration of our Baldwin-relations. For our application of model atmosphere and spectra calculations to determine Baldwin-relations, the differences in the result of the ISA-WIND and the POTSDAM model atmosphere code is somewhat discouraging. It means that shortcomings are present in today's model atmosphere codes that can have a significant effect on the prediction of stellar parameters and the shape of synthetic spectra.

For the hottest WN stars (i.e. stars of the WNE class), we conclude that the predicted strength of the He lines, and hence the theoretically predicted Baldwin-relations, are reliable. For the cooler WN stars (the WNL type stars), the accuracy of the prediction of the He line strengths is not always sufficient to apply the predicted Baldwin-relations for the determination of stellar distances. An *empirical calibration* of the Baldwin-relations is therefore recommended. The validation and calibration of the predicted Baldwin-relations will be the subject of Ch. 5.

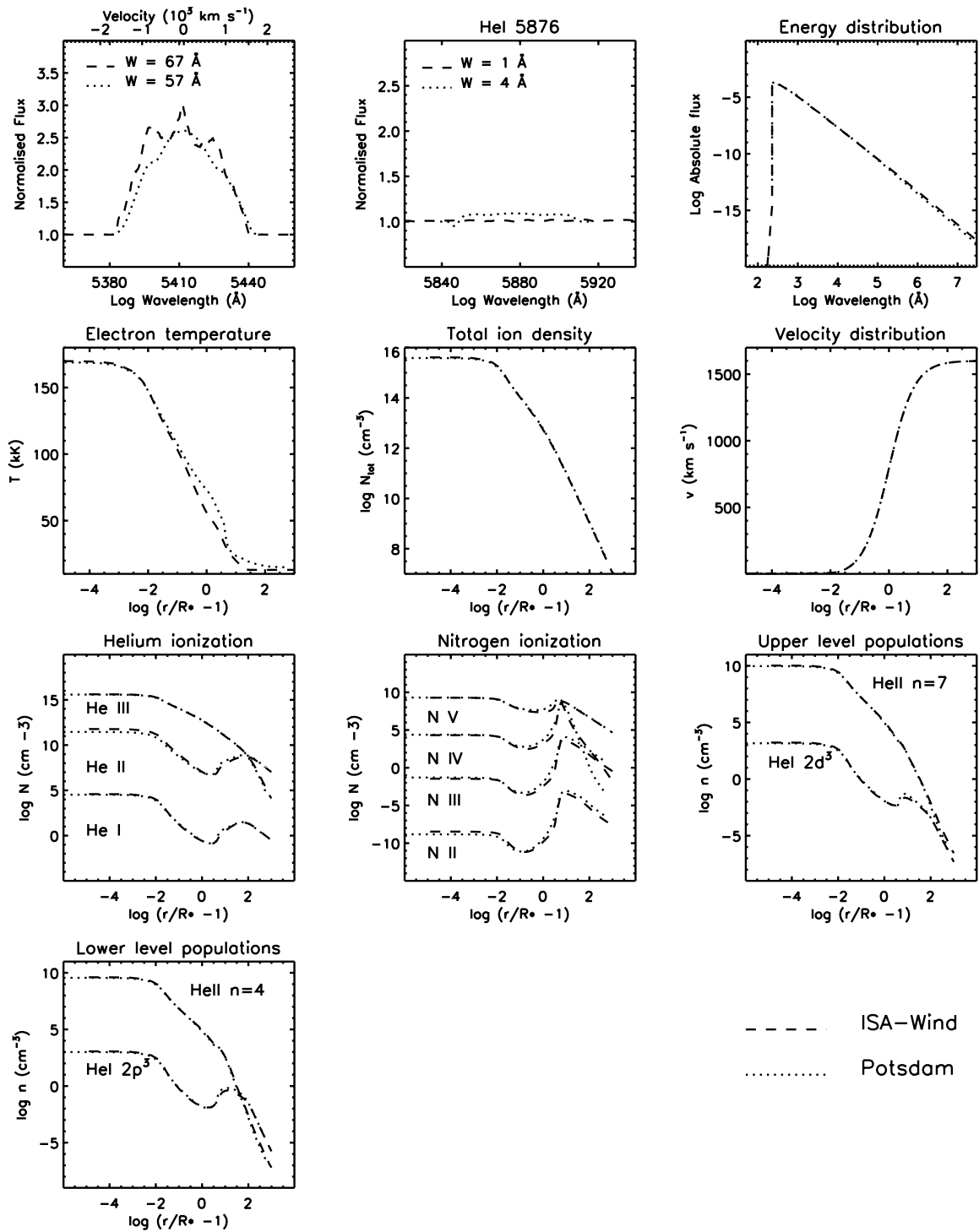


Figure 4.10: Comparison of the ISA-WIND and the POTSDAM code for helium line profiles and different atmosphere characteristics of model A. Dashed lines refer to the ISA-WIND model, dotted lines to the POTSDAM model. Shown are, successively from left to right, from top to bottom: the He II $\lambda 5412$ profile, the He I $\lambda 5876$ profile, the spectral energy distribution, the electron temperature distribution, the total ion density distribution, the velocity structure, the helium ionization balance, the nitrogen ionization balance, and the population of the upper and lower levels, respectively, of the afore mentioned He II and He I transitions.

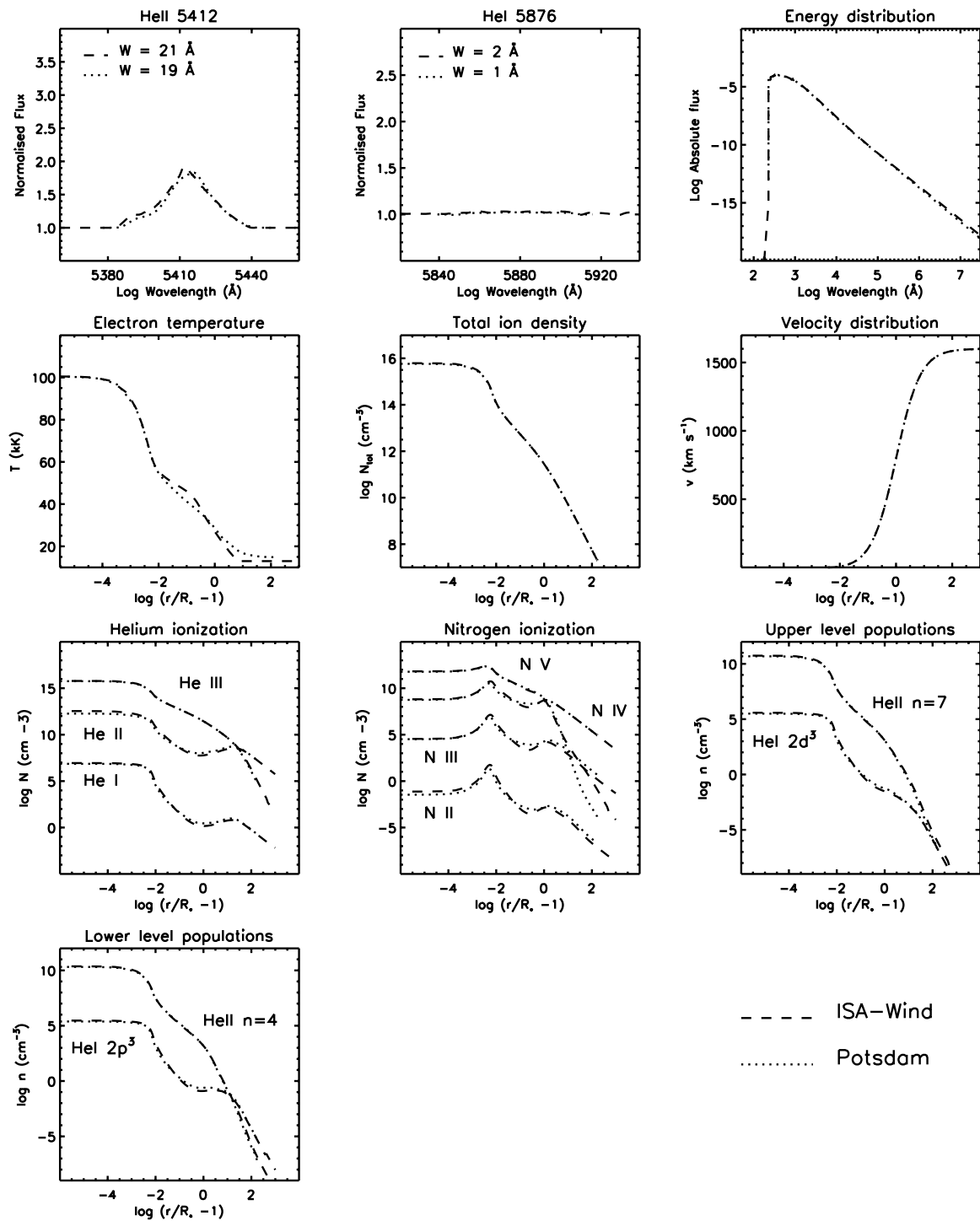


Figure 4.11: Comparison of the ISA-WIND and the POTSDAM code for helium line profiles and different atmosphere characteristics of model B. For explanation, see text below Fig. 4.10.

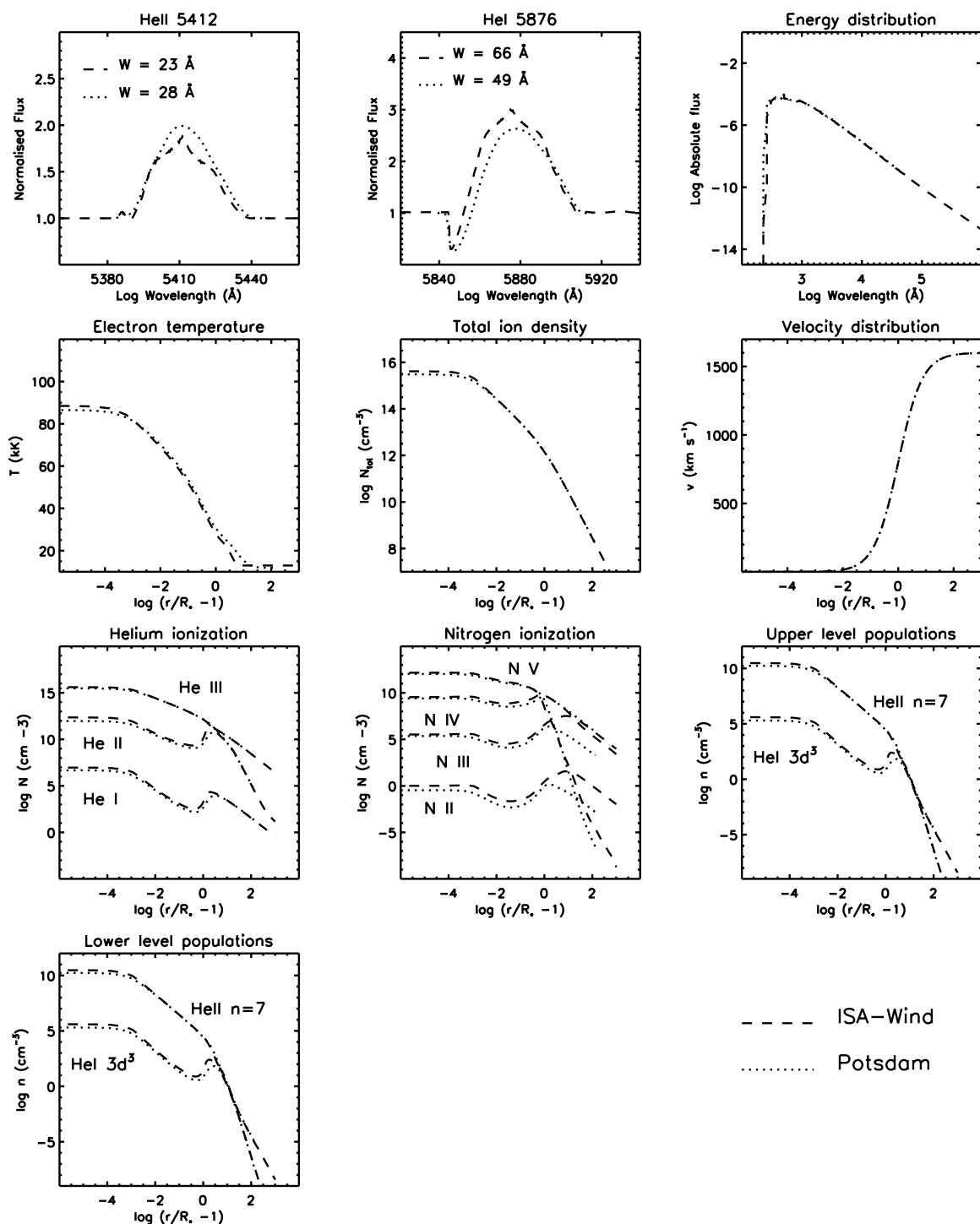


Figure 4.12: Comparison of the ISA-WIND and the POTSDAM code for helium line profiles and different atmosphere characteristics of model C. For explanation, see text below Fig. 4.10.

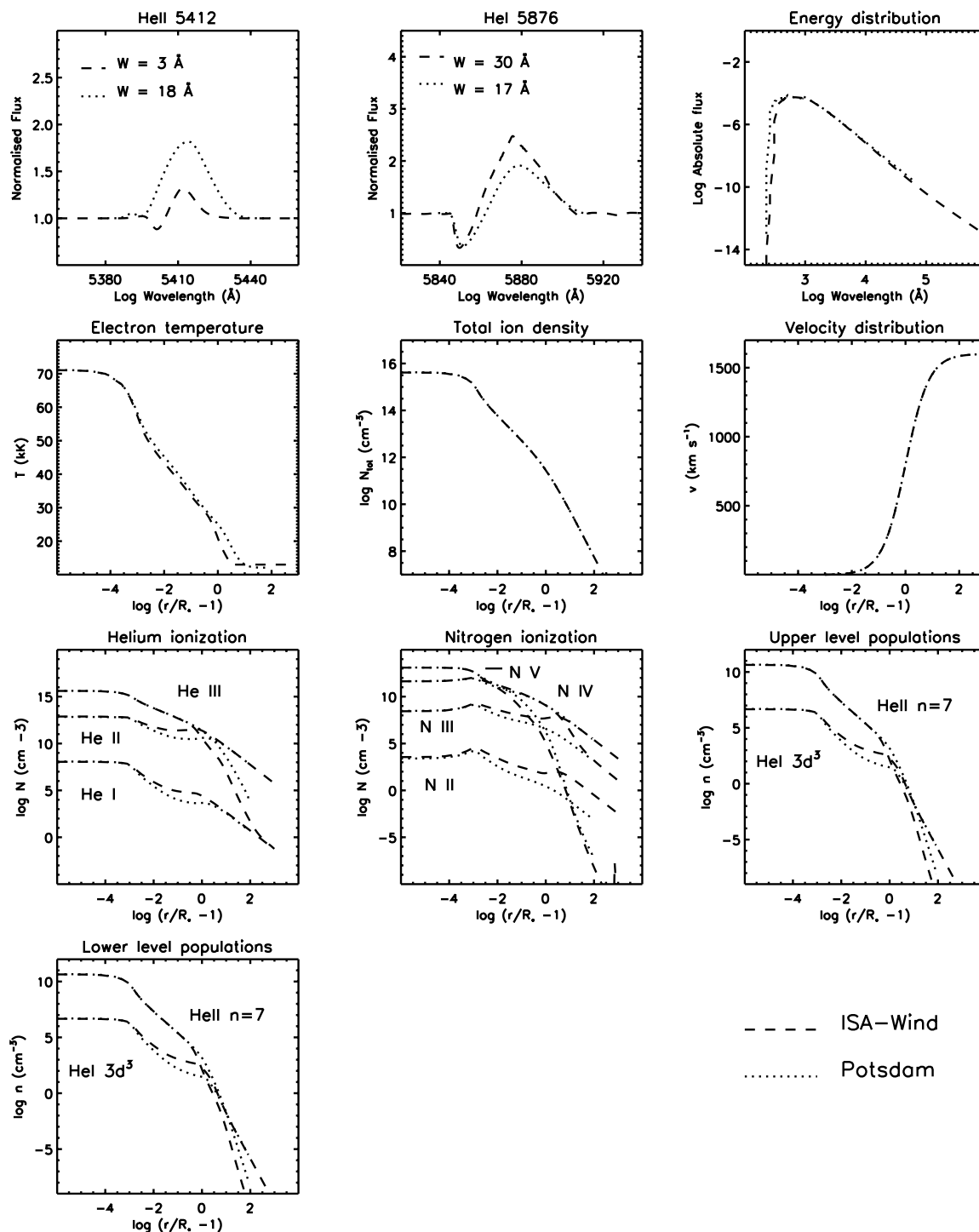


Figure 4.13: Comparison of the ISA-WIND and the POTSDAM code for helium line profiles and different atmosphere characteristics of model D. For explanation, see text below Fig. 4.10.

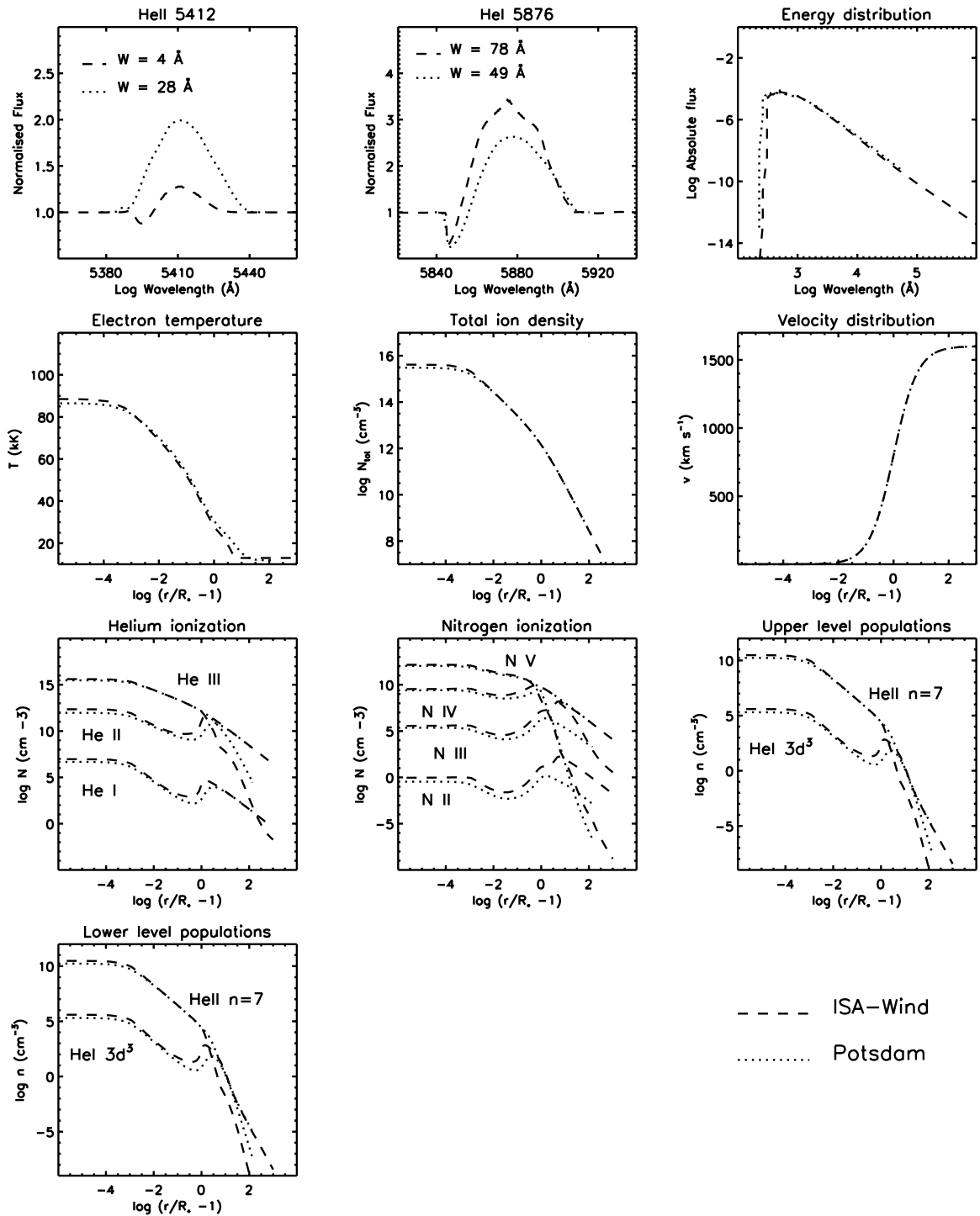


Figure 4.14: Comparison of the ISA-WIND and the POTSDAM code for helium line profiles and different atmosphere characteristics of model C. In the ISA-WIND model, more atomic levels have been used for nitrogen than in the comparison presented in Fig. 4.12. For further explanation, see text below Fig. 4.10.

The validation of predicted Baldwin-relations from He-N models for WN stars

5.1 Introduction

Spectral observations of WN stars in the Large Magellanic Cloud (LMC) show a relation with negative slope between the line equivalent width and monochromatic continuum luminosity at the line wavelength for emission line features (Morris et al. 1993a). This is the *Baldwin-effect*, named after a similar relation found for Active Galactic Nuclei (AGNs) by Baldwin (1977).

In van Gent et al. (2000) (or this book, Ch. 3) relations have been presented between line equivalent width and monochromatic continuum luminosity for five He II transitions of Wolf-Rayet star model spectra. From these *Baldwin-relations* and the study of model atmospheres, it was found that the Baldwin-effect is caused by differences in wind density among stars.

The Baldwin-effect can in principle provide a powerful independent tool to measure stellar distances from the observed spectra. In order to apply the Baldwin-relations as a distance measuring tool, one needs to have some knowledge about a star's mass-loss rate and effective temperature (see Sect. 5.7). Furthermore, it is also required to perform a good calibration of the Baldwin-relations, taking into account all major assumptions made in the model calculations. The influence of these assumptions on the line equivalent width has been the subject of chapter 4.

In chapter 3 we used simple mathematical expressions, followed by detailed model atmosphere calculations to get insight in the physical processes that cause the Baldwin-effect of He II emission lines in WN star spectra. Here we briefly repeat the main results from that chapter.

A given sample of WN stars will show an inverse correlation between the equivalent width of He II emission features and the monochromatic continuum luminosity at the central wavelength of the considered spectral line. The cause of this Baldwin-effect was found to be caused by differences in radius among stars. Different temperatures, mass-loss rates, and terminal wind velocities cause a spread in the relation.

For the Baldwin-effect to occur in He II lines, helium needs to be (almost) fully double ionized over the line forming region of the stellar wind. If there are stars in the considered sample for which this is not the case (because they are too cool or have a too dense wind), the relation between line equivalent width and continuum luminosity will be less prominent or not be present at all.

The Baldwin-relations presented in Ch. 3 were not meant to be directly applicable to measure stellar distances. The goal of that study has been merely to give insight in the physical

phenomena behind the Baldwin-effect. Furthermore, those Baldwin-relations are based on pure helium model atmospheres. As will be explained further on in this chapter, the pure helium approach is a too crude assumption for the accurate prediction of Baldwin-relations.

In this chapter we will present new Baldwin-relations, based on model atmospheres consisting of helium and nitrogen. These relations will be calibrated by considering the model assumptions, described in Ch. 4 and by testing the relations with observed spectra of LMC WN stars, of which the distance is accurately known.

The used LMC WN stars spectra are described in Sect. 5.2. The new model atmosphere calculations and the corresponding synthetic spectra will be described in Sect. 5.3, which is followed by the presentation of new predicted Baldwin-relations (Sect. 5.4). The main model assumptions and their influence on the Baldwin-relations will be discussed in Sect. 5.5. Sect. 5.6 treats the validation of the new Baldwin-relations as distance estimators. In Sect. 5.7 a new strategy to measure WN stars distances by means of the Baldwin-relations will be presented. Discussion and concluding remarks follow in Sect. 5.8.

5.2 Observations

The spectra of LMC WN stars used for this study consist of ultraviolet (UV) and optical observational data. The UV data were obtained from the archive of the International Ultraviolet Explorer (IUE) satellite. The observations were performed using the Short Wavelength Prime (SWP) spectrograph, covering the wavelength range of 1150-2000 Å. The optical data were obtained over several years with the 1.5 m. telescope of the CTIO facility in Chile. A more extensive description of the reduction of the optical data can be found in Torres-Dodgen & Massey (1988). For more details on the UV and optical data, see Ch. 2.

5.3 Model atmospheres

Models were calculated with the non-LTE model atmosphere code ISA-WIND. For a detailed description of this code we refer to de Koter (1993, 1997), and the discussion in Chapter 4. Here, we only mention the main properties.

The geometry of the models is that of a spherically symmetric, stationary outflow. Both photospheric and stellar wind structure are calculated (unified atmosphere), as opposed to the core-halo approach, in which the photospheric radiation field is defined as input at the base of the extended envelope of the model star. In the unified models, the density and velocity structures as function of radius are connected through the equation of mass continuity:

$$\dot{M} = 4\pi r^2 \rho(r) v(r), \quad (5.1)$$

where \dot{M} is the mass-loss rate, r is the radial distance from the stellar centre, ρ is the density, and v is the velocity. For each model the mass-loss rate is assumed to be time-independent.

The equations that describe the transfer of the continuum radiation through the atmosphere are solved under the constraint of statistical equilibrium, through the method of approximate lambda iteration. For the line radiation transfer an improved Sobolev approximation (ISA) is used, which takes into account the diffuse radiation field in the outflowing atmosphere, as well as continuum processes within the line resonance volume (Puls & Hummer 1988).

5.3.1 Atmosphere structure

The photospheric density structure in each model is determined by an inner radius, R_* , which determines the size of the *core* underlying the outflowing atmosphere, the effective gravity acceleration, g_{eff} , and the density at the core, ρ_* . The latter is chosen such, that the total Rosseland optical depth, κ_R , has a value between 20 and 25. Following Hamann (1985a), and follow up papers, we set the scale height in the photosphere by assuming $\log(g_{\text{eff}}) = 3.5$ for WN stars. With the above parameters setting the boundary conditions, the density structure then follows from the solution of the momentum equation for a stationary wind. This equation is given by

$$v \frac{dv}{dr} + \frac{1}{\rho} \frac{dp}{dr} + \frac{GM(1-\Gamma)}{r^2} = 0 \quad (5.2)$$

with velocity field v , gas pressure p , and stellar mass M . Radiative acceleration by electron scattering is included in the equation by the parameter Γ , which denotes the ratio between radiative and gravitational acceleration:

$$\Gamma = \frac{g_{\text{rad}}}{g_{\text{N}}} = \frac{\sigma_e L}{4\pi c GM} = 7.66 \times 10^{-5} \sigma_e \left(\frac{M}{M_\odot} \right)^{-1} \left(\frac{L}{L_\odot} \right) \quad (5.3)$$

where L is the stellar luminosity and σ_e the Thomson scattering coefficient. In the subsonic region the velocity structure follows from the density structure by using the equation of mass continuity (Eq. 5.1).

In the wind region a β -type velocity law is used

$$v(r) = v_\infty \left(1 - \frac{r_0}{r} \right)^\beta \quad (5.4)$$

and the corresponding density structure follows from mass continuity. The photosphere and wind regions are smoothly connected by requiring continuity of both the velocity field and its gradient. These conditions are met by iteratively solving for the radius where the two regions are connected, r_{con} , and the parameter r_0 in Eq. (5.4). It turns out that r_{con} lies close to the sonic radius.

For the models with the densest wind this smooth connection of the two velocity fields fails; in those cases a β -law was used to describe the velocity field through the whole atmosphere.

The bolometric luminosity is specified by the *stellar temperature*, T_* , as

$$L = 4\pi R_*^2 \sigma T_*^4, \quad (5.5)$$

where T_* corresponds to the effective temperature at the core radius, R_* , of the model. T_* is not the real effective temperature T_{eff} , as R_* is not the effective radius. A unique effective radius is hard to define, as it is intrinsically wavelength dependent. We will define the radius, R_{eff} , as the radial distance where the thermalization optical depth equals $1/\sqrt{3}$ at $\lambda = 5500 \text{ \AA}$ (Schmutz et al. 1990). This radius thus follows from the model output, as does T_{eff} , through the luminosity and the radius.

The electron temperature structure follows from the assumption of radiative equilibrium in a grey atmosphere in local thermodynamic equilibrium (LTE). We allow the temperature to drop with radius down to a minimum temperature T_{min} , after that it remains constant. In the former pure helium models, we used a value of $T_{\text{min}} = T_*/2$, suggested for O-stars by Drew (1989).

Table 5.1: Number of explicitly treated levels and line transitions for the ISA-WIND and the POTSDAM codes.

Ion	POTSDAM		ISA-WIND	
	levels	lines	levels	lines
He I	17	55	17	136
He II	16	120	20	190
He III	1	0	1	0
N II	1	0	5	10
N III	33	118	14	91
N IV	38	153	12	66
N V	17	80	14	91
N VI	1	0	1	0

Model calculations for Wolf-Rayet stars in which the temperature distribution is fully calculated in non-LTE, under the assumption of radiative equilibrium, indicate that the temperature drops in the outer wind regions to a value roughly between 9 and 15 kK, independent of the value of T_* (Koesterke, private communication). From this, and based on non-LTE temperature distributions presented in Hillier (1988) and Hamann et al. (1994), we choose a constant value of $T_{\min} = 13$ kK for the new models.

5.3.2 Chemical composition

The models are composed of helium and nitrogen. The nitrogen abundance is set at constant value of 1.5% by mass, following the galactic average used by Hamann & Koesterke (1998a). Although the inclusion of nitrogen is generally thought to be of little influence on the ionization and line equivalent width of helium (e.g. Hamann & Koesterke 1998a), particularly for late type Wolf-Rayet star models (WNL stars), the influence can be substantial (Ch. 4, Sect. 4.3.2 and 4.4.3).

The model atoms used in the calculations are presented in Table 5.3.2. Compared to the pure helium models, used in Ch. 3, we increased the number of He II levels in our models from 10 to 20. This was found to be necessary to get sufficiently strong He II lines at the highest values of T_* in the model grid.

5.3.3 Convergence

Most models were found to converge well. Like for the pure helium models, as a criterium for convergence we required that for two succeeding iteration steps the populations of all atomic levels at all radii to differ not more than 0.1 %.

For some models this criterium was not met; those models kept “flipping” between two solutions that differed mostly less than 1 percent. In those cases it was also found that the two solutions result in almost identical synthetic spectra, with less than one percent difference in flux levels at all wavelengths. Therefore we included those cases in our model sample.

Table 5.2: Helium transitions for which the Baldwin-effect is presented.

Central wavelength (Å)	Levels $n - m$	
He I	5876	3d ³ -2p ³
He II	1640	3-2
He II	2511	7-3
He II	2533	6-3
He II	3203	5-3
He II	4686	4-3
He II	5412	7-4

5.3.4 Synthetic spectra

We calculated synthetic spectra by solving the radiative transfer equations through the model atmospheres. Spectra were calculated for the same five He transitions given in Table 5.2. In addition, spectra were calculated for two He I transitions, as it was found that for the lowest temperatures in our grid they also show a Baldwin-effect. The line transitions for which spectra were calculated are listed in Table 5.2

The reason for selecting these lines is that they belong to the strongest helium lines in observed Wolf-Rayet star spectra, and that they are relatively free of blends by other lines. For example, in many observed Wolf-Rayet spectra the He II Balmer lines from even numbered upper levels suffer from blends from the hydrogen Lyman series. This may hamper the applicability of the Baldwin-effect in those WN stars that have still significant hydrogen left (i.e. mostly the WNL-type stars). The He II $\lambda 10124$ transition, included in the calculations of Ch. 3, was left out of the He-N calculations. This line was found to show a Baldwin-effect over only a very limited range in the equivalent width versus continuum luminosity domain. The strong He I transition at 10830 Å would in principle be useful in the study of the Baldwin-effect. This line is formed over a large part of the wind volume, however, and it was found very hard to accurately predict this line. This is due to its high sensitivity to fixed model parameters such as the minimum temperature, T_{\min} .

Some major assumptions in our model atmospheres that may influence the appearance of the spectra are: *i*) the assumption of spherical symmetry, *ii*) a homogeneous density distribution, i.e. the effects of clumping are ignored, and *iii*) we ignore the effect of electron scattering of line radiation. The influence of these assumptions will be discussed in Sect. 5.5.

5.4 The synthetic Baldwin-effect for He-N models

5.4.1 Grid parameters

We calculated a grid of atmosphere models that covers virtually the whole range of basic stellar parameters as they occur in real Wolf-Rayet stars (Hamann & Koesterke 1998a). We chose a terminal velocity of 2000 km s^{-1} , which is a good representation for the average velocity found in galactic and LMC WR stars. The parameters of our model grid are presented in Table 5.3.

Table 5.3: Input parameters of the ISA-Wind model atmospheres

R_* (R_\odot)	1,2,3,5,10,15,20,30
T_* (kK)	30,35,40,50,60, 70,80,90,100,120
v_∞ (km s^{-1})	2000
$\dot{M}/v_\infty(10^{-5}M_\odot\text{yr}^{-1})/(10^3 \text{ km s}^{-1})$	0.5, 1.0, 2.5, 5, 10
$\log g$	3.5
β	1

5.4.2 Line profiles and ionization

The majority of the He II line profiles in our model spectra are almost purely in emission. This indicates that recombination processes are the main mechanism behind the line formation in most of our models and that in the line formation region of the He II transitions, the dominant ionization stage is He III. At lower values of T_* , scattering processes may dominate over recombination, resulting in a P Cygni component in the line profiles.

The He I profiles only show strong emission in the lower temperature range of our grid, roughly between 30 kK and 50 kK (depending on the wind density). Going to higher values of T_* , most helium becomes doubly ionized and the He I lines disappear.

In chapter 3 we found that for the He II lines to show a Baldwin-effect, helium must be almost completely double ionized to He III. For that reason we did not expect a Baldwin-effect to be visible for He I recombination lines, as this would require a similar degree of ionization for He II for stars wind different wind densities. The He II population is found to vary strongly with wind density, however, for the majority of our models.

Interestingly enough, for low stellar temperatures He II is the dominant ionization stage in the major part of the wind, particularly in the outer wind region. As the He I line are generally formed further out in the wind than the He II lines, the He I lines do show a Baldwin-effect, for models with low T_* , whereas the He II line do not.

To illustrate this, helium line profiles of WNL type models are shown in Fig. 5.1, together with the spectral energy distributions (SEDs). The corresponding ionization structures of helium and nitrogen are shown in Fig. 5.2. The shown models differ only in core radius, R_* . The stellar temperature is $T_* = 40$ kK, the mass-loss rate is $2 \times 10^{-4} M_\odot \text{yr}^{-1}$, and the terminal wind velocity is 2000 km s^{-1} .

Clearly, for the largest part of the wind volume, the dominant ionization stage is He II for models with a small core radius. When going to larger radii (less dense wind), the ionization gradually shifts from He II to He III. This makes that in going from high to low wind densities, the He II equivalent width rises, whereas the He I line equivalent width drops. The monochromatic continuum luminosity at the central wavelength of the line increases with core radius for both the He I and the He II transition, simply following the R_*^2 proportionality of the SED (Fig. 5.1 c).

So, despite the lower density at large core radii, the increased He III population leads to an increase of the He II line equivalent width with monochromatic continuum luminosity, a behaviour opposite to the Baldwin-effect. At the same time, the He I equivalent width drops with rising continuum luminosity, both because of the lower wind density at larger R_* and the lower He II population. The He I line therefore shows a steep Baldwin-relation.

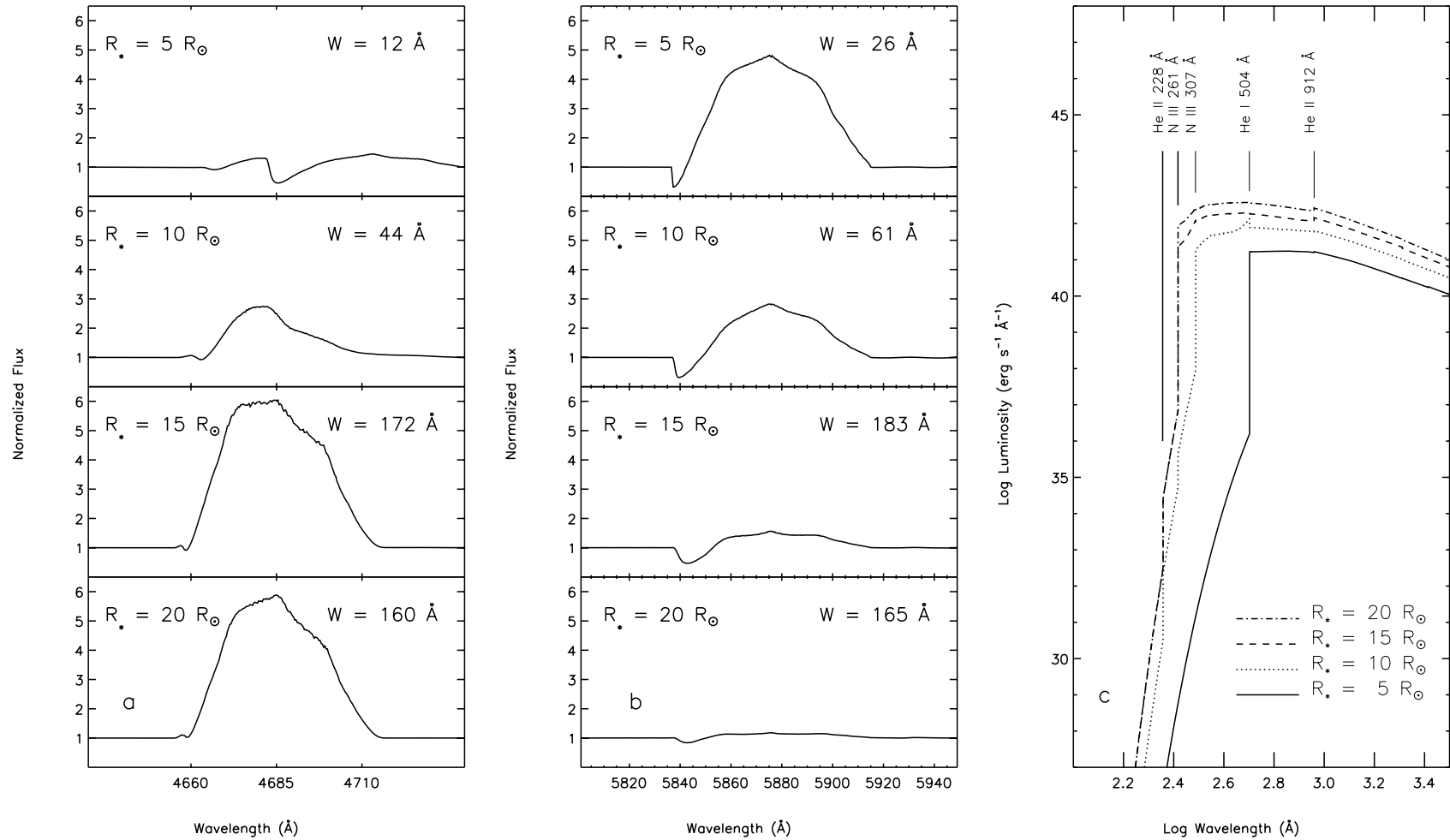


Figure 5.1: Four WNL star models that show the variation of line equivalent width with wind density. Panel a: Continuum normalised spectra of the He II $\lambda 4686$ transition. W is the equivalent width in \AA . Panel b: Continuum normalised spectra of the He I $\lambda 5876$ transition. Panel c: Corresponding spectral energy distributions. R_* indicates the core radius in R_\odot . For all four models: $T_* = 40\text{kK}$, $\dot{M} = 2 \times 10^{-4} M_\odot \text{ yr}^{-1}$, and $v_\infty = 2000 \text{ km s}^{-1}$. Going from small to large core radius, the equivalent width of the He II line increases, whereas that of the He I line drops. The latter line therefore shows a Baldwin-effect.

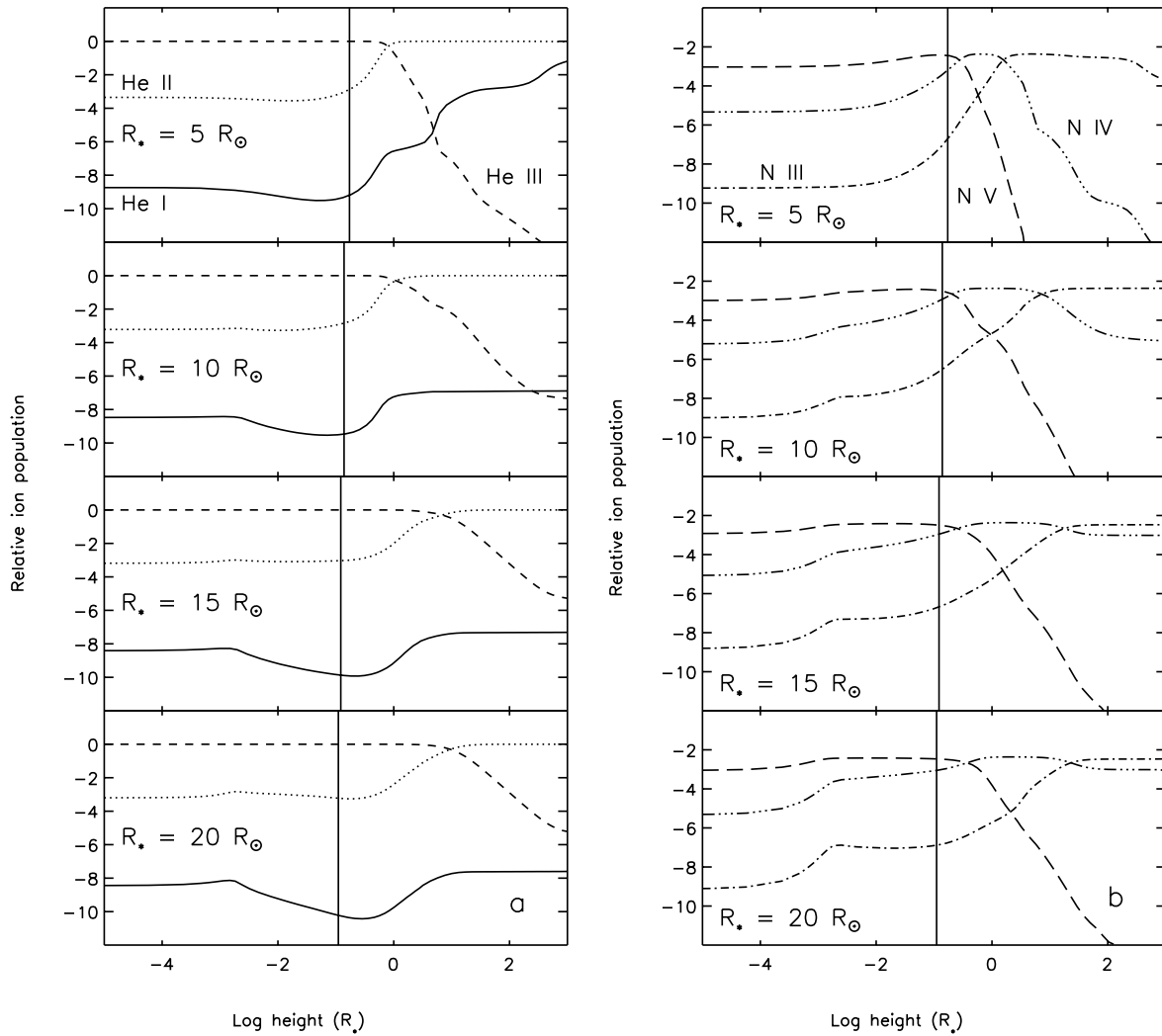


Figure 5.2: Ionization structure of helium (panel a) and the most important nitrogen ions (panel b). Shown is the relative ion population as function of height above the stellar core. R_* indicates the core radius. Vertical lines indicate the effective radius. The shown models are the same as those used for Fig. 5.1. The different line styles represent different ionization stages, as indicated in the top panels.

The fact that He I transitions can also show the Baldwin-effect may prove to be very helpful in applying the Baldwin-relations for the determination of stellar distances of WNL stars. After all, it is the WNL regime in our model grid where the Baldwin-effect of the He II lines breaks down. Fortunately, the He I lines take their place.

So far, we only considered the helium ionization. However, the presence of nitrogen in the model atmospheres has some influence on the He line equivalent width and through that plays a role in the determination of the slope of the He Baldwin-relations. The SEDs show two N III continuum edges, at 261 and 307 Å, respectively. Although the radial optical depth in the He I continuum (below 504 Å) reduces with decreasing wind density (increasing R_*), this effect is reduced by the N III continua, which leads to weaker He lines compared to pure He atmospheres. Compared to a pure He atmosphere, the radiation field and the gas are therefore stronger coupled in the He-N models (see the discussion in Ch. 4.3.2), which means that electron

temperature structure in a He-N model plays a larger role in the ionization balance. Since the temperature structure drops with radial distance, a He-N model of a WNL star will show weaker He II lines and stronger He I line than a similar model that only consists of helium. This will not occur at higher values of T_* , where the N III population decreases in favour of higher ions.

5.4.3 Theoretical Baldwin-relations for WN stars

We present new Baldwin-relations for WN star helium lines in Figs. 5.3 to 5.9. For the He II lines (Fig. 5.3 to 5.8), the relations generally “tumble over” at smaller core radii, where the wind density is high and the dominant helium ionization stage shifts from H III to He II. At the low density end (small mass-loss rate, large R_*), the Baldwin-relations break down because the wind becomes optically thin. The line emission therefore does not originate completely from the wind anymore, but partly from the photosphere. The He I $\lambda 5876$ line shows a Baldwin-effect over the whole wind density range, but only at the lowest values of T_* . At higher T_* , most He II has disappeared in favour of the He III stage, which makes the He I lines disappear.

5.5 Model assumptions

Assumptions in the calculations of the model atmospheres and spectra introduce uncertainties in the predicted equivalent width values. Therefore, before the Baldwin-relations can be applied for determining stellar distances, we must now the uncertainties in the Baldwin-relations introduced by these assumptions, and calibrate the Baldwin-relations, if required. To do so, we will discuss the three assumptions in the model calculations that have the largest effect on the predicted line equivalent widths. These are the assumption of a constant nitrogen abundance, the assumption of a smooth, monotonically decreasing density structure in the wind and the neglect of Thomson scattering in the formation of spectral lines.

Several other assumptions exist in the models which generally have less influence on the predicted Baldwin-relations. However, they can still be important. For example, we neglected the effects of line blending and blanketing on the the ionization structure in the model calculations. Although in general the inclusion of these effects is not expected to have a dramatic influence on the shape of the Baldwin-relations (Ch. 4.3.5), tailored studies on specific WR stars do show changes in derived stellar parameters if blending and blanketing effects are included (e.g. Crowther et al. 1999; De Marco et al. 2000).

The final calibration of the Baldwin-relations therefore has to be performed by means of stars at well known distance, for which parameters have been reliably derived (Sect. 5.6).

5.5.1 Nitrogen abundance

As indicated in Sect. 5.3.2, we have adopted a constant nitrogen abundance in our models of 1.5 % by mass. This is the Galactic average as used by Hamann & Koesterke (1998a). However, we have seen in Sect. 5.4.2, that nitrogen influences the ionization structure of helium because of the presence of N III continuum edges in the UV wavelength range. Nitrogen therefore also affects the strength of the helium lines. The He line strength is thus expected to depend on the nitrogen abundance. This is important for the application of the Baldwin-relations as a distance estimator, since it would mean that knowledge about the chemical composition of a star must

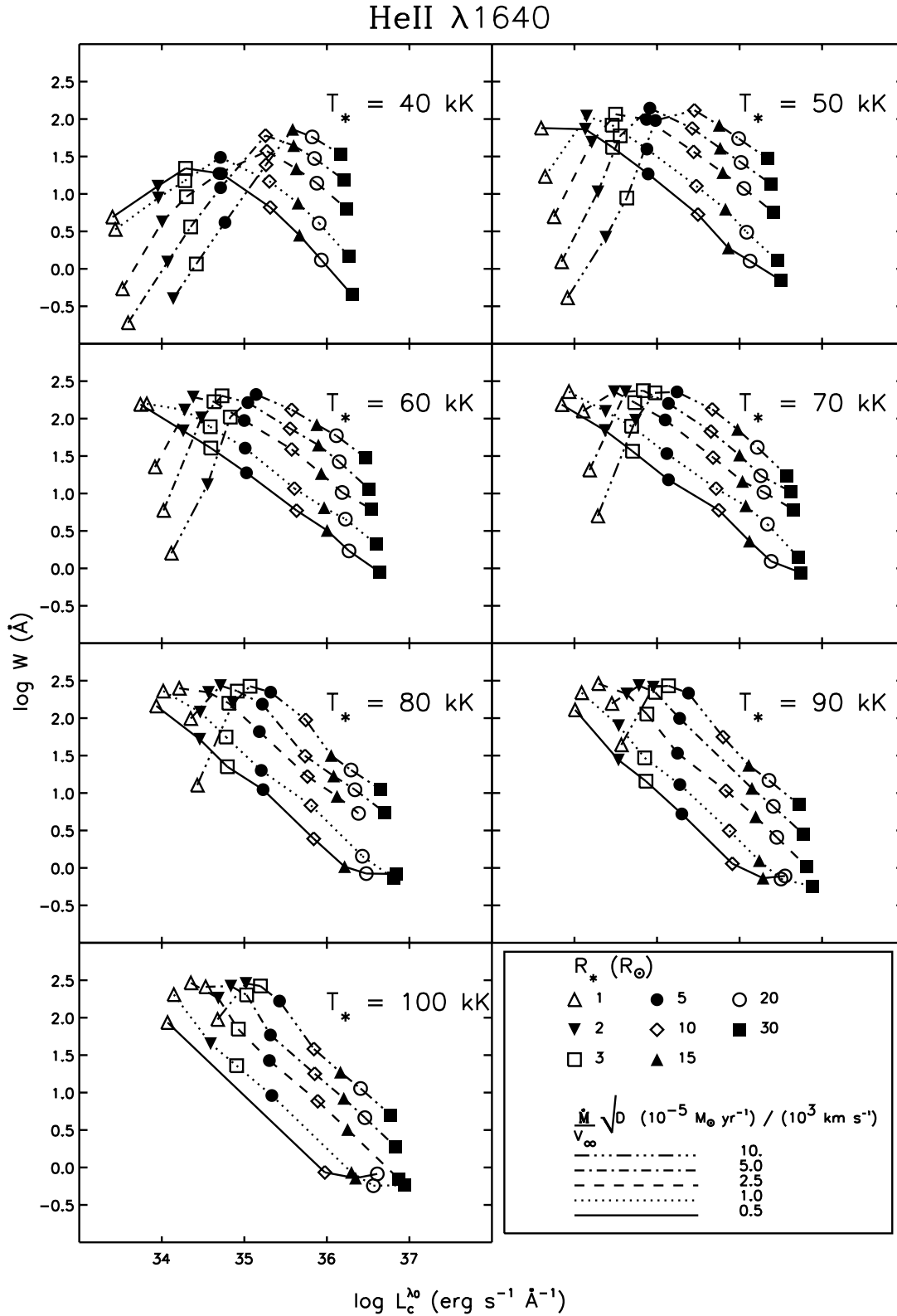


Figure 5.3: Line equivalent width W vs. monochromatic continuum luminosity $L_c^{\lambda_0}$ for the He II $\lambda 1640$ line. Each panel shows $\log(W)$ as function of $\log(L_c^{\lambda_0})$ for models with the same value of T_* , and for different values of \dot{M} and R_* . The terminal wind velocity is $v_\infty = 2000 \text{km s}^{-1}$ for all models. Models with the same value of \dot{M} are connected by lines; the values of R_* are indicated by symbols. Line styles and symbols are explained in the bottom right panel. The relations follow from unclumped models. For stars with clumped winds and clumping factor D , the Baldwin-relation corresponding to $\dot{M} \sqrt{D}$ applies, (see Sect. 5.5.2).

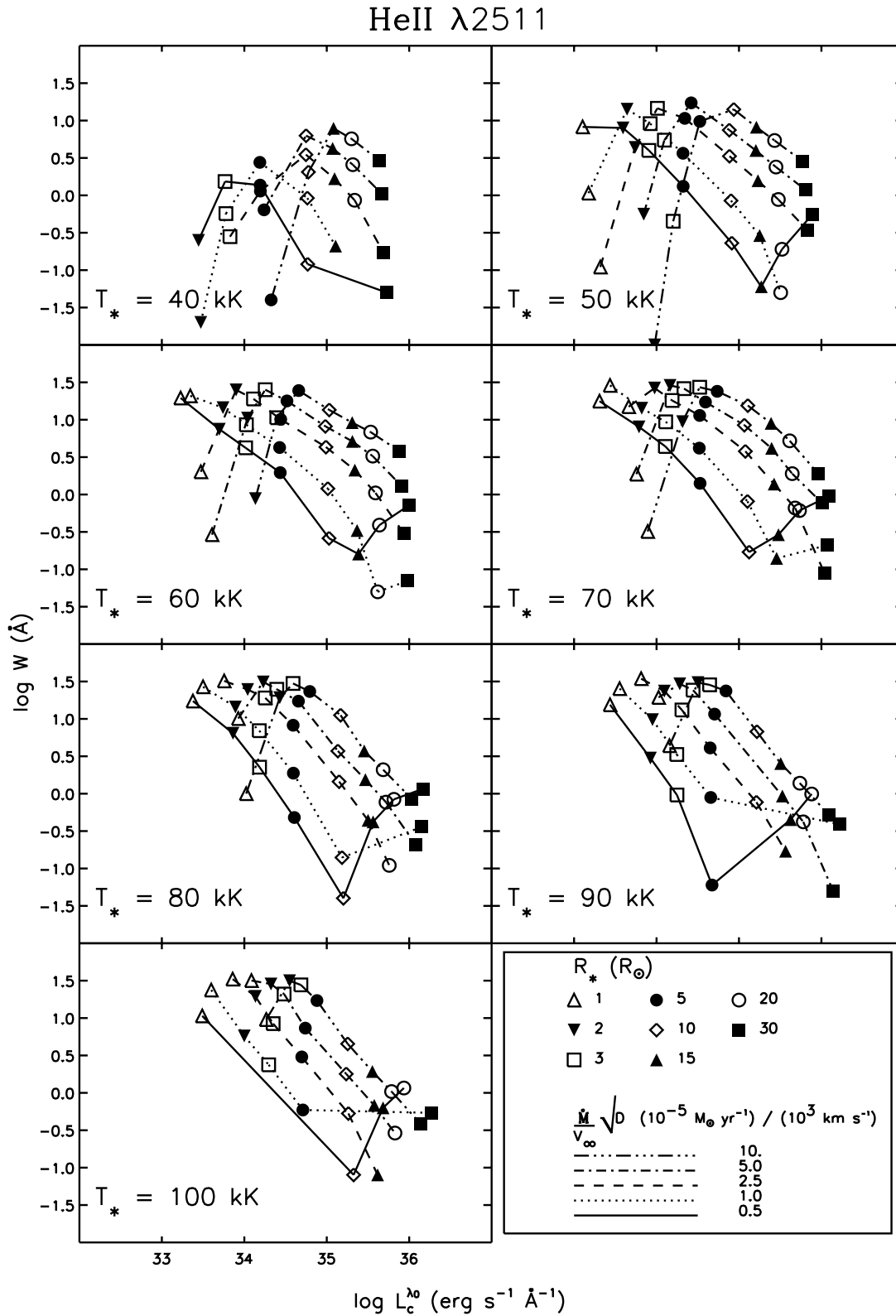


Figure 5.4: Line equivalent width W vs. monochromatic continuum luminosity $L_c^{\lambda_0}$ for the He II $\lambda 2511$ line. For explanation, see the text below Fig. 5.3.

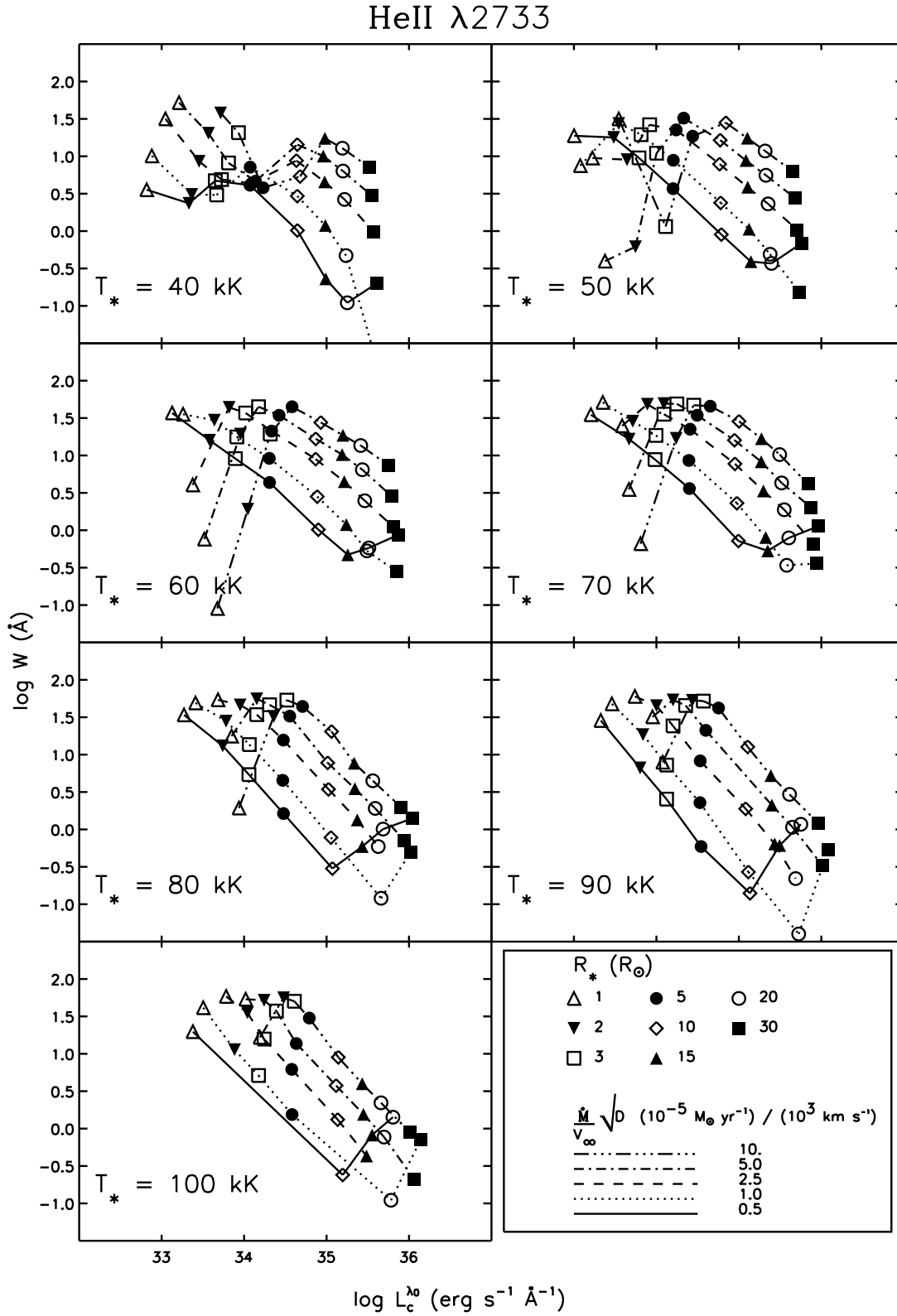


Figure 5.5: Line equivalent width W vs. monochromatic continuum luminosity $L_c^{\lambda_0}$ for the He II $\lambda 2733$ line. For explanation, see the text below Fig. 5.3.

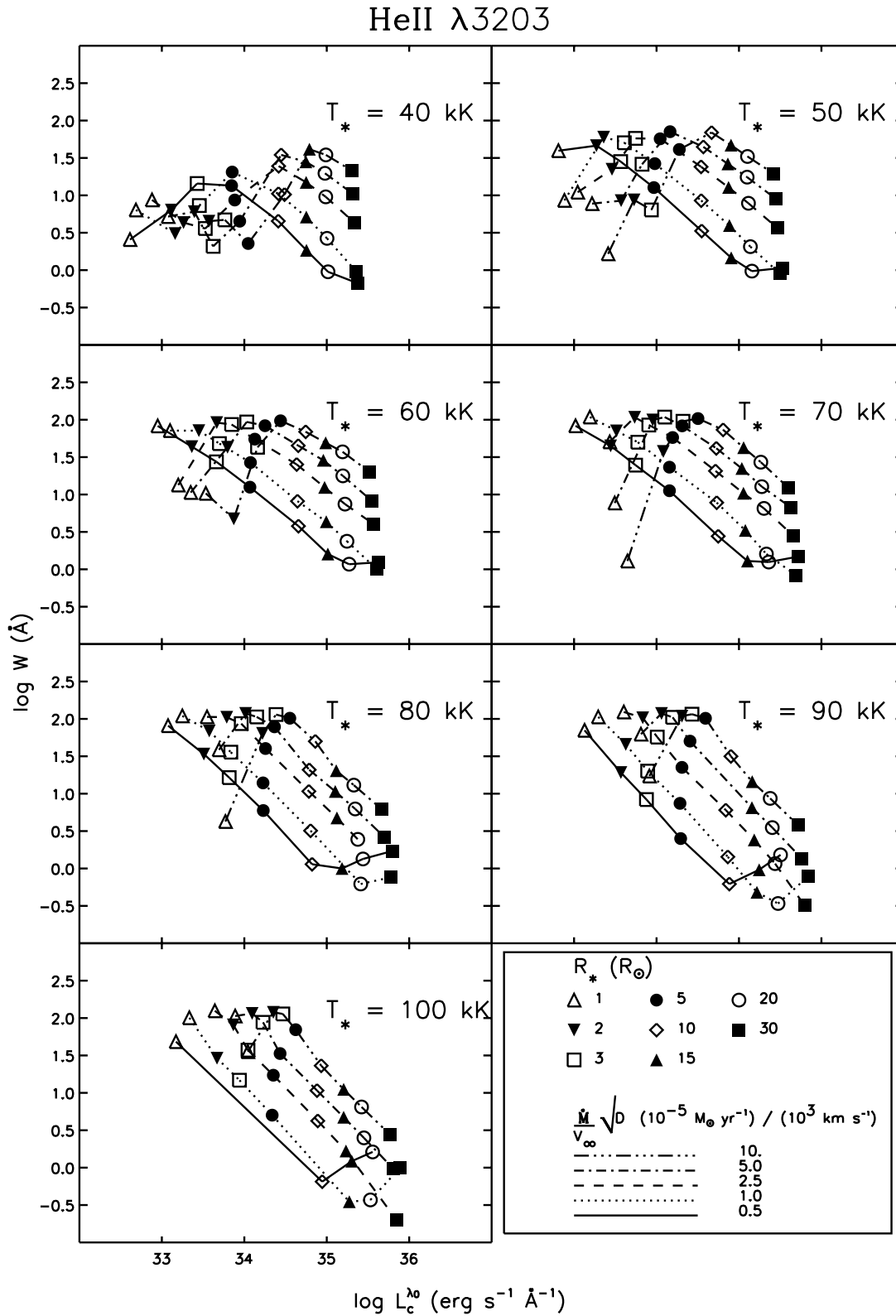


Figure 5.6: Line equivalent width W vs. monochromatic continuum luminosity $L_c^{\lambda_0}$ for the He II $\lambda 3203$ line. For explanation, see the text below Fig. 5.3.

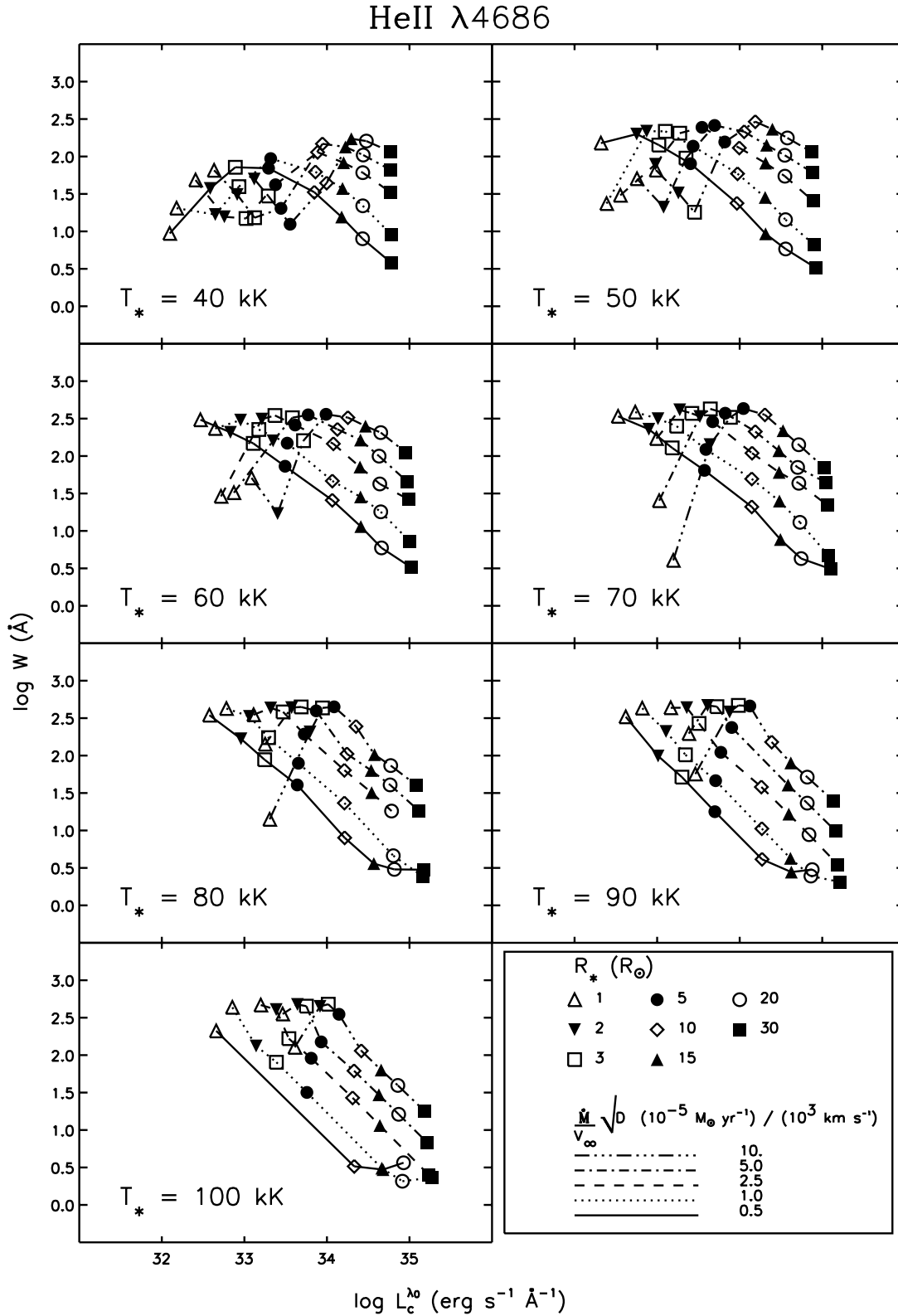


Figure 5.7: Line equivalent width W vs. monochromatic continuum luminosity $L_c^{\lambda_0}$ for the He II $\lambda 4686$ line. For explanation, see the text below Fig. 5.3.

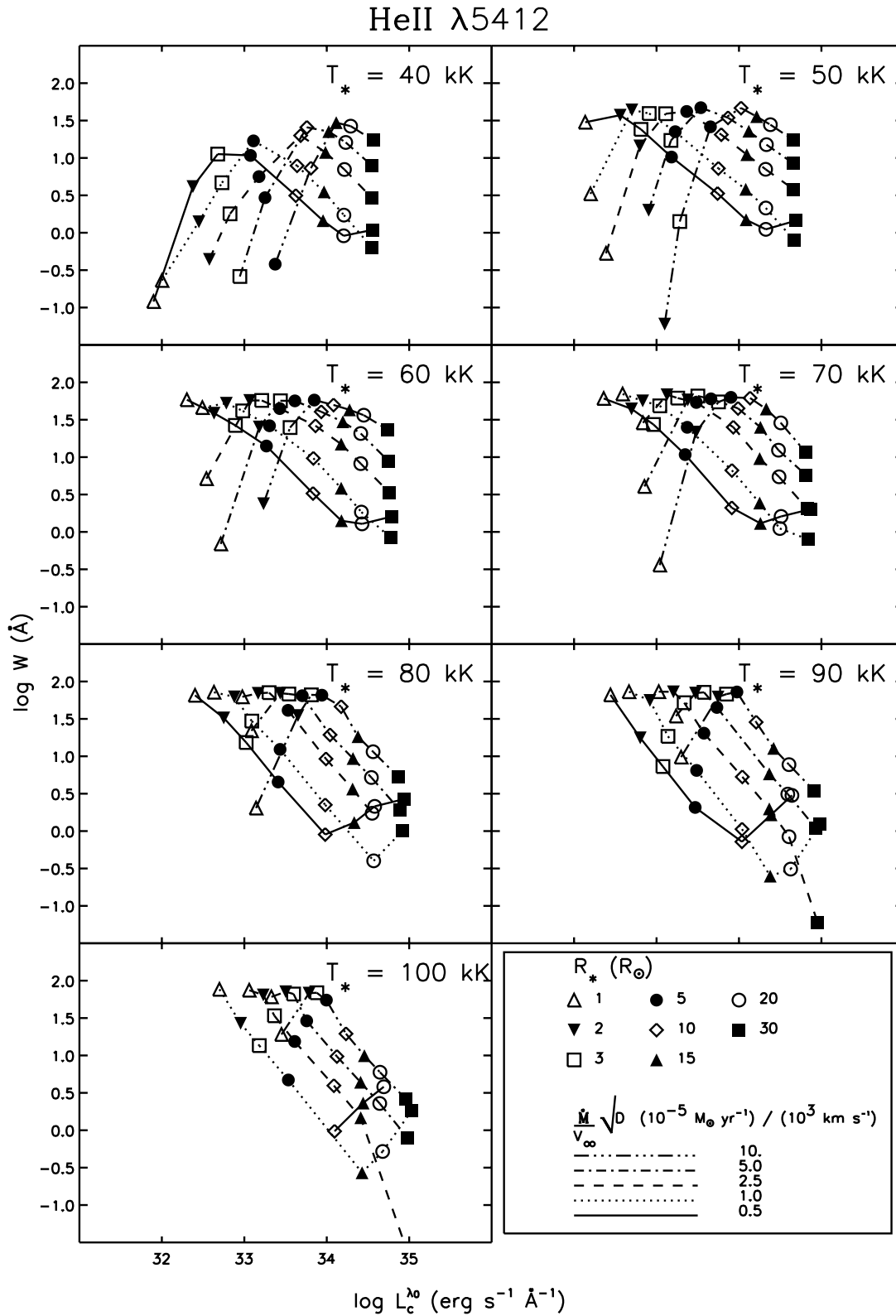


Figure 5.8: Line equivalent width W vs. monochromatic continuum luminosity $L_c^{\lambda_0}$ for the He II $\lambda 5412$ line. For explanation, see the text below Fig. 5.3.

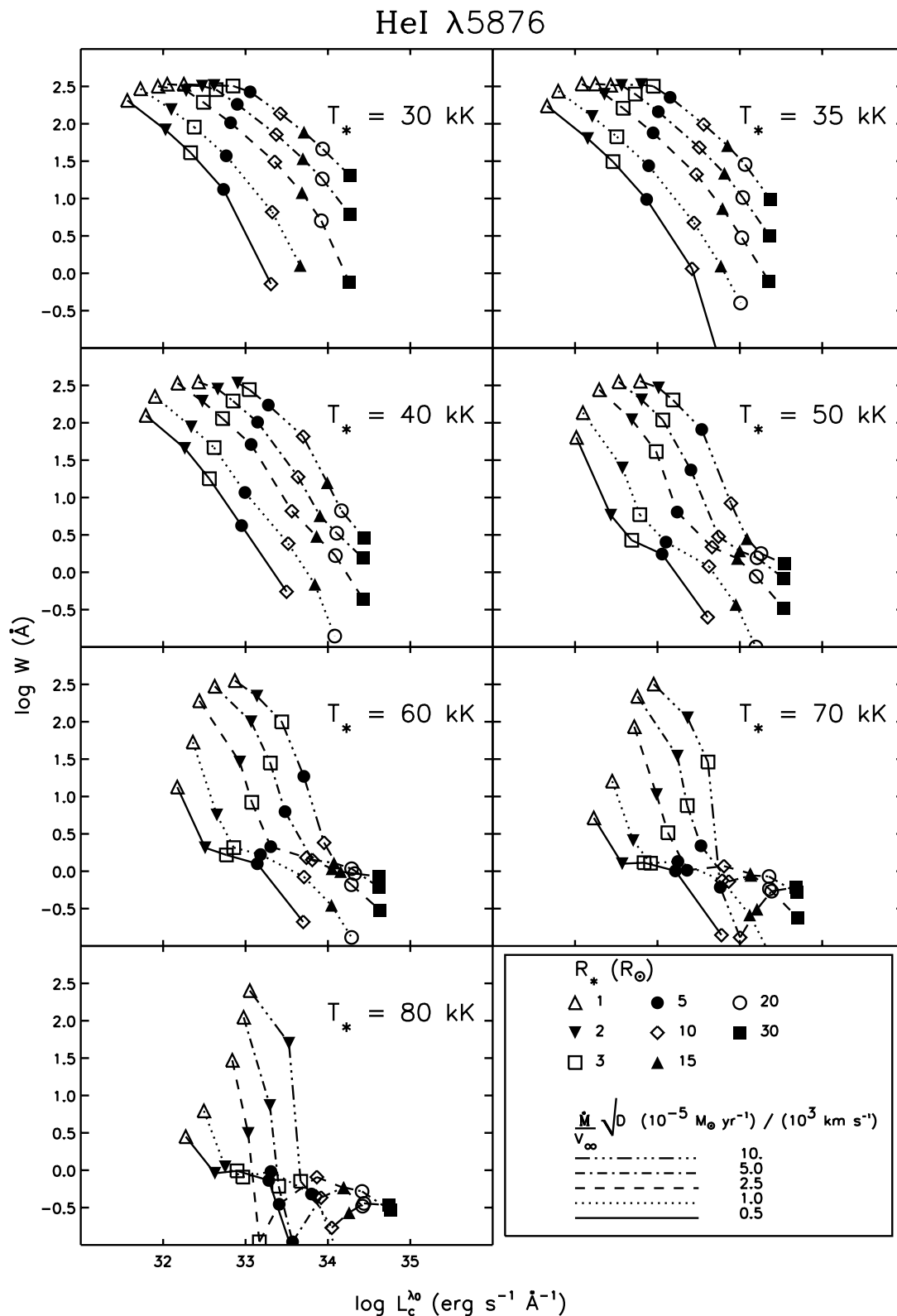


Figure 5.9: Line equivalent width W vs. monochromatic continuum luminosity $L_c^{\lambda_0}$ for the He I $\lambda 5876$ line. For explanation, see the text below Fig. 5.3.

be known before its distance can be measured by means of predicted Baldwin-relations with the suitable N abundance.

In Sect. 5.6 we will test the predicted Baldwin-relations, presented in Sect. 5.4.3, by measuring the distance to stars in the LMC, of which the distance is known. For the LMC WN stars, an average nitrogen abundance of 0.8% by mass applies (Hamann & Koesterke 2000), which is about half of the Galactic value of 1.5%. Since we adopted the latter value in our model calculations to predict the Baldwin-relations, we want to know the influence of the nitrogen abundance on the He line profiles. We therefore compare models with a nitrogen abundance of 0.8 and 1.5% in Fig. 5.10. The figure shows line profiles for the He I $\lambda 5876$ line (left panels) and the He II $\lambda 5412$ line (right panels). Line profiles are shown for models of stellar temperatures of $T_* = 30$ and 50 kK, and a radius of $R_* = 20$ and $5 R_\odot$. The mass-loss rate and terminal wind velocity are the same in all models.

Clearly, for the relatively low temperature of $T_* = 30$ kK, the difference between the LMC and the Galactic N abundance has no visible influence on the He line profiles. The reason is the high N III population in the wind, which causes the N III continuum of the $2p^2$ level (continuum edge at 261 Å) to be optically thick. This is true for both values of the N abundance, resulting in almost the same He ionization for both cases. For the model with a radius of $R_* = 5 R_\odot$ (dense wind), even the He I continuum below 504 Å is optically thick, and nitrogen has little effect on the He ionization.

The largest influence of the nitrogen abundance on the helium ionization is to be expected for the temperature range in which the N III continua become optically thin. In this temperature range, $35 \text{ kK} \lesssim T_* \lesssim 50 \text{ kK}$, different N abundances have the largest influence on the optical depth of the N III continua and therefore on the He line strengths.

Indeed, in Fig. 5.10 we see a noticeable influence of the N abundance on the He line profiles for $T_* = 50$ kK. Still the effect is not large. For the two studied values of the N abundance, we have found differences in line equivalent width of typically 10-20%, which is generally not larger than the uncertainty in the measurement of the line equivalent width of our observed spectra. For values of $T_* \gtrsim 50$ kK, the N III population reduces in favour of higher ion species, resulting in less affection of the He line strength by the presence of nitrogen.

We conclude that the predicted Baldwin-relations, calculated with a galactic N abundance, are also applicable for WN stars in the LMC. However, the nitrogen abundance in WN stars does have some influence on the He line strength in the temperature range between ≈ 35 and 50 kK, and therefore on our Baldwin-relations, calculated with the Galactic average N abundance of 1.5%. For WN stars in this temperature range and with a nitrogen content of more than $\approx 3 - 4$ times lower (or higher) than the Galactic average, we think our model predictions to be inaccurate, and separate Baldwin-relations for the specific N abundance should be calculated.

5.5.2 Clumping

Theoretical and observational evidence indicate that Wolf-Rayet stars winds are inhomogeneous (Hillier 1984; Moffat et al. 1988; Nugis et al. 1998). Most model atmosphere codes that take this *clumping* into account define some density enhancement D , which denotes the density contrast of the clumped material with respect to a homogeneous (i.e. non clumped) model with equal mass-loss rate (Schmutz 1997). The wind medium between the clumps is considered void. The clumps therefore fill a volume fraction $f_V = 1/D$.

In our model calculations, in which clumping has not been explicitly included, the effects

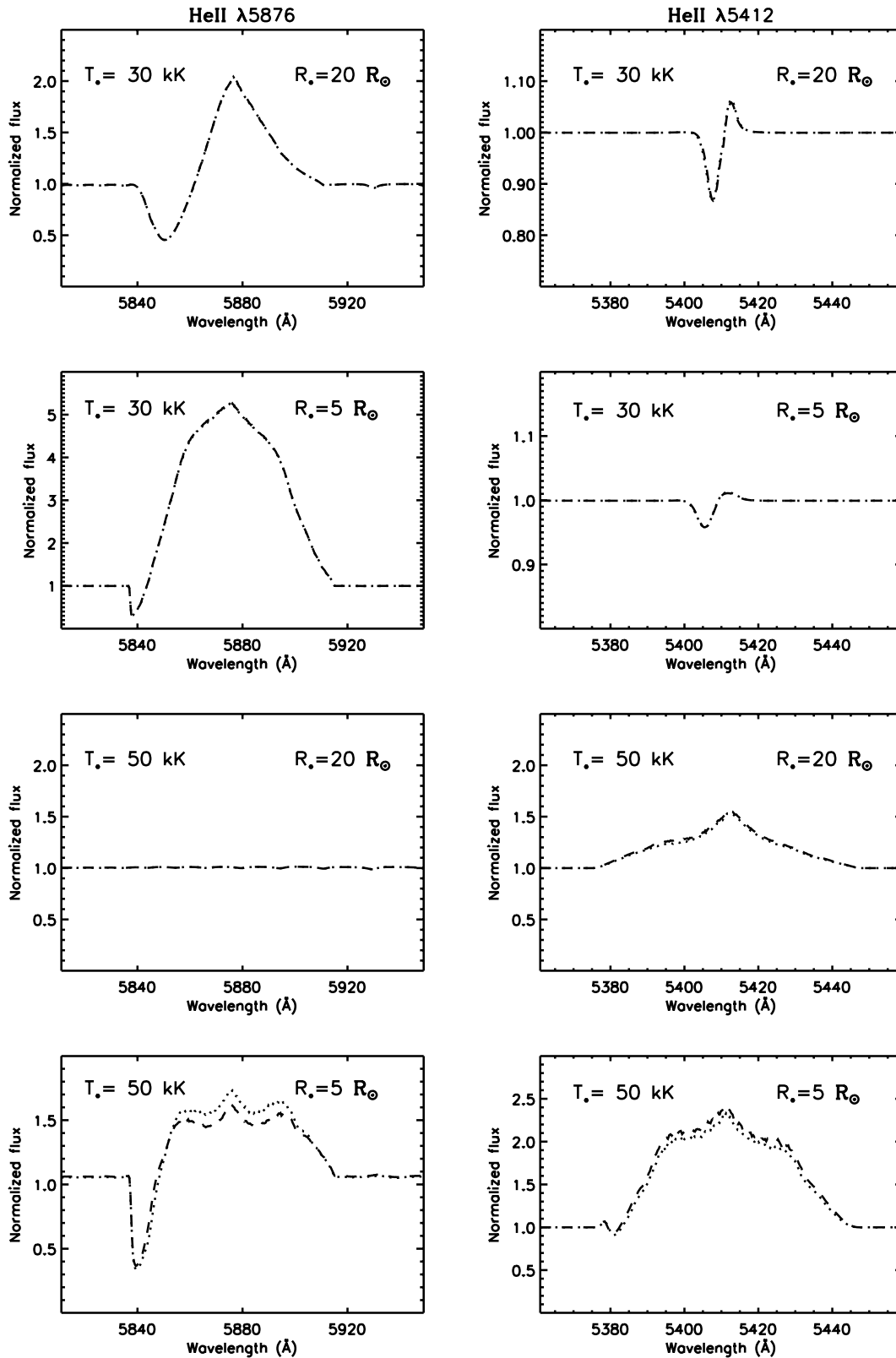


Figure 5.10: The influence of the nitrogen abundance on helium spectral lines. Left panels: He I $\lambda 5876$ line; right panels: He II $\lambda 5412$ line. Dashed lines: N abundance of 0.8 % by mass; dotted lines: N abundance of 1.5 % by mass. Stellar temperature and radius are indicated. For all models: $\dot{M} = 1 \times 10^{-4} M_{\odot} \text{ yr}^{-1}$; $v_{\infty} = 2000 \text{ km s}^{-1}$.

of clumping on the predicted spectra can be accounted for if it is realized that the emission line features in WR spectra are dominated by ρ^2 processes. For this kind of emission features it has been found that the value of the equivalent width is approximately invariant for models with the same value of the *transformed radius*, R_t (Hamann & Schmutz 1987; Hamann & Koesterke 1998b). Including wind clumping, the expression for the transformed radius is:

$$R_t = R_* \times \left(\frac{v_\infty}{2500 \text{ km s}^{-1}} / \frac{\dot{M} \sqrt{D}}{10^{-4} M_\odot \text{ yr}^{-1}} \right)^{\frac{2}{3}}. \quad (5.6)$$

A clumped model with clumping factor D will yield the same R_t (and thus line equivalent width) as a same model with a smooth (unclumped) wind if the mass-loss rate is scaled down by a factor \sqrt{D} . For a certain value of D , the Baldwin-relations can thus simply be scaled with help of Eq. 5.6.

5.5.3 Thomson scattering in lines

As mentioned in Sect. 5.3.4, our model calculations do not take into account frequency redistribution of line radiation by Thomson electron scattering. Our predicted line equivalent width may therefore be in error, as electron scattering wings may contribute significantly to the total equivalent width (Hillier 1991). We cannot scale our Baldwin-relations for Thomson scattering by means of the properties of the transformed radius, as scattering processes scale linearly with ρ rather than with ρ^2 . However, as suggested by Hamann & Koesterke (1998b), it may be realized that for a certain value of T_* , the emitted luminosity by scattering processes from a wind volume V , scales with ρV . The luminosity also scales with R_*^2 . Therefore, if at constant T_* the luminosity of a model is increased (by increasing R_*), it must be possible to maintain the equivalent width of both the recombination line *and* its scattering wings if *i*) the clumping is increased according to $D \propto R_*$, and *ii*) the mass-loss rate is reduced such that the transformed radius stays the same.

The validity of this possible scaling property of the scattering wing strength has never been thoroughly investigated. However we will use the concept to get a feeling of the influence of electron scattering on the shape of the Baldwin-relations.

To do so, we have obtained a grid of models generated by the POTSDAM synthetic stellar atmosphere code (Hamann 1985b; Hamann & Wessolowski 1990) for a constant luminosity of $\log(L) = 5.3$ (Koesterke, private communication). All models are available both with and without electron scattering included, so the separate contribution by electron scattering processes to the total line equivalent width can be determined.

We have used both the above described scaling properties of the electron scattering wings and of the transformed radius to interpolate the relative contribution of the scattering processes to the line equivalent width of the grid of ISA-WIND models.

Fig 5.11 shows the resulting influence of Thomson scattering on the Baldwin-relations for the He I $\lambda 5876$ line and the He II $\lambda 5412$ line. The Baldwin-relations are shown for different values of the stellar temperature and the clumping factor. Each time, the most left panels show the Baldwin-relations without electron scattering taken into account. Note again that these Baldwin-relations without scattering included are valid for each value of the clumping factor D , as long as the mass-loss rate is scaled accordingly. When we compare the Baldwin-relations

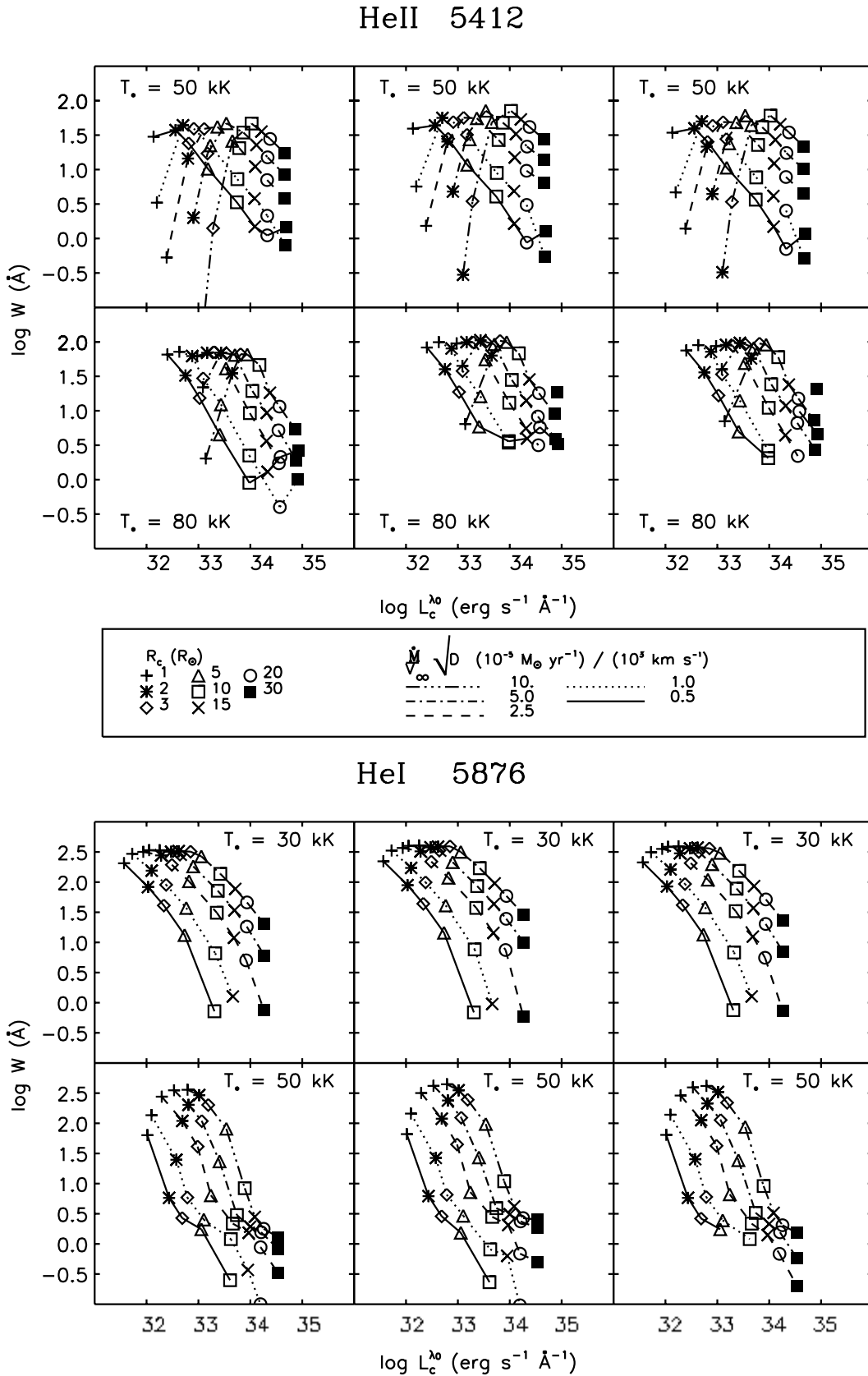


Figure 5.11: The influence of Thomson scattering on the Baldwin-relations for the He II $\lambda 5412$ line (top) and the He I $\lambda 5876$ line (bottom). Symbols are explained in the mid frame. For each line and temperature, the left panel shows the Baldwin-relations without scattering; the middle panel shows the influence of scattering for a clumping of $D = 2.4$; and the right panel shows the influence of scattering for $D = 9$.

without scattering for the He II line with the Baldwin-relations with scattering taken into account and a clump density enhancement of $D = 2.4^1$, it appears that the largest difference between equivalent width values occur for models with a large core radius. Modification of the equivalent width up to a factor two (0.3 dex) occurs for $R_* = 30 R_\odot$. This is explained by the different dependence on the density of the emission from the scattering wings ($\propto \rho$) and the line emission due to recombination processes ($\propto \rho^2$); for a certain value of T_* , models with a large luminosity therefore show relatively strong scattering wings in their spectra.

At a higher clumping factor ($D = 9$, right panels of Fig. 5.11), the lines show weaker electron scattering wings at the same luminosity. This is because for both values of D , the Baldwin-relations are shown for the same values of the transformed radius, which varies with $(v_\infty/\dot{M}\sqrt{D})^{2/3}$.

The influence of Thomson scattering on the total line equivalent width is less pronounced for He I lines. This is because the He II lines are generally formed deeper into the atmosphere, where the line radiation is stronger affected by electron scattering.

Overall, we find that frequency redistribution of line radiation by Thomson scattering is not large for the major part of the parameter domain of our models. A typical correction of less than 0.1 dex in equivalent width can be expected for He II lines, which would lead to a difference of about 0.05 dex in the continuum luminosity derived from the Baldwin-relations. The difference with the models without scattering is even less for the He I transitions, as the He I lines are formed further out in the atmosphere. Still, we think that for WNL type models, inclusion of electron scattering in the models would provide better predicted Baldwin-relations.

5.6 Testing the Baldwin-relations: stars with a well known distance

As mentioned in Sect. 5.1, the obvious practical utility of well-defined correlations between emission line equivalent width and monochromatic continuum luminosity is for determining stellar distances. Vice versa, we can use stars of which the distance is accurately known for a final calibration of the Baldwin-relations. In this section, we will use our Baldwin-relations to determine the distance of WN stars in the LMC. Since the distance to the LMC is already accurately known, and the reddening toward the system is low, this method provides a test of the Baldwin-relations and a final scaling of the relations can be performed if required.

The determination of a star's distance by means of the Baldwin-relations boils down to obtaining a reasonable estimate of the ratio of the mass-loss rate and its terminal wind velocity. The terminal velocity can in general accurately be obtained directly from a star's line spectrum, without knowledge of the star's distance being required. Finding an accurate estimate of the mass-loss rate is a more complex process if the star's distance is unknown, since the mass-loss rate is coupled to the stellar radius and therefore to the luminosity (see also the properties of the transformed radius, Sect. 5.5.2). As the distance of the LMC is well established, mass-loss determinations for LMC stars are relatively reliable. A recent study of LMC WN stars comes from Hamann & Koesterke (2000). They have analysed the spectra of 18 LMC WN stars by

¹A density enhancement of $D = 2.4$ was found as an average for Galactic WR stars by Nugis et al. (1998), from mass-loss rates derived from radio and optical spectra. Mass-loss derivations from fits by model atmospheres indicate an average clumping of $D = 4$ (Hamann & Koesterke 1998b)

means of model atmospheres of helium and nitrogen content. Wind clumping has been taken into account by adopting an average clumping factor of $D = 4$. Interestingly, the results from this study indicate that the parameters of the LMC stars show no systematic differences with those of their Galactic counterparts, despite the lower interstellar metallicity in the LMC²

We used the parameters of the LMC stars from Hamann & Koesterke (2000) to measure the distance to these stars by means of our predicted Baldwin-relations. The procedure is as follows. The mass-loss rates of Hamann & Koesterke (2000) have been derived for a constant clumping of $D = 4$ and we therefore multiplied the mass-loss rates by a factor 2, as the predicted Baldwin-relations are calculated without clumping. Then, for each star the ratio of mass-loss rate and terminal velocity was determined. After that, the equivalent width values from the *observed* spectra were used to derive a continuum luminosity for each spectral line from our predicted Baldwin-relations. As a final step, the derived continuum luminosities were compared with those derived from the observed spectra. In this comparison, the colour excesses $E(B - V)$ from Hamann & Koesterke (2000) were used, in order to minimize the influence of observational aspects on the comparison. For the derivation of the luminosity from the spectra, the LMC distance modulus of $Y_{\text{LMC}} = 18.5$ from Panagia et al. (1991) was adopted.

The comparison of the observed continuum luminosity with that derived from the predicted Baldwin-relations is presented in Fig. 5.12. In general, the agreement between the observed luminosity and the luminosity derived from the Baldwin-relations is very satisfactory, as also indicated by the standard deviations to the one-to-one relation, indicated in the figure. A few outlying points are visible, though. One of these concerns the WNL star Br 24, which has a temperature of $T_* = 39.8$ kK. This is the star showing the biggest luminosity discrepancy for the He II $\lambda 2733$ and $\lambda 4686$ lines. The “problem” with this star is that it lies very close to the points where the Baldwin-relations for these He II transitions tumble over. This is the region where the helium ionization balance is very sensitive to small differences in density and temperature. Differences between our model code and the POTSDAM code, used in the study of Hamann & Koesterke (2000), may therefore well explain the unsatisfying result for Br 24. Indeed, the observed and predicted luminosity for this star agree much better for the He I $\lambda 5876$ line, which shows a nice Baldwin-effect around the stellar temperature of Br 24.

For the stars Br 47 and Br 56, which are classified as WNL and a weak-lined WNE type, respectively, it is the He I $\lambda 5876$ line for which the agreement between predicted and observed luminosity has the worst agreement. The continuum luminosity at the central wavelength of He I $\lambda 5876$, as derived from the Baldwin-relations, is much lower for these stars than the continuum luminosity that follows from their observed spectra. Part of this discrepancy may be due to the omission of Thomson electron scattering processes in the calculation of the line profiles of our models. However, as discussed in the previous section, the error in the derived continuum luminosity is unlikely to be more than ≈ 0.1 dex. Furthermore, the large luminosity discrepancy for Br 47 and Br 56 is not visible for the He II lines, which generally show stronger scattering wings.

For both these stars, in the new study of Hamann & Koesterke (2000), the stellar temperature has been revised to a much higher value than found in the previous study of Koesterke et al. (1991), which was based on model atmospheres consisting of helium only. Several studies on the spectra of WN stars that include metals in the analyses conclude that good fits to the metal lines of the spectra co-involve poor helium line fits (Hamann & Koesterke 1998a; Crowther et al. 1995b). More in particular, good fits to the spectra of N and He II often go along with predicted

²See, however, our discussion in Ch. 6

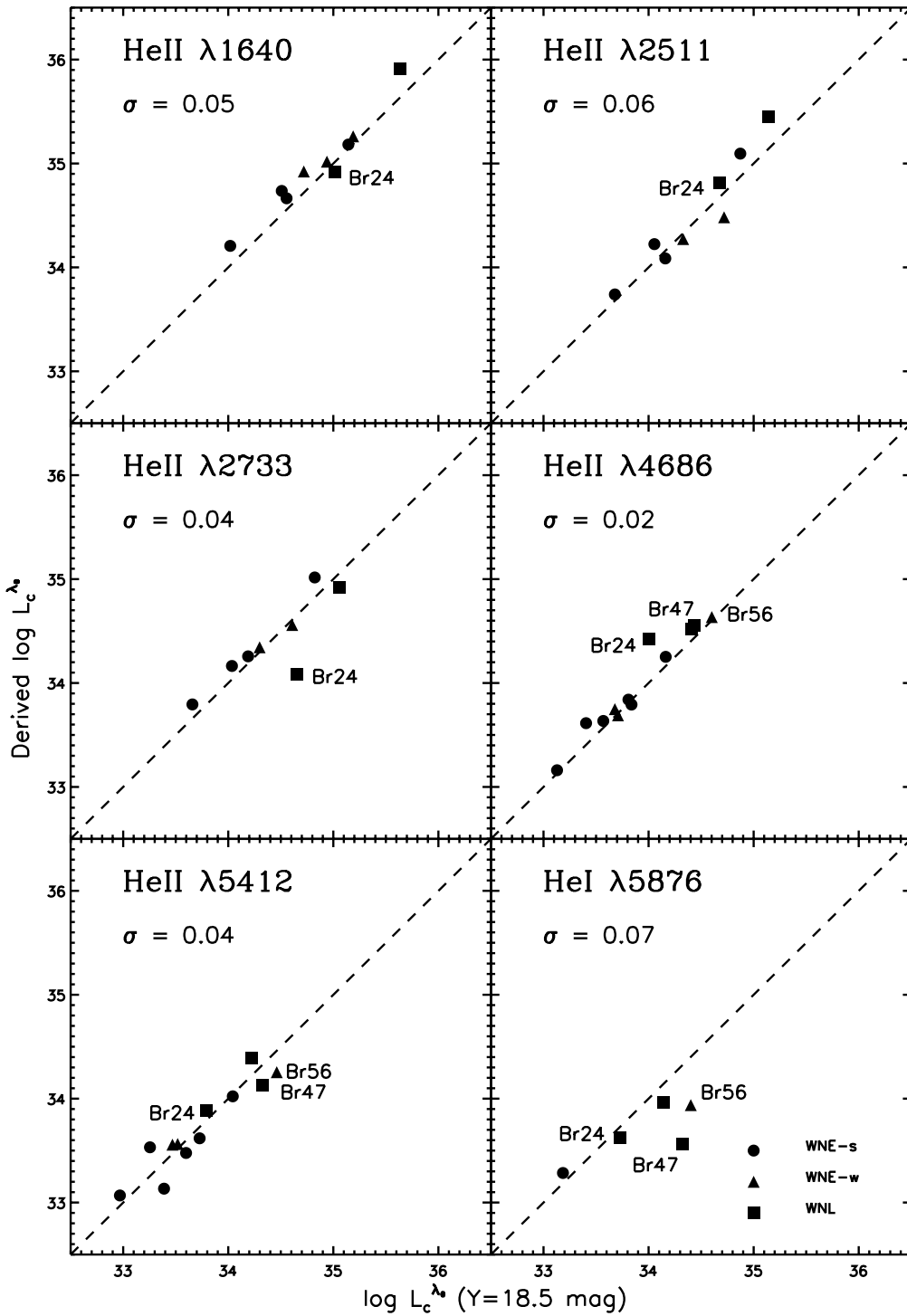


Figure 5.12: Monochromatic continuum luminosity of LMC WN stars derived with the theoretical Baldwin-relations versus the luminosity corresponding to a LMC distance modulus of $Y = 18.5$ mag. Used stellar parameters are from Hamann & Koesterke (2000) (see text). The standard deviation is indicated in each panel.

He I lines that are weaker than the observations. In the derivation of stellar parameters of the LMC WN stars by Hamann & Koesterke (2000), the emphasis has been laid on the nitrogen spectrum, which explains the poor result for Br 47 and Br 56 in Fig. 5.12.

We conclude that with a good estimate of the mass-loss rate and terminal velocity of a star, the Baldwin-relations provide a very good method to estimate the continuum luminosity from the spectrum. Since the stellar distance scales with $L^{1/2}$, the method performs even better as a distance estimator. From the test of our predicted Baldwin-relations for LMC WN stars, no systematic discrepancies were found between the observed continuum luminosity and the luminosity derived from the Baldwin-relations. Therefore, no correction of the predicted Baldwin-relations is found to be required. In the application of the Baldwin-effect as a distance estimator, care has to be taken though for the WNL stars. For those stars the application of the Baldwin-effect relies more on He I lines, which for some cases may be underestimated by our models, if the predictions of metal spectra in literature are to be trusted.

5.7 A new strategy for determination of WN star distances

In the previous section we have found, that the existence of a relation between line equivalent width and monochromatic continuum luminosity can provide an accurate method for the determination of stellar distances, as long as a good estimate of the stellar mass-loss rate and terminal wind velocity has been obtained. The determination of the distance of stars is the subject of the next chapter, in which our theoretical results are applied to Galactic WN stars; in this section we will preview the basic approach.

Initially, reasonably well-defined correlations between line equivalent width and monochromatic continuum luminosity were found for several ultraviolet and optical lines in the spectra of WN stars in the Large Magellanic Cloud (Morris et al. 1993a, Morris 1995). Least-squares fits to these Baldwin-relations were adopted to estimate distances to Galactic WN stars, under the assumption that the scatter in the trends arise solely from gaussian observational uncertainties in the line and continuum measurements and the interstellar reddening corrections, plus a systematic error component for the distance to the LMC (Morris 1995). Our theoretical investigations in Ch. 3 have shown that an *intrinsic* spread due to different mass-loss rates and terminal velocities among stars must be present as well, and that ionization effects lead to non-linear regressions of the He II lines at low stellar temperatures and high wind densities. When the spread due to \dot{M} and v_∞ is ignored, and some average equivalent width versus $L_c^{\lambda_0}$ relation is used for each value of T_* , the Galactic star distances derived through the theoretical Baldwin-relations are biased towards a mean mass-loss rate of the models used to predict the Baldwin-relations. Moreover, because of the ionization effects, the He II trends may give very uncertain results for stars with relatively dense winds, particularly in the case of the cooler WNL stars.

We cannot make assumptions on the mass-loss rate for any given star, since this depends strongly on the stellar radius (or luminosity, and thus distance). We do recognize from studies by Hamann & Koesterke (1998a), however, that groups of WN stars exhibit general mass-loss trends according to line strength. In Fig. 5.13 we show mass-loss rates as determined by Hamann & Koesterke (1998a) versus spectral type for Galactic WN stars. Clear trends in the values of \dot{M} can be seen for the separate groups of strong-lined and weak-lined WNE stars, while the WNL stars are less concentrated. Note that scatter in the values of \dot{M} determined by Hamann & Koesterke 1998a is present and due in part to distance-related uncertainties of

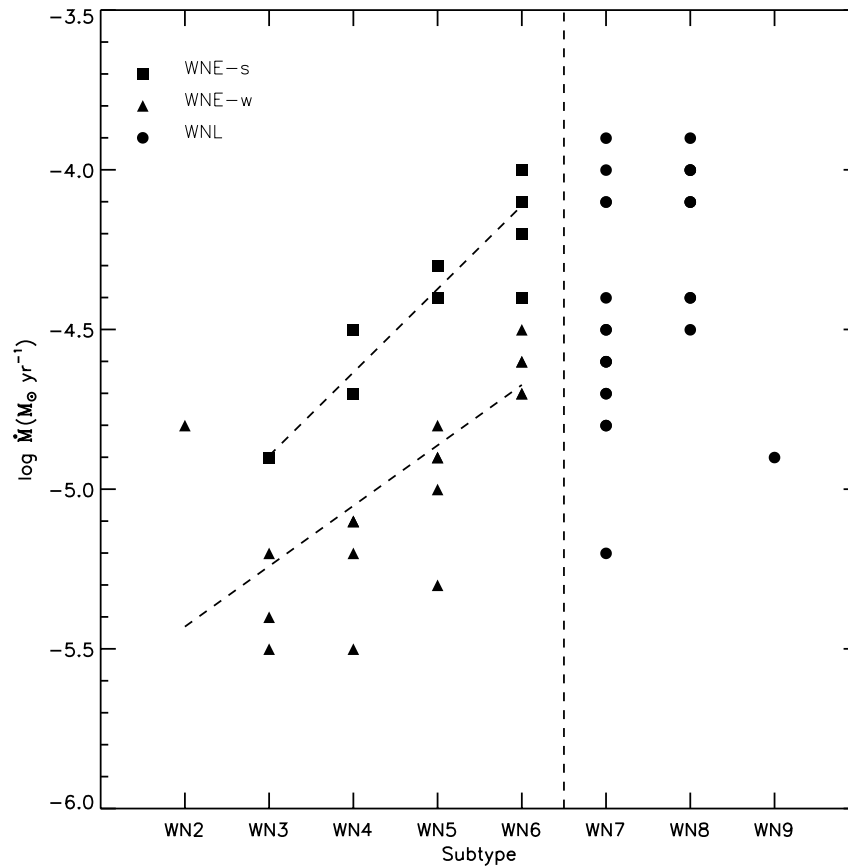


Figure 5.13: Mass-loss rate versus spectral subtype for Galactic WN stars. Mass loss rates are from Hamann & Koesterke (1998a), but scaled down by a factor 2 to account for an average clumping factor $D = 4$. The vertical dashed line divides the WNE and WNL star domains; the two tilted dashed lines show least-squares fits to the separate groups of strong lined and weak lined WNE stars, respectively. Note that the figure does not distinguish stars of same subtype with equal mass-loss rates.

i) alleged membership in OB associations or clusters³; ii) cluster/association distance; or iii) a mean relation of spectral type versus absolute visual magnitude (M_V), derived from assumed cluster/association members.

For the determination of stellar distances, our strategy will be to use the curves of equivalent width versus $L_c^{\lambda_0}$ closest to the mass-loss rate given by the fit of spectral type versus \dot{M} for each group in Fig. 5.13. For the WNL stars, we will simply adopt the equivalent width versus $L_c^{\lambda_0}$ curves corresponding to the mean WN7-WN9 mass-loss rate. For these stars we will rely more heavily on the He I $\lambda 5876$ line.

For this method to work, some parametrisation of the Baldwin-relations is to be given. We have fitted our theoretical Baldwin-relations with second order polynomials and present the resulting fit parameters in Tables 5.4 to 5.10.

In the fitting process, the reversion at high wind density of the equivalent width versus L_c relations, due to ionization effects, is ignored by leaving out all models for which the equivalent width does not monotonically decrease with rising continuum luminosity. This is justified

³We are reminded of the case of γ^2 Velorum (Schaerer et al. 1997; van der Hucht et al. 1997)

Table 5.4: Parameters from second order polynome fits to the relations between the equivalent width, W , and monochromatic continuum luminosity, $L_c^{\lambda_0}$, for the He II $\lambda 1640$ line shown in Fig. 5.3. Listed are the coefficients from the fit $\log L_c^{\lambda_0} = a_0 + a_1 \log W + a_2 \log^2 W$.

He II $\lambda 1640$					
T_* (kK)	$\frac{\dot{M}\sqrt{D}}{V_\infty}$ ($\dot{M} \text{ yr}^{-1} \text{ km}^{-1} \text{ s}$)	a_0	a_1	a_2	σ
30000	0.50	–	–	–	–
	1.00	–	–	–	–
	2.50	–	–	–	–
	5.00	–	–	–	–
	10.0	–	–	–	–
35000	0.50	35.882	–1.067	–1.094	0.047
	1.00	36.140	0.127	–1.370	0.017
	2.50	10.266	57.692	–31.939	0.000
	5.00	35.749	14.890	–12.856	0.000
	10.0	–	–	–	–
40000	0.50	36.081	–0.680	–0.401	0.040
	1.00	36.322	–0.322	–0.502	0.012
	2.50	36.642	–0.122	–0.477	0.000
	5.00	35.213	2.443	–1.354	0.010
	10.0	31.811	6.619	–2.465	0.000
50000	0.50	36.259	–0.887	–0.192	0.055
	1.00	36.512	–0.690	–0.216	0.014
	2.50	36.874	–0.374	–0.349	0.030
	5.00	37.098	–0.234	–0.362	0.010
	10.0	37.720	–0.636	–0.205	0.002
60000	0.50	36.562	–1.106	–0.081	0.007
	1.00	36.871	–0.901	–0.184	0.034
	2.50	37.113	–0.600	–0.244	0.021
	5.00	36.714	0.341	–0.511	0.017
	10.0	36.570	0.882	–0.643	0.006
70000	0.50	36.586	–1.129	–0.051	0.021
	1.00	36.867	–0.868	–0.156	0.013
	2.50	37.672	–1.362	0.013	0.018
	5.00	37.533	–0.801	–0.136	0.019
	10.0	36.753	0.376	–0.427	0.012
80000	0.50	36.440	–1.328	0.086	0.048
	1.00	36.638	–1.019	–0.029	0.018
	2.50	36.907	–0.665	–0.159	0.038
	5.00	37.623	–1.320	0.070	0.029
	10.0	37.601	–0.925	–0.033	0.032
90000	0.50	36.065	–1.167	0.090	0.020
	1.00	36.436	–1.173	0.078	0.028
	2.50	36.837	–0.960	–0.013	0.023
	5.00	37.202	–0.968	–0.002	0.014
	10.0	37.738	–1.318	0.116	0.021
100000	0.50	35.677	–4.432	1.861	0.000
	1.00	36.266	–1.104	0.077	0.016
	2.50	36.730	–0.999	0.022	0.019
	5.00	37.175	–1.172	0.091	0.017
	10.0	37.540	–1.159	0.072	0.023
120000	0.50	35.873	–1.190	0.099	0.018
	1.00	36.206	–1.152	0.091	0.021
	2.50	36.632	–1.086	0.074	0.013
	5.00	37.004	–1.084	0.062	0.020
	10.0	37.506	–1.340	0.157	0.018

Table 5.5: Parameters from second order polynome fits to the relations between the equivalent width, W , and monochromatic continuum luminosity, $L_c^{\lambda_0}$, for the He II $\lambda 2511$ line shown in Fig. 5.4. Listed are the coefficients from the fit $\log L_c^{\lambda_0} = a_0 + a_1 \log W + a_2 \log^2 W$.

He II $\lambda 2511$					
T_* (kK)	$\frac{\dot{M}\sqrt{D}}{V_\infty}$ ($M_{\text{yr}}^{-1} \text{ km}^{-1} \text{ s}$)	a_0	a_1	a_2	σ
30000	0.50	–	–	–	–
	1.00	–	–	–	–
	2.50	–	–	–	–
	5.00	–	–	–	–
	10.0	–	–	–	–
35000	0.50	–	–	–	–
	1.00	–	–	–	–
	2.50	–	–	–	–
	5.00	–	–	–	–
	10.0	–	–	–	–
40000	0.50	33.932	0.059	1.096	0.080
	1.00	34.731	–0.964	–0.602	0.000
	2.50	35.289	–0.798	–0.360	0.001
	5.00	35.674	–0.493	–0.816	0.009
	10.0	–	–	–	–
50000	0.50	34.463	–0.955	–0.259	0.060
	1.00	34.862	–0.793	–0.224	0.008
	2.50	35.434	–0.928	–0.206	0.018
	5.00	35.883	–1.092	–0.072	0.003
	10.0	36.358	–1.320	0.071	0.001
60000	0.50	34.651	–0.929	–0.139	0.027
	1.00	35.076	–0.831	–0.326	0.015
	2.50	35.610	–0.798	–0.307	0.010
	5.00	36.006	–0.738	–0.367	0.009
	10.0	36.745	–1.453	–0.039	0.007
70000	0.50	34.678	–0.767	–0.255	0.009
	1.00	35.050	–0.711	–0.277	0.008
	2.50	35.562	–0.729	–0.270	0.009
	5.00	35.911	–0.608	–0.377	0.016
	10.0	35.980	0.087	–0.737	0.019
80000	0.50	34.436	–0.692	–0.109	0.016
	1.00	34.811	–0.602	–0.201	0.015
	2.50	35.315	–0.640	–0.210	0.025
	5.00	35.625	–0.731	–0.107	0.018
	10.0	35.954	–0.706	–0.120	0.022
90000	0.50	34.222	–0.521	–0.122	0.007
	1.00	34.620	–0.607	–0.102	0.115
	2.50	35.133	–0.645	–0.113	0.017
	5.00	35.526	–0.677	–0.097	0.011
	10.0	35.786	–0.515	–0.189	0.025
100000	0.50	15.135	0.302	17.056	0.000
	1.00	34.548	–0.718	0.018	0.210
	2.50	35.052	–0.631	–0.094	0.014
	5.00	35.443	–0.717	–0.067	0.026
	10.0	35.697	–0.525	–0.138	0.014
120000	0.50	34.115	–0.604	–0.134	0.124
	1.00	34.486	–0.662	–0.059	0.061
	2.50	34.974	–0.753	0.030	0.007
	5.00	35.372	–0.878	0.073	0.013
	10.0	35.787	–1.113	0.235	0.012

Table 5.6: Parameters from second order polynome fits to the relations between the equivalent width, W , and monochromatic continuum luminosity, $L_c^{\lambda_0}$, for the He II $\lambda 2733$ line shown in Fig. 5.5. Listed are the coefficients from the fit $\log L_c^{\lambda_0} = a_0 + a_1 \log W + a_2 \log^2 W$.

He II $\lambda 2733$					
T_* (kK)	$\frac{\dot{M} \sqrt{D}}{V_{\infty}} (\text{Myr}^{-1} \text{ km}^{-1} \text{ s})$	a_0	a_1	a_2	σ
30000	0.50	—	—	—	—
	1.00	—	—	—	—
	2.50	—	—	—	—
	5.00	—	—	—	—
	10.0	—	—	—	—
35000	0.50	—	—	—	—
	1.00	—	—	—	—
	2.50	—	—	—	—
	5.00	—	—	—	—
	10.0	—	—	—	—
40000	0.50	34.621	-0.951	-0.362	0.052
	1.00	35.038	-0.829	-0.298	0.017
	2.50	35.562	-0.672	-0.331	0.155
	5.00	35.676	0.139	-0.881	0.106
	10.0	35.817	0.365	-0.838	0.000
50000	0.50	34.840	-1.030	-0.165	0.056
	1.00	35.141	-0.849	-0.163	0.009
	2.50	35.708	-0.848	-0.238	0.026
	5.00	36.105	-0.894	-0.182	0.006
	10.0	36.609	-1.166	-0.037	0.000
60000	0.50	34.940	-0.965	-0.124	0.009
	1.00	35.342	-0.906	-0.221	0.028
	2.50	35.835	-0.788	-0.254	0.009
	5.00	36.113	-0.536	-0.379	0.007
	10.0	36.557	-0.625	-0.347	0.003
70000	0.50	34.981	-0.988	-0.093	0.028
	1.00	35.274	-0.736	-0.226	0.004
	2.50	35.771	-0.735	-0.221	0.007
	5.00	36.037	-0.521	-0.336	0.020
	10.0	35.846	0.396	-0.699	0.024
80000	0.50	34.674	-0.782	-0.078	0.010
	1.00	35.013	-0.765	-0.087	0.017
	2.50	35.468	-0.621	-0.194	0.026
	5.00	35.817	-0.813	-0.057	0.018
	10.0	36.110	-0.756	-0.075	0.020
90000	0.50	34.410	-0.792	0.039	0.013
	1.00	34.762	-0.715	-0.028	0.011
	2.50	35.278	-0.691	-0.077	0.017
	5.00	35.662	-0.748	-0.042	0.011
	10.0	36.012	-0.805	-0.025	0.024
100000	0.50	24.236	-9.674	12.921	0.000
	1.00	34.774	-0.949	0.102	0.006
	2.50	35.210	-0.774	-0.011	0.012
	5.00	35.585	-0.751	-0.044	0.024
	10.0	35.959	-0.878	0.038	0.012
120000	0.50	34.261	-0.690	-0.069	0.001
	1.00	34.601	-0.645	-0.077	0.013
	2.50	35.102	-0.746	0.009	0.030
	5.00	35.485	-0.717	-0.044	0.017
	10.0	35.872	-0.967	0.125	0.013

Table 5.7: Parameters from second order polynome fits to the relations between the equivalent width, W , and monochromatic continuum luminosity, $L_c^{\lambda_0}$, for the He II $\lambda 3203$ line shown in Fig. 5.6. Listed are the coefficients from the fit $\log L_c^{\lambda_0} = a_0 + a_1 \log W + a_2 \log^2 W$.

He II $\lambda 3203$						
T_* (kK)	$\frac{\dot{M}\sqrt{D}}{V_{\infty}} (\dot{M} \text{ yr}^{-1} \text{ km}^{-1} \text{ s})$	a_0	a_1	a_2	σ	
30000	0.50	–	–	–	–	–
	1.00	–	–	–	–	–
	2.50	–	–	–	–	–
	5.00	–	–	–	–	–
	10.0	–	–	–	–	–
35000	0.50	–	–	–	–	–
	1.00	–	–	–	–	–
	2.50	–	–	–	–	–
	5.00	–	–	–	–	–
	10.0	–	–	–	–	–
40000	0.50	35.100	–1.042	–0.200	0.053	
	1.00	35.331	–0.461	–0.488	0.017	
	2.50	35.627	–0.121	–0.538	0.002	
	5.00	33.802	3.535	–2.012	0.015	
	10.0	29.137	9.934	–3.982	0.000	
50000	0.50	35.108	–0.997	–0.055	0.012	
	1.00	35.434	–0.778	–0.193	0.017	
	2.50	35.799	–0.393	–0.391	0.035	
	5.00	35.957	–0.102	–0.463	0.009	
	10.0	37.181	–1.365	–0.000	0.001	
60000	0.50	35.279	–0.976	–0.119	0.014	
	1.00	35.578	–0.725	–0.265	0.036	
	2.50	36.021	–0.641	–0.265	0.017	
	5.00	35.770	0.269	–0.570	0.015	
	10.0	35.503	1.055	–0.800	0.003	
70000	0.50	35.318	–1.058	–0.062	0.030	
	1.00	35.572	–0.820	–0.160	0.015	
	2.50	36.026	–0.752	–0.179	0.009	
	5.00	36.305	–0.682	–0.191	0.010	
	10.0	35.890	0.193	–0.430	0.013	
80000	0.50	35.036	–1.022	0.004	0.037	
	1.00	35.243	–0.785	–0.083	0.013	
	2.50	35.610	–0.587	–0.169	0.033	
	5.00	36.094	–0.948	–0.009	0.019	
	10.0	36.368	–0.905	–0.012	0.020	
90000	0.50	34.680	–0.937	0.053	0.006	
	1.00	35.007	–0.864	0.012	0.014	
	2.50	35.460	–0.741	–0.054	0.016	
	5.00	35.881	–0.895	0.018	0.011	
	10.0	36.321	–1.111	0.109	0.015	
100000	0.50	33.868	–5.221	2.855	0.000	
	1.00	34.888	–0.847	0.030	0.011	
	2.50	35.446	–0.937	0.043	0.014	
	5.00	35.891	–1.125	0.128	0.011	
	10.0	36.139	–0.939	0.052	0.012	
120000	0.50	34.700	–1.475	0.342	0.059	
	1.00	34.852	–0.906	0.040	0.011	
	2.50	35.341	–0.969	0.084	0.013	
	5.00	35.823	–1.168	0.141	0.013	
	10.0	36.524	–1.723	0.349	0.014	

Table 5.8: Parameters from second order polynome fits to the relations between the equivalent width, W , and monochromatic continuum luminosity, $L_c^{\lambda_0}$, for the He II $\lambda 4686$ line shown in Fig. 5.7. Listed are the coefficients from the fit $\log L_c^{\lambda_0} = a_0 + a_1 \log W + a_2 \log^2 W$.

He II $\lambda 4686$					
T_* (kK)	$\frac{\dot{M}\sqrt{D}}{V_\infty}$ ($M_{\odot}\text{yr}^{-1}\text{km}^{-1}\text{s}$)	a_0	a_1	a_2	σ
30000	0.50	—	—	—	—
	1.00	—	—	—	—
	2.50	—	—	—	—
	5.00	—	—	—	—
	10.0	—	—	—	—
35000	0.50	—	—	—	—
	1.00	—	—	—	—
	2.50	—	—	—	—
	5.00	—	—	—	—
	10.0	—	—	—	—
40000	0.50	34.778	0.292	-0.644	0.052
	1.00	34.039	1.781	-1.075	0.024
	2.50	32.886	3.373	-1.403	0.002
	5.00	19.130	17.652	-4.979	0.024
	10.0	-62.973	93.569	-22.390	0.000
50000	0.50	35.321	-0.864	-0.098	0.023
	1.00	35.035	0.138	-0.429	0.028
	2.50	35.218	0.441	-0.479	0.003
	5.00	32.660	3.458	-1.244	0.023
	10.0	34.736	1.519	-0.705	0.004
60000	0.50	35.308	-0.584	-0.214	0.018
	1.00	35.631	-0.538	-0.214	0.016
	2.50	35.847	-0.229	-0.289	0.021
	5.00	33.879	1.953	-0.782	0.009
	10.0	23.774	11.260	-2.833	0.019
70000	0.50	35.405	-0.827	-0.111	0.027
	1.00	35.312	-0.162	-0.309	0.017
	2.50	36.385	-0.810	-0.135	0.018
	5.00	36.404	-0.548	-0.183	0.019
	10.0	34.386	1.390	-0.569	0.020
80000	0.50	35.477	-1.314	0.076	0.050
	1.00	35.447	-0.838	-0.056	0.020
	2.50	36.065	-1.010	-0.006	0.012
	5.00	36.917	-1.617	0.159	0.021
	10.0	37.763	-2.139	0.287	0.016
90000	0.50	35.089	-1.249	0.107	0.020
	1.00	35.432	-1.221	0.091	0.027
	2.50	35.749	-1.013	0.037	0.011
	5.00	36.148	-1.027	0.035	0.012
	10.0	37.078	-1.671	0.201	0.016
100000	0.50	39.405	-11.840	3.847	0.000
	1.00	35.248	-1.160	0.093	0.015
	2.50	35.900	-1.294	0.114	0.019
	5.00	36.617	-1.699	0.225	0.017
	10.0	37.151	-1.849	0.257	0.009
120000	0.50	34.995	-1.384	0.152	0.017
	1.00	35.089	-1.011	0.035	0.021
	2.50	35.719	-1.253	0.122	0.011
	5.00	36.595	-1.777	0.244	0.018
	10.0	38.577	-3.373	0.629	0.019

Table 5.9: Parameters from second order polynome fits to the relations between the equivalent width, W , and monochromatic continuum luminosity, $L_c^{\lambda_0}$, for the He II $\lambda 5412$ line shown in Fig. 5.8. Listed are the coefficients from the fit $\log L_c^{\lambda_0} = a_0 + a_1 \log W + a_2 \log^2 W$.

He II $\lambda 5412$						
T_* (kK)	$\frac{\dot{M} \sqrt{D}}{V_{\infty}} (\dot{M} \text{ yr}^{-1} \text{ km}^{-1} \text{ s})$	a_0	a_1	a_2	σ	
30000	0.50	–	–	–	–	–
	1.00	–	–	–	–	–
	2.50	–	–	–	–	–
	5.00	–	–	–	–	–
	10.0	–	–	–	–	–
35000	0.50	–	–	–	–	–
	1.00	–	–	–	–	–
	2.50	–	–	–	–	–
	5.00	–	–	–	–	–
	10.0	–	–	–	–	–
40000	0.50	34.147	–0.929	–0.281	0.053	
	1.00	34.418	–0.635	–0.330	0.016	
	2.50	34.786	–0.330	–0.396	0.004	
	5.00	32.575	4.514	–2.584	0.022	
	10.0	19.085	24.639	–9.802	0.000	
50000	0.50	34.340	–1.177	0.037	0.012	
	1.00	34.593	–0.757	–0.211	0.016	
	2.50	35.313	–1.099	–0.060	0.005	
	5.00	34.904	0.369	–0.699	0.014	
	10.0	35.385	0.085	–0.540	0.000	
60000	0.50	34.385	–0.774	–0.213	0.029	
	1.00	34.677	–0.659	–0.242	0.017	
	2.50	34.851	0.103	–0.584	0.011	
	5.00	33.573	2.711	–1.559	0.022	
	10.0	28.737	9.536	–3.764	0.001	
70000	0.50	34.254	–0.657	–0.199	0.031	
	1.00	34.638	–0.740	–0.163	0.034	
	2.50	34.905	–0.239	–0.371	0.027	
	5.00	34.673	0.665	–0.696	0.029	
	10.0	33.662	2.334	–1.188	0.032	
80000	0.50	33.938	–0.702	–0.071	0.012	
	1.00	34.277	–0.725	–0.059	0.023	
	2.50	34.721	–0.720	–0.021	0.007	
	5.00	35.101	–0.751	–0.051	0.024	
	10.0	35.345	–0.617	–0.093	0.027	
90000	0.50	33.852	–1.068	0.166	0.016	
	1.00	34.028	–0.624	–0.038	0.021	
	2.50	34.560	–0.668	–0.051	0.021	
	5.00	34.964	–0.781	0.019	0.003	
	10.0	35.469	–1.135	0.179	0.004	
100000	1.00	34.001	–0.745	0.024	0.008	
	2.50	34.548	–0.797	0.017	0.018	
	5.00	34.994	–1.002	0.116	0.011	
	10.0	35.393	–1.086	0.151	0.008	
120000	0.50	33.636	–0.823	0.046	0.000	
	1.00	34.016	–0.910	0.097	0.023	
	2.50	34.473	–0.846	0.061	0.016	
	5.00	34.941	–1.025	0.118	0.013	
	10.0	35.578	–1.540	0.334	0.010	

Table 5.10: Parameters from second order polynome fits to the relations between the equivalent width, W , and monochromatic continuum luminosity, $L_c^{\lambda_0}$, for the He II $\lambda 5876$ line shown in Fig. 5.9. Listed are the coefficients from the fit $\log L_c^{\lambda_0} = a_0 + a_1 \log W + a_2 \log^2 W$.

He I $\lambda 5876$					
T_* (kK)	$\frac{\dot{M}\sqrt{D}}{V_\infty}$ (\dot{M} yr $^{-1}$ km $^{-1}$ s)	a_0	a_1	a_2	σ
30000	0.50	33.278	-0.238	-0.217	0.002
	1.00	33.683	-0.233	-0.225	0.004
	2.50	34.218	-0.187	-0.263	0.027
	5.00	34.238	0.328	-0.426	0.046
	10.0	33.228	1.841	-0.826	0.059
35000	0.50	33.460	-0.436	-0.162	0.004
	1.00	33.837	-0.445	-0.158	0.007
	2.50	34.286	-0.384	-0.182	0.013
	5.00	34.442	-0.080	-0.280	0.031
	10.0	34.513	0.172	-0.325	0.013
40000	0.50	33.357	-0.518	-0.103	0.014
	1.00	33.731	-0.516	-0.107	0.013
	2.50	34.197	-0.596	-0.070	0.021
	5.00	34.442	-0.512	-0.091	0.027
	10.0	34.493	-0.166	-0.175	0.021
50000	0.50	—	—	—	—
	1.00	—	—	—	—
	2.50	—	—	—	—
	5.00	—	—	—	—
	10.0	—	—	—	—
60000	0.50	—	—	—	—
	1.00	—	—	—	—
	2.50	—	—	—	—
	5.00	—	—	—	—
	10.0	—	—	—	—
70000	0.50	—	—	—	—
	1.00	—	—	—	—
	2.50	—	—	—	—
	5.00	—	—	—	—
	10.0	—	—	—	—
80000	0.50	—	—	—	—
	1.00	—	—	—	—
	2.50	—	—	—	—
	5.00	—	—	—	—
	10.0	—	—	—	—
90000	0.50	—	—	—	—
	1.00	—	—	—	—
	2.50	—	—	—	—
	5.00	—	—	—	—
	10.0	—	—	—	—
100000	0.50	—	—	—	—
	1.00	—	—	—	—
	2.50	—	—	—	—
	5.00	—	—	—	—
	10.0	—	—	—	—
120000	0.50	—	—	—	—
	1.00	—	—	—	—
	2.50	—	—	—	—
	5.00	—	—	—	—
	10.0	—	—	—	—

from the range of bolometric luminosities of $\log(L/L_{\odot}) \approx 5.0 - 6.5$, found for Galactic and LMC WN stars (e.g. Hamann & Koesterke 1998a; Hamann & Koesterke 2000). Most of our theoretical models for which the Baldwin-effect breaks down fall outside this luminosity range.

In the application of the fitted Baldwin-relations we will select the curves calculated at values of the stellar temperatures estimated by Hamann & Koesterke (1998a) from the He I and He II line ratios. The strategy of using the ISA-WIND curves in conjunction with temperatures and mass-loss rate ranges determined by Hamann & Koesterke (1998a), using co-moving frame model atmospheres, has been justified in the previous sections. This scheme will also prove marked improvement over the method of using a mean spectral type- M_v relation.

5.8 Discussion

We have presented theoretical relations between the equivalent width of WN star emission lines and the monochromatic continuum luminosity at the central line wavelength. These *Baldwin-relations* follow from calculations of model stellar atmospheres consisting of helium and nitrogen.

The purpose of presenting Baldwin-relations is their applicability as an estimator of Wolf-Rayet star distances. We have tested the capability of the Baldwin-relations as distance estimators by applying them to LMC star observational data, using determined mass-loss rates and terminal wind velocities derived from model atmospheres by Hamann & Koesterke (2000).

We conclude that the Baldwin-relations perform very well in the determination of stellar distances, as long as the terminal velocity, v_{∞} , and the mass-loss rate, \dot{M} , of the stars are well determined. Values of v_{∞} can be accurately derived from the stellar spectrum. Unfortunately, since derived mass-loss rate values depend on the stellar luminosity (and therefore the distance), average mass-loss rates have to be adopted. This reduces the accuracy of the Baldwin-relations in distance measurements. However, we have devised a scheme in which average mass-loss rates are determined for the separate subgroups of WNE-s, WNE-w and WNL type stars. The thus found mass-loss rates can be combined with polynome fits to the theoretical Baldwin-relations to derive monochromatic continuum luminosities. This method will lead to improved distance estimates, compared to the use of a mean equivalent width versus $L_c^{\lambda_0}$ relation, as performed by Morris (1995).

The application of this strategy will be the subject of the next chapter, where we will use the theoretical Baldwin-relations to estimate the distance of Galactic WN stars.

6

Distances of WN stars from the Baldwin-effect

6.1 Introduction

Spectral observations of Wolf-Rayet (WR) stars of the WN class in the Large Magellanic Cloud (LMC) have shown a relation with negative slope between the line equivalent width, W , of spectral emission lines and monochromatic continuum luminosity at the line wavelength, $L_c^{\lambda_0}$ (Morris et al. 1993a). A similar relation was already known to exist in the spectra of Active Galactic Nuclei (Baldwin 1977), after which the phenomenon has been called the *Baldwin-effect*. The existence of a relation between line equivalent width and continuum luminosity can provide a powerful independent method to derive distances of WR stars. Distances of WR stars have been found hard to derive, as their intrinsic colours and temperatures do not correlate well with luminosity or spectral subtype (e.g. Hamann & Koesterke 1998a, from now on HK98). Moreover, WR stars within one spectral subtype show a range of colours and absolute visual magnitudes, M_v (van der Hucht 2000). WR star distances based on photometry therefore give spurious results, with an uncertainty of more than a factor two in some cases.

The Baldwin-effect in the WR stars spectra provides a distance estimator that depends on the properties of the stellar spectrum alone. Morris (1995) used least-square fits to the observationally found W versus $L_c^{\lambda_0}$ relations to estimate distances of Galactic WN stars. The spread in these *Baldwin-relations* were considered to be gaussian and mainly due to uncertainties in the derivation of line and continuum measurements, as well as reddening corrections. Van Gent et al. (2000) (this thesis, Ch. 3) used model atmosphere calculations to show that the spread in the Baldwin-relations is physical and due to differences in mass-loss rates and terminal velocities among stars. The accuracy of distance determinations with the Baldwin-effect can therefore be refined if the mass-loss rates and terminal velocities of stars of interest are known. This was shown in Ch. 5.6, where we used parameters of WN stars in the LMC from Hamann & Koesterke (2000) to show that the theoretically predicted Baldwin-relations give accurate estimates of stellar luminosities.

Unfortunately, the mass-loss rate that is derived for WR stars is influenced by the adopted stellar distance. However, as was described in Ch. 5, the mass-loss rate of early type WN (WNE) stars is found to progress with spectral subtype¹. For WNE stars, average mass-loss rates for each spectral subtype can therefore be applied to use the Baldwin-relations to estimate

¹Hamann et al. (1995) subdivide the WNE stars in those with relatively strong emission lines and stars with weak lines, indicating this by the labels “s” and “w”, respectively. By definition, a star is labelled WNE-s when the equivalent width of the He II $\lambda 5412$ feature is larger than 37 Å. Throughout this chapter, we adopt this system of three classes of WN stars: WNE-s, WNE-w, and WNL.

their distances.

In this chapter we will apply the theoretically predicted Baldwin-relations to estimate the distance of Galactic WN stars. The observed spectral data used in this study are discussed in Sect. 6.2. Mass-loss determinations of WN stars are the subject of Sect. 6.3. The method to apply the Baldwin-relations to derive stellar distances is explained in Sect. 6.4. We derive Galactic WN stars distances in Sect. 6.5.

6.2 Observations

The spectra of LMC WN stars used for this study consist of ultraviolet (UV) and optical observational data. The UV data were obtained from the archive of the International Ultraviolet Explorer (IUE) satellite. The observations were performed using the Short Wavelength Prime (SWP) spectrograph, covering the wavelength range of 1150-2000 Å. The optical data were obtained over several years with the 1.5 m. telescope of the CTIO facility in Chile. A more extensive description of the reduction of the optical data can be found in Torres-Dodgen & Massey (1988).

For the colour excesses, used to deredden the observed spectra, we adopt mostly the values of Morris et al. (1993b) for the LMC stars. Only for those stars for which Morris et al. (1993b) derived a total colour excess $E(B - V)$ smaller than the average foreground extinction of $E(B - V) = 0.03$, we adopted the excess values of Hamann & Koesterke (2000).

For the Galactic stars, we adopt colour excesses from Morris et al. (1993b) and Conti & Morris (1990). For stars studied in common in these two studies, average values were taken. For more details on the UV and optical data and the adopted colour excesses, see Ch. 2.

6.3 Mass-loss rate determinations

The spread in the theoretically predicted Baldwin-relations is partly caused by difference in temperature among stars, but mainly by different mass-loss rates and terminal wind velocities (Ch. 3). The terminal wind velocities can be derived directly from the stellar spectrum, as Doppler broadening of WR emission lines reflects the velocity field of the stellar wind. Accurate derivations of mass-loss rates of WR stars are hampered, however, by the fact that the derived mass-loss rate value depends on the stars luminosity and therefore on its adopted distance. Most reliable mass-loss determinations are therefore to be expected for stars with a well known distance, such as stars in the LMC. Since we are interested in *finding* stellar distances by means of the theoretical Baldwin-relations, the mass-loss rate is not a-priori known. Although most studies that derive mass-loss rates have to assume a distance for the considered stars, their results can be used to test our Baldwin-relations as a distance estimator. We will therefore look into different approaches, used to derive WR star mass-loss rates. After that we will combine these studies to find average mass-loss rates for each WN spectral subtype, which can be applied with the Baldwin-relations to estimate WN star distances.

6.3.1 Mass-loss rates from detailed modelling

Detailed modelling of specific WR stars by means of model atmospheres has provided mass-loss rates for most of the known WR stars in the Galaxy and the LMC (e.g. Crowther & Smith 1997;

Hamann & Koesterke 1998a; Hamann & Koesterke 2000). Results of the different studies show overall reasonable agreement and general consensus exists on the improvements to be made in the years to come. Hamann & Koesterke (2000) accounted for inhomogeneities in the stellar wind in a study on the stellar parameters of LMC WN stars. Following Schmutz (1997), they assume the wind volume to be filled with clumps with a density that is a factor D higher than the density of a smooth, unclumped wind with the same mass-loss rate². Among the difficulties encountered in WN star studies with detailed models is the disagreement between results from studies that analyse the observed He spectrum and studies that focus on the metal lines (e.g. Hamann & Koesterke 1998a; Crowther et al. 1995c). These discrepancies are expected to be reduced when blanketing and line blending effects can be fully taken into account (Hillier & Miller 1998).

The results from detailed modelling of LMC WN stars by Hamann & Koesterke (2000) were used in Ch. 5 to test and validate our theoretically predicted Baldwin-relations. From this we learned that the Baldwin-relations give accurate results, when the mass-loss rate of the studied stars is known. In our study here, we will therefore refrain from using mass-loss rates from detailed model studies to test our Baldwin-relations in estimating Galactic and LMC stellar distances. We will use these mass-loss rates however in defining suitably average mass-loss rates for WN stars subtypes, which is discussed in Sect. 6.3.3.

6.3.2 Mass-loss rates from optical and radio observations

Nugis et al. 1998 derived clumping-corrected mass-loss rates for Galactic WR stars, based on the observed strength of optical emission lines of He II, N IV, and N V and on radio continuum spectra. As opposed to what is usually done in detailed modelling with model atmospheres, the method of Nugis et al. (1998) describes the density enhancement due to clumps as function of the radial distance to the star and separately for each star. This is different from the strategy in detailed modelling with model atmospheres, where usually clumping is described by means of a constant density enhancement throughout the wind.

Nugis & Lamers (2000) (NL, from now on) used the method of Nugis et al. 1998 to study the dependence of mass-loss rate on stellar parameters and found that the mass-loss rate of Galactic WN stars strongly depends on luminosity and chemical composition. The mass-loss rates and luminosities of the *single* WN stars from Nugis & Lamers (2000) are shown in Fig. 6.1. For comparison we show the same parameters derived with model atmosphere calculations; for the WN stars sample of HK98 (panel a) and from studies of Crowther and co-workers (panel b). Many stars in these three sample are studied in common and differences in resulting mass-loss rate and luminosity are sometimes large. All three groups show that there is a tendency of the mass-loss rate to progress with luminosity. A dependence of the mass-loss rate on luminosity was suggested by Abbott et al. (1986). They found the mass-loss rate of WN stars to progress with stellar mass and combined this with the dependence of luminosity on stellar mass, following from stellar evolution theory.

NL found the spread in their \dot{M} versus L relation to be mainly due to differences in hydrogen content of the stars. The spread in the relation of HK98 is somewhat larger than in that of NL.

² D represents the density enhancement of the clumps with respect to the density of a smooth, “unclumped” wind. The wind medium between the clumps is considered void. Hamann & Koesterke (1998b) showed a *clumping factor* of $D = 4$ to be a good representation for the inhomogeneities in all three WN subclasses (WNE-s, WNE-w, WNL). For more details about the treatment of clumping in model atmospheres, we refer to Ch. 5.5.2.

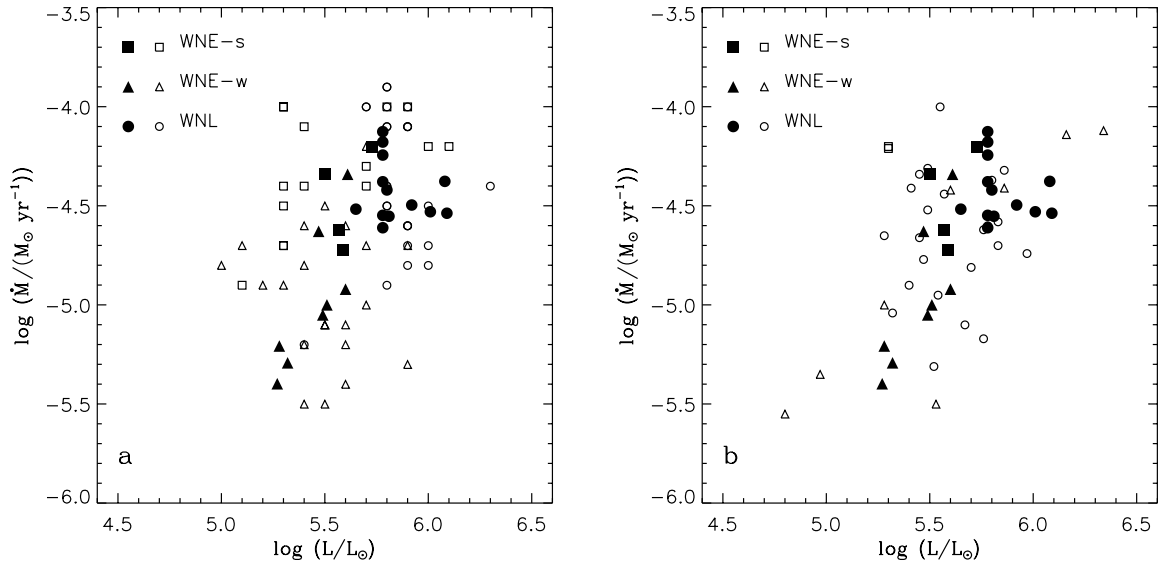


Figure 6.1: Mass loss rate versus bolometric luminosity for single Galactic WN stars. WN subclasses are distinguished by different symbol shapes, as indicated in the figure. Open symbols represent stars from HK98 (panel a) or studies from Crowther and colleague (panel b); filled symbols refer to NL.

This is for the larger part caused by the revision of the parameters of the WNE-w stars, which were assigned larger luminosities in a study of their nitrogen spectra. As mentioned in the previous subsection, problems with the detailed analyses of metal line spectra exist. The results from NL therefore provide a method to test the validity of the predicted Baldwin-relations that is independent of model atmosphere calculations.

6.3.3 Average mass-loss rates as function of spectral subtype

In Ch. 5.7 we devised a strategy to derive WN star distances by means of the theoretically predicted Baldwin-relations, combined with average mass-loss rates as function of WN spectral subtype. The idea was based on the progressive dependence of the mass-loss rates of WNE type stars with spectral subtype, found from the stellar parameters derived by HK98. Here we will combine the results from different studies to find suitable averaged mass-loss rates as function of spectral subtype. WN stars mass-loss rate is shown versus spectral subtype in Fig. 6.2. The figure combines mass-loss rates from studies on LMC WN stars by Crowther & Smith (1997) and Hamann & Koesterke (2000) and on Galactic WN stars by Crowther et al. (1995b); Crowther et al. (1995c); Crowther & Smith (1996); Crowther & Dessart (1998), and HK98. In the study of HK98 and the studies by Crowther and colleague, wind clumping was not taken into account. In Fig. 6.2 we therefore scaled down their mass-loss rates by a factor 2, accounting for an average clumping of $D = 4$. In the previous subsection we mentioned that different studies sometimes disagree in the derived parameters of similar objects. In Fig. 6.2, this is illustrated, for example, by the WN2 early type star from HK98 and that from NL. Both cases concern the same Galactic star: WR 2.

In Fig. 6.2 the three WN star subclasses of WNE-s, WNE-w and WNL stars are clearly distinguished. The strong lined WNE stars show on average larger mass-loss rates than the WNE stars with weak lines. For both these classes there is a trend of increasing mass-loss rate

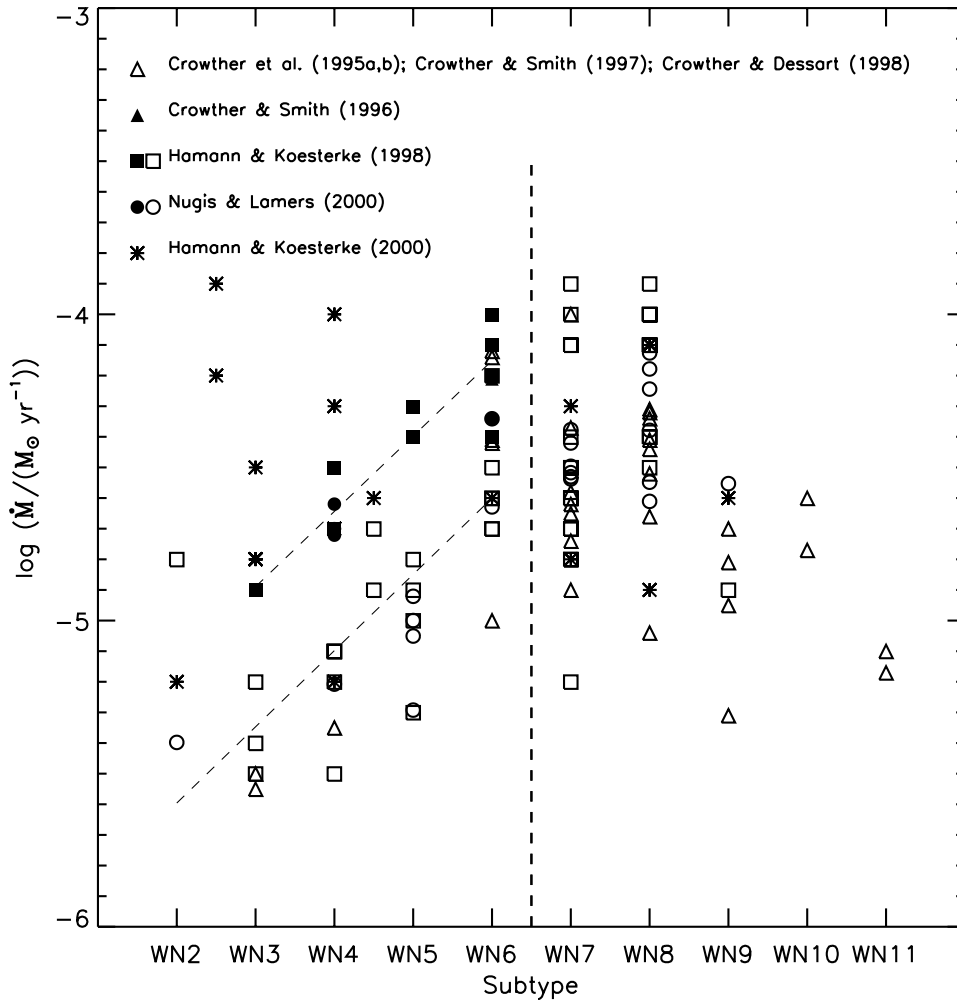


Figure 6.2: Mass loss rate versus spectral subtype from different studies. Different studies are indicated by different symbol shapes. Filled symbols distinguish the strong lined early type stars (WNE-s). The vertical dashed line separates the WNE and WNL stars. Tilted dashed lines are least square fits to the WNE-s and WNE-w stars, respectively. Stars indicate the LMC WN stars studied by Hamann & Koesterke (2000). These are excluded in the regression of the WNE-s stars (see text).

with spectral subtype. Such a trend is not visible for the WNL type stars. Each spectral subtype group of these stars shows a large range of mass-loss rates.

In looking for a representative value of the mass-loss rate for each of the three WN star classes it was suggested in Ch. 5.7 that linear regression relations between $\log(\dot{M})$ and spectral subtype are used for the WNE-s and WNE-w classes. These regression relations are indicated in Fig. 6.2 by dashed lines. Here we rather choose average values of $\log(\dot{M})$ per spectral subtype, as for the WNE-w stars the regression relations tend to overestimate the mass-loss rate for the WN3-w to WN5-w stars, due to relatively large spread in mass-loss rate for the WN6-w stars.

Average mass-loss rates for each spectral subclass, derived from the data in Fig. 6.2, are given in Table 6.1. The large standard deviation for the WNL stars indicates that the use of average mass-loss rates in the determination of stellar distances with the Baldwin-relations is expected to give unreliable results. Good results can be expected for the WNE stars. In deter-

Table 6.1: Average mass-loss rates ($\log \dot{M}/(M_{\odot} \text{yr}^{-1})$) for WN spectral subtypes.

Subtype:	WN 2	WN3	WN4	WN4.5	WN5	WN6	WN7	WN8	WN9
WNE-s	–	–4.90	–4.65	–	–4.37	–4.16	–	–	–
σ	–	–	0.09	–	0.06	0.14	–	–	–
WNE-w	–5.10	–5.43	–5.22	–4.80	–5.03	–4.49	–	–	–
σ	0.42	0.14	0.15	0.14	0.18	0.25	–	–	–
WNL	–	–	–	–	–	–	–4.51	–4.32	–4.87
σ	–	–	–	–	–	–	0.29	0.26	0.26

mining the average mass-loss values for the WNE-s stars, we have excluded the results from Hamann & Koesterke (2000). This study on LMC WN star parameters shows systematic higher mass-loss rates for the LMC WNE-s stars than the values of their Galactic counterparts. The latter are mainly derived by HK98, which use the same method as Hamann & Koesterke (2000), except that wind clumping was not accounted for. It is unclear what causes the different results from the two studies. In a study on WNL stars in the LMC, including some WN6 type stars, Crowther & Smith (1997) did not find any systematic different mass-loss rates in comparison to similar Galactic stars, although the highest mass-loss values of WN6-w stars in Fig. 6.2 are from this study. Apparently, WNE stars in the LMC have, on average, a higher mass-loss rate than their Galactic counterparts. This is contrary to theoretical expectations, because of the lower metallicity of the LMC!

Three methods to determine the mass-loss rates of WN stars have been described above:

(i) The mass-loss rates are obtained by detailed modelling with model atmospheres. Mass-loss rates from Hamann & Koesterke (2000), derived in this way, were used in Ch. 5 to test our theoretically predicted Baldwin-relations. Derived continuum luminosities from the Baldwin-relations were found to agree closely with those observed.

(ii) The mass-loss rates derive from radio continuum observations and the strength of optical emission lines. For a large part of our sample of Galactic WN star observations, mass-loss rates obtained by this method are given by Nugis & Lamers (2000) (NL). These mass-loss rates provide another test for our Baldwin-relations, independent from model atmosphere calculations. NL does not give mass-loss rates for LMC stars, so we can only test our Baldwin-relations with this method for Galactic stars. This will be done in Sect. 6.5.1.

(iii) Average mass-loss rates are determined for each WN spectral subtype. The performance of the theoretical Baldwin-relations as distance estimators, using these average mass-loss rates, can be tested by means of stars with a well known distance. This method is therefore applied in Sect. 6.5.2, focussing at Galactic stars for which the distance is known from alleged membership of an open star cluster or OB association.

6.4 Strategy

The method by which we apply the theoretically predicted Baldwin-relations to estimate stellar distances is the following. An estimate of the stars mass-loss rate is obtained, according to one of the methods described in the previous section: either the mass-loss rate from NL is adopted, which derives from observations of radio continuum spectra and from the strength of optical emission lines; or the average mass-loss rates belonging to the stars spectral type is used, as listed in Table 6.1. If the adopted mass-loss rate is derived for a clumped wind, it is enhanced by a factor two (corresponding to an average wind clumping of $D = 4$) to be used with our Baldwin-relations, which follow from “unclumped” model atmosphere calculations. Based on the terminal wind velocities presented by HK98 the ratio of mass-loss over terminal velocity can be determined. An estimate of the stellar temperature, T_* , is also obtained from HK98. For each available spectral line, we can now find the parametrisations of the Baldwin-relations presented in Ch. 5.7, that correspond closest to the value of T_* and $\dot{M}\sqrt{D}/v_\infty$ of our star of interest. If the star lies between two *Baldwin curves*, we interpolate in $\log(\dot{M})$ space. With the value of the line equivalent width from our observed spectra we then find the stars continuum luminosity, which is then used to derive its distance.

6.5 Distance to Galactic WN stars

In Ch. 5.6 it was demonstrated that the theoretically devised Baldwin-relations can provide accurate stellar distances if mass-loss rates from detailed modelling with stellar atmospheres are used. Since accurate derivation of a stars mass-loss rate by detailed modelling requires the distance to be known, we will look at two other approaches in this section to estimate stellar mass-loss rates. We will then use these mass-loss rates together with the theoretical Baldwin-relations to derive distances of Galactic WN stars. We will express the derived distances in terms of the *distance modulus*, Y , which is defined as the difference between the apparent magnitude and the absolute magnitude of an object

$$Y = m_0 - M = 5 \log(d) - 5, \quad (6.1)$$

where the apparent magnitude m_0 is derived from the unreddened spectrum and d is the distance in pc.

6.5.1 Mass-loss rates from observations

In Ch. 5, the theoretically predicted Baldwin-relations were tested by deriving the luminosity of LMC WN stars based on mass-loss rates from model atmosphere calculations of Hamann & Koesterke (2000). The test showed good agreement between the derived luminosities and those determined from the observed spectra.

However, problems exist in the calculation of stellar parameters with model atmospheres and inhomogeneities in the stellar wind and the effects of blanketing are not always accounted for (see Sect. 6.3.1). We therefore also want to use independently derived mass-loss rates, not based on model atmosphere calculations, to test our Baldwin-relations as distance estimators. Such independently obtained mass-loss rates are given by NL and were discussed in Sect. 6.3.2.

Distance moduli, derived with our predicted Baldwin-relations, and based on the mass-loss rates of NL (derived from observations), are given in Table 6.2, column 5. In the table, we

only list those stars for which the distance is already thought to be known from their alleged membership of a stellar cluster or association. Unless indicated otherwise, the acknowledged distance moduli of cluster/associations in Table 6.2 are taken from Lundström & Stenholm (1984). These authors studied the cluster/association membership of 50 Galactic Wolf-Rayet stars, of which 37 are of WN type. The alleged cluster or association membership was classified to be *definite*, *probable*, or *possible*. These cluster/association distance moduli from literature are given in column 4 of Table 6.2.

Our estimated distance moduli, with the mass-loss rate from NL, are compared with their alleged cluster/association distance modulus in Fig. 6.3 a.

We will now discuss the results in order of certainty of cluster/association membership.

Stars with definite membership These stars should give us the most reliable information about the quality of our distance estimates, as they are almost certainly members of a cluster/association of well known distance. We see varying results, however. The distance moduli derived by us for WR 22 and WR 89 agree well with their acknowledged cluster/association distance. Particularly for WR 141, the result seems less favorable. Our used colour excess of $E(B - V) = 1.12$ agrees quite well with that used by NL ($E(B - V) = 1.14$). NL give a mass-loss rate of $\log(\dot{M}) = -4.92$ for this star, whereas the (unclumped) mass-loss rate found by HK98 is $\log(\dot{M}) = -3.9$. Even when accounting for clumping ($D = 4$) the latter value is still 5 times higher than the mass-loss rate of NL. A clumping correction of $D = 100$ (!) would have to be applied on the value of HK98 to get the mass-loss rate that NL obtained for this star.

Stars with probable membership Ten stars are presented in this category and membership is confirmed for about half of them. For the poor results of WR 2 and WR 138 we again notice that NL present a much lower mass-loss rate than HK98. The high distance modulus obtained for WR 51, WR 67 and WR 115 can not be explained by different mass-loss rates. Before stating that the membership for these stars probably needs to be revised, we await our results of the next subsection, where we derive distance moduli for these stars based on average mass-loss rates of their spectral subtype.

Stars with possible membership Most of these stars do not belong to the program stars of NL. For the only available star, WR 6, discussion is ongoing on its membership of the open cluster Cr 121. Lundström & Stenholm (1984) give a distance modulus of $Y = 9.8$ mag. for this cluster. Based on the strength of interstellar spectral lines, Howarth & Schmutz (1995) concluded the star to be at a much larger distance, $Y = 11.3$ mag., in close agreement to our result obtained here. Membership of Cr 121 is however reconfirmed by the proper motion and parallax measured by HIPPARCOS (de Zeeuw et al. 1999).

From the above evaluation of cluster and association membership of Galactic WN stars, we found that stellar distances obtained from the Baldwin-relations are often underestimated when mass-loss values of NL are used. In the next subsection we discuss distance parameters for the same Galactic WN stars, this time based on average mass-loss rates prescribed for each WN spectral subtype.

6.5.2 Mass-loss rate as function of spectral subtype

In this section, we will estimate the distances of Galactic WN stars, based on prescribed mass-loss averages as function of spectral subtype. The average mass-loss rates for each WN spectral subtype are given in Table 6.1. Following the strategy described in Sect. 6.4, we obtain distance moduli for our sample of Galactic WN stars. For the stars with alleged cluster or association membership, the derived distance moduli are listed in column 7 of Table 6.2. Fig. 6.3 b compares our obtained distance moduli with that of the corresponding cluster or association. We discuss the results again in order of reliability of cluster/association membership.

Stars with definite membership Quite similar results are obtained as in Sect. 6.5.1, were we used mass-loss rates from NL. The distance of WR 141, however is remarkably different and is in much closer agreement with the distance of the Cyg OB1 cluster.

Stars with probable membership Our results for this class of stars seems better than from the method used in Sect. 6.5.1. This is mainly due to higher mass-loss rates for WR 2 and WR 138. In Sect. 6.5.1 we obtained a distance for WR 51, WR 67 and WR 115 that is much larger than of their alleged host cluster. These high values for the distance modulus of these stars is confirmed with our method here. Van der Hucht (2000) lists a *photometric* distance modulus for WR 51 of $Y = 14.53$ mag, based on the relation of average absolute visual magnitude with spectral subtype. Membership of WR 51 may therefore need to be reconsidered.

Stars with possible membership For four of the eight stars in this category, membership is confirmed by our results. The result for WR 6 is not very good, but membership of the Cr 121 cluster seems to be ruled out, in agreement with our result in Sect. 6.5.1. Membership of WR 18, WR 66, and WR 120 seem doubtful.

From the study of Galactic WN stars that are thought to be a member of an open cluster or stellar association, we conclude that theoretically predicted Baldwin-relations give reasonably well distance estimates if average mass-loss rates as function of spectral subtype are used.

Although the uncertainties are sometimes large, for the application of the Baldwin-relations in estimating stellar distances, we prefer the use of average mass-loss rates for each WN spectral subtype above those obtained from NL. This is because the latter performs slightly worse in confirming the membership of stars of which membership of a cluster/association is thought “definite” or “probable”. Moreover, we observe that with the mass-loss rates, the discrepancy between the derived distance modulus and the distance modulus of the alleged host cluster/association is largest for the stars WR 138 (a ‘probable’ member) and WR 141 (definite membership). Interestingly, these are the only stars in Table 6.2 that are known to be (possibly) in a binary. However, an O or B star companion generally only contaminates the *continuum* spectrum of the WR star; a large contribution of the companion to the *flux* of spectral lines is not to be expected. If indeed the WR star continuum spectrum is diluted by the companion, and a correct estimate is made of the WR stars mass-loss rate, the measured line *equivalent widths* are lower than if the WR star would have been single. The slope of our theoretically predicted relations between line equivalent width and continuum luminosity (the Baldwin-relations) is roughly $\alpha = -1$ or slightly steeper (see Ch. 5). Due to spectral dilution by the companion star, the derived continuum luminosity will therefore most likely be slightly underestimated.

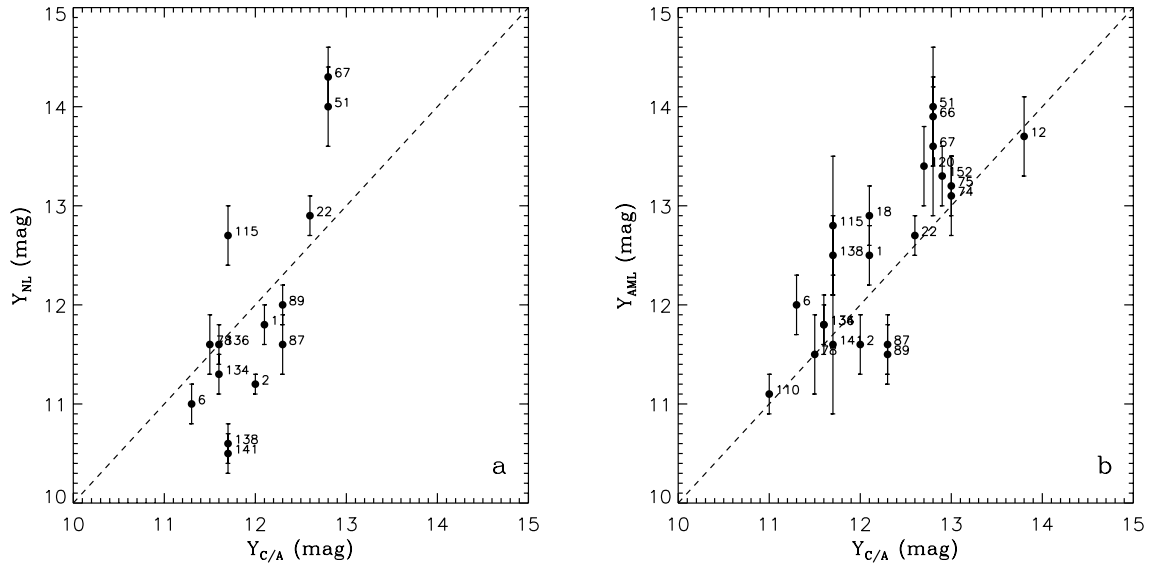


Figure 6.3: Distance modulus derived with the Baldwin-relations versus distance modulus of cluster/association. Panel a: using mass-loss rates from Nugis & Lamers (2000), derived from observed radio spectra and optical emission lines. Panel b: using average mass-loss rates for each WN spectral subtype.

An overestimate of the distance is the result. This indicates that, for WR 138 and WR 141, adopting the average mass-loss rate of their spectral type provides a better estimate of their true mass-loss, than the mass-loss rates from NL.

We therefore apply the method of using average mass-loss rates for each spectral subtype to present distance estimates for our complete sample of Galactic WN stars. The results are listed in Table 6.3. The value of the distance modulus in column 10 in this table, is the average over the separate derivations for the different He lines (columns 3 to 9).

6.6 Discussion

We have applied theoretically predicted Baldwin-relations to estimate the distances of single WN stars in the Milky Way galaxy. It was already shown in Ch. 5 that good results are obtained from the Baldwin-relations if mass-loss estimates from model atmosphere calculations, presented in literature, are used. As an independent way to validate the Baldwin-relations, we used mass-loss rates from Nugis & Lamers (2000, NL), derived from optical and radio observations, to derive distance estimates for Galactic WN stars that have a well known distance from their membership of an open cluster or OB association. The results are less accurate than with the mass-loss rates from model atmospheres, obtained in Ch. 5. The best results were obtained for those stars for which the mass-loss rate from NL closely agrees to that derived from model atmosphere calculations (e.g. HK98).

Using average mass-loss rates generally gave better results than using the mass-losses from NL. As the latter method generally performs less in confirming cluster/association membership than using average-mass-loss rates, we conclude that our theoretically Baldwin-relations are well predicted and the mass-loss rates of NL may in some cases be less reliable than those

Table 6.2: Distance moduli of Galactic WN stars in open clusters and OB associations.

WR ^a	Subtype ^b	Cluster/ Association	$Y_{C/A}$ ^c (mag)	Y_{NL} ^d (mag)	$\sigma_{Y_{NL}}$ (mag)	Y_{AML} ^e (mag)	$\sigma_{Y_{AML}}$
Definite							
22	WN7 + abs	Car OB1	12.6 ^f	12.9	0.2	12.7	0.2
87	WN7	HM 1	12.3	11.6	0.3	11.6	0.3
89	WN7	HM 1	12.3	12.0	0.2	11.5	0.3
141	WN6-w	Cyg OB1	11.7	10.5	0.2	11.6	0.7
Probable							
1	WN5-s	Cas OB7	12.1	11.8	0.2	12.5	0.3
2	WN2-w	Cas OB1	12.0	11.2	0.1	11.6	0.3
51	WN4-w	Sk 16	12.8 ^g	14.0	0.4	14.0	0.6
67	WN6-w	Pi 20	12.8	14.3	0.3	13.6	0.7
78	WN7	NGC 6231	11.5	11.6	0.3	11.5	0.4
115	WN6-w	Ser OB1	11.7	12.7	0.3	12.8	0.7
134	WN6-s	Cyg OB3	11.6	11.3	0.2	11.8	0.2
136	WN6-s	Cyg OB3	11.6	11.6	0.2	11.8	0.3
138	WN5+abs	Cyg OB1	11.7	10.6	0.2	12.5	0.4
152	WN3-w	Cep OB1	12.9	–	–	13.3	0.3
Possible							
6	WN5-s	Cr 121	11.3 ^h	11.0	0.2	12.0	0.3
12	WN7	B0 7	13.8	–	–	13.7	0.4
18	WN5-s	Car OB1	12.1	–	–	12.9	0.3
66	WN8	Pi 20	12.8	–	–	13.9	0.3
74	WN7	Nor OB4	13.0	–	–	13.1	0.4
75	WN6-s	Nor OB4	13.0	–	–	13.2	0.3
110	WN6-s	Sgr OB1	11.0	–	–	11.1	0.2
120	WN7	Do 33	12.7	–	–	13.4	0.4

^aWR numbers are from van der Hucht et al. (1981).^bClassification from Smith (1968), amended by Hamann et al. (1995) to discriminate between WNE-s and WNE-w stars.^cCluster/Association distance moduli from Lundström & Stenholm (1984), unless stated otherwise.^dDistance moduli from the Baldwin-relations, using mass-loss rates from observations, presented by Nugis & Lamers (2000).^eDistance moduli from the Baldwin-relations, using average mass-loss rates.^fCudworth et al. 1993.^gvan der Hucht (2000). derives a photometric distance modulus of 14.53 mag. for this star.^hDistance modulus of WR 6, from Howarth & Schmutz (1995). These authors derive this value as an underlimit.

Table 6.3: Distance moduli of Galactic WN stars as estimated with the theoretical Baldwin-relations.

WR ^a	Subtype ^b	Y							\bar{Y}	$\sigma_{\bar{Y}}$
		He II $\lambda 1640$	He II $\lambda 2511$	He II $\lambda 2733$	He II $\lambda 3203$	He II $\lambda 4686$	He II $\lambda 5412$	He I $\lambda 5876$		
1	WN5-s	12.5	12.5	12.4	12.6	12.6	—	—	12.5	0.3
2	WN2-w	11.7	—	11.6	11.7	11.6	11.6	—	11.6	0.3
3	WN3a-w+c	13.0	—	—	13.5	12.7	12.5	—	12.9	0.2
6	WN5-s+c?	12.4	11.7	12.0	12.0	12.1	—	—	12.0	0.3
7	WN4-s	14.2	13.8	14.0	13.8	14.0	13.8	—	13.9	0.7
10	WN4.5-w	16.0	—	14.5	—	15.7	15.8	—	15.5	0.5
12	WN7	—	—	—	—	—	—	13.7	13.0	0.4
16	WN8	—	—	—	—	—	—	13.5	13.5	0.4
18	WN5-s	13.2	12.8	12.8	—	12.9	—	—	12.9	0.3
20	WN4.5-w	—	—	—	—	15.1	14.7	—	14.9	0.6
22	WN7a+c	—	—	—	—	—	—	12.7	12.7	0.2
35	WN6-w	—	—	—	—	—	17.2	16.7	17.0	0.6
36	WN4-s	—	—	—	—	13.5	13.6	—	13.6	0.4
37	WN3-s	—	—	—	—	11.9	12.1	—	12.0	0.4
40	WN8	—	—	—	—	—	—	12.4	12.4	0.5
44	WN4-w	14.6	14.5	14.6	14.6	14.7	14.7	—	14.6	0.4
46	WN3pec-w	12.7	—	12.5	—	12.3	12.3	—	12.5	0.3
49	WN5-w	—	—	—	—	15.3	15.1	—	15.2	0.7
51	WN4-w	—	—	—	—	14.0	13.9	—	14.0	0.6
55	WN7	14.8	13.1	14.0	15.0	—	14.0	13.4	14.0	0.2
58	WN4-s	—	—	—	—	15.7	15.5	—	15.6	0.4
61	WN4.5-w	15.3	14.0	14.6	16.2	14.0	14.6	15.4	14.9	0.4
66	WN6	—	—	—	—	—	—	13.9	13.9	0.3
67	WN6-w	—	—	—	—	13.2	13.7	14.0	13.6	0.6
74	WN7	—	—	—	—	13.4	13.7	12.4	13.2	0.3
75	WN6-s	14.8	12.1	13.1	13.3	13.4	12.8	—	13.2	0.3
78	WN7	—	—	—	—	—	—	11.5	11.5	0.4
82	WN8	—	—	—	—	—	15.7	14.4	15.0	0.3
84	WN6-w	—	—	—	—	—	13.8	13.7	13.7	0.7
87	WN7	—	—	—	—	—	—	11.6	11.6	0.3
89	WN7	—	—	—	—	—	—	11.5	11.5	0.3
91	WN6-s	—	—	—	—	—	10.4	—	10.4	1.2
110	WN6-s	11.0	11.0	11.2	—	11.1	11.2	—	11.1	0.2
115	WN6-w	—	—	—	—	—	13.3	12.9	13.1	0.5
120	WN8	—	—	—	—	—	—	13.4	13.4	0.4
123	WN8+c	—	—	—	—	—	—	15.0	15.0	0.5
124	[WN8]?+h	—	—	—	—	—	—	14.6	14.6	0.7
128	WN4-w	13.8	13.4	13.7	14.0	13.8	14.0	—	13.8	0.4
129	WN4-w	—	—	—	—	13.7	13.4	—	13.6	0.6
130	WN8	—	—	—	—	—	—	13.4	13.4	0.3
131	WN7a	—	—	—	—	—	—	15.1	15.1	0.4
134	WN6-s+c	12.0	11.6	12.4	11.5	11.7	11.8	—	11.8	0.2
136	WN6-s+c	12.2	11.2	11.8	11.6	11.9	11.9	—	11.8	0.3
138	WN6a-w	12.7	12.4	12.4	12.5	12.3	12.5	12.5	12.5	0.4
141	WN6-w+c	—	—	—	—	—	—	11.6	11.6	0.7
147	WN7+c	—	—	—	—	—	—	11.3	11.3	0.4
148	WN7+c	—	—	—	—	—	—	14.4	17.2	0.2
149	WN6-s	—	—	—	—	17.0	16.0	—	16.5	0.3
152	WN3-w	13.4	13.4	13.2	13.5	13.1	13.1	—	13.3	0.3
155	WN7+c	—	—	—	—	—	—	14.1	11.9	0.3
156	WN8	—	—	—	—	—	—	14.3	14.3	0.4
157	WN4.5-w	—	—	14.6	—	14.6	13.8	—	14.3	0.5
158	WN7	—	—	—	—	—	—	14.4	15.5	0.2

^aWR numbers are from van der Hucht et al. (1981).

^bClassification from Smith (1968), amended by Hamann et al. (1995) to discriminate between WNE-s and WNE-w stars.

derived from model atmosphere calculations.

Sometimes, the uncertainty in our derived distance moduli is uncomfortably large, particularly for the WNL stars. For those stars our method to estimate the distance does not perform much better than using the relation between average absolute magnitudes and spectral subtype (e.g. HK98). Improvements for the Baldwin-relations as distance estimators are however to be expected, when increased knowledge of clumping phenomena and blanketing effects in WR star winds will lead to more consensus about the mass-loss rates of Wolf-Rayet stars.

Any dependence of the mass-loss rate on spectral subtype is not observed for WN stars in the LMC. The LMC WNE stars show on average higher mass-loss rates compared to the Galactic WNE stars, which is not what is expected from the metallicity content of the LMC. However, the deviating mass-loss behaviour of WNE stars in the LMC means that more knowledge is required about the mass-loss rates of WR stars in other galaxies before theoretically predicted Baldwin-relations can be applied to measure extra-galactic distances.

Summary and prospects

Summary of the thesis

This thesis describes the Baldwin-effect in Wolf-Rayet (WR) stars, a relation between the equivalent width of emission lines and the monochromatic luminosity at the line wavelength of the underlying continuum. The connection between spectral characteristics and stellar luminosity directly suggests the Baldwin-effect could function as a distance estimator of WR stars.

The importance of accurate determination of WR star distances has become obvious in Ch. 1, which is an introductory chapter to the rest of the thesis. Because of the optically thick stellar wind, observational properties of WR stars, such as intrinsic colours and absolute magnitudes, do not correlate well with each other. Methods to derive stellar distances, that work well for other stars, therefore do not apply to WR stars. Furthermore, Ch. 1 introduced the Baldwin-effect in WR stars: its observational discovery and its value as a distance estimator, because it seems to depend on properties of the observed spectra alone.

Ch. 2 described the spectral observations used in this thesis project. After some general words about interstellar extinction, several techniques to derive interstellar extinction properties were described. Particularly, attention was paid to the methods that were applied to derive the colour excesses that have been used in this thesis.

In Ch. 3 the physics behind the Baldwin-effect was studied. This was done by means of model atmosphere calculations and synthetic spectra of He II lines. Theoretically predicted relations between line equivalent width and monochromatic continuum luminosity (Baldwin-relations), based on pure helium model atmospheres, were presented for five He II transitions. Separate relations were presented for different values of the stellar temperature, T_* . The idea was confirmed that differences in wind density among stars cause the Baldwin-effect. For a certain terminal wind velocity and mass-loss rate, stars with a smaller radius have the highest wind density. Accordingly, the spectral emission lines are relatively strong, whereas the small radius causes a low luminosity. Vice versa, larger stars show weaker lines and a higher continuum luminosity. In the spectral observations of LMC WN stars, the relation between equivalent width and monochromatic continuum shows a certain spread; Previously, this spread was mainly attributed to a gaussian distributed uncertainty in the measured line equivalent width values and level of the continuum, as well as uncertainties in the reddening corrections. The model calculations, however, showed that the spread is physical in nature, and reflects differences in mass-loss rate and terminal wind velocity among stars. The range in basic WR star parameters, over which the Baldwin-effect shows, was found to be limited. The He II line spectra showed that the Baldwin-effect disappears if the considered sample of stars shows too large differences

in the ionization balance in the wind. Mainly, it was observed that the Baldwin-effect breaks down for the densest winds and the lowest stellar temperatures. This is because He III recombines to He II, reducing the equivalent width of the He II recombination lines. Finally, it was suggested that the application of theoretically predicted Baldwin-relations, to measure stellar distances, may be hampered by the fact that the spread in the relations is largely caused by differences in mass-loss rate. A reasonable estimate of the mass-loss rate would therefore be required, before a distance can be derived. This is not straightforward, as was already seen in Ch 1.

Model atmosphere calculations are always a simplified representation of the outer layers of a star as they appear in nature. Therefore, before theoretically predicted Baldwin-relations can be used to derive stellar distances, their calibration may be required. This can be done by studying the major assumptions made in the model atmosphere calculations. With the Baldwin-effect in mind, the use of model atmospheres in WR star studies was discussed in Ch. 4. Several assumptions were described, such as spherical symmetry, chemical composition, and representations of the temperature structure in the stellar wind. It was found that model atmosphere calculations perform better for early type WN stars than for late types. Also, the results of two model atmosphere computer codes were compared. Differences between the two codes in the predicted ionization balance of nitrogen were found, but could not be explained. However, a better treatment of the model atoms of metals seems warranted.

In Ch. 5 the validation of predicted WN star Baldwin-relations from model atmosphere calculations was described. The omission in the model atmosphere calculations of two physical processes was discussed. These processes are electron scattering of line photons and clumping phenomena in the stellar wind. It was found, that the influence of electron scattering on the predicted Baldwin-relations is not large, although including this process will give better Baldwin-relations, particularly for late type WN stars. Clumping can be accounted for by a simple scaling of the Baldwin-relations.

New theoretical Baldwin-relations were presented, based on model atmospheres consisting of helium and nitrogen. The application of these predicted Baldwin-relations as a distance estimator of stellar distances was tested. This was done by means of WN stars in the Large Magellanic Cloud (LMC), for which the distance is accurately known. In estimating the distances of these stars, mass-loss rates from literature were used. The distances obtained from the predicted Baldwin-relations were found to agree closely to the acknowledged distance modulus of the LMC of $Y = 18.5$.

Anticipating the use of the Baldwin-relations to estimate the distance of *Galactic* WN stars, a scheme was devised that describes average mass-loss rates for each WN spectral subtype.

Based on average mass-loss rates for the spectral subtypes of WN stars, distances of Galactic WN stars were estimated in Ch. 6 by means of the theoretically predicted Baldwin-relations. The accuracy of the method was tested by means of WN stars that are thought to be a member of an open star cluster or OB association. It was found that the Baldwin-relations provide reasonable accurate distances for early type WN stars. For late type stars, the range in mass-loss rate for any spectral subtype is large, resulting in uncertain distances.

Prospects

The physics that causes the Baldwin-effect in Wolf-Rayet stars has become clear in this thesis. Unfortunately, it has also been found that currently the Baldwin-effect does not perform very well as a distance estimator. As we have seen, the main reason for this is that the mass-loss rate of a star must be known, ere its distance can be determined through the Baldwin-relations. Currently, several methods exist to derive mass-loss rates of Wolf-Rayet stars, but many of them depend on prior knowledge of the stellar distance. Even for Wolf-Rayet stars with known distances the scatter in derived mass-loss rates can be large.

Our method of determining average mass-loss rates for each WN star subtype did not result in the derivation of accurate distances by means of the Baldwin-effect. However, the method has made clear, that the spread in mass-loss rates for a certain spectral subtype is not completely physical. Uncertainties in the applied methods to derive these mass-loss rates play a role. Improved insight in the values of the mass-loss rates as function of spectral subtype may however be expected.

This kind of progress will for a large part come from improved model atmosphere calculations. The inclusion of clumping and blanketing effects in Wolf-Rayet star model calculations are already showing promising results.

Although improved knowledge on the mass-loss behaviour of Wolf-Rayet stars is required in order to apply the Baldwin-relations as an estimator of Wolf-Rayet star distances, the Baldwin-effect is likely to perform better in this way for O stars. O stars are expected to show a Baldwin-effect for far infrared emission lines. At those wavelengths, the continuum radiation field becomes dominated by free-free processes and is formed in the stellar wind, therewith meeting the requirements for the occurrence of the Baldwin-effect.

For O stars, derived mass-loss rates are much more reliable than for Wolf-Rayet stars, which provides good ground to investigate the behaviour of the Baldwin-effect as a distance estimator of O stars.

Het Baldwin-effect in Wolf-Rayet sterren.

Het was een mooie middag. De zon straalde en het was warm. Het enig hoorbare geluid was het zoemen van de moter, de wind die langs het openstaande raampje wakkerde en af en toe het geblaas van een schaap dat verschrikt naar de zijkant van de weg vluchtte, als het je auto in de gaten kreeg.

Wat was begonnen als rondrit door dit heuvellandschap, zonder duidelijke bestemming, was veranderd in een doelgericht afstevnen op de witte bergtop, daar heel in de verte. Al toen de eerste heuvels links en rechts van de auto verschenen, had deze imposante bergtop zich afgetekend aan de horizon. Binnen twee uur ben ik daar wel, had je gedacht, en wie weet zou je met de auto wel zo hoog kunnen komen dat je even de koele sneeuw door je handen kon laten glijden.

De uren verstreken; het werd middag en de berg leek nog altijd even ver weg als hij die morgen had geleken. De aanvankelijk fris groen gekleurde heuvels werden langzaam donkergeel en toen oranje. Schaduwen van heuveltoppen werden langer en bedekten al gauw het grootste deel van de omgeving. En toen, onverwacht snel, verdween de zon achter een lage heuvelrug en werd het snel donkerder. En met het verdwijnen van het laatste streepje zonlicht beseftte je dat je je behoorlijk vergist had in de afstand tot de berg. Het ding was in werkelijkheid waarschijnlijk veel groter dan je je kon voorstellen. Onbewust had je geschat dat de afmetingen van de berg ongeveer overeen moesten stemmen met de heuvels om je heen en aldus geconcludeerd dat de afstand er heen wel meeviel. En ja, de berg leek wel niet zo groot, maar was het wel en stond ook op een veel grotere afstand dan in een middag was te overbruggen.

En plotseling was het dus donker. Aardedonker zelfs. Want straatverlichting was hier niet en het laatste dorp had je alweer een uur geleden gepasseerd. De betovering van de bergtop had er bovendien voor gezorgd dat je niet echt opgelet had waar je je bevond. Het beste was dus gewoon door te rijden tot het volgende dorp en daar een overnachtingsplek te zoeken. Geleid door het licht van de koplampen reed je rustig verder, tot na een half uur eindelijk een lichtje in de verte zichtbaar werd; waarschijnlijk een boerderijtje. Nee, er was nog een tweede lichtje er vlakbij, een beetje zwakker. Een huisje wat verder weg. Misschien was er vlak daarna wel een heel dorp. Hopelijk wist men bij één van de twee huisjes hoever het eerstvolgende hotelletje nog was of misschien bood men er zelfs wel een slaapplek aan.

Maar wat nu? De lichtjes werden helderder! Feller en feller, hoewel er één het helderst bleef. Langzaam werd ook een ronkend geluid hoorbaar. Het licht was nu bijna oogverblindend. Dan een zovend geluid en... de vrachtauto was voorbij. Een vrachtauto met één heldere en één niet goed functionerende, minder heldere koplamp, maar die wel steeds allebei even ver van je vandaan waren geweest.

Hier op aarde zijn we gewend de afstand van de dingen die we zien te schatten aan de hand van hoe groot die dingen lijken en aan de hand van hoe de dingen in hun omgeving passen. Zoals

hierboven is gebleken, kan deze informatie soms nogal bedrieglijk zijn en hebben we zaken als kilometerpaaltjes of landkaarten nodig om een werkelijk idee van de afstand te hebben. Ook de helderheid van dingen geeft ons informatie over hun afstand. Maar, zoals we zagen is een lamp die zwak lijkt niet altijd ver weg; Hij kan ook zwak overkomen omdat hij gewoon minder licht uitstraalt.

Dezelfde problemen met betrekking tot afmetingen en helderheid komen we tegen bij afstandmetingen in de sterrenkunde. Dit proefschrift gaat over een eigenschap van bepaalde sterren, waarmee mogelijk afstanden tot sterren te bepalen zijn: het *Baldwin-effect in Wolf-Rayet sterren*.

We zullen eerst kijken naar wat sterren nu eigenlijk zijn. Daarna kijken we naar methoden die in de sterrenkunde gebruikt worden om afstanden van sterren te bepalen. Vervolgens bekijken we een bepaald soort sterren, de Wolf-Rayet sterren en we zullen begrijpen dat het bepalen van hun afstand niet eenvoudig is. Daarna kijken we naar het Baldwin-effect, waar dit proefschrift over gaat. Tot slot volgt er een korte beschrijving van de inhoud van elk hoofdstuk van dit proefschrift.

Sterren, wat zijn ze en waarom is kennis over hun afstand belangrijk?

Sterren zijn grote bollen gas, die licht uitstralen omdat in hun binnenste *kernfusie* optreedt, een proces waarbij atomen samensmelten tot een nieuw, zwaarder atoom. Bij dit proces komt energie vrij in de vorm van licht. Onze zon is ook een ster. Dat de zon zo veel helderder lijkt dan alle sterren die we 's nachts zien, komt enkel en alleen omdat de zon zoveel dichterbij staat dan die andere sterren.

Sterren zijn er in vele soorten. Er zijn grote en kleine sterren, zware en lichte, hete en koude, heldere en zwakke. Sterren komen zelfs voor in allerlei kleuren. Die verschillende eigenschappen betekenen ook dat sterren een verschillende levensloop hebben. Bij een ster met veel massa (een "zware" ster) is door de zwaartekracht de materie in zijn binnenste veel meer samengeperst en daardoor heter dan bij een minder massieve ster. Dit heeft gevolgen voor het verloop van de kernfusie, want die gaat veel sneller bij hogere temperaturen. Een massieve ster is dus ook sneller door zijn "brandstof" heen en leeft daardoor korter dan een lichtere ster.

Het is belangrijk de afstand te weten tot alle sterren die we zien. Dit leert ons namelijk iets over de verdeling van de sterren om ons heen en daarmee over de geboorte en levensloop van sterren en de structuur en geschiedenis van het heelal. Zijn er bijvoorbeeld in een bepaald gebied meer zware sterren dan in een ander gebied? Worden er om ons heen overal evenveel sterren per jaar gevormd? Horen sterren die je in groepjes bijeen ziet werkelijk bij elkaar en zijn ze samen ontstaan? Of staan ze alleen maar in dezelfde richting en staat de een veel verder weg dan de andere? En voor de meest lichtsterke sterren, die je tot heel ver weg nog kan zien, kan hun precieze afstand ons zelfs iets leren over de manier waarop ons heelal uitdijt.

Afstandsbepalingen van sterren

We hebben al gezien dat voor "aardse zaken" de schijnbare grootte en helderheid van een object valse informatie kunnen geven omtrent de afstand tot dat object. Een groot object dat ver weg

staat of een klein object dichtbij, kunnen allebei even groot *lijken*. Net zo kan een veraf staand object dat veel licht uitzendt net zo helder lijken als een lichtzwakker object op kleine afstand.

De afstanden van sterren zijn nauwelijks aan de hand van hun grootte te meten. Zelfs al zou je de werkelijke grootte van een ster kennen, dan zou je nog niets hebben aan hoe groot hij aan de hemel lijkt. Alle sterren (behalve de zon) staan namelijk zo ver weg dat het allemaal puntjes blijven, al gebruik je de grootste telescoop. Als voorbeeld: stel dat je zo snel zou kunnen vliegen dat je in 8 minuten bij de zon bent, die 150 miljoen kilometer van ons verwijderd is ¹. Met die snelheid zou je nog meer dan 4 jaar nodig hebben om de dichtstbijzijnde ster te bereiken. Helderheid lijkt dus een betere manier op afstanden te bepalen dan de grootte. Zoals we inmiddels weten, is de schijnbare helderheid niet genoeg. Je moet eerst weten hoeveel licht de ster werkelijk uitstraalt voordat zijn helderheid aan de hemel je informatie over zijn afstand geeft. Ofwel, is de ster een 60 of een 100 Watt lamp?²

Nu is de volgende vraag dus: Hoe weet je hoeveel licht een ster uitstraalt? Gelukkig blijkt voor de meeste sterren, dat de hoeveelheid licht die ze uitstralen gekoppeld is aan de kleur die ze hebben. En dat heeft weer te maken met de temperatuur van de ster. Hoe dat precies zit zullen we hier buiten beschouwing laten, maar je kan het vergelijken met een stuk ijzer dat gaat gloeien als je het in het vuur houdt. Hoe heter het wordt, hoe feller het oplicht. Bovendien zal met de stijging van de temperatuur de kleur van het gloeiende ijzer langzaam veranderen: van rood-oranje zal het geel worden, dan blauw en tenslotte wit. Kortom, lichtsterkte en kleur variëren met de temperatuur en zijn dus aan elkaar gekoppeld. Dit fenomeen is erg handig bij de afstandsbeoordeling van sterren. Van veel sterren is dan ook aan de hand van hun kleur de afstand bepaald.

Helaas gaat deze methode niet op voor alle sterren. Juist voor veel van de meest lichtkrachtige sterren blijkt de kleur niet gerelateerd aan hun lichtkracht. En de helderste sterren zijn heel belangrijk, omdat ze op grote afstand nog zichtbaar zijn.

Voor deze heldere sterren blijken er soms andere methoden te bestaan om achter hun afstand te komen. Een goede afstandsbeoordeling kan, bijvoorbeeld, worden verkregen wanneer zo'n heldere ster onderdeel is van een hele groep sterren. Van de zwakkere sterren in de groep kan je dan wel de afstand aan de hand van hun kleur bepalen en weet je zodoende ook hoe ver de heldere ster van je af staat. Lang niet elke heldere ster behoort echter tot zo'n sterrengroep. Andere methoden om hun afstanden te bepalen zijn dan ook nodig. We zullen nu eerst eens kijken wat voor sterren dat zijn, waarvan de kleur en de lichtkracht zo slecht van elkaar afhangen.

Sterrenwinden, spectra en Wolf-Rayet sterren

Materieverlies van sterren

De sterren die het meeste licht uitzenden vertonen een bijzonder gedrag. We hebben het dan over sterren die honderdduizend tot een miljoen maal zoveel licht uitzenden als de zon. Die grote lichtkracht heeft als resultaat dat de buitenste lagen van de ster geleidelijk worden weggeblazen. Net zoals de wind in het zeil van een zeilboot duwt en hem zo laat varen, zo kan licht ook iets voortduwen. En als een ster dus maar lichtsterk genoeg is wordt een deel van het gas

¹de snelheid die je dan hebt is de snelheid waarmee licht zich door de ruimte voortplant

²Als je de werkelijke lichtkracht van sterren in Watt zou willen uitdrukken, dan krijg je een getal van zo'n 26 cijfers!

waaruit de ster bestaat het heelal in geblazen, een continu proces dat tienduizenden tot honderdduizenden jaren kan duren. We spreken dan van een *sterrenwind*. Of een bepaalde ster een sterrenwind vertoont, kan je zien aan het *spectrum* van een ster.

Spectra van sterren

Het licht dat onze zon uitstraalt is op het eerste gezicht wit-geel van kleur. Als je echter zonlicht door een prisma laat vallen, dan zie je een brede band met, letterlijk, alle kleuren van de regenboog. Dit *spectrum* van de zon ontstaat doordat het prisma het wit-gele zonlicht uiteenrafelt in al zijn afzonderlijke kleuren, net zoals regendruppels dat doen als er een regenboog zichtbaar is. Blijkbaar is zonlicht samengesteld uit talloze verschillende kleuren, die bij elkaar gemengd op ons een wit-gele indruk maken.

Net zoals bij de zon, kan je van elke ster een spectrum nemen. Behalve de continue kleurenband, waarbij de ene kleur naadloos overgaat in de andere, en die dan ook het *continuüm* wordt genoemd, zul je bij de meeste sterren nog iets zien. Op bepaalde plekken in het spectrum zul je smalle, donkere lijnen zien. Het lijkt of het licht van heel bepaalde kleurtinten ontbreekt in het spectrum, of in ieder geval veel zwakker is. Dit is ook inderdaad zo. De donkere lijnen worden namelijk veroorzaakt door chemische elementen in de ster, zoals waterstof, helium, koolstof, stikstof, zuurstof en nog veel meer. De atomen van deze elementen zijn in staat licht van een bepaalde kleur, of beter gezegd: *golflengte*, te absorberen. Ieder element heeft zijn eigen bepaalde golflengten waarop het licht kan absorberen. Het licht bij die golflengten zie je dus ook niet, of slechts heel zwak, in het spectrum van de ster. Vandaar de donkere lijnen, die dan ook *absorptielijnen* worden genoemd. Omdat ieder element zijn eigen golflengten kent waarop het licht absorbeert, kan je uit de plaats van de donkere lijnen in het spectrum zien wat de samenstelling van de ster is. Zo bestaat de ene ster bijna helemaal uit helium, terwijl je in het spectrum van een andere ster helemaal geen heliumlijnen zult zien, maar bijvoorbeeld weer wel veel van waterstof.

Maar nu even terug naar de sterrenwinden. Want het blijkt dat je aan het spectrum van een ster kunt zien of een ster een sterrenwind heeft of niet. Als een ster materie verliest, dan zie je in zijn spectrum naast absorptielijnen ook nog *emissielijnen*. Dit zijn lijnen bij een bepaalde golflengte die juist helderder zijn dan de continue kleurenband. Blijkbaar zitten er dus chemische elementen in zo'n sterrenwind die zelf licht uitstralen en zodoende het spectrum van de ster bij bepaalde golflengten een beetje helderder maken.

Wolf-Rayet sterren

We weten dus nu, hoe je kunt zien of een ster materie verliest in een sterrenwind. Dit *massaverlies* kan behoorlijk groot zijn. Voor enkele sterren is dit zelfs zo groot, dat in enkele tienduizenden jaren net zoveel materie wordt weggeblazen als waaruit onze zon bestaat. Als je zolang zoveel materie wilt wegblazen, betekent dat natuurlijk wel dat de ster in het begin uit veel meer materie dan onze zon moet bestaan. Inderdaad tref je zulke sterke sterrenwinden alleen aan bij sterren, die aanvankelijk meer dan 25 maal zo zwaar waren als de zon.

Die sterren met zo'n hele sterke sterrenwind noemen we *Wolf-Rayet* sterren, genoemd naar de astronomen Wolf en Rayet. Zij ontdekten namelijk in 1867 dat er sterren waren die alleen maar emissielijnen in hun spectrum vertonen en geen absorptielijnen (Zie Fig. 1 in Hoofdstuk 1). Nu weet men dat dat komt omdat de wind van deze sterren zo sterk en dicht is, dat je alleen

de wind nog maar ziet. De onderliggende ster wordt geheel aan het oog onttrokken. Je zien dus alleen nog maar de emissielijnen in het spectrum, die, zoals we eerder zagen, in de sterrenwind gevormd worden. Zelfs het continuüm van het spectrum wordt bij Wolf-Rayet sterren gevormd door licht dat uitgestraald wordt door het gas van de wind en niet van de ster zelf.

We kunnen nu terugkeren naar de eerder gemaakte opmerking, dat bij de helderste sterren de lichtkracht niet goed uit de kleur af te leiden is. Dit is het sterkst het geval bij Wolf-Rayet sterren. Dat komt doordat bij Wolf-Rayet sterren al het licht uit de sterrenwind komt en niet van de onderliggende ster. De kleur van de ster zegt daarom niet zoveel meer over de temperatuur en de lichtkracht van de ster die diep in de wind verborgen is.

De afstand van Wolf-Rayet sterren: het Baldwin-effect

Voor Wolf-Rayet is de kleur dus geen goede manier om de lichtkracht en daarmee de afstand, te bepalen. Maar, er is mogelijk een andere manier waarmee de afstand van Wolf-Rayet bepaald kan worden. Voor een bepaalde groep Wolf-Rayet sterren heeft men namelijk ontdekt, dat de helderheid van de emissielijnen samenhangt met de hoeveelheid licht van het onderliggende continuüm dat de ster *uitzendt*. En wel zodanig dat sterren met een lichtsterk continuüm de zwakste lijnen vertonen en omgekeerd. Dit effect wordt het Baldwin-effect genoemd, omdat de astronoom Baldwin het ooit ontdekt heeft, zij het voor een ander soort objecten dan Wolf-Rayet sterren.

Het Baldwin-effect kan een manier zijn om de afstand van Wolf-Rayet sterren te bepalen. Als namelijk de helderheid van de emissielijnen iets zegt over hoeveel continuümlicht de ster uitzendt, dan kan je dus, bij wijze van spreken, aan de helderheid van de emissielijnen zie of de ster een 60 of een 100 Watt lamp is. Vergelijk je dat dan met hoe helder de ster aan de hemel staat, dan weet je zijn afstand. De natuurkunde en de toepasbaarheid van het Baldwin-effect in Wolf-Rayet sterren is bestudeerd in dit proefschrift.

Overzicht van dit proefschrift

Hoofdstuk 1 is een inleidend hoofdstuk. Het beschrijft wat Wolf-Rayet sterren zijn, hun natuurkundige eigenschappen en levensloop. Verder komen afstandsbepalingen aan bod en wordt het Baldwin-effect geïntroduceerd.

Om meer te weten te komen over het Baldwin-effect in Wolf-Rayet sterren is onder meer gebruik gemaakt van waargenomen spectra van Wolf-Rayet sterren. Deze worden beschreven in Hoofdstuk 2. Tevens wordt hier beschreven wat het effect is op het sterlicht van stof dat zich tussen de ster en de waarnemer bevindt. Verschillende methoden worden bekeken waarmee gecorrigeerd kan worden voor de effecten van het stof.

Een studie naar de natuurkundige oorzaak van het Baldwin-effect is het onderwerp van Hoofdstuk 3. Er wordt gebruik gemaakt van kunstmatige spectra die door een computermodel werden gegenereerd. Zodoende kan het uiterlijk van het sterspectrum worden bekeken als functie van, bijvoorbeeld, afmeting van de ster, massaverlies en snelheid van de sterrenwind. Ook kunnen kunstmatig “Baldwin-relaties” worden vervaardigd, grafieken waarbij de helderheid van de emissielijnen wordt getoond als functie van de sterkte van het continuüm.

Uit de berekeningen blijkt, dat het Baldwin-effect een algemeen verschijnsel is voor Wolf-Rayet sterren. De oorzaak blijkt grotendeels te liggen in verschillen in afmeting (straal) van de sterren. De relatie tussen de helderheid van de emissielijnen en het onderliggende continuüm, vertoont echter een zekere spreiding. Deze blijkt te worden veroorzaakt tussen verschillen in massaverlies en windsnelheid.

De computerprogramma's waarmee de kunstmatige spectra worden gegenereerd zijn zogenaamde *modelatmosfeer-programma's*. Eigenlijk berekent zo'n programma de structuur en natuurkundige omstandigheden van een sterrenwind. Vervolgens wordt gekeken wat er met het sterlicht gebeurt als het zich door deze kunstmatige sterrenwind voortbeweegt. Zodoende wordt een kunstmatig spectrum verkregen. Het gebruik van modelatmosfeer-programma's bij het bestuderen van Wolf-Rayet sterren wordt bekeken in Hoofdstuk 4. De belangrijkste vereenvoudigingen worden besproken en de resultaten van twee verschillende programma's worden met elkaar vergeleken.

In Hoofdstuk 5 worden berekende Baldwin-relaties gepresenteerd die gebruikt kunnen worden voor het schatten van afstanden van Wolf-Rayet sterren. De belangrijkste vereenvoudigingen van de modelberekeningen worden besproken en bekeken wordt of door de vereenvoudigingen aanpassingen van de Baldwin-relaties noodzakelijk is. Tot slot wordt het functioneren van de Baldwin-relaties als afstandindicatoren getest door de lichtsterkte te schatten van sterren waarvan de afstand al goed bekend is. Het blijkt dat de methode goed werkt als het massaverlies van de sterren van tevoren bekend is.

In Hoofdstuk 6 wordt het Baldwin-effect gebruikt om de afstanden te bepalen van de Wolf-Rayet sterren om ons heen. Van sommige Wolf-Rayet sterren is de afstand al bekend, omdat ze bij een groep sterren horen waarvan de afstand uit hun kleur bepaald is. Deze sterren vormen dus een extra test voor de kwaliteit van de Baldwin-relaties als afstandmeter. Er is gebruik gemaakt van een schatting van het massaverlies van de sterren, omdat dat vaak niet goed bekend is. Er wordt geconcludeerd dat de verkregen afstanden vaak goed zijn, maar dat een betere bepaling van het massaverlies van Wolf-Rayet sterren nodig is om tot echt nauwkeurige resultaten te komen.

Curriculum Vitae

Lang geleden, op 17 januari 1969, zag ik het eerste streepje daglicht, in de mooie stad Amsterdam. Het grootste deel van mijn leven heb ik in die stad doorgebracht.

De lagere en middelbare school doorliep ik aan de Vrije Scholengemeenschap Geert Groote, tot het behalen van het VWO diploma op 20 juli 1988.

De interesse in de sterrenkunde was toen al jaren aanwezig, en de studiekeuze lag dus voor de hand. De keuze viel op Utrecht, mede vanwege de brede natuurkundige basis van de sterrenkundestudie aldaar. Naarmate de studie vorderde bleek mij interesse te liggen in de combinatie van de theoretische aspecten van het vak met de interpretatie van waarnemingen. Dat laatste werd mede ingegeven door een korte stage aan de Radiosterrenwacht Dwingeloo.

De combinatie van theorie en waarnemingen bepaalde grotendeels de keuze van mijn afstudeeronderzoek, welke ik begon bij Henny Lamers. Het onderzoek betrof het proberen verklaren van afwijkende profielen van spectraallijnen in ultraviolet spectra, gemaakt met de Hubble Space Telescoop van massieve sterren in de Andromedanevel, M31.

Het doctoraaldiploma Algemene Sterrenkunde werd “met genoegen” aan mij uitgereikt op 29 augustus 1994.

Het duurde even voor ik de kans kreeg het sterrenkundig onderzoek voort te zetten, maar uiteindelijk was het opnieuw Henny Lamers bij wie ik een promotieonderzoek begon. Het onderwerp daarvan moge bekend zijn. In deze periode bezocht ik diverse conferenties, in Luik (België), München (Duitsland), Puerto Vallarta (Mexico) en Tartu (Estland). Ook bracht ik driemaal een werkbezoek aan het Space Telescope Science Institute in Baltimore, waar ik samenwerkte met Luciana Bianchi aan Wolf-Rayet spectra en met Thomas Gäng aan spectra van Luminous Blue Variables. In April van dit jaar bezocht ik Pat Morris aan het California Institute of Technology in Pasadena, hetgeen onder meer de basis legde voor het schrijven van hoofdstuk 4 van dit proefschrift.

Terwijl ik dit schrijf is inmiddels duidelijk dat ik mijn werk niet binnen de sterrenkunde zal voortzetten. Sinds 15 september werk ik bij het KNMI in De Bilt, waar ik zal werken aan de ontwikkeling van een stralingstranport-code waarin de voortplanting en verstrooiing van zonlicht in de aardatmosfeer zal worden beschreven. Wie dit proefschrift gelezen heeft zal begrijpen dat de gemaakte stap vanuit de sterrenkunde niet zo groot is.

List of Figures

1.1	The first page of the article by Wolf & Rayet (1867)	2
1.2	Spectrum of a WNE-s (top), WNE-w (middle), and WNL star	4
1.3	The Observed <i>Baldwin-effect</i> for He II transitions in the spectra of WN stars in the LMC	12
2.1	Observed Spectra of a Galactic and an LMC WN3 star	21
3.1	Dimensionless effective radius, $x_c = r_c/R_*$, vs. optical depth parameter, Γ_τ , for different β -type velocity laws	28
3.2	Line luminosity L_l (panel a) and equivalent width W (panel b) vs. continuum luminosity for the He II $\lambda 1640$ transition for isothermal atmospheres	29
3.3	Four models that show the Baldwin-effect	34
3.4	Four models that do not show the Baldwin-effect	35
3.5	Line equivalent width vs. monochromatic continuum luminosity for the He II $\lambda 1640$ line	37
3.6	Line equivalent width vs. monochromatic continuum luminosity for the He II $\lambda 3203$ line	38
3.7	Line equivalent width vs. monochromatic continuum luminosity for the He II $\lambda 4686$ line	39
3.8	Line equivalent width vs. monochromatic continuum luminosity for the He II $\lambda 5411$ line	40
3.9	Line equivalent width vs. monochromatic continuum luminosity for the He II $\lambda 10124$ line	41
3.10	Tangential Sobolev optical depth, τ_{tan} , for the He II $\lambda 1640$ line, as function of core radius (x-axis) and mass-loss rate (y-axis) for different stellar temperatures	43
3.11	The Baldwin relations of the He II $\lambda 1640$ line, but now as a function of T_{eff} rather than T_*	47
4.1	Helium spectral lines for a WNL type H-He model for three different H/He abundance ratios	57
4.2	Hydrogen and helium ionization structure of the models for which helium lines are shown in Fig. 4.1	57
4.3	Model spectra of helium lines for the H-He model (full lines) and a model with the same stellar parameters but consisting of H-He-N (dashes)	58
4.4	Ionization structure for the $T_* = 33$ kK H-He model (panel a) and H-He-N model (panel b). Panel c shows the temperature stratification for the H-He (full line) and H-He-N (dashes) models	58

4.5	Spectral energy distributions of the H-He model (full line) and the H-He-N model (dashes) at $T_* = 33$ kK	60
4.6	Model spectra of helium lines for a H-He model (full lines) and a model with the same stellar parameters but consisting of H-He-N (dashes)	61
4.7	Ionization structure for the $T_* = 50$ kK H-He model (panel a) and H-He-N model (panel b). Panel c shows the temperature stratification for the H-He (full line) and H-He-N (dashes) models	62
4.8	Spectral energy distributions of the H-He model (full line) and the H-He-N model (dashes) at $T_* = 50$ kK	62
4.9	Equivalent width contours for the He II $\lambda 5412$ line and the He I $\lambda 5876$ line)	67
4.10	Comparison of the ISA-WIND and the POTSDAM code for helium line profiles and different atmosphere characteristics of model A	73
4.11	Comparison of the ISA-WIND and the POTSDAM code for helium line profiles and different atmosphere characteristics of model B	74
4.12	Comparison of the ISA-WIND and the POTSDAM code for helium line profiles and different atmosphere characteristics of model C	75
4.13	Comparison of the ISA-WIND and the POTSDAM code for helium line profiles and different atmosphere characteristics of model D	76
4.14	Comparison of the ISA-WIND and the POTSDAM code for helium line profiles and different atmosphere characteristics of model C	77
5.1	Four WNL star models that show the variation of line equivalent width with wind density	85
5.2	Ionization structure of helium and the most important nitrogen ions	86
5.3	Line equivalent width W vs. monochromatic continuum luminosity $L_c^{\lambda_0}$ for the He II $\lambda 1640$ line	88
5.4	Line equivalent width W vs. monochromatic continuum luminosity $L_c^{\lambda_0}$ for the He II $\lambda 2511$ line	89
5.5	Line equivalent width W vs. monochromatic continuum luminosity $L_c^{\lambda_0}$ for the He II $\lambda 2733$ line	90
5.6	Line equivalent width W vs. monochromatic continuum luminosity $L_c^{\lambda_0}$ for the He II $\lambda 3203$ line	91
5.7	Line equivalent width W vs. monochromatic continuum luminosity $L_c^{\lambda_0}$ for the He II $\lambda 4686$ line	92
5.8	Line equivalent width W vs. monochromatic continuum luminosity $L_c^{\lambda_0}$ for the He II $\lambda 5412$ line	93
5.9	Line equivalent width W vs. monochromatic continuum luminosity $L_c^{\lambda_0}$ for the He I $\lambda 5876$ line	94
5.10	The influence of the nitrogen abundance on helium spectral lines	96
5.11	The influence of Thomson scattering on the Baldwin-relations for the He II $\lambda 5412$ line and the He I $\lambda 5876$ line	98
5.12	Monochromatic continuum luminosity of LMC WN stars derived with the theoretical Baldwin-relations versus the luminosity corresponding to a LMC distance modulus of $Y = 18.5$ mag	101
5.13	Mass-loss rate versus spectral subtype for Galactic WN stars	103
6.1	Mass loss rate versus bolometric luminosity for single Galactic WN stars	116

6.2	Mass loss rate versus spectral subtype from different studies	117
6.3	Distance modulus derived with the Baldwin-relations versus distance modulus of cluster/association	122

List of Tables

1.1	WR classification scheme by Smith (1968)	5
1.2	Basic physical parameters of Wolf-Rayet stars, compared to those of O-stars and the Sun	6
2.1	Galactic WN stars	13
2.2	WN stars in the LMC	15
3.1	He II transitions for which the Baldwin-effect was studied	32
3.2	Input parameters of the ISA-Wind model atmospheres	33
3.3	Fit coefficients and parameter range limits for the Baldwin relations	44
4.1	Number of explicitly treated levels and line transitions for the ISA-WIND and the POTSDAM codes	68
4.2	Basic parameters of the four WR star models for which the ISA-WIND code and the POTSDAM code are compared	69
5.1	Number of explicitly treated levels and line transitions for the ISA-WIND and the POTSDAM codes	82
5.2	Helium transitions for which the Baldwin-effect is presented	83
5.3	Input parameters of the ISA-Wind model atmospheres	84
5.4	Parameters from second order polynome fits to the relations between the equivalent width, W , and monochromatic continuum luminosity, $L_c^{\lambda_0}$, for the He II $\lambda 1640$ line	104
5.5	Parameters from second order polynome fits to the relations between the equivalent width, W , and monochromatic continuum luminosity, $L_c^{\lambda_0}$, for the He II $\lambda 2511$ line	105
5.6	Parameters from second order polynome fits to the relations between the equivalent width, W , and monochromatic continuum luminosity, $L_c^{\lambda_0}$, for the He II $\lambda 2733$ line	106
5.7	Parameters from second order polynome fits to the relations between the equivalent width, W , and monochromatic continuum luminosity, $L_c^{\lambda_0}$, for the He II $\lambda 3203$ line	107
5.8	Parameters from second order polynome fits to the relations between the equivalent width, W , and monochromatic continuum luminosity, $L_c^{\lambda_0}$, for the He II $\lambda 4686$ line	108
5.9	Parameters from second order polynome fits to the relations between the equivalent width, W , and monochromatic continuum luminosity, $L_c^{\lambda_0}$, for the He II $\lambda 5412$ line	109

5.10	Parameters from second order polynome fits to the relations between the equivalent width, W , and monochromatic continuum luminosity, $L_c^{\lambda_0}$, for the He II $\lambda 5876$ line	110
6.1	Average mass-loss rates ($\log \dot{M}/(M_{\odot} \text{ yr}^{-1})$) for WN spectral subtypes	118
6.2	Distance moduli of Galactic WN stars in open clusters and OB associations	123
6.3	Distance moduli of Galactic WN stars as estimated with the theoretical Baldwin-relations	124

References

- Abbott D. C., 1982, *ApJ* 259, 282
- Abbott D. C., Conti P. S., 1987, *ARA&A* 25, 113
- Abbott D. C., Torres A. V., Biegging J. H., Churchwell E., 1986, *ApJ* 303, 239
- Baldwin J. A., 1977, *ApJ* 214, 679
- Baldwin J. A., Burke W. L., Gaskell C. M., Wampler E. J., 1978, *Nat* 273, 431
- Barlow M. J., Hummer D. G., 1982, in *IAU Symp. 99: Wolf-Rayet Stars: Observations, Physics, Evolution*, Vol. 99, p. 387
- Bhatia A. K., Underhill A. B., 1986, *ApJS* 60, 323
- Bhatia A. K., Underhill A. B., 1988, *ApJS* 67, 187
- Bhatia A. K., Underhill A. B., 1990, *ApJ* 358, 240
- Breysacher J., 1981, *A&A Suppl.* 43, 203
- Brownsberger K. R., 1995, Ph.D. thesis, University of Colorado at Boulder
- Brussaard P. J., van de Hulst H. C., 1962, *Reviews of Modern Physics* 34, 507
- Castor J. I., Abbott D. C., Klein R. I., 1975, *ApJ* 195, 157
- Chiosi C., Maeder A., 1986, *ARA&A* 24, 329
- Conti P. S., 1976, *Mem. Soc. Roy. Sci. Liège*, 6e série, IX, 193
- Conti P. S., 1999, *New Astronomy* 4, 489
- Conti P. S., Massey P., 1989, *ApJ* 337, 251
- Conti P. S., Morris P. W., 1990, *AJ* 99, 898
- Conti P. S., Underhill A. B., 1988, *O stars and Wolf-Rayet stars*, Washington, NASA
- Conti P. S., Vacca W. D., 1990, *AJ* 100, 431
- Conti P. S., Garmany C. D., Massey P., 1989, *ApJ* 341, 113
- Conti P. S., Massey P., Vreux J. M., 1990, *ApJ* 354, 359
- Crowther P. A., 2000, *A&A* 356, 191
- Crowther P. A., Dessart L., 1998, *MNRAS* 296, 622
- Crowther P. A., Smith L. J., 1996, *A&A* 305, 541
- Crowther P. A., Smith L. J., 1997, *A&A* 320, 500
- Crowther P. A., Hillier D. J., Smith L. J., 1995a, *A&A* 293, 172
- Crowther P. A., Hillier D. J., Smith L. J., 1995b, *A&A* 293, 403
- Crowther P. A., Pasquali A., De Marco O., Schmutz W., Hillier D. J., de Koter A., 1999, *A&A* 350, 1007
- Crowther P. A., Smith L. J., Hillier D. J., 1995c, *A&A* 302, 457
- Crowther P. A., Smith L. J., Hillier D. J., Schmutz W., 1995d, *A&A* 293, 427
- Cudworth K. M., Martin S. C., Degioia-Eastwood K., 1993, *AJ* 105, 1822
- de Koter A., Schmutz W., Lamers H. J. G. L. M., 1993, *A&A* 277, 561
- de Koter A., Heap S. R., Hubeny I., 1997, *ApJ* 477, 792

- De Marco O., Schmutz W., Koesterke L., Hamann W.-R., de Koter A., 1999, in: van der Hucht, K. A., Koenigsberger, G., Eenens, P. J. R. (eds.), *Wolf-Rayet Phenomena in Massive Stars and Starburst Galaxies*, proc. IAU Symp. 193, (San Francisco: ASP), p. 231
- De Marco O., Schmutz W., Crowther P. A., Hillier D. J., Dessart L., de Koter A., Schweickhardt J., 2000, *A&A* 358, 187
- de Zeeuw P. T., Hoogerwerf R., de Bruijne J. H. J., Brown A. G. A., Blaauw A., 1999, *AJ* 117, 354
- Drew J. E., 1989, *ApJS* 71, 267
- Eggen O. J., 1981, *ApJ* 247, 507
- Fitzpatrick E. L., Massa D., 1988, *ApJ* 328, 734
- Fitzpatrick E. L., Massa D., 1990, *ApJS* 72, 163
- Gräfener G., Hamann W.-R., Hillier D. J., Koesterke L., 1998, *A&A* 329, 190
- Hamann W.-R., 1985a, *A&A* 145, 443
- Hamann W.-R., 1985b, *A&A* 148, 364
- Hamann W.-R., Koesterke L., 1998a, *A&A* 333, 251
- Hamann W.-R., Koesterke L., 1998b, *A&A* 335, 1003
- Hamann W.-R., Koesterke L., 2000, *A&A*, accepted
- Hamann W.-R., Schmutz W., 1987, *A&A* 174, 173
- Hamann W.-R., Wessolowski U., 1990, *A&A* 227, 171
- Hamann W.-R., Wessolowski U., Koesterke L., 1994, *A&A* 281, 184
- Hamann W.-R., Koesterke L., Wessolowski U., 1995, *A&A* 299, 151
- Hillier D. J., 1984, *ApJ* 280, 744
- Hillier D. J., 1987, *ApJS* 63, 947
- Hillier D. J., 1988, *ApJ* 327, 822
- Hillier D. J., 1990a, *A&A* 231, 116
- Hillier D. J., 1990b, *A&A* 231, 111
- Hillier D. J., 1991, *A&A* 247, 455
- Hillier D. J., Miller D. L., 1998, *ApJ* 496, 407
- Hiltner W. A., Schild R. E., 1966, *ApJ* 143, 770
- Howarth I. D., Schmutz W., 1995, *A&A* 294, 529
- Kingsburgh R. L., Barlow M. J., Storey P. J., 1995, *A&A* 295, 75
- Koesterke L., Hamann W.-R., Wessolowski U., Schmutz W., 1991, *A&A* 248, 166
- Kudritzki R.-P., Lennon D. J., Puls J., 1995, in: Walsh, J. R., Danziger, I. J. (eds.), *Science with the VLT*, Springer Verlag, p246
- Lamers H. J. G. L. M., Cassinelli J. P., 1999, *Introduction to stellar winds*, Cambridge, Cambridge University Press
- Lamers H. J. G. L. M., Leitherer C., 1993, *ApJ* 412, 771
- Lamers H. J. G. L. M., Rogerson J. B., 1978, *A&A* 66, 417
- Lamers H. J. G. L. M., Waters L. B. F. M., 1984, *A&A* 136, 37
- Lamers H. J. G. L. M., Nota A., Panagia N., Smith L. J., 2000, *ApJ*, in press
- Langer N., Maeder A., 1995, *A&A* 295, 685
- Leitherer C., 1988, *ApJ* 326, 356
- Lépine S., Moffat A. F. J., 1999, *ApJ* 514, 909
- Lucy L. B., 1971, *ApJ* 163, 95
- Lundström I., Stenholm B., 1984, *A&A Suppl.* 58, 163

- Maeder A., 1996, in: Vreux, J.-M., Detal, A., Fraipont-Caro, D., Gosset, E., Rauw, G. (eds.), Proc. 33rd Liège Int. Astroph. Coll., Liège, Univ. of Liège, p. 1
- Massey P., 1984, ApJ 281, 789
- Mathis J. S., 1990, ARA&A 28, 37
- Mihalas D., 1978, Stellar atmospheres, 2nd edition, San Francisco, W. H. Freeman and Co.
- Moffat A. F. J., Drissen L., Lamontagne R., Robert C., 1988, ApJ 334, 1038
- Morgan W. W., Keenan P. C., Kellman E., 1943, An atlas of stellar spectra, with an outline of spectral classification, , Chicago, The University of Chicago press
- Morris P. W., 1995, Ph.D. thesis, University of Colorado at Boulder
- Morris P. W., Conti P. S., Lamers H. J. G. L. M., Koenigsberger G., 1993a, ApJ 414, L25
- Morris P. W., Brownsberger K. R., Conti P. S., Massey P., Vacca W. D., 1993b, ApJ 412, 324
- Nugis T., Lamers H. J. G. L. M., 2000, A&A 360, 227
- Nugis T., Crowther P. A., Willis A. J., 1998, A&A 333, 956
- Panagia N., Gilmozzi R., Macchetto F., Adorf H. ., Kirshner R. P., 1991, ApJ 380, L23
- Pauldrach A., Puls J., Kudritzki R. P., 1986, A&A 164, 86
- Pozzo M., Jeffries R. D., Naylor T., Totten E. J., Harmer S., Kenyon M., 2000, MNRAS 313, L23
- Puls J., Hummer D. G., 1988, A&A 191, 87
- Puls J., Kudritzki R. ., Herrero A., Pauldrach A. W. A., Haser S. M., Lennon D. J., Gabler R., Voels S. A., Vilchez J. M., Wachter S., Feldmeier A., 1996, A&A 305, 171
- Puls J., Springmann U., Lennon M., 2000, A&A Suppl. 141, 23
- Savage B. D., Mathis J. S., 1979, ARA&A 17, 73
- Schaerer D., Schmutz W., Grenon M., 1997, ApJ 484, L153
- Schmutz W., 1997, A&A 321, 268
- Schmutz W., Vacca W. D., 1991, A&A Suppl. 89, 259
- Schmutz W., Hamann W.-R., Wessolowski U., 1989, A&A 210, 236
- Schmutz W., Abbott D. C., Russell R. S., Hamann W. R., Wessolowski U., 1990, ApJ 355, 255
- Seaton M. J., 1979, MNRAS 187, 73P
- Smith L. F., 1968, MNRAS 140, 409
- Smith L. F., Maeder A., 1989, A&A 211, 71
- Smith L. F., Shara M. M., Moffat A. F. J., 1990, ApJ 358, 229
- Smith L. F., Shara M. M., Moffat A. F. J., 1996, MNRAS 281, 163
- Smith L. J., Stroud M. P., Esteban C., Vilchez J. M., 1997, MNRAS 290, 265
- Spitzer L., 1978, Physical processes in the interstellar medium, New York, New York Wiley-Interscience
- Thompson R. W., 1983, NASA IUE Newsletter 21, 39
- Thompson R. W., Turnrose B. E., 1983, NASA IUE Newsletter 20, 34
- Torres-Dodgen A. V., Massey P., 1988, AJ 96, 1076
- Vacca W. D., 1992, Ph.D. thesis, University of Colorado at Boulder
- Vacca W. D., Torres-Dodgen A. V., 1990, ApJS 73, 685
- van der Hucht K. A., 1992, A&AR 4, 123
- van der Hucht K. A., 2000, New Astronomy Review, submitted
- van der Hucht K. A., Conti P. S., Lundström I., Stenholm B., 1981, Space Science Reviews 28, 227
- van der Hucht K. A., Hidayat B., Admiranto A. G., Supelli K. R., Doom C., 1988, A&A 199, 217

-
- van der Hucht K. A., Schrijver H., Stenholm B., Lundström I., Moffat A. F. J., Marchenko S. V., Seggewiss W., Setia Gunawan D. Y. A., Sutantyo W., van den Heuvel E. P. J., de Cuyper J. ., Gomez A. E., 1997, *New Astronomy* 2, 245
- van Gent J. I., Lamers H. J. G. L. M., de Koter A., Morris P. W., 2000, *A&A*, submitted
- Vink J. S., de Koter A., Lamers H. J. G. L. M., 1999, *A&A* 350, 181
- Vink J. S., de Koter A., Lamers H. J. G. L. M., 2000, *A&A*, accepted
- Voors R. H. M., Waters L. B. F. M., de Koter A., Bouwman J., Morris P. W., Barlow M. J., Sylvester R. J., Trams N. R., Lamers H. J. G. L. M., 2000, *A&A* 356, 501
- Vreux J. M., Dennefeld M., Andrillat Y., 1983, *A&A Suppl.* 54, 437
- Vreux J. M., Dennefeld M., Andrillat Y., Rochowicz K., 1989, *A&A Suppl.* 81, 353
- Walborn N. R., 1977, *ApJ* 215, 53
- Waters L. B. F. M., Lamers H. J. G. L. M., 1984, *A&A Suppl.* 57, 327
- Wessolowski U., Schmutz W., Hamann W.-R., 1988, *A&A* 194, 160
- Wolf C. J. E., Rayet G., 1867, *Compt. Rend. Acad. Sci. Paris* 65, 292